ISTANBUL TECHNICAL UNIVERSITY ★ GRADUATE SCHOOL OF SCIENCE ENGINEERING AND TECHNOLOGY

ANTIBACTERIAL AMPHIPHILIC POLYMERS BASED ON ENZYMATICALLY SYNTHESIZED POLYCAPROLACTONE

Ph.D. THESIS

Nazif Uğur KAYA

Department of Polymer Science and Technology

Polymer Science and Technology Program

FEBRUARY 2017

ISTANBUL TECHNICAL UNIVERSITY ★ GRADUATE SCHOOL OF SCIENCE ENGINEERING AND TECHNOLOGY

ANTIBACTERIAL AMPHIPHILIC POLYMERS BASED ON ENZYMATICALLY SYNTHESIZED POLYCAPROLACTONE

Ph.D. THESIS

Nazif Uğur KAYA
(515102002)

Department of Polymer Science and Technology

Polymer Science and Technology Program

Thesis Advisor: Prof. Dr. F. Yüksel AVCIBAŞI GÜVENİLİR

FEBRUARY 2017

İSTANBUL TEKNİK ÜNİVERSİTESİ ★ FEN BİLİMLERİ ENSTİTÜSÜ

ENZİMATİK OLARAK SENTEZLENMİŞ POLİKAPROLAKTON BAZLI ANTİBAKTERİYEL AMFİFİLİK POLİMERLER

DOKTORA TEZİ

Nazif Uğur KAYA
(515102002)

Polimer Bilim ve Teknolojisi Anabilim Dalı

Polimer Bilim ve Teknolojisi Programı

Tez Danışmanı: Prof. Dr. F. Yüksel AVCIBAŞI GÜVENİLİR

ŞUBAT 2017

Nazif Uğur KAYA, a Ph.D. student of ITU Graduate School of Science Engineering and Technology, Polymer Science and Technology Department with student ID 515102002, successfully defended the dissertation entitled "Antibacterial Amphiphilic Polymers Based On Enzymatically Synthesized Polycaprolactone", which he prepared after fulfilling the requirements specified in the associated legislations, before the jury whose signatures are below.

Thesis Advisor :	**Prof. Dr. F. Yüksel AVCIBAŞI GÜVENİLİR** Istanbul Technical University	.....
Jury Members :	**Prof. Dr. Ayşen ÖNEN** Istanbul Technical University	.....
	Prof. Dr. Ülker BEKER TUBITAK-MAM, Gebze	.....
	Prof. Dr. İ. Ersin SERHATLI Istanbul Technical University	.....
	Assoc. Prof. Dr. Didem SALOĞLU DERTLİ Yalova University	.....

Date of Submission : 26 December 2016
Date of Defense : 03 February 2017

To my dearest family,

FOREWORD

I would first like to thank to my supervisor, Prof. Dr. Yüksel GÜVENİLİR for accepting me as a PhD student, her valuable mentoring, supporting my abroad studies and guidance not only for my thesis but also for life.

I greatly appreciate to my thesis supervisor comitee Prof. Dr. Ayşen ÖNEN and Prof. Dr. Ülker BEKER for their continuous advices and supports.

I am indebted to Prof. Dr. Metin Hayri ACAR and Assoc. Prof. Dr. Didem SALOĞLU DERTLİ for their helps in using laboratory equipments.

I also would like to acknowledge Prof. Dr. Filip Du Prez for opening the laboratories and facilities in University of Gent for my PhD studies and collaborative researches.

I am cordially appreciated to Asst. Prof. Dr. Nezha BADI for her invaluable technical advices and teaching and providing a positive working environment.

I would like to acknowledge Pervin SAYGIN and ARÇELİK for their helps in antibacterial tests.

I am thankful to my chiefs in SASA Polyester A.Ş. for permitting me to allocate sufficient time for my PhD studies.

I would also like to express my sincere gratitude to the my colleagues Cansu ÜLKER, Erhan ÖZSAĞIROĞLU, Nurefşan GÖKALP and other group members of "Biotechnology Lab" research group for the warm and synergetic working environment.

I am very grateful to Assoc. Prof. Dr. Özgür SEYDİBEYOĞLU, Dr. Hale ÖZTÜRK DÜŞKÜNKORUR for their helps and advices in the beginning of my PhD journey.

I am grateful to Dr. Y.Andelip AYDIN for her advices in the laboratory.

It would be very hard without the opportune helps of Şenel KARANCI and my other colleagues in I.T.U. Chemical Engineering Department.

I would like to send my deepest thanks to my dear friends, Akın EVİRGEN, Aslı GENÇTÜRK, Aylin KERTİK, Aysu ARSLAN, Başak DEMİRCİOĞLU ÖZ, , Çağlar FIRAT, Derya AKÇÖREN, Didem AYTAÇ, Dinçay AKÇÖREN, Ercan MUTLU, Giray ERSÖZOĞLU, Gültekin ÖZ, Hüsniye BALKAN, İlayda OKSAL, İlknur GERGİN, Kaan DEMİRKAZIKSOY, Masoud TEYMOURFAMIAN, Melike BALADİN, Pelin TONKA, Mecit GÖKÇE, Muhsin SONAY, Orçun ÇINAR, Selda ŞEN TANUĞUR, Timuçin BALKAN, Tolga SATICI, Tuluhan ERGİN, Yusuf TANUĞUR, Zeliha GÜLER GÖKÇE.

My thanks and appreciations go to the "PCR Group" members Bastian, Benjamin, Bernhard, Cristina, Duchan, Lucie, Frank, Görkem, Hannes, Jonas, Josh, Kevin, Laetitia, Maarten, Martijn, Matthias, Otto, Pieter, Rémi, Sare, Seda, Steven, Susanne, Sophie, Subrata, Şensu, Wim, Xiangqiang and Yann for being cooperative in a joyful and positive lab environment. I would like to express my greatest gratitude to Daniël

FRANK, Jonas VAN DAMME, Andrea HUFENDIEK and Seda ÇAKIR from PCR in my Ghent adventure for their precious friendship and limitless helps. I appreciate Pınar SİNEM OMURTAG for her helps to my journey to Ghent.

I would like to thank to my friends in Ghent, Aina, Alex, Alicia, Alejandro, Berna, Cana, Carola, Ceren, Delphi, Edoardo, Fabio, Marta, Melda, Marcelina, Onur, Oriana, Paschalis, Pierluigi, Sinem and Soizic for always being joyful, entertaining and full of life.

I always felt the love and limitless support of my family in my heart keeping me on; it wouldn't be possible for me to pursue my studies without them.

December 2016

Nazif Uğur KAYA
(Chemical Engineer)

TABLE OF CONTENTS

Page

ABBREVIATIONS

ACN	**:** Acetonitrile
AHLs	**:** N-acyl homoserine lactones
AK	**:** Pseudomonas fluorescens
AMPs	**:** Antimicrobial peptides and proteins
Asp	**:** Aspartate
ATRP	**:** Atom transfer radical polymerization
BuA	**:** Butyl acrylate
BzA	**:** Benzyl acrylate
CALB	**:** Candida antarctica lipase B
CL	**:** ε-caprolactone
DAG	**:** Diacylglycerol
DCM	**:** Dichloromethane
DDL	**:** Dodecalactone
DMA	**:** Dimethylacetamide
DMATC	**:** 2-dimethylaminotrimethylene carbonate
DMF	**:** Dimethylformamide
DMPCL	**:** Dimethacrylated polycaprolactone
DMPKL	**:** Polikaprolakton dimetakrilat
DMSO	**:** Dimethylsulfoxide
DSC	**:** Differential scanning calorimetry
DTK	**:** Diferansiyel taramalı kalorimetre
EGDA	**:** Ethylene glycol diacrylate
EGDMA	**:** Ethylene glycol dimethacrylate
ELISA	**:** Enzyme-linked immunosorbent assay
eROP	**:** Enzymatic ring-opening polymerization
FTIR-ATR	**:** Fourier transform infrared spectroscopy-Attenuated total reflection
Glu	**:** Glutamate
Gln	**:** Glutamine
HEA	**:** 2-hydroxyethyl acrylate
HEMA	**:** 2-hydroxyethyl methacrylate
His	**:** Histidine
Irgacure 819	**:** Bis(2,4,6-trimethylbenzoyl)-phenylphosphineoxide
Irgacure 2959	**:** (1-[4-(2- Hydroxyethoxy)-phenyl]- 2-hydroxy-2-methyl-1-propane-1-one)
LED	**:** Light emitting diode
Lipase A	**:** Lipase from Aspergillus niger
Lipase CC	**:** Lipase from Candida cylindracea
Lipase CR	**:** Lipase from Candida rugosa
Lipase PF	**:** Lipase from Pseudomonas fluorescence
Lipase PR	**:** Lipase from Penicillium roqueforti
Lipase RD	**:** Lipase from Rhizopus delemer
Lipase RJ	**:** Lipase from Rhizopous japanicus

MAG : Monoacylglycerol
MeOH : Methanol
MSCRAMM : Microbial surface components recognizing adhesive matrix molecules
N435 : Novozyme-435
NMR : Nuclear magnetic resonance
NO : Nitric oxide
P(CL)$_n$-*b*-P(BuA)$_m$: Block copolymer of polycaprolactone and poly(butyl acrylate)
P(CL)$_n$-*b*-P(BzA)$_m$: Block copolymer of polycaprolactone and poly(benzyl acrylate)
P(CL)$_n$-*b*-P(THFA)$_m$: Block copolymer of polycaprolactone and poly(tetrahydrofurfuryl acrylate)
P(CL)$_n$-*b*-P(TFEA)$_m$: Block copolymer of polycaprolactone and poly(trifluoroethyl acrylate)
P(CL)$_n$-*b*-P(HEA)$_m$: Block copolymer of polycaprolactone and poly(2-hydroxyethyl acrylate)
P(CL)$_n$-*b*-P(PEGMEA)$_m$: Block copolymer of polycaprolactone and poly(PEGMEA-480)
P(CL)$_n$-*b*-P(PEGMEA)$_m$ -*b*-P(SBMA)$_k$: Block copolymer of polycaprolactone poly(PEGMEA-480) and poly(sulfobetaine methacrylate)
PA6 : Poly(ε-caprolactam)
PA66 : Poly(hexamethylene adipamide)
PBAT : Poly(butylene adipate-co-terephthalate)
PBS : Polybutylenesuccinate
PBT : Poly(butylene terephthalate)
PC : Polycarbonate
PCBMA : Poly(carboxybetaine methacrylate)
PCL : Polycaprolactone
PDEA : Poly(diethylamino ethyl methacrylate)
PDI : Polydispersity index
PDL : Pentadecaloactone
PDMS : Poly(dimethylsiloxane)
PE : Polyethylene
PEF : Polyethylenefuranoate
PEG : Poly(ethylene glycol)
PEGMA-950 : Poli(etilen glikol) metil eter metakrilat-950
PEGMEA-480 : Poli(etilen glikol) metil eter akrilat-480
PET : Poly(ethylene terephthalate)
PG : Polyglycerol
PHA : Polyhydroxyalkanoate
PHB : Poly[(R)-3-hydroxybutyrate]
PHEMA : Poly(2-hydroxyethyl methacrylate)
PHPMA : Poly(3-hydroxypropyl methacrylate)
PKL : Polikaprolakton
PLA : Polylactic acid
POEGMA : Poly(oligo(ethylene glycol) methacrylate)
PP : Polypropylene
PPBMA : Poly(phopshobetaine methacrylate)
PPDL : Polypentadecalactone

PPL : Porcine pancreatic lipase
PS-30 : Pseudomonas cepacia
PSBMA : Poly(sulfobetainemethacylate)
PSerMA : Poly(serine methacrylate)
PTT : Poly(trimethylene terephthalate)
QACs : Quaternary ammonium compounds
QAS : Quaternary ammonium salts
QPS : Quaternary phosphonium salts
SAMs : Self-assemble monolayers
SBMA : Sülfobetain metakrilat
SBMA : Sulfobetaine methacrylate
SI-ATRP : Surface-initiated atomic transfer radical polymerization
QS : Quorum-sensing
ROP : Ring-opening polymerization
SEC : Size exclusion chromatography
Ser : Serine
TAG : Triacylglycerol
TBT : Tributyltin
TFEA : 2,2,2-trifluoroethyl acrylate
THF : Tetrahydrofuran
THFA : Tetrahydrofurfuryl acrylate
Thr : Threonine
TMPTA : Trimethylolpropane triacrylate
UCC : Union Carbide Corporation
UDL : Undecalactone
UV : Ultraviolet
VL : δ-valerolactone

SYMBOLS

7	**:** H atoms belonging to the methylene groups on the 2-bromoisobutyryl bromide end-groups
a, b	**:** Aromatic H atoms of the macrophotoinitiator
a_1, a_2, b_1, b_2	**:** H atoms belonging to double-bonded end-groups of PCL
A, A', B	**:** H atoms belonging to THFA repeating unit and THFA monomer
A, A', F	**:** H atoms belonging to reacted and unreacted PEGMEA-480 macromonomers
A, D, E	**:** H atoms belonging to the THFA repeating units
c, 1, 2, 3, 4, 5	**:** CL repeating units along PCL
D, D'	**:** H atoms of the ester neighbouring methylene bridge in the reacted and unreacted BzA monomers
e, f	**:** EG moiety inside the chains
e	**:** H atoms belonging to the methyl group of the methacrylate end-groups
EPR^0_{Exp}	**:** Estimated total peak height ratios of the peaks at 1637 cm^{-1} and 1720 cm^{-1} calculated with the molar feed ratios
F', H	**:** Unreacted vinylic double bond H atoms of tetrahydrofurfuryl acrylate and H atoms belonging to the methylene bridge of PTHFA backbone
G', C, C'	**:** Double bond H atoms of butyl acrylate monomer
h, c	**:** HEMA end-groups of PCL
I_a, $I_{5'}$	**:** Peak integrals of the peaks c and 5'
I_c, I_d, I_g, I_h	**:** Peak integrals of the peaks c, d, h and h
I_A, $I_{A'}$, I_B	**:** Peak integrals of the peaks A, A' and B
I_A, $I_{A'}$, I_F	**:** Peak integrals of the peaks A, A' and F
I_A, I_D, I_E	**:** Peak integrals of the peaks A, D and E
I_D, $I_{D'}$	**:** Peak integrals of the peaks D and D'
$[I]^d_A$, $[I]^d_5$	**:** Peak integrals of the peaks A and 5 of the dry polymer
$[I]^f_{A'}$ $[I]^f_5$	**:** Peak integrals of the peaks A' and 5 of the mixture before photopolymerization
$[I]^d_D$, $[I]^d_5$	**:** Peak integrals of the peaks D and 5 of the dry polymer
$[I]^f_{D'}$ $[I]^f_5$	**:** Peak integrals of the peaks D' and 5 of the mixture before photopolymerization
$I_{F'}$, I_H	**:** Peak integrals of the peaks F' and H
$I_{G'}$, I_C, $I_{C'}$	**:** Peak integrals of the peaks G, C and C'
m, d	**:** Methacrylate end-groups of PCL
$\overline{M_n}$	**:** Number average molecular weight
$\overline{M_n^{SEC}}$	**:** Number average molecular weight calculated via SEC
m/n	**:** Ratio of the repeating units of THFA to the repeating units of CL
m_{feed}/n_{feed}	**:** Feed ratio of THFA monomer to the repeating units of CL in the macrophotoinitiator

PR^{0}_{DMPCL} : Peak height ratios of the peaks at 1637 cm^{-1} and 1720 cm^{-1} belonging to the crude DMPCL

$PR^{0}_{PEGMA-950}$: Peak height ratios of the peaks at 1637 cm^{-1} and 1720 cm^{-1} belonging to the crude PEGMA-950

$PR^{p}_{Exp.}$: Peak height ratios of the peaks at 1637 cm^{-1} and 1720 cm^{-1} after photopolymerization

T_g : Glass transition temperature

$T_{g,1}$: First glass transition temperature

$T_{g,2}$: Second glass transition temperature

T_m : Melting temperature

$T_{m,1}$: First melting temperature

$T_{m,2}$: Second melting temperature

v, w, g, h, 5' : Hydroxyl end-groups

x_1, x_2, y_1, y_2 : H atoms belonging to double-bonded end-groups of PCL

δ : Chemical shift in nuclear magnetic resonance (ppm)

ΔC_p : Specific heat change per gram of polymer

ΔH_f : Enthalpy of fusion per gram of polymer

$\Delta H_{f,1}$: Enthalpy of fusion per gram of polymer for first melting

$\Delta H_{f,2}$: Enthalpy of fusion per gram of polymer for second melting

ΔH^{c}_{f} : Enthalpy of fusion per gram of polymer for 100% crystalline polymer

χ_c : Degree of crystallinity

χ_{DMPCL} : Molar feed ratio of DMPCL for photopolymerization

$\chi_{PEGMA-950}$: Molar feed ratio of PEGMA-950 for photopolymerization

LIST OF TABLES

Page

LIST OF FIGURES

Page

ANTIBACTERIAL AMPHIPHILIC POLYMERS BASED ON ENZYMATICALLY SYNTHESIZED POLYCAPROLACTONE

SUMMARY

Amphiphilic polycaprolactone (PCL) based polymers were synthesized utilizing three different approaches including the combination of enzymatic ring-opening polymerization (eROP) either with photopolymerization and atom transfer radical polymerization (ATRP). The side reactions during the synthesis of methacrylate initiated eROP of ε-caprolactone (CL) was scrutinized to reveal the formation of different end-groups. Effect of reaction time initiator/lactone ratio and the synergetic effect of temperature and initiator/lactone ratio as 2-hydroxyethyl methacrylate (HEMA) was the nucleophilic initiator, Novozyme-435 (N435) was the immobilized lipase catalyst. α,ω-methacrylated PCL macromonomer was synthesized to have the benefit of the side reactions investigated at the first place, utilizing ethylene glycol dimethacrylate (EGDMA). Since, water acted as the nucleophilic initiator in the beginning of the reaction, EGDMA was degraded by N435 and tailored onto the ends of the PCL chains resulting in mixture of macromonomers comprising a combination of methacrylate, HEMA, and hydroxyl end-groups together with ethylene glycol (EG) moieties along the chain. The mixture of PCL chains were concisely called as dimethacrylated PCL or α,ω-methacrylated PCL (DMPCL). DMPCL was employed as a long crosslinking agent in the photopolymerizaton of poly(ethylene glycol) methyl ether methacrylate-950 (PEGMA-950) with the aid of trimethylolpropane triacrylate (TMPTA) and Irgacure-819 as the initiator under light emitting diod (LED) ultraviolet (UV) bulbs. To achieve amphiphilic copolymer of PCL and poly(ethylene glycol) (PEG) with another strategy, a macrophotoinitiator based on PCL was again synthesized via eROP when Irgacure-2959 was used as the nucleophilic initiator. Light-induced polymerization was again applied to reach PCL copolymers with butyl acrylate (BuA), benzyl acrylate (BzA), tetrahydrofurfuryl acrylate (THFA), 2,2,2-trifluoroethyl acrylate (TFEA), 2-hydroxyethyl acrylate (HEA) and poly(ethylene glycol) methyl ether acrylate-480 (PEGMEA-480). PEGMEA-480 and sulfobetaine methacrylate (SBMA) were also installed on enzymatically synthesized PCL to achieve AB and ABC type block copolymers via ATRP. Following the end-functionalization of enzymatically synthesized PCL with 2-bromoisobutyryl bromide, diblock copolymer of $P(CL)_n$-*b*-$P(PEGMEA)_m$ and triblock copolymer of $P(CL)_n$-*b*-$P(PEGMEA)_m$-*b*-$P(SMBA)_k$ were achieved. The structures of the abovementioned polymers were analysed with ^1H nuclear magnetic resonance (NMR), fourier transform infrared spectroscopy-attenuated total reflection (FTIR-ATR), differential scanning calorimetry (DSC) and size exclusion chromatography (SEC). The antibacterial properties of the polymers were investigated via zone inhibition test method.

The side reactions during the synthesis of methacrylate initiated enzymatic ring-opening polymerization of ε-caprolactone (CL) was scrutinized. It was revealed that N435 has high activity enough to catalyze enzyme-monomer complex formation, initiation, and propagation, cleaving the ester bond of the hydroxyl bearing acrylate

initiator at the same time. Therefore, it was revealed that it might be preferable to study at lower reaction temperatures to reduce the side reactions inside the sufficient activity range of N435 or other lipase types. It is obvious to finalize the eROP at low reaction times and conversions in order to obtain lower side reactions and comparable HEMA addition. Furthermore, the lower enzyme amount might be preferable in order to realise higher HEMA addition, lower methacrylate transfer, comparable total methacrylate end-groups, and minimum EG inside the chains. HEMA/CL ratio can also be chosen minimum as both of the side reactions seemed to be lower at both temperatures and enzyme amounts, still conserving the total methacrylate amount sufficient. In addition to these, higher molecular weight and polymerization yield of macromonomers can be obtained at lower initiator/lactone ratios.

To synthesize α,ω-methacrylated macromonomer for the application as a crosslinking agent in UV polymerization, it was benefited from the previously investigated side-reactions during eROP of CL when an ester containing initiator presented in the reactor. The double methacrylation of the PCL chains was evaluated to be a successful route, since the one-pot synthesis comprised of the primary synthesis of PCL enzymatically, and subsequent tailoring of the methacrylate groups onto the chains provided that all the water molecules were removed from the reaction mixture with high vacuum for high a conversion time. Furthermore, the conversion values without the usage of either PEGMA-950 or DMPCL didn't give high conversion values of DMPCL and PEGMA-950. Therefore, the concurrent usage of DMPCL and PEGMA-950 in photopolymerization provided a synergetic influence for the conversion of both macromonomers with the help of TMPTA. The feed mole ratios 0.25, 0.50 and 0.75 for DMPCL (DMPCL/Total macromonomers) inside the photopolymerization mixture all gave high polymerization yields. Consequently, enzymatically polymerized dimethacrylated PCL macromonomer with average molecular weight of 4400 g/mole and 0.84 ratio of the total methacrylate end-groups was found to be an efficient crosslinking agent in photopolymerization and obtaining amphiphilic networks. It was noteworthy that the low T_g and T_m values of the amphiphilic networks revealed the rubbery and elastic behaviour of the materials.

The enzymatic synthesis of PCL-based macrophotoinitiator was performed successfully. The macrophotoinitiator successfully photopolymerized the acrylate monomers: butyl acrylate, benzyl acrylate, tetrahydrofurfuryl acrylate, 2,2,2-trifluoroethyl acrylate, 2-hydroxyethyl acrylate and poly (ethylene glycol) methyl ether acrylate ~ 480 g/mole). Benzyl acrylate and tetrahydrofurfuryl acrylate had the highest conversion values. The block copolymer structure of poly(CL-b-BzA) and high conversion was confirmed with a single and broad Tg value with a high step decrease of the specific heat capacity. The relatively high dry polymer conversions for gel formation by using HEA and PEGMEA-480 monomers in photopolymerization also proved the efficiency of amphiphilic polymer synthesis via PCL based macrophotoinitiator. The low T_g value, thus the rubbery state, of the amphiphilic gels also made it possible for their usage in biomedical applications together with the biocompatible nature of the employed macromonomers.

A chemoenzymatic route was utilized in order to synthesize amphiphilic diblock copolymer ($P(CL)_n$-*b*-$P(PEGMEA)_m$) and an amphiphilic triblock copolymer comprising zwitterionic monomer units ($P(CL)_n$-*b*-$P(PEGMEA)_m$-*b*-$P(SMBA)_k$). It should be noted that the third polymer segment was installed by the synthesis of a methacrylate via ATRP onto an polyacrylate based diblock macroinitiator. Furthermore, the low solubility of the diblock copolymer in the reaction solvent

ethanol/water mixture was also one of the challenging points of the third monomer addition. Another barrier for both PEGMEA-480 and SBMA ATRP polymerizations might be the steric hinderence of PEGMEA-480 brush segments together with the possible entaglements of the PEG chains. However, PEGMEA-480 conversion was calculated as 65% and SBMA was proven to be polymerized with diblock ATRP macroinitiator.

Amphiphilic diblock copolymers comprised of PCL and PEG synthesized via photopolymerization and ATRP approaches both had antibacterial activity against S. aureus (Gram positive) and E. coli (Gram negative). The triblock copolymer, based on PCL, PEG and PSMBA was only antibacterial against S. aureus. However, neither of the polymers provided antifungal activity against A. niger. Antifouling feature assay might also be performed for the synthesized polymers, since composing antifouling surfaces is one of the candidate routes to obtain antibacterial activity due to their capability of inhibition of the protein based molecules which are employed by microorganisms to simplify their settlemt on surfaces. Protein adsorption test might be a method to investigate antifouling features. Consequently, enzymatic ring-opening polymerization in combination with photopolymerization or ATRP was found to be an approach to synthesize polymers performing antibacterial properties which might find applications in biomedical and marine uses.

ANTİBAKTERİYEL ÖZELLİK TAŞIYAN ENZİMATİK OLARAK SENTEZLENMİŞ POLİKAPROLAKTON BAZLI AMFİFİLİK POLİMERLER

ÖZET

Polikaprolakton (PKL) bazlı amfifilik polimerler, enzimatik halka açılım polimerizasyonunun (eROP) fotopolimerizasyon veya atom transfer radikal polimerizasyon (ATRP) yöntemleri ile beraber kullanılarak sentezlenmiştir. ε-kaprolaktonun (KL) eROP yöntemi ile polimerizasyonu reaksiyonunda ester içeren nükleofilik başlatıcı kullanılarak oluşan yan reaksiyonlar incelenmiştir. Reaksion süresi, başlatıcı/lakton oranı ve reaksiyon sıcaklığı ile başlatıcı/lakton oranının sinerjik etkilerinin bu yan reaksiyonlara, dolayısıyla uç grup oluşumlarına etkileri incelenmiştir. Nükleofilik başlatıcı olarak 2-hidroksietil metakrilat (HEMA) ve biyokatalizör olarak Novozyme-435 (N435) immobilize lipaz enzimi kullanılmıştır. PKL bazlı amfifilik polimerlerin elde edilmesinde üç farklı yönteme başvurulmuştur. Birinci yöntemde yukarıda bahsedilen yan reaksiyonlardan faydalanılarak iki ucu da metakrilat içeren PKL bazlı makromonomer sentezlenmiştir. Reaksiyonun başlangıcında su nükleofilik başlatıcı olarak görev yapmıştır. Bununla birlikte etilen glikol dimetkrilat (EGDMA) da N435 tarafından parçalanmıştır. Reaksiyonun başlamasından bir süre sonra ortamdaki suyun vakumla uzaklaştırılması ile birlikte metakrilat fonksiyonel grupları PKL zincirlerinin uç gruplarına eklenmiştir. Elde edilen PKL' nin, HEMA ve metakrilat uç gruplarının yanı sıra farklı hidroksil uç gruplarını da çeşitli kombinasyonlar oluşturacak şekilde içerdiği görülmüştür. Dolayısıyla, bu PKL karışımı dimetakrilatlı polikaprolakton (DMPKL) olarak adlandırılmıştır. Bir sonraki aşamada, poli(etilen glikol) metil eter metakrilat-950' nin (PEGMA-950) fotopolimerizasyon reaksiyonunda, DMPKL ve trimetilpropan triakrilat (TMPTA) beraber çapraz bağlayıcı olarak ve ışık yayan diyot-ultraviyolet (LED-UV) kullanılmıştır. Amfifilik ağsı yapıların oluşturulduğu bu yöntemde Irgacure-819' a fotobaşlatıcı olarak başvurulmuştur. PKL bazlı amfifilik yapıların elde edilmesi için diğer bir yöntem, hidroksil fonksiyonel gruplu Irgacure-2959 fotobaşlatıcısı, CL' nun enzimatik polimerizasyonunda nükleofilik başlatıcı olarak kullanılmıştır. Böylece bir ucu fotobaşlatıcı, diğer ucu ise hidroksil fonksiyonlu PKL bazlı makrofotobaşlatıcı elde edilmiştir. Elde edilen makrofotobaşlatıcı, bütil akrilat (BuA), benzil akrilat (BzA), tetrahidrofürfüril akrilat (THFA), 2,2,2-trifloroetil akrilat (TFEA), 2-hidroksietil akrilat (HEA) ve poli(etilen glikol) metil eter akrilat-480 (PEGMEA-480) monomerlerinin UV polimerizasyonunda kullanılmıştır. Üçüncü yöntem olarak da, ATRP yöntemi ile önce PKL ve PEGMEA-480 içeren diblok kopolimeri, daha sonradan bu diblok kopolimer kullanılarak sülfobetain metakrilat (SBMA) tekrarlanan ünitelerini içeren triblok kopolimeri sentezlenmiştir. Bunun için önceden eROP yöntemi ile sentezlenen PKL, 2-bromoizobütiril bromit ile fonksiyonlandırılarak makrobaşlatıcıya dönüştürülmüştür. Yukarıda bahsedilen polimerik yapılar ^{1}H nükleer magnetik rezonans (NMR), fourier transform kızılötesi spektroskopi-azaltılmış toplam yansıma (FTIR-ATR), diferansiyel taramalı

kalorimetre (DSC), boyut dışlama kromatografisi (SEC) yöntemleri ile karakterize edilmiştir. Antibakteriyel özellikler ise zon inhibisyonu testi ile analiz edilmiştir.

Enzimatik halka açılım polimerizasyonu yöntemi ile metakrilat bazlı başlatıcı kullanılarak gerçekleştirilen PKL makromonomeri sentezi reaksiyonunda ana ve yan reaksiyonlar incelendiğinde, N435 lipaz katalizörünün, hem enzim-monomer kompleksini oluşturduğu hem de hidroksil fonksiyonel gruplu ester grubu içeren metakrilat başlatıcıdaki (HEMA) ester bağlarını parçalayarak yan reaksiyonlara sebep olacak ürün oluşturduğu görülmüştür. Bu çalışmalar ışığında, daha düşük monomer dönüşümü göz önüne alınarak reaksiyon sürelerinin de kısaltılması, yan reaksiyonların azaltılmasında bir başka yöntem olabilir.

N435 enziminin ester içeren başlatıcılara karşı yüksek aktivitesinden faydalanılarak iki ucu da metakrilat içeren PKL makromonomeri sentezlenmiştir. Bu sentez yönteminin ilk bölümde gerçekleştirilen enzimatik sentezlerden farkı; ilk aşamada polimerizasyonun, monomer, enzim ve reaktörün içerisinde bulunan eser miktardaki suyun başlatıcı olarak kullanılması, daha sonra reaktöre yüksek vakum uygulayarak bu suyun ortamdan uzaklaştırılması ve enzimin ortamda bulunan metakrilat bazlı monomerik çapraz bağlayıcıyı (EGDMA) parçalayarak PKL' nin iki ucuna eklemesidir. Bu şekilde sentezlenen dimetakrilatlı, çapraz bağlayıcı özellikli DMPKL, ultraviyolet polimerizasyonuna tabi tutularak PEGMA-950 ile amfifilik kopolimerleri sentezlenmiştir. Sabit triakrilat çapraz bağlayıcı konsantrasyonunda; PEGMA-950 ve DMPKL makromonomerlerinin konsantrasyonları (0.00, 0.25, 0.50, 0.75, 1.00) değiştirildiğinde, her iki monomerin dönüşümü değerlendirildiğinde PEGMA-950 ve DMPKL birlikte kullanıldığı durumlarda, amfifilik kopolimerler elde edildiği gözlenmiştir. Aksi durumda, monomer dönüşümleri düşük çıkmaktadır.

İkinci yaklaşım olarak amfifilik polimerlerin elde edilmesinde, enzimatik olarak PKL bazlı makrofotobaşlatıcı sentezi gerçekleştirilmiş ve fotopolimerizasyon yöntemi ile BuA, BzA, THFA, TFEA, HEA ve PEGMEA-480 monomerleri ile polimerizasyon reaksiyonları incelenmiştir. En yüksek polimerizasyon verimi benzil akrilat monomeri ile sağlanmıştır. Aynı zamanda, PEGMEA-480 ve HEA ile PKL bazlı amfifilik yapılar farklı bir yolla sentezlenebilmiştir. Sentezlenen amfifilik polimerlerin oda sıcaklığında jel formunda olması, DSC analizlerine göre düşük camsı geçiş noktası değerlerine sahip olması, kauçuğumsu yapıda oldukları, ana maddelerine göre amorf yapılarının arttığı ve bu nedenle biyomedikal uygulamalarda kullanılabilir olmasını sağlamaktadır.

Son yaklaşım olarak, PEGMEA-480 ve SBMA içeren diblok ve triblok amfifilik kopolimerler sentezlenmiştir. ATRP yöntemi ile amfifilik diblok ve triblok kopolimerlerin daha kontrollü bir şekilde sentezlenmeleri hedeflenmiştir. Bunun için enzimatik olarak sentezlenmiş PKL önce 2-bromoizobutiril bromit ile ATRP makrobaşlatıcısına dönüştürülmüş ve PEGMEA-480 makromonomerinin ATRP reaksiyonu sonucu AB tipli $P(KL)_n$-*b*-$P(PEGMEA)_m$ diblok kopolimeri elde edilmiştir. AB tipli kopolimer de yine makrobaşlatıcı olarak kullanılarak SBMA monomerinin ATRP reaksiyonu gerçekleştirilmiş ve ABC tipli $P(KL)_n$-*b*-$P(PEGMEA)_m$-*b*-$P(SMBA)_k$ triblok kopolimeri elde edilmiştir. PEGMEA-480 makromonomerinin polimerizasyon verimi ^{1}H NMR yöntemi ile hesaplanabilmiştir, ancak triblok kopolimerinin çözünürlük probleminden dolayı ^{1}H NMR'dan yalnızca kopolimerin varlığı ispatlanmış, ancak polimerizasyon verimi hesaplanamamıştır.

Sentezlenmiş olan polimerik yapıların antibakteriyel özellikleri zon inhibisyon metodu ile incelenmiştir. PKL bazlı makrofotobaşlatıcı kullanılarak elde edilen PEGMEA-480

makromonomerinin fotopolimerizasyon ürünü *Staphylococcus aureus* (*S. aureus*) (Gram pozitif) ve *Escherichia coli* (*E. coli)* (Gram negatif) bakterilerine karşı antibakteriyel etki göstermiştir. Aynı şekilde enzimatik ve ATRP yöntemlerinin kombinasyonu ile elde edilen AB tipi $P(KL)_n$-*b*-$P(PEGMEA)_m$ diblok kopolimeri de bu iki bakteriye karşı antibakteriyel özellik göstermiştir. Bunun yanında, yine AB tipli diblok kopolimeri kullanılan ABC tipi $P(KL)_n$-*b*-$P(PEGMEA)_m$-*b*-$P(SMBA)_k$ triblok kopolimerinin yalnızca *S. aureus*'a karşı antibakteriyel etkiye sahip olduğu gözlemlenmiştir. Bu polimerlerin *Aspergillus niger* (*A. niger*) mikroorganizmasına karşı antifungal etkisi gözlemlenememiştir. Elde edilen diğer polimerik yapılarda ise bahsi geçen mikroorganizmalara karşı antibakteriyel ve antifungal nitelik bulunamamıştır. PEGMEA-480 makromonomeri ve PKL içeren amfifilik yapıların antibakteriyel özellik göstermesi, PEGMEA-480 makromonomerinin yoğun bir şekilde tekrarlanan üniteler halinde polimerik yapıların içerisinde yer alabilmesinden kaynaklanmaktadır. Kullanılan polimerizasyon yöntemleri ve antibakteriyel testler, enzimatik halka açılım polimerizasyonunun ATRP veya ultraviyole polimerizasyonu yöntemleri ile kombinasyonları ile antibakteriyel polimerlerin sentezlenebildiğini göstermektedir. Bu, polimerlerin antibakteriyel özellik isteyen biyomedikal uygulamalarda (yara örtüsü, kateter) ve denizcilik uygulamalarında (boya hammaddesi) kullanılabilir olduğunu göstermektedir. İleride yapılacak yeni çalışmalarda bu bulgular yol gösterici olacaktır.

1. INTRODUCTION

1.1 Purpose and Scope of Thesis

In this study, it was purposed to obtain polycaprolactone (PCL) based amphiphilic polymers performing antibacterial properties for their usage in bioapplications. The enzymatic polymerization was employed for the synthesis of PCL unlikely the conventional methods for its usage in biomedical applications. The main and side reactions during the enzymatic ring opening polymerizaiton of methacrylate initiated caprolactone (CL) synthesis were scrutinized. Followingly, chiefly PEG and SBMA based acrylates and methacrylates were installed onto the PCL backbone either via photopolymerization strategies or controlled radical polymerization approach. Antibacterial properties of the selected synthesized materials were investigated to decide which polymers were suitable for antibacterial end-uses.

1.2 Literature Overview

1.2.1 Biopolymers

No matter most of the commercially available synthetic polymers are based on fossil fuels and manufactured by synthetic routes, polymers based on renewable sources were in the market long before. Indeed, until 1850, all of the commodity products were supplied from plants which means the main source was the wood. However, a transition to oil-driven economical model in the late 18th century affected the polymer industry, opening novel polymers and synthetic technologies (Ulber, 2011, Chapter 8).

In recent years environmental friendly polymers based on renewable resources has been gaining great interest again. As their physical and chemical properties enhanced and achieving comparable prices with the petroleum based polymers, they have already been replaced in some applications, especially in the packaging and coating industry (Endres, 2011). There are many driving forces accelerating this transition in favour of biopolymers: (1) Decaying fossil fuel stock; (2) volatility of the prices in fossil fuel market; (3) global climate change issues pointing greennhouse gas

emissions; (4) consideration of inequity in political terms; (5) additional waste utilization requirement in fuel-based synthetic polymers (Niaounakis, 2013). Another advantages of this "green" technology are (6) safer production standarts; (7) drammatically reduced auxiliary materials such as solvents, blocking groups etc.; (8) decreased maintenance costs in facilities owing to lower energy consumption and absence of auxiliary substances; (9) increased effectiveness in recycling due to inherenlty thermoplastic and biodegradable nature of the polymers. Considering the above issues, an acceleration in demand for "green" polymers in the 21st century wouldn't be unrealistic any longer as many environmental legislations and regulations became valid or planned (Mülhaupt, 2013).

A certain description of the terms degradable, biodegradable, bio-based, compostable, and biopolymers was not yet precisely decided in the literature and patents, since these concepts often include common features and interpenetrating.

Degradability, is a term embracing polymers or plastics being disintegrated by various mechanisms such as physical decomposition, chemical degradation, and biodegradation via biological routes. Therefore, accoridng to this definition, degradability term comprises biodegradability.

Biodegradable property is evaluated as a capability of degradation of a material under the exposure of microorganisms such as molds, fungi, and bacteria in a certain period and environment. Polymers decomposing into carbon dioxide, methane, water, inorganic compounds, or biomass led by the mechanism of enzymatic processes of microorganisms that can be measured by standart tests, over a specific period of time, exhibiting acquirable disposal states referred as "biodegradable" with reference to ASTM D5488-84de1. The following international standards are:

Biodegradable polymers are also authorized by the international standards; ISO 17088:2012; EN 13432:2000; EN 14995:2006; ASTM D6400-12.

Apart from "degradable" and "biodegradable" concepts, biobased term is considered in the perspective of raw materials obtained from renewable resources. Raw materials are entitled as renewable if they can be built up via natural routes faster than thie consumption rate.

In order to make a description of "biodegradable" and "biopolymer/bioplastic" features, two main criterias are taken into account as the raw material source and

degradation medium of the polymer. So, classification of biopolymers might be defined as:

(A) Biopolymers which are obtained from renewable resources (biobased) and biodegradable; (B) biopolymers which are obtained from renewable resources (biobased) but not biodegradable; (C) biopolymers attained from fossil fuels (not biobased) and biodegradable. (Niaounakis, 2015, Chapter 1). Biopolymers classified in this context were represented n Table 1.1.

Table 1.1 : Biodegradable versus biobased polymers (Niaounakis, 2015, Chapter 1).

Origin	Biodegradable	Nonbiodegradable
Bio-based	CA, CAB, CAP, CN, P3HB, PHBHV, PLA, starch, chitosan	PE (LDPE), PA-11, PA-12, PET, PTT
Partially bio-based	PBS, PBAT, PLA blends, starch blends	PBT, PET, PTT, PVC, SBR, ABS, PU, epoxy resin
Fossil fuel-based	PBS, PBSA, PBSL, PBST, PCL, PGA, PTMAT, PVOH	PE (LDPE, HDPE), PP, PS, PVC, ABS, PBT, PET, PS, PA-6, PA-66, PU, epoxy resin, synthetic rubber

ABS, acrylonitrile-butadiene-styrene; CA, cellulose acetate; CAB, cellulose acetate butyrate; CAP, cellulose acetate propionate; CN, cellulose nitrate; HDPE, high density polyethylene; LDPE, low density polyethylene; PA-6, polyamide 6; PA-66, polyamide 6,6; PA-11, aminoundecanoic acid-derived polyamide; PA-12, laurolactam-derived polyamide; PBAT, poly(butylene adipate-co-terephthalate); PBS, poly(butylene succinate); PBSA, poly(butylene succinate-co-adipate); PBSL, poly(butylene succinate-co-lactide); PBST, poly(butylene succinate-co-terephthalate); PBT, poly(butylene terephthalate); PCL, poly(ε-Caprolactone); PE, polyethylene; PET, poly(ethylene terephthalate); PGA, poly(glycolic acid), polyglycolide; P3HB, poly(3-hydroxybutyrate); PHBHV, poly(3-hydroxybutyrate-co-3-hydroxyvalerate); PLA, poly(lactic acid), polylactide; PP, polypropylene; PS, polystyrene; PTMAT, poly(methylene adipate-co-terephthalate); PTT, poly(trimethylene terephthalte); PVOH, poly(vinyl alcohol); PVC, poly(vinyl chloride); PU, polyurethane; SBR, styrene-butadiene rubber.

There are many commercial biobased and/or biodegradable polymers in the market such as Polylactic acid (PLA), epoxies, cellulose derivatives, polycaprolactone (PCL), biobased polyethyleneterephthalate (PET), biobased polybutyleneterephthalate (PBT), poly(trimethylene terephthalate) (PTT), polyethylenefuranoate (PEF), polyhydroxyalkanoate derivatives (PHA), poly(butylene adipate-co-terephthalate) (PBAT), polybutylenesuccinate derivatives (PBS), ligno-cellulosics, chitin, chitosan, poly(esther-amide)s, poly(ether-amide)s, biobased polyurethane family, biobased polyethylene (PE), biobased polypropylene (PP), butadiene polymers, natural rubber, vegetable oil-based coatings, starch-based thermoplastics, polymers from corn and soy proteins, poly(α-amino acid)s (Álvarez-Chávez et al, 2012). In Table 1.2, it can also be seen the main distinguish of biopolymers regarding the different types of biobased organisms, fossil based and biodegradability. However, it should be noted that some of these biopolymers such as polylactide (PLA), pol(butylene succinate) (PBS),

pol(trimethylene terephthalate) (PTT), etc. can be obtained both from biobased and fossil based pathways.

Table 1.2 : Classification of Biopolymers (Niaounakis, 2015, Chapter 1).

Biodegradable				Nonbiodegradable
Bio-Based			Fossil-Based	Bio-Based
Plants	Microorganisms	Animals		
Cellulose and its derivatives[1] (polysaccharide)	PHAs (e.g., P3HB, P4HB, PHBHV, P3HBHH$_x$)	Chitin (polysaccharide)	Poly(alkylene dicarboxylate)s (e.g., PBA, PBS, PBSA, PBSE, PEA, PEA, PES, PESE, PESA, PPF, PPS, PTA, PTMS, PTSE, PTT)	PE (LDPE, HDPE), PP, PVC
Lignin	PHF	Chitosan (polysaccharide)	PGA	PET, PPT
Starch and its derivatives (monosaccharide)	Bacterial cellulose	Hyaluronan (polysaccharide)	PCL	PU
Alginate (polysaccharide)	Hyaluronan (polysaccharide)	Casein (protein)	PVOH	PC
Lipids (triglycerides)	Xanthan (polysaccharide)	Whey (protein)	POE	Poly(ether-ester)s
Wheat, corn, pea, potato, soy, potato (protein)	Curdlan (polysaccharide)	Collagen (protein)	Polyanhydrides	Polyamides (PA-11, PA-410, PA-610, PA-1010, PA-1012)
Gums (e.g. *cis*-1, 4-polyisoprene)	Pullulan (polysaccharide)	Albumin (protein)	PPHOS	Polyester amides
Carrageenan	Silk (protein)	Keratin, PFF (protein)		Unsaturated polyesters
PLA (from strach or sugar cane)		Leather (protein)		Epoxy
				Phenolic resins

HDPE, high density polyethylene; LDPE, low density polyethylene; P3HB, poly(3-hydroxybutyrate); P3HBHH$_x$, poly(3-hydroxybutyrate-co-3-hydroxyhexanoate); P4HB, poly(4-hydroxybutyrate); PBA, poly(butylene adipate), PBS, poly(butylene succinate); PBSA, poly(butylene succinate-co-adipate); PBSE, poly(butylene sebacate); PC, polycarbonate; PCL, poly(ε-Caprolactone); PE, polyethylene; PEA, poly(ethylene adipate); PES, poly(ethylene succinate); PESA, poly(ethylene succinate-co-adipate); PESE, poly(ethylene sebacate); PET, poly(ethylene terephthalate); PFF, poultry feather fiber; PGA, poly(glycolic acid), polyglycolide; PHA, poly(hydroxy alkanoate); PHBHV, poly(3-hydroxybutyrate-co-3-hydroxyvalerate); PHF, polyhydroxy fatty acid; PHH, poly(hydroxy hexanoate); PLA, poly(lactic acid), polylactide; POE poly(ortho ester); PP, polypropylene; PPF, poly(propylene fumarate); PPHOS, polyphosphazenes; PPS, poly(propylene succinate); PTA, poly(tetramethylene adipate); PTMS, poly(tetramethylene succinate); PTSE, poly(tetramethylene sebacate); PTT, poly(trimethylene terephthalte); PVC, poly(vinyl chloride); PVOH, poly(vinyl alcohol); PU, polyurethane.
[1]*Acetyl cellulose might be biodegradable or nonbiodegradable. This case depends on the acetylation degree. Low acetylation degree provide biodegradability. However, highly substituted materials are nonbiodegradable.*

Biopolymers can also be classified in terms of their thermoprocessabilities as thermoplastics, thermosets and elastomers. Another way to categorize biopolymers is considering their composition as blends, composites, or laminates. A commercial product including biopolymers is Ecovio ® (BASF AG), a blend of PLA and PBAT (Ecoflex ®, BASF AG). Biocomposites is a group of materials based on biopolymers and/or synthetic polymers reinforced with natural fibers, such as sisal, flax, hemp, jute,

banana, wood, and various grasses, and/or fillers and additives (Niaounakis, 2015, Chapter 1).

Table 1.3 : Biopolyesters manufactured and commercially available globally. [a]Biosourcing (%): The percentage of carbon originating from biomass sources among the total organic carbon (Jiang and Loos, 2016).

Biobased polyester	Biosourcing (%) [a]	Manufacturer	Trademark
PLA	up to 100	Natureworks (Minnetonka, MS, USA)	Ingeo™, NatureWorks®
		Synbra (Etten-Leur, The Netherlands)	BioFoam®
		Zheijang Hisun Biomaterials Biological Engineering (Taizhou, Zheijang, China)	REVODE 100 and 200 Series
		Nantong Jiuding Biological Engineering (RugaO, Jiangsu, China)	-
		Teijin (Chiyoda, Tokyo, Japan), Mitsui Chemicals (Minato, Tokyo, Japan)	BIOFRONT™
		Mitsui Chemicals (Minato, Tokyo, Japan)	LACEA®
		Futerro (Celles, Belgium)	Futerro®
		Corbion Purac (Amsterdam, The Netherlands)	LX175, L175, L130, L105, D070
PHAs	100	Metabolix (Cambridge, MA, USA) and ADM (Decateur, IL, USA)	Mirel™
		MHG (Bainbridge, GA, USA)	Nodax™
		Bio-on (San Giorgio di Piano, Bologna, Italy)	MINERV-PHA™
		Tianjin Green Biosciences (Tianjin, China)	GreenBİo
		Kaneka (Tokyo, Japan)	Kaneka PHBH
		Tianan Biological Materials (Ningbo, Zheijang, China)	ENMAT™
		PHB Industrial S/A (Serrana, Brazil)	BIOCYCLE®
PBS	50	PTT MCC Biochem (Chatuchak, Bangkok, Thailand)	BioPBS™
		Showa DEnko K.K. (Tokyo, Japan)	Bionolle™
		Mitsubishi Chemical (Chiyoda-ku, Tokyo, Japan)	GS Pla®
PEF	100	Avantium (Geleen, The Netherlands)	-
PET	up to 30	Coca Cola (Atlanta, GA, USA)	PlantBottle™
PTT	37	DuPont (Wilmington, DE, USA)	Sorona®
	up to 35		Biomax®
PBAT	30-70	Novamont (Novara, Italy)	Origo-Bi™
		BASF (Ludwigshafen, Germany)	Ecoflex® FS
Co-polyester	9-30	SK Chemicals (Seongnam-si, Gyeonggi-do, Korea)	ECOZEN®
Co-polyester	-	DuPont (Wilmignton, DE, USA)	Biomax®

Recently, various biopolyesters are commercially available. In 2013, the biobased polymer capacity worldwide does not exceed 2 % of the total polymer production in 2013, which is projected to be 4% in 2020 (Table 1.1) (Jiang and Loos, 2016).

1.2.2 Enzymatic polymerization

In living cells, there is a wide range of enzymes catalyzing metabolic pathways. Polysaccharides, proteins, polyesters, nucleic acids (DNA, RNA), polyaromatics, natural rubber are synthesized by enzymes in nature (Albertsson and Srivastava, 2008; Kobayashi, 2011). For example, more than 10^{12} tons of biomaterials such as cellulose and starch are produced per year via natural pathways which is four-fve times more than the amount of polymers manufactured from petroleum feedstock (Albertsson and Srivastava, 2008).

The enzymes are categorized by the Enzyme Commission in six main groups according to their reactions (Table 1.4) (Kobayashi, 2011; Pugh et al, 2015). On the other hand, three enzyme groups were so far applied for enzymatic polymerization (Kobayashi, 2011).

Enzymatic polymerization is a synthetic in-vitro polymerization technique when an isolated enzyme is used as a catalyst. There are studies in the literature investigating

Table 1.4 : Enzyme classification (Kobayashi, 2011).

Enzymes	Example enzymes	Synthesized polymers
1. Oxidoreductases	Peroxidase, laccase, tyrosinase, glucose oxidase	Polyphenols, polyanilines, vinyl polymers
2. Transferases	Phosphorylase glycosyltransferase, acyltransferase	Polysaccharides, cyclic oligosaccharides, polyesters
3. Hydrolases	Glycosidase (cellulase, amylase, chitinase, hyaluronidase), lipase, peptidase, protease	Polysaccharides, polyesters, polycarbonates, polyamides, polyphosphates, polythioesters
4. Lyases	Decarboxylase, aldolase, dehydratase	
5. Isomerases	Racemase, epimerase, isomerase	
6. Ligases	Ligase, synthase, acyl CoA synthetase	

enzymatically synthesis natural polysaccharides such as cellulose, amylose, xylan and chitin (Albertsson and Srivastava, 2008; Gijsen et al, 1996; Kobayashi et al, 1991; Salmon and Hudson, 1997). Moreover, enzymatic polymerization technique brought a new synthetic way to obtain some useful polymers which might be harder to synthesize. Aliphatic polyesters, polycarbonates, polyphosphates, even polyaromatics and vinyl polymers are examples of biodegradable polymers that were synthesized via enzymatic route. These polymers were implied in biomedical applications such as orthopedic devices, tissue engineering, adhesion barriers, and controlled drug delivery vehicles (Albertsson and Srivastava, 2008). One of the main reasons of preferring enzymatic polymerization is the residues of organometallic catalysts such as Zn, Al, Sn, Sb, Ti, Bi, Ge in the polymers in the case of commercial ring opening polymerization (ROP) of various lactones and condensation polymerization, since these metallic catalysts are intrinsically toxic (Albertsson and Srivastava, 2008; Chatti et al, 2006; Kricheldorf, 2009).

In addition to this, enzymatic polymerization has more prevailing features as compared with organic synthesis such as higher catalytic activity, milder reaction conditions (i.e.

temperature, pressure and pH etc.), better enantioselectivity, chemoselectivity and regioselectivity, lesser by-product formation. Provided complex formation, enzymatic polymerization brings more precise structural control, yet not requiring protection/deprotection strategies. Thus, there is little or no side products. On the other hand, the compatibility of the substrates with the enzymes limits the variation of enzyme-monomer combinations. It should also be noted that the enzymes generally might not be cost-effective (Kobayashi et al, 2001b; Pugh et al, 2015).

Enzymes can also be used in bulk, organic solvents and at numerous interfaces. Enzymes are supplied from renewable feedstocks, easy to be recovered from the polymer and resusable (Yang et al, 2011). It should also be noted that water roles as an initiator in eROP, thereby eliminating the laborous water removal procedures in organic synthesis (Albertsson and Srivastava, 2008). Although, in case another nucleophilic initiator would be chosen rather than water, removal of water becomes crucial (Xiao et al, 2009). Consequently, enzymatic polymerization is evaluated as an environmental friendly synthesis method (Puskas et al, 2009; Yang et al, 2011).

1.2.3 Hydrolases

Hydrolases are by far the mostly preferred enzyme class, approximately 75 % of the industrially utilized enzymes perform hydrolytic characteristic. Proteases and carbohydrases possess almost 40 % of the global enzyme sales, however lipases still are the most preferred class employed in organic chemistry (de Regil and Sandoval, 2013).

1.2.3.1 Lipases

1.2.3.2 Definition of Lipases

Lipases belong to the serine hydrolase family referred as triacylglycerol acylhydrolases (E.C. 3.1.1.3) which are distinguishable from esterases (E.C. 3.1.1.1) regarding the fact of their substrates. The first approach to differentiate lipases and esterases, i.e., activation in presence of an interface called “interfacial activation”, was inappropriate since this phenomenon is not applicable to some lipases. Some well-known examples of this case are Lip4 from Candida rugosa and Candida antarctica B (Casas-Godoy et al, 2002, Chapter 1; Tang et al, 2001; Uppenberg et al, 1994). Hence, accordingly the lipases were described as enzymes which are able to hydrolyzing the

carboxyl esters of acylglycerols possessing more than or equal to 10 carbon atoms, as esterases hydrolyzing the carboxyl esters of acylglycerol having less than or equal to 10 carbon atoms. On the other hand, since both lipases and esterases performs a wide range of substrate specifity, both of these phenomena might be considered (Casas-Godoy et al, 2002, Chapter 1; Chainian et al, 2002; Verger, 1997). Another perspective on the differentiation of lipases and esterases is considering the amino acid composition and the electrostatic distribution on protein surface (Casas-Godoy, 2012, Chapter 1; Fojan et al, 2000). Cutinases are able to eventuate the hydrolysis of ester bonds in cutine polymers. On the other hand, they can also hydrolyze both long and short chain triglycerides whether there is an interfacial activation or not. Therefore they are regarded as an intermediate class between lipases and esterases (Casas-Godoy, 2012, Chapter 1).

1.2.3.3 Lipase catalyzed reactions

Lipases intrinsically catalyze the hydrolysis the ester bonds on triglycerides, diglycerides and monogylcerides (Figure 1.1) (Casas-Godoy et al, 2012, Chapter 1).

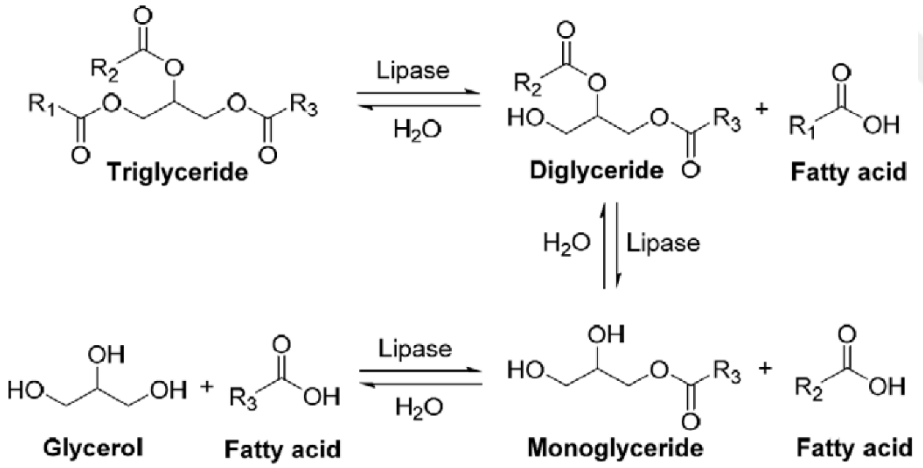

Figure 1.1 : Hydrolysis of triglyceride via lipase (Jiang and Loos, 2016).

Mostly, these reactions are performed at the interface of a biphasic medium due to the immiscibility of a hydrophobic organic phase and water. Transesterification and esterification reactions are also catalyzed by lipases. Throughout an esterification reaction, a fatty acid is bound to an alcohol, resulting an ester bond and delivering a water molecule. Thioester and amide bond formations are analogous to esterification reactions, where thiol and amine molecules are employed as substrates respectively. Acidolysis, aminolysis, alcoholysis and interesterification reactions are the

transesterification reactions that lipases are able to catalyze (Figure 1.2) (Casas-Godoy et al, 2012, Chapter 1).

Lipases can be extracted from animal or plant tissue, or by cultivation of microorganisms. Although, the lipases obtained from the animals are hardly pure in order to be used in food industry. The impurities might include animal viruses, hormones and trypsine which cause a bitter taste. Therefore, most of the commercially available lipases are obtained from microorganisms due to more robust production procedures and abundance (Casas-Godoy et al, 2012, Chapter 1; Schmid and Verger, 1998; Vakhlu and Kour, 2006).

The first isolated lipases were from Bacillus prodigiosus, Bacillus pyocyaneus, and Bacillus fluorescens, recently called as Serratia marcescens, Pseudomonas aeruginosa, and Pseudomonas fluorescens, respectively (Casas-Godoy et al, 2012, Chapter 1).

Developments in genetic engineering methods provided more lipases commercially produced from recombinant bacteria and yeasts. For instance, a lipase used in detergent industry, is commercially manufactured in large scale via fermentation of Aspergillus Oryzae of which the gene coding was modified with the one of the fungus Humicula lanuginosa. and are able to execute to hydrolyzation of triglycerides (or esters) at water-oil interface. This process is purposed for the degradation of food and fats. Besides, they are also employed as drugs against digestive disorders and diseases of pancreas, additive in detergent formulations to remove fat stains and as catalysts for the production of specialty chemicals. Lipase is one of the most multi-purposed biocatalyst category in organic synthesis owing to its capability of hosting a vast range of synthetic substrates still preserving regioselectivity and chiral recognition (Schmid and Verger, 1998).

1.2.3.4 Structure of the lipases

In the literature, researches on the structure and flexibility of lipases in various organic solvents can be found (Trodler and Pleiss, 2008). To enhance the flexibility, thus the activity, of the lipases, several researches including mutagenesis were studied (Hong, 2013). To reveal the activity and thermal stability of *Candida antarctica lipase B* (CALB), one of the most preferred lipases, numerous researches were performed (Li et al, 2010). Immobilization onto various substrates such as acrylic resin (Novozym ® 435, commercially available product of Novozymes) and zeolites are mostly employed

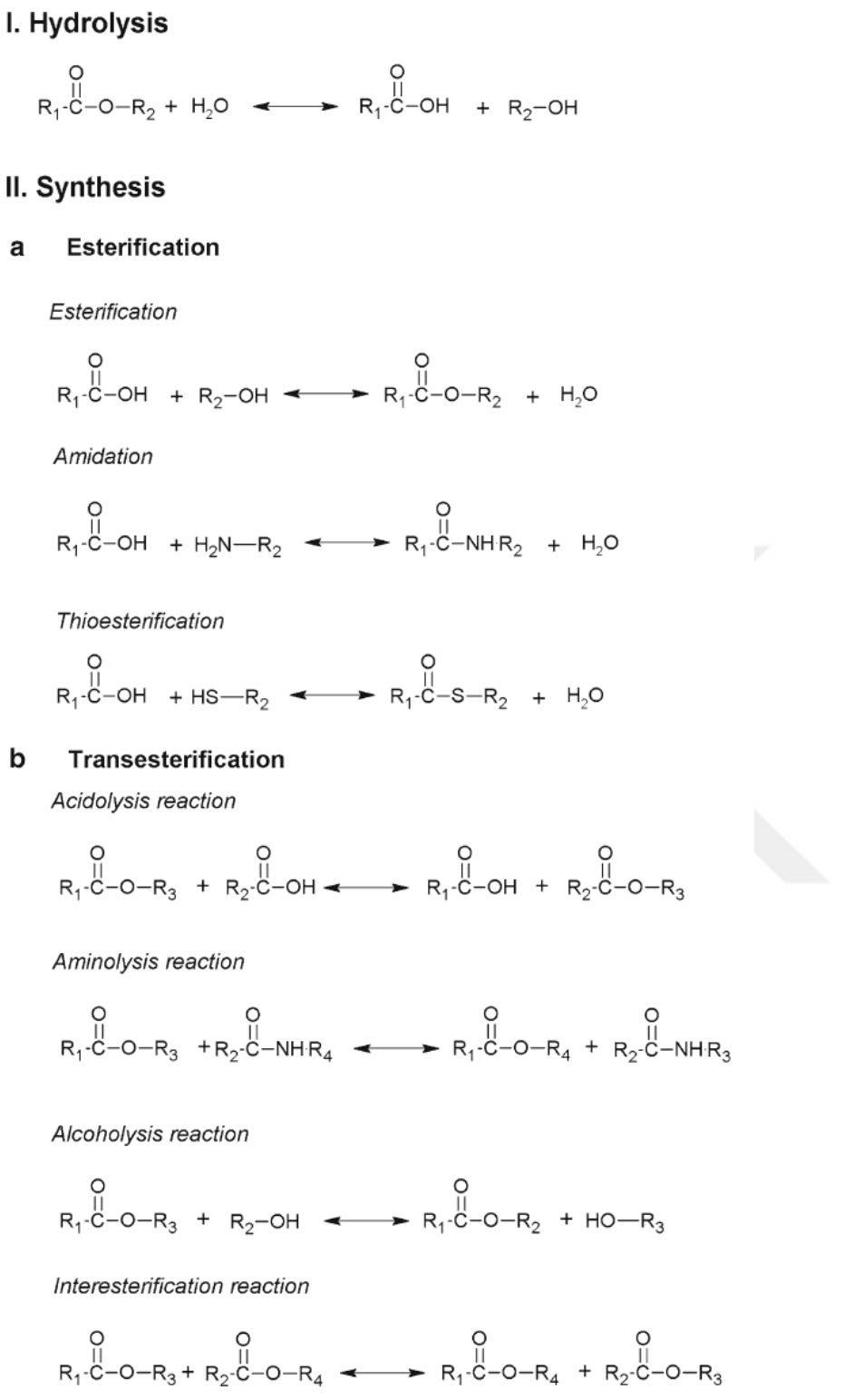

Figure 1.2 : Lipase catalyzed reactions (Casas-Godoy et al, 2012, Chapter 1).

substrates for increasing the thermal stability of CALB as well as mutagenesis (Carlsson et al, 2014; Costa et al, 2009; Öztürk-Düşkünkorur et al, 2014; Poojari and Clarson, 2013).

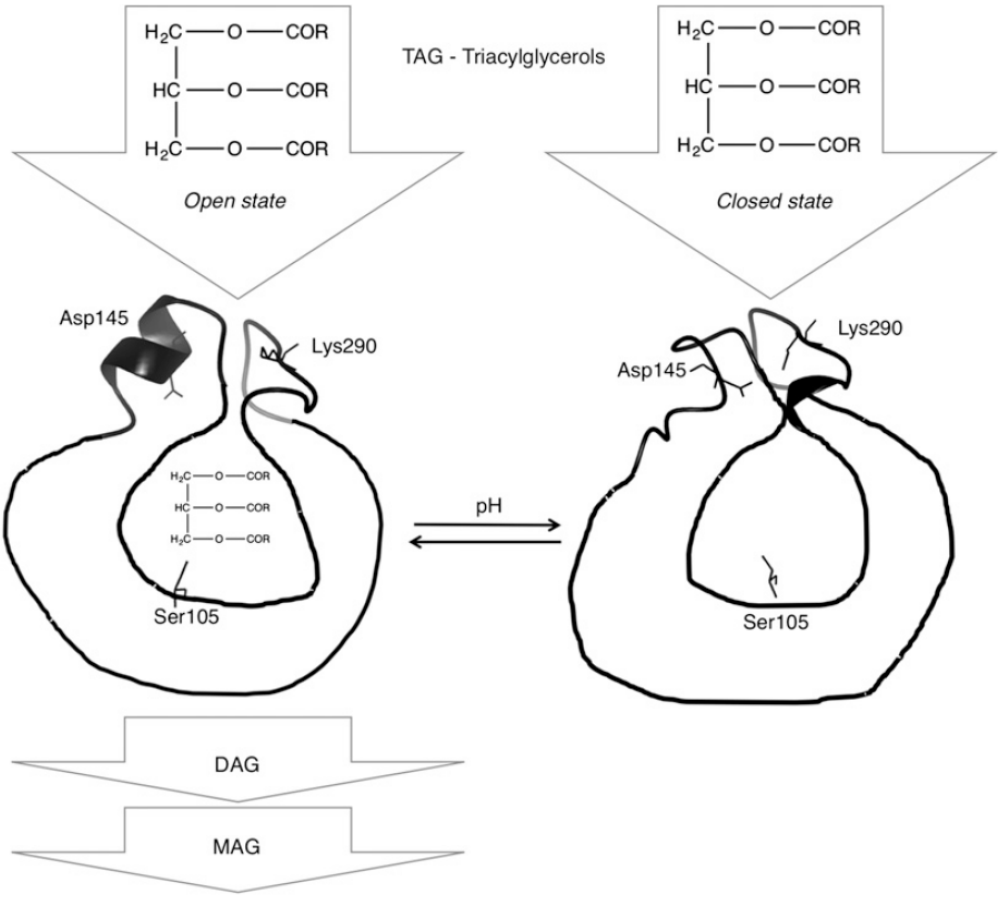

Figure 1.3 : Representation of the open and closed conformations of CALB. Hydrolysis of triacylglycerol molecule (TAG) to diacylglycerol (DAG) and monoacylglycerol (MAG) when CALB is present in open conformation (Stauch et al, 2015).

The typical structure and functional resemblance of lipases are independent from the difference in molecular masses and from which organism they have been isolated. In most lipases, a lid or flap mechanism composed of an amphiphilic α-helix peptide sequence resides. When the lid is in its closed conformation, the substrate is not allowed to reach the catalytic site (i.e., in the absence of an interphase or organic solvent). But, when the lid is opened, hydrophobic substrate, for instance oil drop, can achieve a large hydrophobic surface (Figure 1.3) (Albertsson and Srivastava, 2008; Schmid and Verger, 1998).

The entire lipases belong to "α/β-hydrolase fold" family having the same architecture consisting of specific sequence of α-helices and β-strands. α-helices surround the core composed of parallel β-strands. The active nucleophilic serine site resides in a hairpin turn between β-strand and α-helix (Albertsson and Srivastava, 2008; Schmid and Verger, 1998). α-helix is connected to the middle of a β-sheet array with a sharp turn,

referred to as the nucleophilic elbow. Lipases particularly hold the same catalytic triad composed of either an aspartate (Asp) or a glutamate (Glu) residue (acidic part), a histidine (His) (as base) and a nucleophilic serine (Ser) (Figure 1.4) (Nardini and Dijkstra, 1999; Veld and Palmans, 2010).

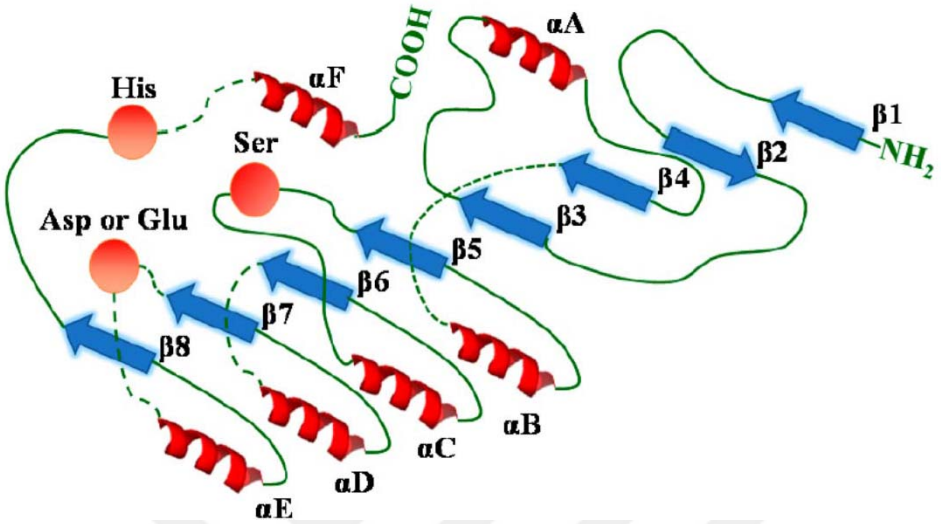

Figure 1.4 : Secondary structure of lipases demonstrating α/β hydrolase fold and catalytic triad; α-helixes are shown as helixes and β-sheets are referred as arrows (Jaeger et al, 1999; Jiang and Loos, 2016).

is located at one side of the Ser, while the oxyanion hole contributes to the stabilization of the opposite side of the Ser residue with a hydrogen bonds. CALB can be used as a reference to explain the catalytic mechanism of α/β-hydrolase class due to its vastly implication in enzymatic polymerizaton reactions (Veld and Palmans, 2010). In 1990, two lipase structures were revealed with X-Ray crystallography (Human pancreatic lipase and Mucor miehei triglyceride lipase). The three-dimensional structure proposed a mechanism in which the interfacial activation is caused by amphiphilic peptidic loop covering the active site of the enzyme in solution. Similar to a dynamic lid/flap shift analogy, the lid is conformationally rearranged leading the active site be accessible to the substrate (Figure 1.5) (Brady et al, 1990; Brzozowski et al, 1991; Schmid and Verger, 1998; Winkler et al, 1990). Recently, several hundreds of lipase sequences and three-dimensional lipase structures can be found in the Protein Data Base (Url-1).

The catalytic triad of CALB is assembled by Asp187, His224, and Ser105 (Figure 1.6), additionally oxyanion hole is formed by the backbone amide protons of Thr40 (Threonine), Gln106 (Glutamine) and side chain of Thr40. The mechanism starts with

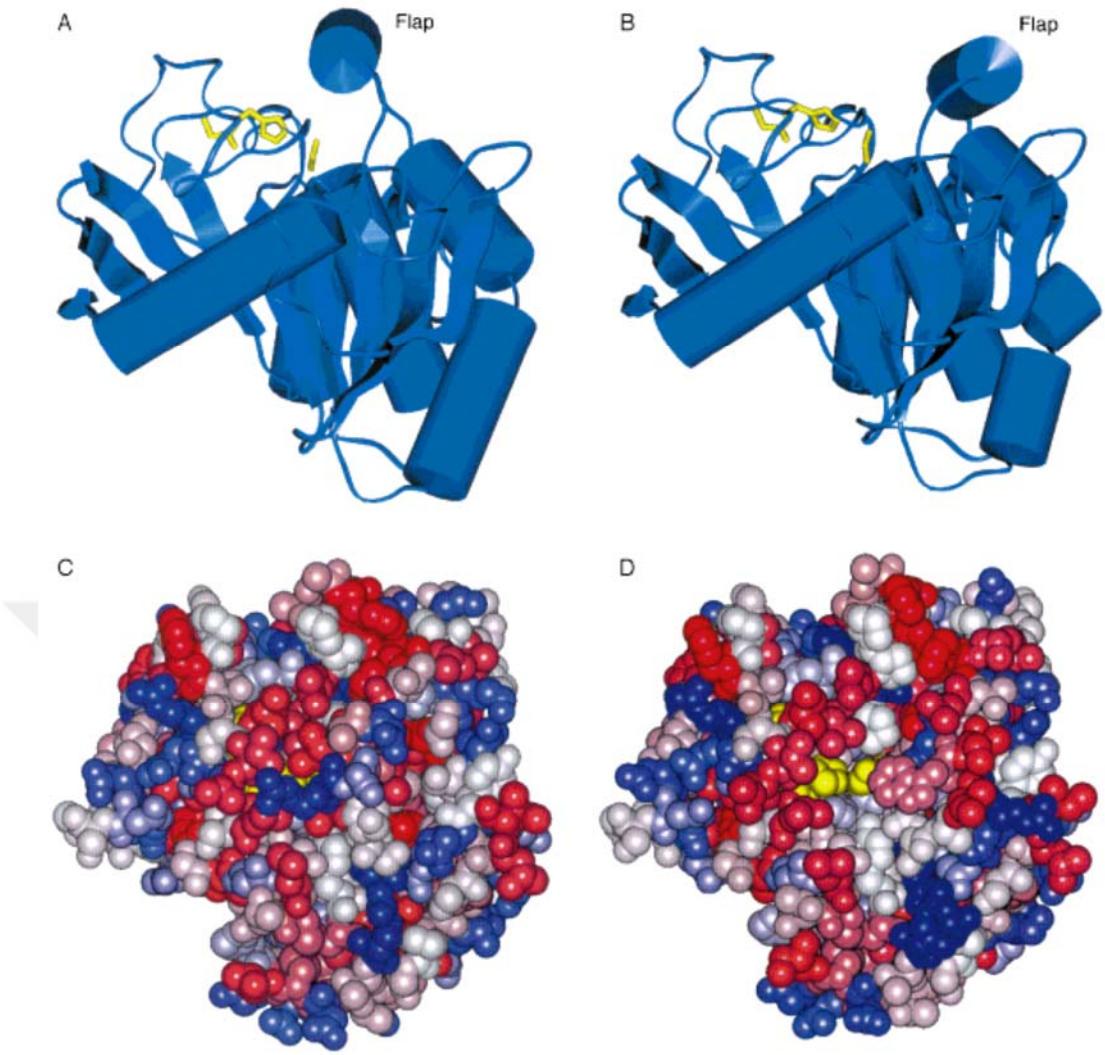

Figure 1.5 : Closed (A, C) and open (B, D) forms of Mucor miehei lipase. A and B (side view): the catalytic triad (yellow) and secondary structure elements demonstrating the α/β-hydrolase fold common in all lipases. C and D (top view): space-filling model, the color decreases with reducing polarity (dark blue - light blue - white - light red - dark red). When the lid opens, the catalytic triad (yellow) becomes accessible (D), and it is noticeable the region binding to the interphase transforms into a more apolar character (Schmid and Verger, 1998).

a reversible complex between the substrate and the free enzyme, called Michaelis-Menten complex. Along with the suitable settlement of the substrate, Ser105 residue nucleophilically attacks onto the carbonyl group of the substrate forming the first tetrahedral intermediate. The negative charge occuring on the former substrate oxygen,

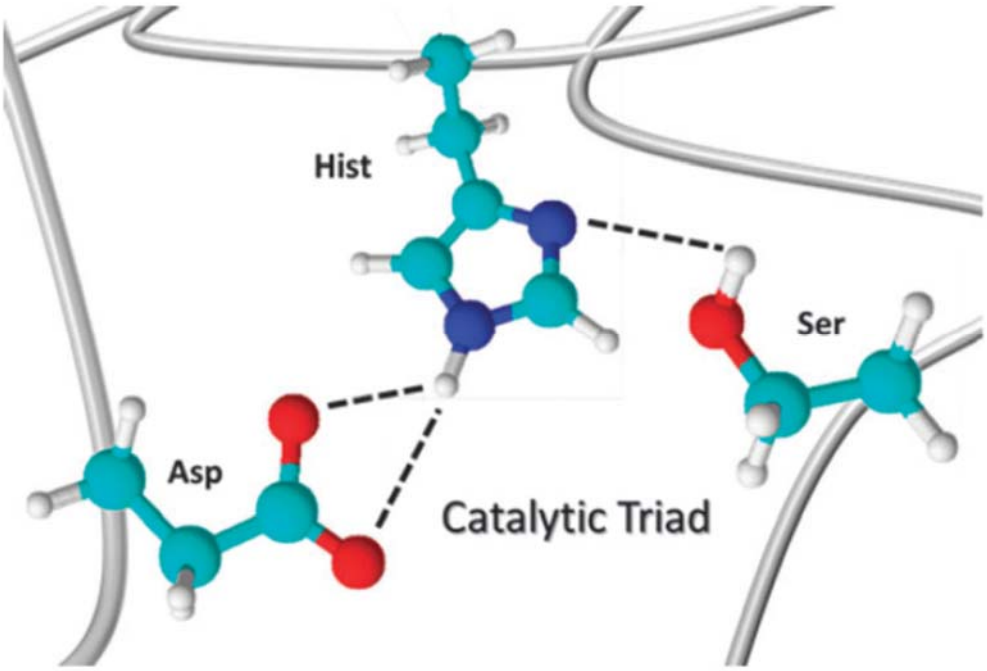

Figure 1.6 : Demonstration of a lipase catalytic triad in a lipase with Asp (acidic), His (basic) and Ser (Nucleophilic) parts (Coulembier et al, 2012).

which presents in the tetrahedral intermediate, is stabilized by threefold hydrogen bonding interactions with the oxyanion hole. In the mean time, the positive charge on His224 is stabilized via an interaciton with Asp187. Afterwads, substrate alkyl oxygen takes a proton from His224, and enzyme releases the alcohol part of the substrate. In the end of this acylation step, and a covalently bound acyl-enzyme complex occurs. If a monomer is used as the substrate, this complex is regarded as the enzyme-activated monomer complex. The next step is the deacylation of acyl-enzyme complex where a nucleophile, such as water, alcohol or amine, attacks on the carbonyl group of the complex. His224 takes the proton from the nucleophile as Asp187 and the oxyanion hole stabilized the positive and negative charges. Subsequently, alkyl oxygen of Ser105 transfers the proton from His224 allowing the reoccurence of the carbonyl group of the substrate. Consequently, an enzyme-product complex appears which is weakly bound to each other. After the reaction product is delivered, the free enzyme is regenerated (Figure 1.7) (Veld and Palmans, 2010).

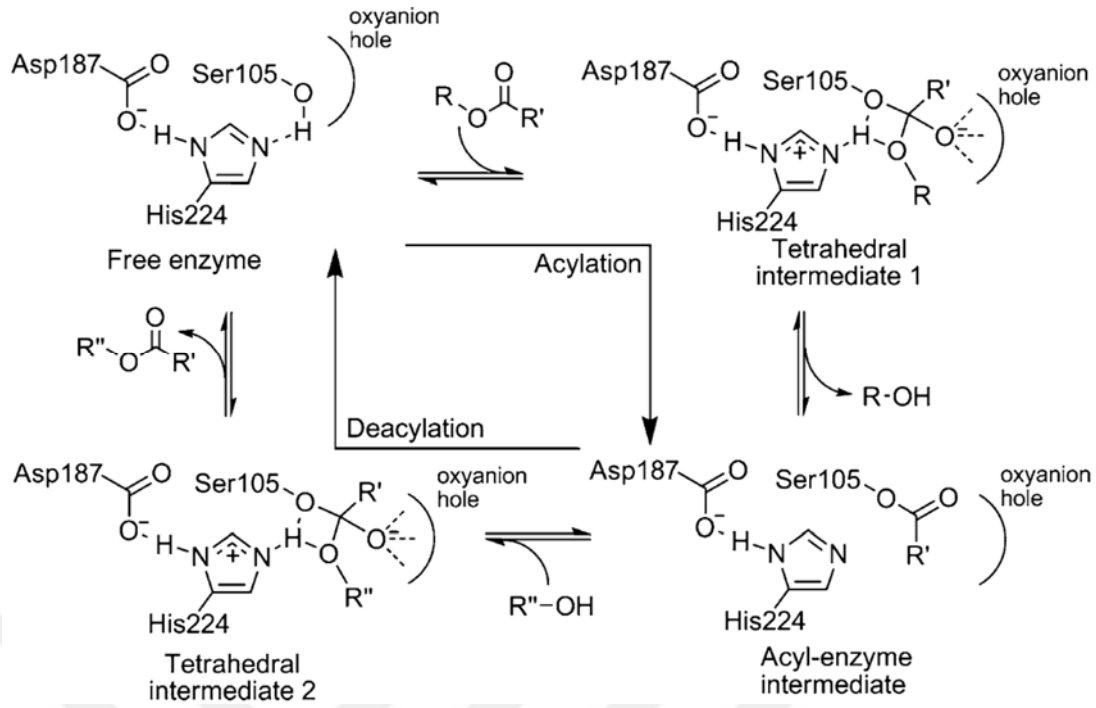

Figure 1.7 : Catalytic mechanism of CALB showing an acylation and deacylation steps (Veld and Palmans, 2010).

CALB is a globular polypeptide chain comprising 317 aminoacids, with a molecular weight of 33 kDa. Despite CALB is known to have the common unique structure of the lipases, there is not an overall consensus of the approaches about the lid structure and interfacial activation. In some reports, it was reported that the most elastic part of the CALB, α5 and α10 helixes might role as the lid, and CALB is activated interfacially which was supported with molecular dynamics simulation (Jiang and Loos, 2016; Skjøt et al, 2009; Zisis et al, 2015). Moreover, this interfacial activation of CALB is established by the hydrophobicity of the interface and the size of the substrate. In contrast, there is another proposition that is not in agreement with the concept of the lid screening the access to the active site, and neither the interfacial activation. But, alternatively, the high selectivity of the CALB was explained with the confined accessable space in the chamber preserving the active site (Jiang and Loos, 2016; Martinelle et al, 1995; Uppenberg et al, 1994). It should also be mentioned that the presence of interfacial activation might change according to the substrate and solvent utilized.

1.2.3.5 Increased stability of the lipases

In the last thirty years, there has been many studies revealed the parameters affecting the structure and function of the enzymes. Molecular dynamics simulations supplied

facilitative experimental findings and enlightened the inhibitory effects of organic solvents, e.g. inflexibility of enzyme conformations, dispossession of the essential water content from the protein structure, leakage of the solvent into the active site causing damage in the protein structure. Numerous investigations for the stability of the enzymes in organic solvents including the addition of stabilizing agents and protein engineering researches (Stepankova et al, 2013).

Despite enzymes including lipases and proteases performs robust in neat organic solvents, a small number of water molecule still binds to the protein molecule, providing a plasticizing effect for the conformational flexibility which is crucial for a sufficient catalyzing efficiency. However, in case the water portion in an organic solvent is greater than a specific degree, consequently the conformational mobility of the enzyme increases and denaturation occurs inevitably. The majority of the enzymes lose their acvitity exceeding a concentration of water in an organic solvent around 60-70% (v/v). The hydrophilic solvents are well known to cause structural changes due to its ease of penetrational ability. It is also critical that hydrophilic solvents decrease the possibility of confrontation of water molecules with the protein sequence which prevents the required protein-water interface. Opposingly, protein structure is more stabile in hydrophobic solvents, since the structural integrity of the enzyme is preserved favorably. Nevertheless, enzmyes lose their activity in completely anhydrous organic solvents due to the lubricating effect of the water molecules on the enzyme and providing a medium for optimum activity level (Stepankova et al, 2013).

There has been studies in the literature to improve the stability of the enzymes including (i) the extraction of a well-purified enzymes that are able to perform at harsh conditions, (ii) alteration of the structure of the enzyme, (iii) remodeling the solvent (Figure 1.8) (Stepankova et al, 2013).

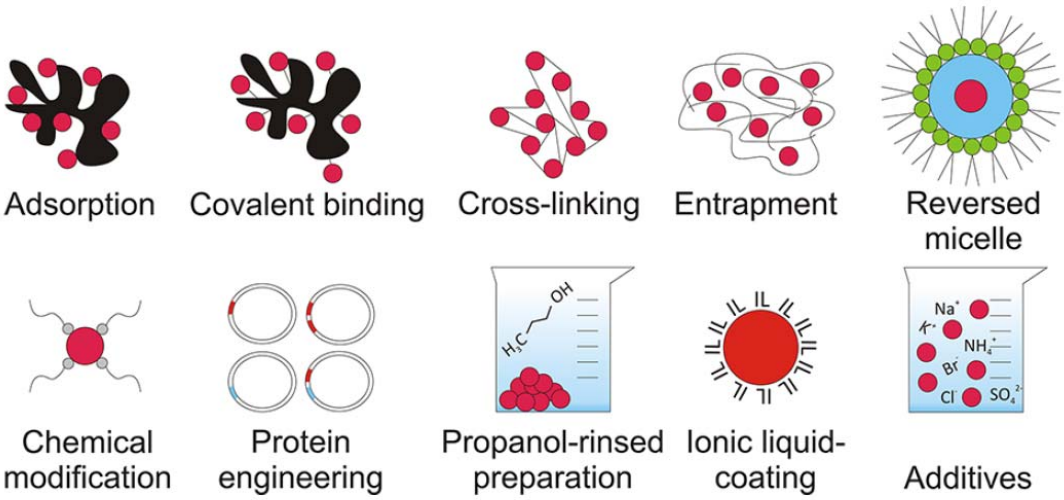

Figure 1.8 : Improvement methods for the stability of the enzymes in organic solvents (Stepankova et al, 2013).

On of the mostly preferred methods to obtain stability is the enzyme immobilization. Immobilization of the lipases are conducted, in order to enhance their endurance in organic solvents, recyclability, reusability, catalytic activity, specificity or selectivity. By preventing the unfolding and keeping the structural integrity of the enzyme, immobilization sustains the efficiency of the active site on the protein sequence. Moreover, immobilization increases the reusability and recyclability of the enzyme reducing the production costs. There are three main methods for immobilizaiton; (i) immobilization onto an inert matrix, (ii) immobilization within an inert matrix, (iii) formation of waterinsoluble particles (Table 1.5) (Stepankova et al, 2013).

Table 1.5 : Immobilization methods of the enzymes (Stepankova et al, 2013).

Immobilization method		Description
immobilization onto an inert matrix	adsorption	formed by an adsorption of an enzyme onto a solid support based on van der Waals, electrostatic, and/or hydrophobic interactions
	covalent binding	formed by chemical bonds between the functional groups of an enzyme and those on the support
immobilization within an inert matrix	entrapment	formed by an incorporation of an enzyme within a gel or polymer
	cross-linked enzyme crystal (CLEC)	formed by covalent bonds between enzyme crystals using a bifunctional agent
formation of waterinsoluble particles	cross-linked enzyme aggregate (CLEA)	formed by precipitation of the enzyme from aqueous buffer followed by covalent bonds between the resulting physical aggregates using a bifunctional agent
	protein-coated microcrystal (PCMC)	formed by dissolving an enzyme in a concentrated solution of a crystalline material followed by coprecipitation by addition of a water-miscible solvent

Among immobilization strategies, physical adsorption is the easiest route to provide the enzmye stability. Numerous commercial enzymes were investigated regarding theie immobilization on various materials. The most widely applied commercially available physically adsorbed enzyme performing efficiently active behavior in neat organic solvents is CALB, adsorbed on macroporous polyacrylate resin, Novozmy® 435 (N435, Novozymes A/S, Copenhagen, Denmark) (Stepankova et al, 2013; Tufvesson et al, 2011). The immobiliztion support is Lewatit® VP OC 1600, a divinylbenzene-crosslinked poly(methyl methacrylate) resin manufactured by Lanxess®. N435 beads have a particle size between 300-800 μm which can be filtered from the reaction mixture (Figure 1.9) (Basso et al, 2013).

Figure 1.9 : N435 beads (Jiang and Loos, 2016).

1.2.4 Enzymatic polymerization via lipases

1.2.4.1 Polycarbonates

Aliphatic polycarbonates perform good biodegradation, low toxicity properties and good biocompatibility, consequently employed by biomedical applications such as flexible sutures and drug delivery. Trimethylene carbonate can be enzymatically polymerized via N435, porcine pancreatic lipase (PPL), Pseudomonas cepacia (PS-30) and Pseudomonas fluorescens (AK); with N435 giving the highest efficiency and molecular weight (Bisht et al, 1997). There are also other types of trimethylene carbonate derivatives, e.g. 2,2-methyltrimethylene carbonate, 5-benzyloxy-trimethylene carbonate, 5-methyl-5-benzyloxycarbonyltrimethylene carbonate, 5-methyl-5-carboxyl-1,3-dioxan-2-one and 5-allyloxy-1,3-dioxan-2-one (Yang et al,

2011). Copolymers of trimethylene carbonate with telechelic hydroxylated poly[(R)-3-hydroxybutyrate] (PHB), ε-caprolactone (CL), ethylene ethyl phosphate, (Dai et al, 2011; Jun et al, 2003). Copolymers with L,L-, D,D- and D,L-lactides were also reported (Matsumura et al, 1999). Water-soluble polycarbonate (PC) was prepared with 2-dimethylaminotrimethylene carbonate (DMATC) monomer via N435 (Zhang et al, 2012). Another water soluble polycarbonate with tertiary amine groups in the backbone via polymerizing 6,14-dimethyl-1,3,9,11-tetraoxa-6,14-diaza-cyclohexadecane-2,10-dione ($(ADMC)_2$) with N435. It is interesting in this study that trial of polymerizing the same monomer with tin(II) 2-ethylheaxanoate [$Sn(Oct)_2$] had failed (Wang et al, 2010). Since trimethylene carbonate is a low melting monomer (48°C), it can also solubilize its comonomers during eROP enabling a solvent-free synthesis (Al-Azemi and Bisht, 2002).

1.2.4.2 Polyphosphates

Polyphosphates are important class of materials due to their flame retarding, adhesion promotive, plasticizer, processability properties, solubility in common solvents and lowering the glass transition temperature (T_g) value (Yang et al, 2011). Enzymatic ring opening polymerization of ethylene isopropyl phosphate was conducted in porcine pancreatic lipase (PPL) in bulk (Wen and Zhuo, 1998). Ethylene isobutyl phosphate was successfully enzymatically polymerized with PPL immobilized on silica beads again in bulk (He et al, 2001).

1.2.4.3 Polythioesters

It is important to obtain polythioesters having molecular weight more than 100,000 g/mole to reach desirable mechanical properties. Enzymatic polymerization of polythioester was proceeded by first synthesizing a cycling monomer (Cyclic hexanedithiol-sebacate monomer) with N435, and subsequent enzymatic polymerization of the same monomer using the same enzyme with a molecular weight of 100,000 g/mole (Kato et al, 2007).

1.2.4.4 Polyamides

Since conventional chemical methods to synthesize polyamides requires high temperature and pressure value, enzymatic polymerization might be a good alternativefor polyamide production (Poulhès et al, 2012). Aliphatic polyamides (PAs)

have been applied as commercially available engineering thermoplastics for several decades, such as poly(ε-caprolactam) (PA6) and poly(hexamethylene adipamide) PA66 (Yan et al, 2016). Most commonly, PAs are synthesized via ROP of cycled and lactams polycondensation of diamines and diacids. Opposingly, amide bonds are not as susceptible as ester and carbonate bonds to hydrolysis, since higher activation energy is needed for enzyme-bound tetrahedral transition state of amides as compared to the more polar esters and carbonates. The electronegative oxygen in ester bonds is more intimate to the adjacent bonds than in amide bonds confining the electron delocalization which decreases the resonance stability at the ground state (Liljeblad et al, 2010; Veld and Palmans, 2010). On the other hand, the restricted resonance stabilization might cause the amide bonds be prone to an attack by water molecules. Hence, smaller ring-sized amides, such as β-lactam (four-membered), are easily hydrolyzable rings. Polyamides via lipases is still limited as compared with polyesters. One of the drawbacks is the reduced solubility of polyamides in apolar solvents which are mostly preferred in lipase catalyzed enzymatic polymerizations (Veld and Palmans, 2010).

Synhtesis of poly(β-alanine) was proceeded via enzymatic ring-opening polymerization by utilizing N435 at 90°C for 96 hours in toluene with a monomer/enzyme ratio of 1:1 (w/w). It should be noted that the average degree of polymerization of the obtained polymer was not exceeding 18, including both linear and cyclic macromolecules (Schwab et al, 2008). Polycondensation reactions of dimethyl adipate with various diamines via N435 gave successful synthesis of polyamides with a release of methanol (MeOH) as side product of polycondensation. Copolymers of polyamides comprising silicon segments was obtained with polycondensation of 1,8-octanediol, α,ω-(diaminopropyl)polydimethylsiloxane and diethyl adipate. Researches reported that the formation of amide bonds occured faster than ester bonds, eventually forming a block-like structure of amide and ester bonds on the backbone (Veld and Palmans, 2010). In one study, poly(amidoamines) were synthesized as dimethyl adipate, diethylene triamine, triethylene tetramine were the polycondensation monomers, N435 and Mucor miehei lipase as enzymatic catalyst (Stavila and Loos, 2015). For the synthesis of optically active polyamides, polycondensation of optically active chiral diamine monomer and diesters were

processed for 10 days at 80°C and reduced pressure, consequently achieving up to 87 % of yield and around 14,700 g/mole of M_n (Poulhès et al, 2012).

1.2.4.5 Polyesters

Enzymatic polyester synthesis requires milder reaction conditions than conventional processes, such as temperature values lower than or equal to 100°C, since chemical synthesis of polyesters are conducted at around 180-280°C (Gross et al, 2010). A wide range of lipases extracted from various resources were applied for enzymatic polyester synthesis, such as Candida antarctica, Candida rugosa, Pseudomonas fluorescens, Pseudomonas cepacia, porcine pancreas, etc. N435, which was explained above, was the most efficient and straightforward lipase type concerning the ability to catalyze a diverse type of monomers, thus scrutinized in the literature (Yang et al, 2011). Chiefly two main routes are followed for the enzymatic synthesis of polyesters: (1) ring-opening polymerization, (2) polycondensation. Polycondensation might either be executed with the reaction of dicarboxylic acids or their diesters with alcohols, or via self-polycondensation of oxyacids or their esters (Figure 1.10) (Kobayashi, 2009).

Some examples of monomers used in enzymatic polycondensation with N435 and cutinase are diethyl succinate, dimethyl 2-mercaprosuccinate, dimethylaminoisophthalate, sebacic acid, adipic acid, symmetrically unsaturated α,ω-dicarboxylic acid methyl esters (C_{18}, C_{20}, C_{26}) as diacids or diesters; 1,4-butanediol, 1,6-hexanediol, 1,8-octanediol, octanediolpolyethylene glycol (PEG) with various chain lenghts, 1,4-cyclohexanedimethanol, α,ω-bis(3-hydroxypropyl) polydimethylsiloxane as diols; cis-9,10-epoxy-18-hydroxyoctadecanoic acid as oxyacid (Gross et al, 2010; Guo et al, 2008; Hunsen et al, 2007; Jiang, 2008; Kato et al, 2009; Kumar et al, 2004; Mahapatro et al, 2004; Olsson et al, 2007; Warwel et al, 2001).

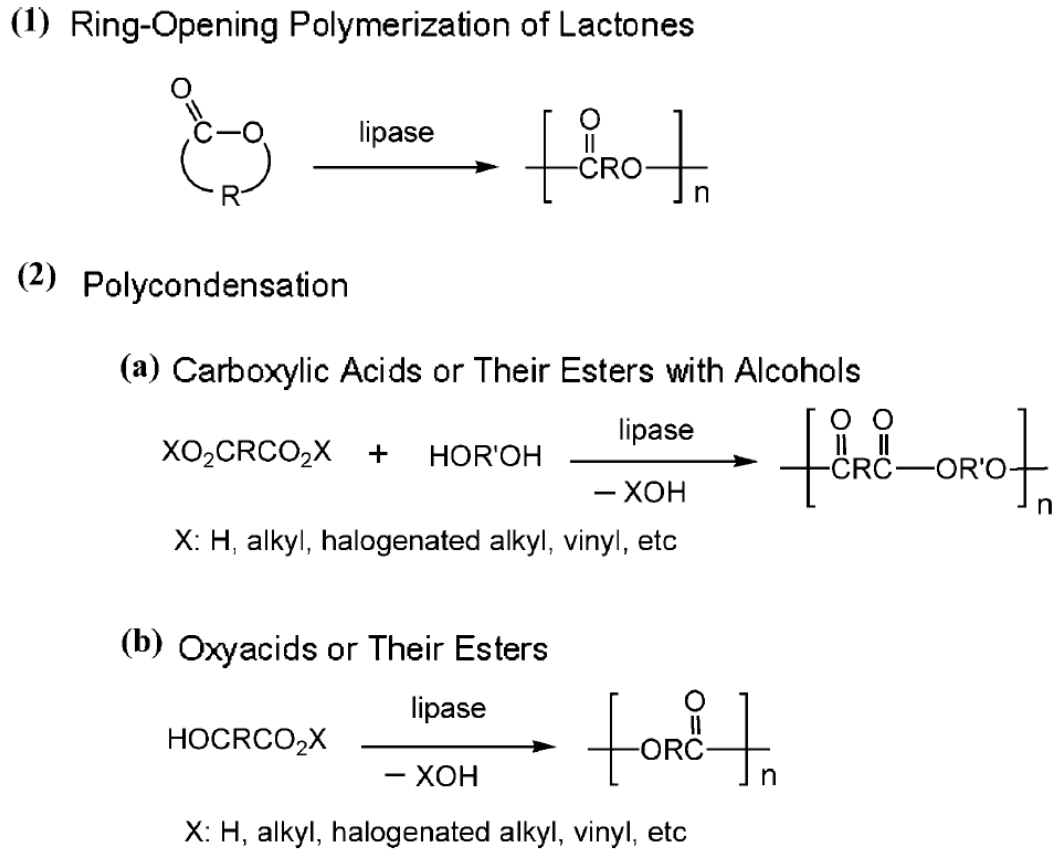

Figure 1.10 : Ring-opening polymerization and polycondensation methods for the enzymatically catalyzed polyesters synthesis (Kobayashi, 2009).

Enzymatic ring-opening polymerization (eROP) of lactones by lipases was first introduced to the literature by two different research groups in 1993 (Knani et al, 1993; Uyuma and Kobayashi, 1993). Within the last two decades, enzymatic polymerization, mainly especially lipase-catalyzed polyester synthesis, has advanced and gained importance becoming a considerable route for the synthesis of polymeric materials (Zhang et al, 2014). Lipase catalyzed eROP of lactons with ring sizes of 4 and 17 members were investigated in the literature (Figure 1.11) (Varma et al, 2005).

Lactones, namely cyclic esters, with various ring sizes composed of either substituted and unsubstituted structures were also examined deeply in the literature (Figure 1.12) (Kobayashi, 2009).

Substrate specification and high selectivity maintaining a vast number of polyesters with various functional initiators and terminators, were highly determined by the location of the active site (Albertsson and Srivastava, 2008; M. Takwa, Xiao, Y., Simpson, N., Malmström, E., Hult, K., Koning, C.E., Heise, A., Martinelle, M.,

2008a). Enzymatic polymerization is catalyzed by the serine fragment. Firstly, acyl-enzyme intermediate generates the enzyme-activated monomer (EM).

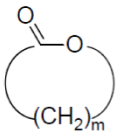

m = 2 (4-membered) : β-PL	m = 10 (12-membered) : UDL
m = 4 (6-membered) : δ-VL	m = 11 (13-membered) : DDL
m = 5 (7-membered) : ε-CL	m = 14 (16-membered) : PDL
m = 7 (9-membered) : 8-OL	m = 15 (17-membered) : HDL

Figure 1.11 : Lactones used in polyester synthesis by eROP (Varma et al, 2005).

Afterwards, the acyl carbon of EM is attacted by the nucleophilic initiator. This stage is called the initiation reaction constituting a ω-hydroxycarboxylic acid (n = 1) which is the precursor leading the propagation step.

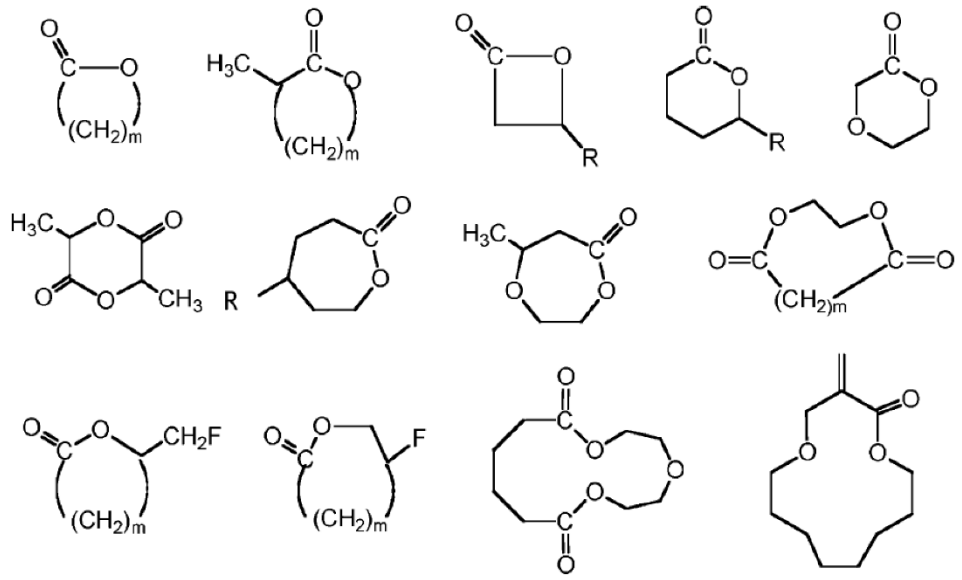

Figure 1.12 : Lactones with varying ring sizes having substituted and unsubstituted structures (Kobayashi, 2009).

Nucleophilic initiator might be water, alcohol, or any hydroxyl bearing component. Propagation step starts with the attack of the hydroxyl end-functionality on the propagation chain to EM thus adding a monomer unit (Figure 1.13) (Uyama and Kobayashi, 2002). The rate of lactone polymerization via eROP is determined by the rate of lactone-lipase complex formation (Jérôme and Lecomte, 2008; Uyama and Kobayashi, 2002). The first kinetic studies of enzymatic polymerization of lactones

(were reported in 1997 with 12-dodecalonide (13-membered lactone) and lipase Pseudomonas fluorescens (lipase PF), by comparing the monomer consumption rates in the presence of 1-octanol, as initiator, and without 1-octanol. In both cases, the monomer consumption rates were the same revealing that acyl-enzyme complex formation was the slower step in polymerization. The kinetic analysis were proceded according to Michaelis-Menten equation (Uyama et al, 1997).

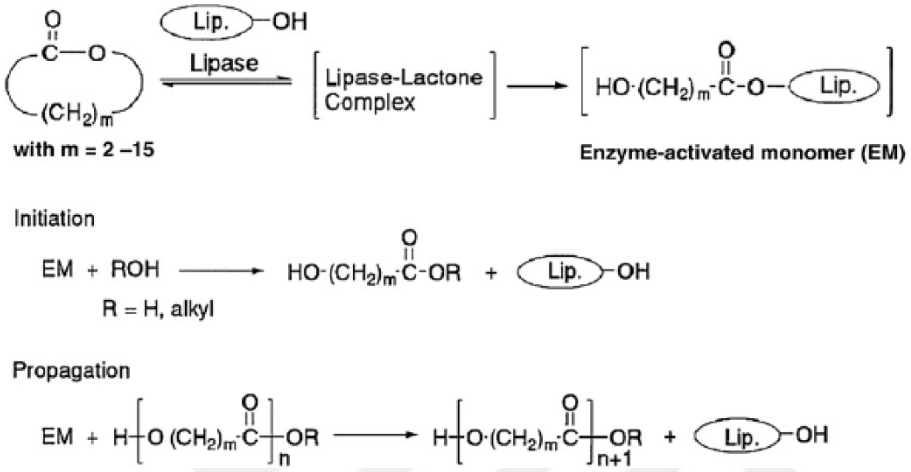

Figure 1.13 : General synthesis mechanism of lipase-catalyzed ROP of lactones (Jérôme and Lecomte, 2008).

The eROP mechanism is different than the chemical ROP (cationic, anionic or radical) in terms of the place where the active center appears and the reactivity of the cyclic compounds. In chemical ROP, the active site is the propagating chain-end. However, in eROP, the monomer is activated in each addition to the propagating backbone. The cyclic compounds also have different reactivity in ionic mediums, the smaller sized lactones participate in higher activity due to their higher ring-strains. On the other hand, larger lactones such as pentadecalactone (PDL, 16-membered), undecalactone (UDL, 12-membered) and dodecalactone (DDL, 13-membered) have high enzymatic polymerization rates than the smaller ring-sized lactones like ε-caprolactone (7-membered) and δ-valerolactone (6-membered) (Kobayashi, 2009).

Many enzymes were screened for the polymerization of lactones including *Aspergillus niger* (lipase A), *Candida cylindracea* (lipase CC), *Candida rugosa* (lipase CR), *Penicillium roqueforti* (lipase PR), *Pseudomonas cepacia* (lipase PC), *Pseudomonas fluorescence* (lipase PF), *Rhizopus delemer* (lipase RD), *Rhizopus japanicus* (lipase RJ), *porcine pancreatic lipase* (PPL) (Kobayashi, 2009; Uyama et al ,1995). On the

other hand, N435 was reported as the most efficient catalyst among all for CL (Kobayashi, 2009; Sivalingam and Madras, 2004).

1.2.5 Polycaprolactone

Polycaprolactone (PCL) is among one of the most important polymer preferred to be applied in medicine and tissue engineering thanks to its mechanical properties, low melting point (59-64°C), crystallinity, miscibility and blend compatibility with a wide range of polymers, good solubility with biocompatibility and biodegradability by numerous bacterias. Thus, since 1970s and 1980s, PCL was being employed widely in drug delivery systems. PCL has good solubility in tetrahydrofuran (THF), toluene, chloroform, dichloromethane (DCM), carbon tetrachloride, benzene, cyclohexanone and 2-nitropropane; weak solubility in acetone, 2-butanone, ethyl acetate, dimethylformamide (DMF), and acetonitrile (ACN); insoluble in alcohols, petroleum ether, diethyl ether and water. (Labet and Thielemans, 2009; Woodruff and Hutmacher, 2010).

The miscibility of PCL is possible with a number of polymes icluding poly(vinyl chloride), poly(styrene-co-acrylonitrile), poly(acrylonitrile-co-butadiene-styrene), polycarbonates, nitrocellulose and cellulose (butyrate). PCL has also mechanical compatibility with polyethylene PE, PP, natural rubber, poly(vinyl acetate) and ethylene propylene rubber (Labet and Thielemans, 2009).

Some of the physical properties of PCL can be found in Table 1.6.

Table 1.6 : Physical properties of PCL (Labet and Thielemans, 2009).

Properties	Range
Number average molecular weight, M_n, (g.mole^{-1})	530-630,000
Density, ρ (g.cm^{-3})	1.071-1.200
Glass transition temperature, T_g (°C)	(-65)-(-60)
Melting temperature, T_m (°C)	56-65
Demposition temperature, T_d (°C)	350
Inherent viscosity, η_{inh} (cm^3.g^{-1})	100-130
Intrinsic viscosity, η (cm^3.g^{-1})	0.9
Tensile strength, σ (MPa)	4-785
Young's Modulus, E (GPa)	0.21-0.44
Elongation at break, ε (%)	20-1000

1.2.5.1 Production of ε-caprolactone

Nowadays, CL is yearly manufactured around multi-1000 tonnes/year via Union Carbide Corporation (UCC) process (Figure 1.20). Cyclohexanone is oxidized by peracetic acid with a converison of 85-90%. Moreover, disadvantages considering toxicity, ecology and safety still remains to be enhanced (Schmidt et al, 2015).

Figure 1.14 : Industrial production of ε-CL from peracetic acid and cyclohexanone (Labet and Thielemans, 2009).

On the other hand, CL can be synthesized enzymatically instead of chemical oxidation which is referred as Baeyer-Villiger monooxygenases (Balke et al, 2012; Schmidt et al, 2015). BVMOs needs only molecular oxygen as an oxidizing reagent and NADPH as cofactor. For the oxidation of cyclohexanone, cyclohexanone monooxygenase extracted from Acinetobacter NCIB 9871 and *Nocardia globerula CL1* might be used (Donohague et al, 1976). CHMO can also be manufactured recombinantly in yeast and *Escherichia coli* (*E.Coli*) (Schmidt et al, 2015).

1.2.5.2 Degradation of polycaprolactone

Depending on its degree of crystalline degree, molecular weight and degradation medium, PCL can be biodegraded from several months to several years. PCL can be fullydegraded by many bacteries. The biodegradation starts from the amorphous phase and causing a rise in the crystalline degree. Subsequently, with the cleavage of the ester bonds, the molecular weight starts to decrease. The final degradation occurs at high temperatures via end-scission, although it degrades via via random chain scission at low temperatures. The carboxylic acid release as a degradation by-product catalyzes the decomposition, while enzymes provide higher rate of degradation (Labet and Thielemans, 2009). PCL is fully degradable in the environment by the bacteries, but in the body it can not be degraded enzymatically in our body (Ikada and Tsuji, 2000; Labet and Thielemans, 2009). The low-molecular weight by-products released by biodegradation of PCL were not found yet harmful to the environment and human body (Vert et al, 1992; Woodruff and Hutmacher, 2010).

1.2.5.3 Enzymatic synthesis of polycaprolactone

CL has got high activity for e-ROP, thus enzymatic polymerization of CL has been widely studied. eROP of CL was successfully conducted via numerous lipases and esterases such as Lipases A, BC, CA (CALB), CC, CR, PR, RJ, *Mucor Miehei*, PPL, *Humicola insolens* cutinase (Divakar, 2004; Henderson et al, 1996; Hunsen et al, 2007; MacDonald et al, 1995; Shoda et al, 2016).

Examples of thermophilic lipase and esterase extracted from *Fervidobacterium nodosum* and *Archaeoglobus fulgidus* were reported to catalyze eROP of CL showing high activity at high temperatures, for instance highest activity at 90°C with *Fervidobacterium nodosum* (Li et al, 2011; Ma et al, 2009; Shoda et al, 2016).

Enzymatic ring-opening polymerization reaction with raw industrial lipases needs a remarkably large amount of enzyme, often more than 40% by weight of the monomer CL, in order to synthesize PCL with a sufficient yield. On the other hand, less than 1% by weight of N435 amount was reported to be efficient enough to obtain a PCL with high catalytic activity (Shoda et al, 2016).

Synthesis mechanism of the enzymatic ring-opening polymerization of eROP of CL is demonstrated in Figure 1.15.

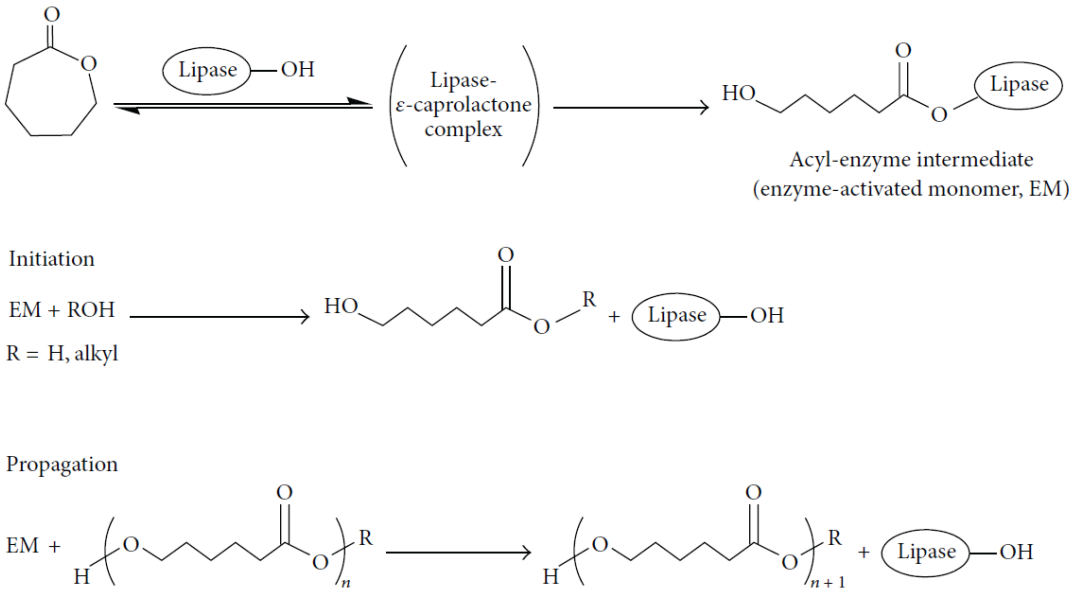

Figure 1.15 : Synthesis mechanism of eROP of CL (Kaya and Guvenilir, 2015).

1.2.6 Photopolymerization

Photopolymerization possesses a substantial interest since it has been applied in coatings, adhesives, inks, printing plates, optical waveguides and microelectronics by

providing economic and environmental benefits together. For instance, photoinitiated polymerization methods might provide room temperature or below synthesis conditions, which is deficient in synthesis methods employing thermal energy such as thermal curing and free-radical polymer synthesis with thermally degradable initiators (Fisher et al, 2001; Yagci et al, 2010). Benzoin, 2-hydroxy-2-methyl-1-phenyl propan-1-one (Darocure 1173), 2-hydroxy-1-[4-(2-hydroxyethoxy)phenyl]-2-methyl propan-1-one (Irgacure 2959) photoinitiators were used in the synthesis of PCL based macrophotoinitiators via stannous octoate catalyzed living ring-opening polymerization (ROP) to induce photopolymerization of methyl methacrylate (MMA) resulting in block copolymers of ε-caprolactone (CL) and MMA (Degirmenci et al, 2002). Similarly, mid-chain macrophotoinitiators comprised of poly(D,L-lactide) homopolymer and tetrablock poly(D,L-lactide)-poly(ε-caprolactone) copolymers were synthesized via ROP and they were utilized in further installation of MMA units via light induced polymerization (Degirmenci et al, 2015).

Irgacure-2959 (Ir2959) was used as the nucleophilic initiator to obtain a macrophotoinitiator by enzymatic ring opening polymerization (eROP) of oxacycloheptadec-10-en-2-one. The α-Ir2959-substituted macrophotoinitiator was also UV-cured (Faucher, 2013).

Poly(benzyl acrylate) (PBzA) was preferred in the literature due to its high thermal and photochemical stability and poly(tetrahydrofurfuryl acrylate) (PTHFA) was noted witt its' recognizable blood compatibility (Mochizuki et al, 2009; Oberti et al, 2008). Homopolymers and copolymers of 2-hydroxyethyl acrylate (HEA) were widely used in biomedical applications as a result of their hydrogel form, tunable properties and biocompatibility (Aran et al, 2010; Chen et al, 2007).

1.2.7 Antimicrobial and antifouling polymers

1.2.7.1 Biofouling process and bacterial adhesion

Animal, mineral, or vegetable surfaces (either biotic or abiotic) are susceptible to biofilm formation and bacterial colonization (Dunne, 2002). Biofilm formation might be observed in maritime, dairy, food, water systems, oil, paper, opticians, dentistry, and hospitals (Garrett et al, 2008). Various biofilm formations were shown in Figure 1.16.

Figure 1.16 : Biofilms (a) mold in households, (b) algae on ship's hull, (c) bacterial biofilm on a catheter (Siedenbiedel and Tiller, 2012).

A wide range of bacterial strains are beneficial and exist as constituents in human body (symbiotic bacteria referred as human microbiome) which participate in regulating human behavior, physiology, development. Nevertheless, there are also unfriendly bacteria harmful to human health (Renner and Weibel, 2011). Bacterial adhesion to human tissue and biomaterial implants, for instance orthopaedic biomaterials, is one of the key steps in the pathogenesis of infection since the bacteria colonize on the surface (Armentano et al, 2007; Montanaro et al, 2007). Several factors affect the bacterial adhesion process such as environmental factors, flow conditions, the presence of serum proteins and antibiotics, the bacterial properties and the material surface properties. This process consists of two main steps (Armentano et al, 2014).

The first step is the initial, instantaneous and reversible physical phase which starts with the attraction of the cells to the surface via Brownian motion, van der Waals interactions, gravitational forces, surface electrostatic (double layer) interaction, and hydrophobic interactions (Arciola et al, 2012; Armentano et al, 2014; Garrett et al, 2008). The first step is also described as long- and short-range interactions, which are crucial for the initiation of bacterial adhesion preparing the molecular and cellular adhesion. The long-term interactions are nonspecific and occurs >50 nm distance between cells and surfaces, while the short-term interactions occur <5 nm with the incorporation of hydrogen bonding, ionic, dipole and hydrophobic interactions. Bacterial adhesion is influenced by bacterial properties (hydrophobicity and the surface charge of the bacteria) and surface properties of the material (chemical composition, surface roughness and surface configuration) (Arciola et al, 2012; Armentano et al, 2014; Krasowska and Sigler, 2014; van Loosdrecht et al, 1987).

In the second step, molecular reactions between the bacterial surface structures and the substrate surfaces which are either coated or uncoated with host matrix proteins (i.e., albumin, fibronectin, fibrinogen, vitronectin, and laminin). The structures on the

bacterial surface such as capsules, fimbriae, or pili and slime assist bacteria adhere on the substrate surface (Armentano et al, 2014). The adherence of *Staphylococcus aureus (S. Aureus)*, as a bacterial pathogen which is primarily extracellular, is driven by protein adhesins of the microbial surface components recognizing adhesive matrix molecules (MSCRAMM) family that are chiefly anchored to the cell wall peptidoglycan (Armentano et al, 2014; Foster and Höök, 1998).

As it was demonstrated in Figure 1.17, the cell wall of the Gram-positive bacteria is comprised of an inner lipid membrane encompassed by a layer of peptidoglycan which is a crosslinked polysaccharide. On the other hand, the Gram-negative bacteria preserve a thinner layer of peptidoglycan, yet have another outer lipid membrane layer surrounding the peptidoglycan layer. The proteins and lipopolysaccharide residing in the outer membrane generate surface charge. Various bacteria possess capsules prolonging toward the outer cell comprised of a thick layer of alginate (an anionic polysaccharide) and other complex polysaccharides. There are extracellular organelles assisting attachment and motility, e.g. pili, curli, fimbrae, and flagella. Therefore, the structure of the surrounding environment and the substrate affect the bacterial adhesion (Renner and Weibel, 2011). The dynamic reversible cell adsorption process eventualize with an irreversible adsorption of a portion of the bacteria. Regarding the irreversible attachment, there is an argument whether the extracellular organelles of the bacteria dominate the eletrostatic repulsive forces (double layer) between the substrate and bacterial surface or not. Following the settlement of the conditioning layer, the extracellular organelles achieve this layer accelerating the contact between the bacteria and the surface which ease the chemical reactions such as oxidation and hydration. There are indications revealing the bacterial adhesion mainly driven by hydrophobic-hydrophilic interaction of the two considered surfaces. The bacteria grow in population after the irreversible settlement process. In condition where the cell division rate is equal to the cell death rate is referred as the stationary phase. When the cell concentration is high, the biofilm utilizes cell signaling mechanisms which are referred entirely as quorum sensing (Garrett et al, 2008). Quorum sensing is a stimuli and response language system supplying the communication to assist their adaptance to the changing environmental medium by regulating the certain genes as a counteract to population density (González and Keshevan, 2006; Whitehead et al, 2001) . Low-molecular-mass molecules are used for signaling and their concentration in outer cell

is determined by the population density of the related bacteria. The bacteria cells sense the signalling molecule providing an act when the medium reaches a critical cell oncentration (Whitehead et al, 2001). In the death phase, the enzymes secreted by the bacterial community itself breakdown the biofilm and releasing the surface bacteria. For example, N-acetyl-heparosan lyase by *Escherichia coli* is secreted. Subsequently, the upregulation of the codes controlling the motility and downregulation of the codes determining the number of porins are driven. Thus, a genetic cycle for biofilm adhesion and cohesion is completed (Garrett et al, 2008; González and Keshevan, 2006). The signalling molecules might briefly be classified as amino acids and short peptides mainly used by Gram-positive bacteria and fatty acid derivatives oftenly used by Gram-negative bacteria (Whitehead et al, 2001).

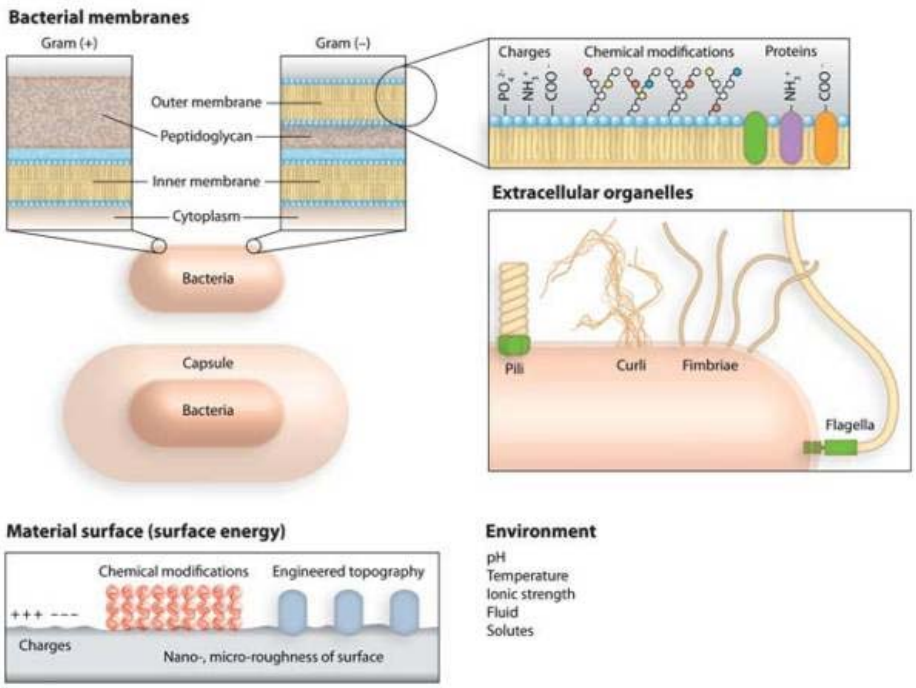

Figure 1.17 : Characteristic elements determining the bacterial and surface related interactions (Renner and Weibel, 2011).

There are examples of bacteria which can form a biofilm with the help of suitable nutrients such as *Staphylococcus epidermidis, Staphylococcus aureus,* and *Streptococcus species* as Gram-positive pathogens; Pseudomonas aeruginosa as Gram-negative pathogens and *Escherichia coli* as Enterobacteriaceae family (a large family of Gram-negative bacteria as well) (Armentano et al, 2014).

The environmental factors affecting the microbial adhesion might be stated as pH, rheological and adhesive properties of biofilms and temperature (Garrett et al, 2008).

1.2.7.2 Antimicrobial polymers

Microbial infections became an issue constituting stress globally by influencing healthcare areas (Santos et al, 2016). There are several strategies to prevent surface contamination including supplying a sterile environment via the utilization of disinfectants such as hypochlorite, hydrogen peroxide, or other reactive oxygen species (ROS). Another way is to use silver salts, quaternary ammonium compounds, alcohols and triclosan (Siedenbiedel and Tiller, 2012). Although microbials have great importance to overcome these problems, low molecular weight antimicrobial agents bring various drawbacks including environmental toxicity and cytotoxicity (especially for triclosan and marine biocides) (Dann and Hontela, 2011; Fusetani, 2011; Juda, 2010). In contrast, macromolecular structures involving antimicrobial functionalities provide the antimicrobial features in a more sustainable way (Kenawy et al, 2007). As compared with the conventional antimicrobial agents, antimicrobial polymers has several advantages such as reducing the environmental complications and preserving a higher density of biologically active groups than their oligomer derivatives. Furthermore, insolubility of the antimicrobial polymers provide availability in biomedical, environmental protection and water treatment end-uses (Hu et al, 2005). Thus, recently, antimicrobial polymers have gained great importance concerning new structures and modifications of known macromolecules in parallel with biological, physicochemical, biological research and engineering design. The growing demand is driven by the requirement of prevention of microbial infection in water purification systems, food, general consumer markets, medical, dental and hygenic applications (Timofeeva and Kleshcheva, 2011). It has been revealed that bacteria evolved in a way that being more resistant to the developed antibiotics which made it necessary to reassess the sufficiency of the common antibiotics and supporting the idea of elaborating new antimicrobial materials. Pharmaceutical antibiotics and antiseptic materials have been investigated as different research areas. However, antimicrobial macromolecules have built a common pathway (Gabriel et al, 2007).

Numerous types of plastics might be sterilized with dry/wet heat, or ionizing radiation. On the other hand, microorganisms are infecting in case these polymers are exposed to the atmosphere. Macromolecular antimicrobials so far supplied straightforward solutions to obtain biomaterials. It is note to mention that polymeric antimicrobial agents are nonvolatile, chemically stable and resistant to migration through the skin.

Antimicrobial polymers might secure lives by preventing infections in medical applications. Pacemakers made of an antimicrobial polymer, as a permanent implant and polymeric catheters slowly releasing an antibiotic are some end-uses of antimicrobial polymers.

Antibiofouling surfaces might be reached via preventing biofilm formation by incorporating an antimicrobial polymer onto the surface of the substrate. To provide the inhibiton of biofilm formation, the material should be able to resistant to adhesion of the surrounding bacteria, which is briefly managed either by repelling or killing the bacteria. Hydrogels structured with poly(ethylene glycol) (PEG) or similar hydrogels are helpful to repel the bacteria. Highyl negatively charged polymers or ultrahydrophobic materials also participate in the repelling mechanism. On the other hand, the killing mechanism works either by biocide release or contact of the polymeric antimicrobial with the bacteria (Figure 1.18) (Siedenbiedel and Tiller, 2012).

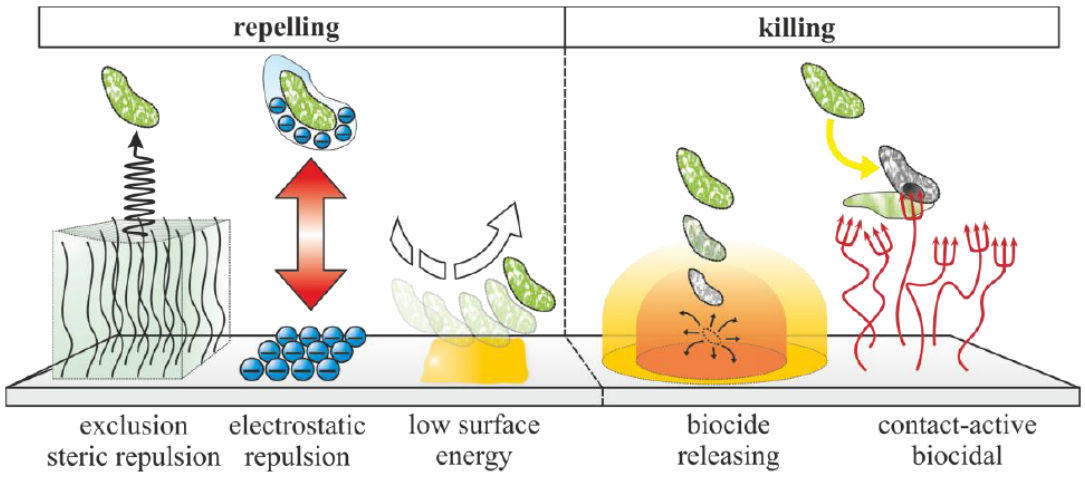

Figure 1.18 : Approaches for achieving antimicrobial surfaces (Siedenbiedel and Tiller, 2012).

Antimicrobial polymers have been in the literature since 1965 when polymers and copolymers of 2-methacryloxytroponones were realized to kill bacteria such as *Staphylococcus aureus, Salmonella typhosa, Salmonella chloraesuis, Escherichia Coli, Streptococcus pyogenes* characterized by zone inhibition test (Cornell and Donaruma, 1965; Siedenbiedel and Tiller, 2012).

Strategies to obtain antimicrobial polymers might be incorporating an organic and inorganic biocide into the polymers during processsing, equipping a biocidal function after processing, polymerizing or copolymerizing a antimicrobial monomer and

grafting antimicrobial agents into natural occurring or synthetic polymers (Kenawy et al, 2007). Intrinsically antimicrobial polymers were reviewed in the literature reporting biomimic studies of the biological activites of antimicrobial natural host-defence peptides (HDPs) (poly(phenylene ethynylenes), polynorbornenes, polymethacrylates), membrane perturbation and biophysical techniques (Gabriel et al, 2007; Timofeeva and Kleshcheva, 2011).

The fundamental necessities of an antimicrobial polymer might be sorted as: (1) Easy an inexpensive synthesis, (2) long-term stability, (3) insolubility in water in case disinfection procedures applied with water, (4) non-toxic decomposure emission, (5) non-toxic and not irritant for the people handling, (6) capability of regeneration with activity loss, (7) activity against a wide range of pathogenic microorganisms in short contact times polymers (Kenawy et al, 2007).

The molecular weight, spacer length between the active site and polymer, hydrophilic-hydrophobic balance, and nature of counterions are the parameters affecting the antimicrobial activity of the polymer (Kenawy et al, 2007).

In the literature, the antibacterial surfaces are achieved mainly by bactericidial approach such as quaternary ammonium compounds (QACs), several other polycations (organometallic dendrimers, chlorhexidine), metal ions (silver, copper, titanium, etc.), antibiotics (e.g., gentamicin), bacterial agents (e.g., bacteriophages, protein synthesis inhibitors, antibacterial enzymes (e.g., lysozyme), antibacterial peptides, natural biomolecules such as chitosan and herbal extracts (e.g., flavanones, chalcones, etc.) and oxidative stress inducing structures. QACs conduct the antibacterial activity through contact by affecting the ion-exchange mechanism and disturbance of the stabilization of the cytoplasmic membranes of the bacteria and consequent leakage of the intracellular fluid. Bactericidial effect progressed through the release of a low-molecular weight antimicrobial agent, such as metal ions and antibiotics, damage the bacterial cell membrane together with disordering the bacterial enzyme, DNA and protein functions. However, the biocidial effect might cause the accumulation of the dead bacteria on the surface (Wo et al, 2016).

The mostly studied synthetic antimicrobial biocidal polymers are cationic polymers including quaternary phosphonium salts (QPS), quaternary ammonium salts (QAS); N-halamine polymers (defined as polymers involving one or more nitrogen-halogen

covalent bonds which are formed by the chlorination of imide, amide or amine groups); polyethyleneimine polymers, other cationic polymers, antimicrobial peptides and proteins (AMPs) (Behlau et al, 2011; Brandenburg et al, 2012; Hui and Debiemme-Chouvy, 2013; Kenawy et al, 2014; Li et al, 2011; Wang, 2014; Xue et al, 2015). Nitric oxide (NO) releasing polymeric coatings are also used for antimicrobial applications (Wo et al, 2016; Yang et al, 2015). Silver (Ag) release, as well as other metal ions, from a polymeric nanocomposites was employed as a route to achieve antibacterial materials (Palza, 2015; Radheshkumar and Münstedt, 2006; Xing et al, 2010). Photoactively bioactive polymeric nanocomposite materials could be handled via blending TiO_2 with various polymer types such as polyurethane, PEG and epoxy (Sadu et al, 2014; Santhosh and Natarajan, 2015; Shah et al, 2008).

1.2.7.3 Antifouling polymeric materials

The protein based film occuring fastly on the substrate surface chiefly interacts with the bacteria when the medium is a physiological fluid. The surface film formation of albumin is invesitagated to change the surface properties of the substrate by rising the hydrophobicity. Bacteria use their adhesins, referred as MSCRAAMs, in order to bind to the protein adsorbed host surface. The proteins which host the bacterial adhesion, referred as "host adhesins", are comprised of fibrinogen, fibronectin, laminişn, vitronectin, clumping factor A and B, bone sialoprotein, elastin, IgV, etc.

In mediums including low concentration of protein or not including protein, the substrates that are antiadhesive and capable of repelling the bacteria generally possess inert characteristics. Self-assembled monolayer, polymer brushes, hydrogel coatings, microstructured and nanostructured surface are some of the approaches to achieve antiadhesive features. Nevertheless, certain inert surfaces might perform antifouling property also in protein-rich medium by preventing the adsorption of the "host adhesins". Polyanionic surfaces might cause electrostatically repel the bacteria which carry negatively charged glycocalices. Gram-negative bacteria usually involve a polyanionic glycocalix. On the other hand, Gram-positive bacteria possess polycationic glycocalix (Campoccia et al, 2013).

Fouling resistant surfaces have been classified according to their common features as: (1) hydrophilicity providing high hydration, (2) electrically neutral charged, (3) hydrogen bond accepting, (4) not being hydrogen bond donor (Zheng et al, 2004).

Superhydrophobicity also assist antifouling via Cassie-Baxter wetting mechanism (Campoccia et al, 2013).

Hydrophilic materials supply a hydration layer on the substrate surface diminishing the protein adsorption onto the substrate. Consequently, proteins needs to overcome and substitute the water molecules at the interface in order to establish a satisfactory concentration for adsorption. There are various routes to obtain a robust hydrated interlayer between the polymer surface and the protein. As hydrophilic polymers employ hydrogen bonds, zwitterionic structures use ionic solvation (Chen et al, 2016).

Some approaches to prevent fouling in various applications such as surgical equipment and protective apparel in hospitals, medical implants, biosensors, textiles, food packaging and food storage, water purification systems, and marine and industrial equipments are shown in Figure 1.19. Furthermore, resistance against microbial and protein adhesion to surfaces holds vital emphasis for catheters, prosthetic devices, and contact lenses, in immunological assays like enzyme-linked immunosorbent assay (ELISA), in devices for drug delivery, and in materials for patterned cell culture (Banerjee et al, 2011).

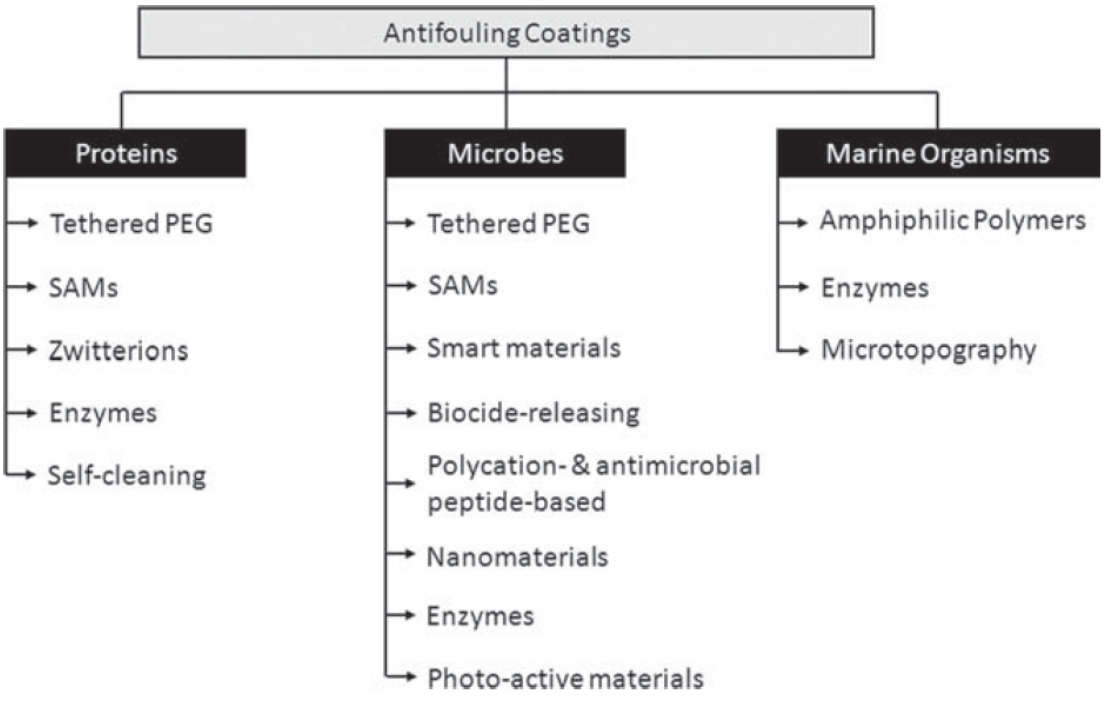

Figure 1.19 : Various methods to achieve antifouling surfaces (Banerjee et al, 2011).

Substantial biomimetic approaches for general foul-release property may be to targeted with self-assemble monolayers (SAMs) and briefly can be referred as:

(1) Polymer brushes (nonionic polymer brushes with hydrophilic groups: poly(oligo(ethylene glycol) methacrylate) (POEGMA), poly(ethylene glycol) (PEG) hydroxyl-containing poly(2-hydroxyethyl methacrylate) (PHEMA), poly(3-hydroxypropyl methacrylate) (PHPMA).

(2) Zwitterionic surfaces: Bioinspiration from antithrombogenic nature of the inner walls of a blood vessel that prevents emboli. These cell walls phospholipids hold the zwitterionic phosphorylcholine head groups (e.g. phosphatidylcholines and sphingomyelin) and the hydrophilic glycosyl head groups (in glycolipids such as cerebroside).

(3) Dendritic coatings: SAMs comprising hydrophilic dendritic architecture provide an intense sheet repelling proteins (polyglycerol (PG) dendrons, branched PEGylated SAMs)

(4) Hydrogel Coatings: Thermally crosslinked poly(N-vinylpyrrolidone).

(5) Hydrophobic and Superhydrophobic Surfaces

(6) Nanopatterned surfaces: Hyperbranched polymer coatings included fluorinated and PEGylated group (Krishnan, 2013, Chapter 6).

Zwitterionic antifouling polymeric materials

Zwitterionic polymers are especially serviced as hydrophilic and antifouling coatings in biomedical applications (Ladd et al, 2008). It should be noted that zwitterionic polymers are evaluated as nonfouling, since the nonfouling criteria claims protein adsorption of <0.3 ng/cm^2 (Chen et al, 2016). Poly(sulfobetaine methacylate) (PSMBA), poly(carboxybetaine methacrylate) (PCBMA), poly(phopshobetaine methacrylate) (PPBMA), poly(serine methacrylate) (PSerMA) and copolymers of some of the related zwitterionic monomers are the examples of the applied zwitterionic polymers and for antifouling approaches (Liu et al, 2013; Tanaka et al, 2015; West et al, 2014). Amphiphilic triblock copolymers of PCL, poly(diethylamino ethyl methacrylate) (PDEA) and PSMBA were also synthesized through azide-alkyne click reaction for pH sensitive drug delivery application as curcumin was the anticancer molecule (Zhai et al, 2014).

PEG based antifouling polymeric materials

PEG became the most applied polymer targeting antifouling end-use. Due to the entropy loss in case the PEG is coated on the surfaces, steric repulsion mechanism

deteriorates the protein adsorption. Another process for the protein adsorption prevention is the high hydrophilic nature of PEG chains causing a hydration layer which hinders the intermolecular interaction between the surface and the protein. The antifouling feature is affected by various parameters such as the brush graft-density, length of the PEG chains, and the configuration in branching structure (Lowe et al, 2015). Furthermore, the bactericidial effet of poly(ethylene glycol) with 400 g/mole of molecular weight (PEG-400) was reported in high concentrations of PEG-400 against *Klebsiella pneumoniae (K. pneumoniae), Pseudomonas aeruginosa (P. aeruginosa), E. coli, and S. aureus* (Chirife et al, 1983).

It was previously reported that the copolymerization of polyethylene glycol methyl ether methacrylate (PEGMA) and 2-hydroxyethyl methacrylate (HEMA), both of which are highly hydrophilic, with vinyl pyridine were applied to improve the biocompatibility still preserving the antimicrobial activity. On the other hand, as a quaternary ammonium salt, the polymer of vinyl pyridine has toxicity against mammalian cells, Gram positive and Gram negative bacteria (Hasan et al, 2013; Sellenet et al, 2007).

1.2.7.4 Natural products comprising antifouling features

There are several steps releasing signals and organizing occasions inducing the establishment and growth of sessile microbial communities enclosed in an extracellular polymer matrix. Though microbial biofilms might be deterred through signal substitution which are responsible for biofilm development or via decomposition of miscellaneous extracellular polymers that form the frames of the biofilm (Dobretsov et al, 2006). Bioassays for antibiofouling are being conducted in order to scrutinize the chemical defence system of the marine organisms in epibiosis control as well as new natural molecules to prevent the microbial adhesion and colonization (Camps et al, 2011).

Apparently, the most challenging obstacle on the route to environmentally non-toxic antifouling agents is the procurement of raw materials . As it is considered antifouling paint demand comprises the remarkable portion of the total marine coating industry, there would also be a necessity of majority amounts. Quorum-sensing (QS) inhibitor is one of the promising area to be investigated. QS inhibitors have the task for organizing biofilm (or microfouling) composition, swarming, production of toxins and

secondary metabolites of which are communicational results between bacterial cells. It is worth to mention that marine organisms commonly inherently have QS inhibition (Fusetani, 2011).

Gram-positive and Gram-negative bacteria emit various, overlapping QS signals. The most extensively investigated class is N-acyl homoserine lactones (AHLs). AHL interfering enzymes comprise hydrolases (lactonases), acylases and oxidoreductases. The extracellular polymer matrix involves monospecific, multispecies biofilms and concurrently composition of polysaccharides, proteins and nucleic acids. Various marine microbes have been represented as disintegrator of biopolymer matrixes via lytic enzymes (Dobretsov et al, 2006).

Encapsulated protease (as a hydrolytic enzyme) in poly(dimethylsiloxane) (PDMS) matrix demonstrated protein antifouling capability. Immobilized hydrolytic enzymes, namely pronase and α-chymotrypsin could be incorporated into biocatalytic film sor oil-based paints. TiO_2 was proven to have photoactive behavior as it can decompose a broad variety of compounds such as stearic acid, and gaseous formaldehyde under visible light so that the surfaces kept clean e.g. glass, textiles and catheters (Banerjee et al, 2011).

Furthermore, bioinspired approaches for antifouling mechanisms point out natural surfaces. There are various marine specimens having antifouling features such as gorgonians, marine mammals, echinoderms, algae, shark, molluscs, fish and crustaceans. Various microtopographies and hierarchical structures exist as well as modified surface properties (surface wettability) (Scardino and de Nys, 2011).

1.2.7.5 Antifouling and antibacterial materials based on PCL and other polyesters

Polyester type polymers have been preferred in antifouling paints due to their combined features: Comprising biobased monomers (e.g. L- or D- Lactic acid, ε-caprolactone, δ-valerolactone, hydroxyalkanoate derivatives), biodegradability via hydrolyzing, benign chemicals released through biodegradation.

Grafting is an option to introduce environmentally benign monomers onto polymer backbone. Target structure was methacrylate and tert-butyl acrylate (as hydrophobic monomer) combination in the backbone while P(DL-Lactic acid) chains were grafted. Firstly, methacrylic acid oligoester (oligo(lactic acid)) were condensated and

macromonomer was synthesized; afterwards the macromonomer and tert-butyl acrylate were copolymerized and graft structure was obtained. Along with defined varnish formulations, application on a vinylester frame and immersion in artificial sea water. Cuprous oxide was used as the bioactive antifouling agent and xylene was the diluting agent It was noted that cuprous oxide release was encouraged by increasing lactic acid units along the grafts (Langlois et al, 2002).

In another study, copolymers of ε-caprolactone, L-lactic acid (L-LA) and δ-valerolactone (VL) were synthesized via ring-opening polymerization (ROP) as tetrabutoxytitane, $Ti(OBu)_4$, was used as the catalyst. The importance of lactic acid and δ-valerolactone monomers was the essential diminish in the crystallinity of poly(ε-caprolactone) (PCL). Thus, P(CL-co-VL) and P(CL-co-LA) copolymers were achieved. The polymerization temperature was 240°C. The paint formulation involved biocide (cuprous oxide), xylene and additives (titanium oxide, zinc oxide). The hydrolysis products were hydroxycaproic acid, hydroxypentanoic acid, and lactic acid. However, the biodecomposition medium was neither the sea water nor its' imitation. Distilled water was employed in order to clearly understand release nature of monomers. The impressive outcome was the efficient hydrolization rate of LA units (14% hydrolyzed groups) as compared with VL based copolymers (1% hydrolyzed groups) within 3 months (Faÿ et al, 2006). Same researches profoundly investigated the antifouling activity of abovementioned P(CL-co-VL) and P(CL-co-LLA) copolymer based paints with a formulation including "booster biocides" in Atlantic Ocean. Excellent antifouling performances were reached via 20,000 g/mole number average molecular weight (M_n) for both copolymers as CL monomer % varying between 83-88. This phenomena was revealed by the faster release of the antifouling agent in lower molecular weights which decrease the antifouling activity (Faÿ et al, 2007).

Lactic acid was also exclusively represented with antifouling feature in natural and artificial sea mediums. Commercial PLLA films were designated for hydrolysis and following slow emission of lactic acid. Whilst lactic acid directly added to the culture medium leaded to a rapid toxicity of cypris larvae, slow release due to hydrolization was confirmed to be a more approved method for permanent antimacrofouling (Ishimaru et al, 2012). Tin(II) octoate ($(Sn(Oct)_2)$) is an alternative catalyst for polyesterification (Odent et al, 2012).

Three active compounds were investigated in terms of their antifouling behaviors with the synergetic effect of P(CL-co-VL) biodegradable polymers. The aforementioned study was conducted in corporation with Nautix Marine Paints (France). Active compounds were chosen as Tween 85, chlorhexidine and zincperoxide all of which were relatively less toxic than zinc pyrithione, dichlofluanid, tributyltin (TBT), diuron, Irgarol 1051 and copper thiocyanate. Biodegradable binder is approved to be a promising antifouling paint inclusion while providing antifouling action for several months, prevention of microfouling with lower toxic chemicals (Carteau et al, 2014).

In bulk enzymatic ROP of lactones, ethylene glycol is also used as co-initiator. In addition to these, a novel method in enzymatic polymerization called miniemulsion method is an option (Målberg, 2010; Taden, 2003).

Grafting of poly(ethylene oxide) PEO chains onto PCL might be an alternative architecture of hydrophilic protein adhesion repellents (Jérôme, 2008). It is evidently known that hydrophilic polymers are more resistant to protein adsorption than hydrophobic polymers. As PEG is a hydrophilic polymer, it holds unique and additional resistance to protein adsorption. There is a synergetic cooperation of concurrent processes of steric repulsion. Firstly, PEG chains are compressed with the protein particulates causing a diminish in the conformational entropy of the polymer chains. As a reaction, chains carry out an elastic repulsion to the proteins. Other contribution to repulsion is the excluded volume effect occurring between the hydrated PEG chains and adhering protein chains consequently leading osmotically repulsion of the protein. Studies demonstrated densely grafting of only a few ethylene glycol molecules perform fine protein antifouling characteristic as well (Banerjee, 2011; Krishnan, 2013).

In the literature, the surfaces of PCL and PET were functionalized to initiate the zwitterionic monomers, sulfobetaine methacylate (SBMA) and carboxybetaine methacylate (CBMA), via surface-initiated atomic transfer radical polymerization (SI-ATRP) method, and eventually nonfouling hemocompatible surfaces were obtained. Another method was to achieve zwitterionic polymer functionalized PCL was the azide-alkyne click reaction in which the zwitterionic polymer was synthesized separately, following the click reaction (Jiang et al, 2011; Li et al, 2013; Wang et al, 2016).

1.2.7.6 Enzymatically synthesis of end-functionalized PCLs

Initiator method

Nucleophiles such as water and alcohols were studied in the literature for their initiation efficiency in eROP of lactones. ω-unsaturated alcohols, alkyl glucopyranosides, bifunctional atom transfer radical polymerization (ATRP) initiators,

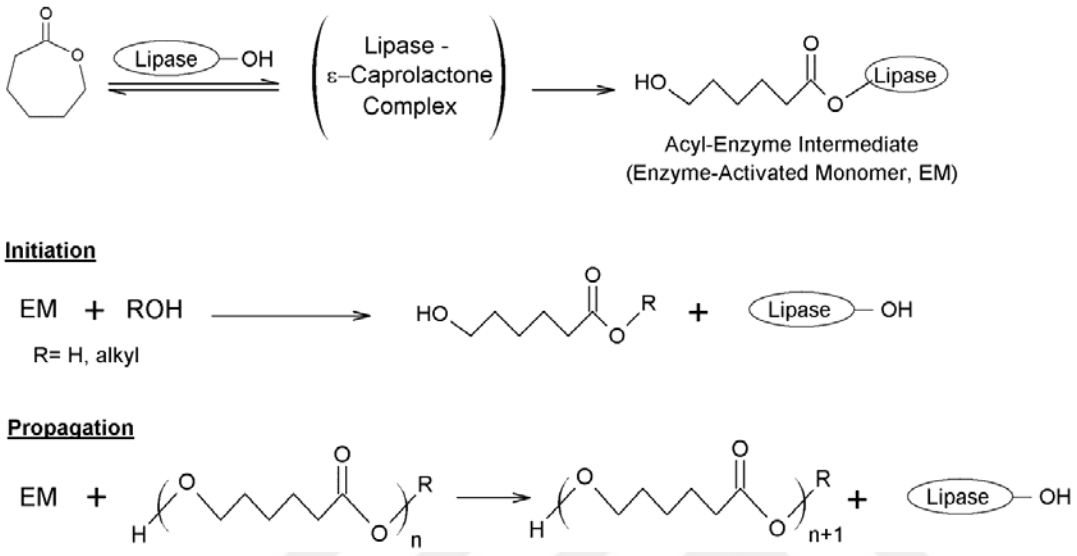

Figure 1.20 : Synthesis mechanism of lipase-catalyzed eROP of CL (Jérôme and Lecomte, 2008; Kaya and Guvenilir, 2015).

are the examples of nucleophiles other than water which initiated eROP of lactones (Kobayashi, 2009; Yang et al, 2014). The hydroxyl groups on the surface of the clay (Silanol) also acted as nucleophilic initiator in the synthesis of surface grafted PCL via CALB immobilized on several clays (Düşkünkorur, 2014). eROP mechanism of CL is demonstrated in Figure 1.20.

There are various studies end-functionalized enzymatic ring-opening polymerizations with many lipase types, lactone monomers and initiators (Kobayashi, 2009; Yang et al, 2011). HEMA and hydroxyethyl acrylate (HEA) initiated CL and PDL enzymatic ring opening polymerization were conducted in order to achieve methacrylate or acrylate end-functionalized polylactones and to reveal the mechanistic aspects of the eROP in case an ester containing initiator is utilized (Takwa et al, 2008a; Xiao et al, 2009).

The proposed mechanism was demonstrated in Figure 1.21. On the other hand, there are several side reactions since the initiator includes breakable ester groups by lipase. The side reactions were explained followingly:

However, closer inspection of the reaction products revealed the formation of several other polymer products in this reaction. It was detected, by ^{1}H NMR and MALDI-TOF MS, that the lipase catalyzed not only the HEMA initiated ROP but also the cleavage of the ester bond within the HEMA moiety of the polymer. This cleavage resulted in two major types of transesterification (acyl transfer) reactions: methacrylate transfer and polyester transfer. The methacrylate transfer led to polymers with four different end-group structures; HEMA end group (1, 3); hydroxyl end group (1, 2); 1,2-ethanediol end group (2, 3); methacrylated hydroxyl end group (3). Furthermore, as a result of the polyester transfer reaction, the 1,2-ethanediol moiety was found to be present within the polyester chain (4) (Takwa et al, 2008a, p.706).

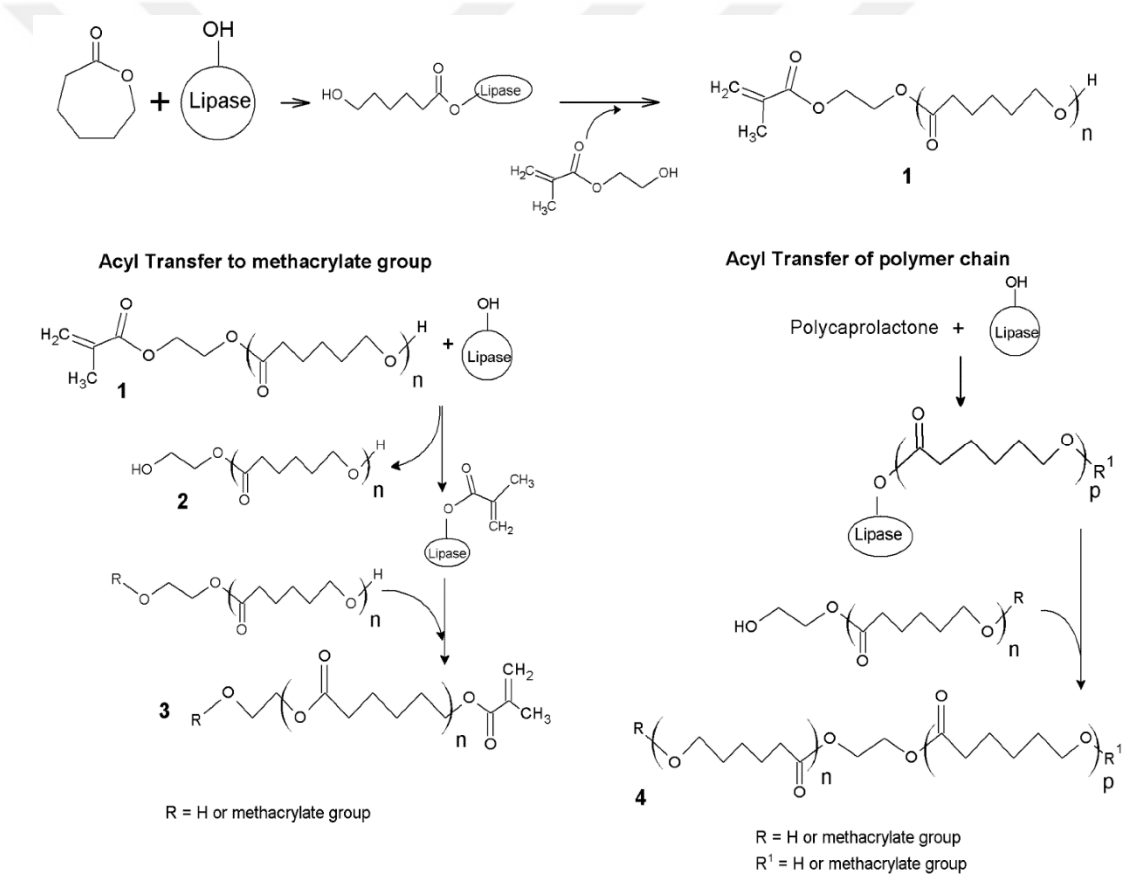

Figure 1.21 : eROP of CL and side reactions thereof:methacrylate transfer (HEMA end-group of the polymer to hydroxyl end-group of polymer); 1,2-ethanediol formation inside the polyester chain (Kaya and Guvenilir, 2015; Takwa et al, 2008a; Xiao et al, 2009).

Regarding these side reactions the polyester structures possibly presenting in the reaction mixture were shown in Figure 1.22. Therefore, it was considereed that the resulting polymer included a combination of macromonomer structures having

different end-groups. For example double methacrylated PCL macromonomer chains also occured in the reaction mixture (Takwa et al, 2008a).

It is known that water moiety during enzymatic ring-opening polymerization is an inhibiting parameter, whilst an optimum amount is required for the enzyme activity. Water has an ability of constituting hydrogen bonds with the enzymes providing a plasticizing effect, which organic solvents are not capable of. This conformational mobility ensures the optimum enzymatic activity. On the other hand, a high water content also inhibits the enzymatic activity by causing the aggregation of enzyme particles resulting in difficulties in diffusion (Varma et al, 2005).

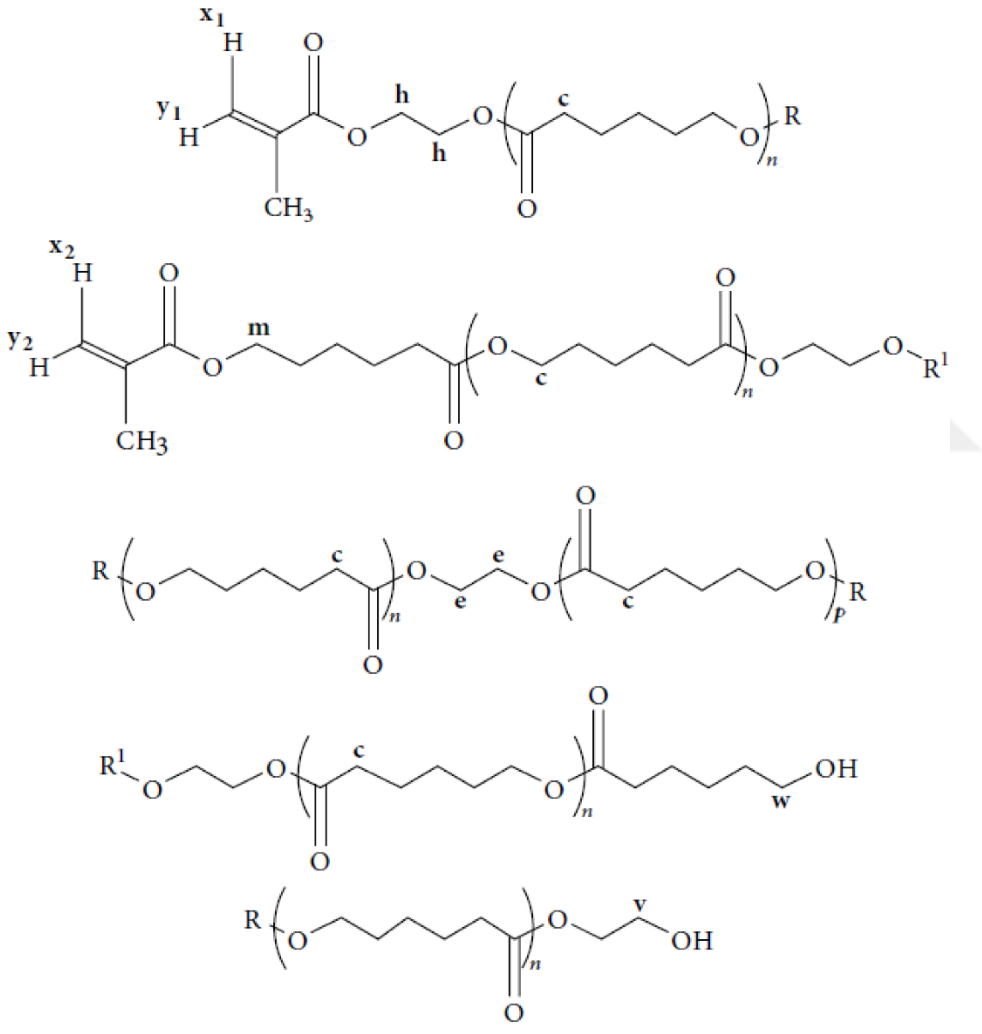

R = H, or methacrylate group

R^1 = H, methacrylate or p(ε-caprolactone) chain

Figure 1.22 : Proposed products obtained in enzymatic ring-opening polymerization of CL as HEMA is the initiator (Kaya and Guvenilir, 2015; Takwa et al, 2008a; Xiao et al, 2009).

In another study, anhydrous conditions were applied, HEMA initiated N435 catalzed ROP of CL was conducted in bulk conditions at 60°C. CL was distilled over CH_2 at vacuum, HEMA was used as received and N435 was dried over P_2O_5 at 0.1 mm Hg for 42 hours before synthesis. All the glassware were flame dried, silanized and stored under N_2 at 0 ppm moisture at glove box. The reaction was proceeded for 5 h, and the polymerization yield was between 69.2 – 56.0%. By eliminating water from the system both might increased the molecular weight and reduced the amount of side reactions. Because, HEMA is the only nucleophilic initiator for CL polymerization, since there is no water or very little amount of water in the reaction medium, it is assumed that all of the PCL chains have one HEMA end-functionalization. Thus, molecular weight could also be calculated with ^{1}H NMR together with size exclusion chromatography (SEC). On the other hand, side reactions and degradation mechanism were not investigated (Srivastava et al, 2007).

Terminator method

In terminator method, the alcohol end-group of a polyester is acylated in single step with a vinyl ester. Macromonomers and telechelics might be obtained by the terminator method (Kobayashi, 2009). For instance polyester with carboxylic acid end-groups at both ends was synthesized when divinyl sebacate participated in the eROP (Kobayashi, 2015). α,ω-functionalized polypentadecalactone (PPDL) was synthesized via eROP again with N435. The variations in the end-group configuration of PPDL strucutres were as follows: (1) two thiol ends, (2) one thiol and one acrylate end, (3) two acrylate ends, (4) two methacrylate ends. In the synthesis of two acrylate ended PPDL and two methacrylate ended PPDL, ethylene glycol diacrylate (EGDA) and ethylene glycol dimethacrylate (EGDMA) were used respectively. But, it should be noted that in these synthesis procedures, water acted as the nucleophilic initiator to achieve a sufficient molecular weight for the macromonomers. Additionally, EGDA and EGDMA were further processed in the side reactions while the water molecules were removed via high-vacuum. Therefore, acrylate and methacrylate end-groups were tailored to the α and ω side of the PPDL (Takwa et al, 2008b).

2. EXPERIMENTAL PART

2.1 Chemicals

2-Hydroxyethyl methacrylate (HEMA) (≥ 99% containing ≤ 50 ppm monomethyl ether hydroquinone as inhibitor), 2-hydroxyethyl acrylate (HEA) (96%, contains 200-650 ppm monomethyl ether hydroquinone as inhibitor), Novozyme®435 (N435) (Candida antactica lipase B immobilized on acrylic resin), ethylene glycol dimethacrylate (EGDMA) (98 %, containing 90-110 ppm monomethyl ether hydroquinone as inhibitor), trimethylolpropane triacrylate (TMPTA) (600 ppm monomethyl ether hydroquinone as inhibitor, technical grade), poly(ethylene glycol) methyl ether methacrylate (PEGMA-950) (Average $\overline{M_n}$ = 950 g/mole, containing 100 ppm MEHQ as inhibitor, 300 ppm BHT as inhibitor), poly (ethylene glycol) methyl ether acrylate ((PEGMEA-480) ($\overline{M_n}$ = 480 g/mole and containing 100 ppm BHT as inhibitor, 100 ppm MEHQ as inhibitor), butyl acrylate (BuA), triethylamine, 2-bromoisobutyryl bromide, copper chloride, 2,2′-Bipyridyl, and [2-(Methacryloyloxy)ethyl]dimethyl-(3-sulfopropyl)ammonium hydroxide (sulfobetaine methacrylate) (SBMA) were purchased from Sigma-Aldrich. ε-caprolactone (CL) (99%) was purchased from Alfa Aesar. Bis(2,4,6-trimethylbenzoyl)-phenylphosphineoxide (Irgacure-819) and (1-[4-(2-Hydroxyethoxy)-phenyl]-2-hydroxy-2-methyl-1-propane-1-one) (Irgacure 2959) were purchased from Ciba Specialty Chemicals. Benzyl acrylate (BzA), 2,2,2-trifluoroethyl acrylate (TFEA) were purchased from TCI Chemicals. Tetrahydrofurfuryl acrylate (THFA) was purchased from Polysciences Inc.. Solvents were supplied from Aldrich.

2.2 Equipments

2.2.1 Size exclusion chromatography

Size exclusion chromatography (SEC) measurements were performed with Agilent 1100 as tetrahydrofuran (THF) was the SEC solvent with 45min of measurement duration.

2.2.2 Differential scanning calorimetry

Differential scanning calorimetry (DSC) measurements were conducted with Mettler-Toledo DSC-1, equipped with an automatic sample robot, a liquid nitrogen-based cooling system and a FRS5 sensor based on a star-shaped arrangement of 56 thermocouples. DSC pans are standard Al pans of 40 µL. STARe Excellence Software was used for data analysis. The DSC measurements were performed in 3 sequential runs: (1) heating from room temperature to 60°C, (2) cooling from 60°C to -100°C, (3) heating from -100°C to 200°C respectively. Heating and cooling were executed in 10°C/min ramps. Between each heating and cooling steps, isothermal steps for 5 min were applied. For the calculation of thermal values, 2nd heating curves were taken into consideration.

2.2.3 Fourier transform infrared spectroscopy

Fourier Transform infrared spectroscopy (FTIR-ATR) measurements were performed with ATR-FTIR-ATR (Affinity-1 FTIR-ATR, Shimadzu) in the range between 600 and 4000 cm^{-1}.

2.2.4 ^{1}H Nuclear magnetic resonance

^{1}H Nuclear Magnetic Resonance (NMR) measurements were performed with Agilent VNMRS 500MHz ($CDCl_3$).

2.2.5 Other equipments

Other equipments which were used in this study were; magnetic stirrer (Ikamag RH), oven (Binder), heater (Ikamag RCT Classic), analytical balance (And, Gr-200).

2.2.6 Methods

2.2.6.1 Synthesis of HEMA Initiated PCL via eROP

CL was dried in the evaporator over molecular sieves at 60°C for 24 h before use. Reactions were carried out in three-necked glass flasks under N_2 atmosphere. Three-necked flasks were dried at 50°C and capped in order to avoid moisture entrance. Before the chemicals were introduced into the reactor, the reactor temperature was set to 60°C under high-flow N_2 for 20 minutes, followingly N435 was added and the one

neck was capped with rubber septum. Enzyme was also dried at 60°C for 20 minutes at high-flow N_2. HEMA and previously dried CL were added via separate syringes through the rubber septum at room temperature. The medium was allowed to mix for 20 minutes before the reaction at room temperature, afterwards the reactor is dipped into the heating oil at the set temperature for reaction. The mixing was provided by magnetic stirrer. N_2 purge continued during the reactions. The reaction was terminated with chloroform addition into the reactor. Chloroform and polymer solution was filtered off the enzyme. Polymer was precipitated with excess cold hexane or cold MeOH for 1 days at -8 ± 2°C at the refrigirator. To hold almost all of the polymer chains, centrifuge operation at -8 ± 1°C (2500 rpm) was carried out for precipitation and washing. 7 times santrifugation with MeOH was performed in order to wash away HEMA, CL and other little molecules arose from undesired side reactions. 90-100 minutes washing is observed as enough for all of the polymer chains to precipitate. Polymers were washed with MeOH were dried under room conditions for 3 days.

2.2.6.2 Photopolymerization of poly(Ethylene glycol) methyl ether methacrylate with α,ω-methacrylated PCL via eROP

Synthesis of α,ω-methacrylated PCL via eROP

EGDMA initiated eROP of CL was carried out at 90°C with EGDMA/CL ratio at 0.1 (mole/mole). N435/CL was 6.1 (g/mole) and 10 g of CL was used. The first step of the reaction was proceeded for 5 hours to provide CL polymerization as moisture was not removed from the reaction media and acted as the nucleophilic initiator. Afterwards, the reactor was kept under vacuum to remove moisture and the reaction proceeded for 48 hours under vacuum. The reaction was terminated with chloroform addition into the reactor. Enzyme was filtered and polymer was precipitated in cold methanol for three times. Precipitated polymer was filtered. In the end, the polymer was dried at 25°C for 3 days. The reaction scheme and the target products were briefly illustrated in Figure 2.1.

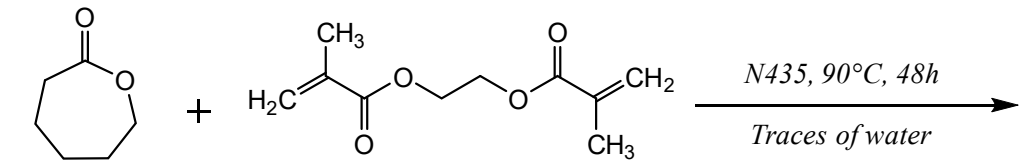

ε-Caprolactone EGDMA

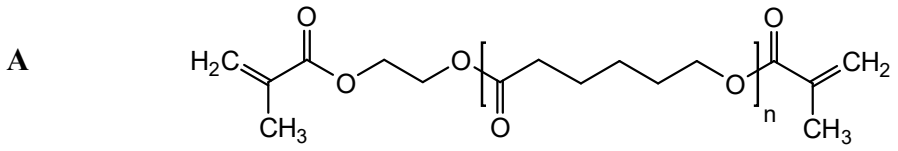

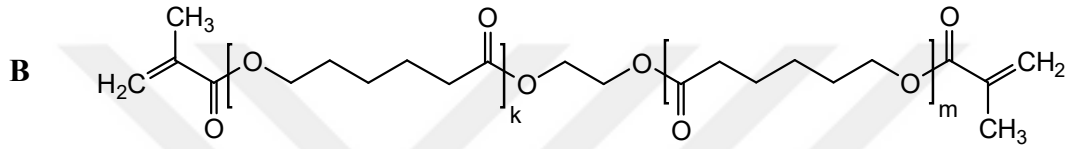

Figure 2.1 : Synthesis of α,ω-methacrylated PCL comprised of A and B structures via eROP (Adapted from Takwa et al, 2008b).

Photopolymerization of PEGMA-950 with α,ω-methacrylated PCL mixture

For the photopolymerization of PEGMA-950, α,ω-methacrylated PCL mixture (DMPCL) was used as crosslinker together with TMPTA (Figure 2.2).

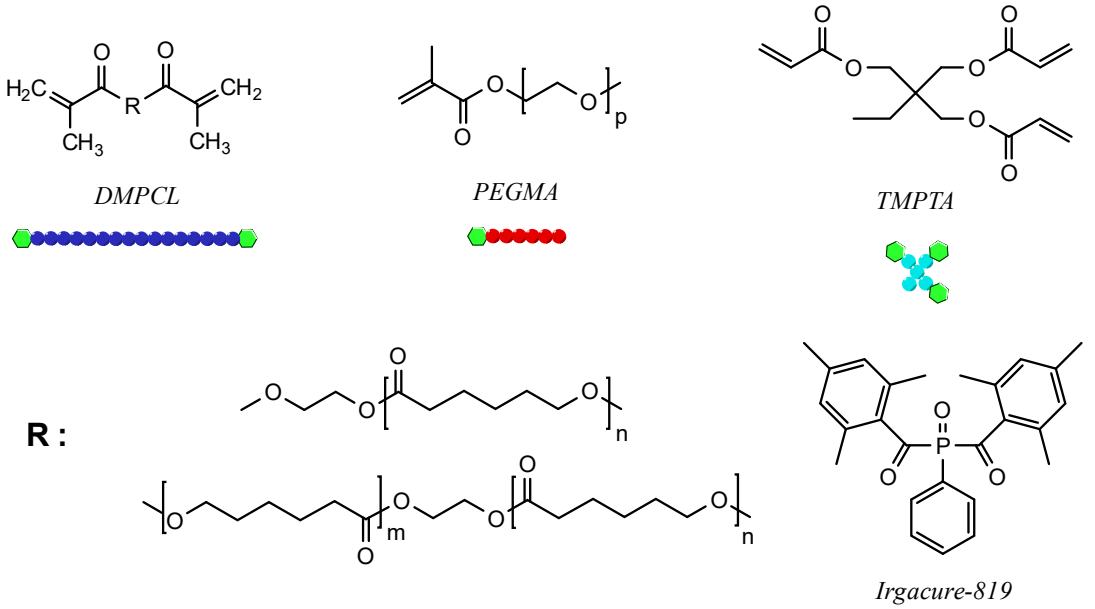

Figure 2.2 : Monomers, macromonomers and the photoinitiator (Irgacure-819) used in the photopolymerization including DMPCL, PEGMA, TMPTA.

The photopolymerization reactions were made using Light Emitting Diode (LED) lamps between 360-400 nm wavelength emission. On the other hand, the efficient UV absorption

spectrum of Irgacure-819 is between 200-440 nm. The decomposition of Irgacure-819 under UV light and formation of the free radicals which are able to initiate the free-radical polymerization was shown in Figure 2.3. To reveal the photopolymerization efficiency between the reactions conducted via solvent casting method and the reactions made in bulk reaction, two different photopolymerization setups were utilized. In the reactions performed in vial, Ar atmosphere was applied and 15° of optical lenses were used for focusing (Figure 2.5). On the other hand, the reactions via solvent casting method, Ar atmosphere was not employed and the optical lenses were not fixed (Figure 2.4). All of the other parameters were kept constant i.e., reaction time, monomer, macromonomer, solvent and photoinitiator amounts.

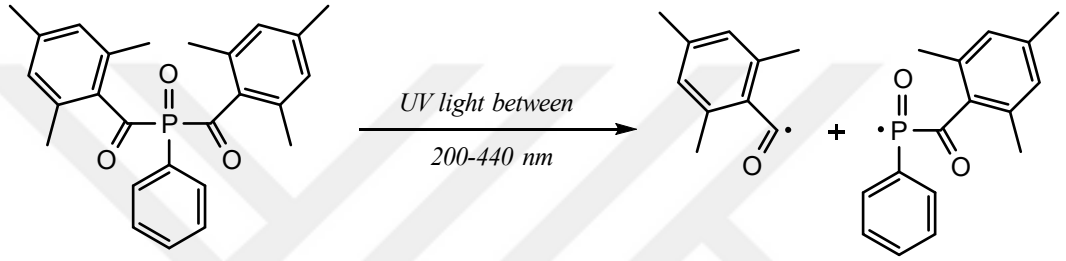

Irgacure-819

Figure 2.3 : Photodecomposure of Irgacure-819 under the UV light between 200-440 nm.

The advantage of the LED lamps is the substantial decrease in heating of the reaction medium, prevention of the solvent evaporation, consequent loss of solvent from the reaction medium.

For the reactions performed in vials, DMPCL, PEGMA-950, Irgacure-819, magnetic stirring bar (8mm x 3mm) (Length x Diameter) and $CHCl_3$ were put into a 10 mL snap-capped glass vial. The vial was purged with Ar gas and the cap was closed immediately after. The mixture was stirred at room temperature for 5 minutes at dark to ensure proper mixing of the components. Then UV polymerization was started while the stirrer was mixing at 1000 revolutions per minute (rpm); the reaction time was kept as 60 minutes.

For the reactions conducted via solvent casting method, the reaction mixture was prepared the same as the reactions in glass vial, and it was poured on microscopic glass slides (25mm x 75mm) (Figure 2.4). The proposed network structure was demonstrated in Figure 2.6. For the calculation of the gel content of V-PCLPEG-0.75, the gel was treated with soxhlet extraction for 24h when $CHCl_3$ was used as the solvent. Afterwards, the gel was dried and weighed.

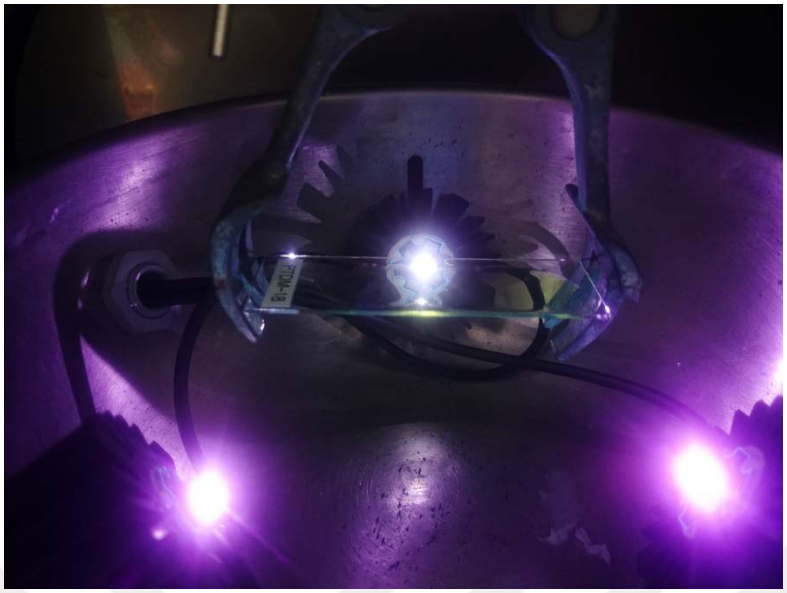

Figure 2.4 : Photopolymerization setup via solvent casting for DMPCL, PEGMA-950 and TMPTA.

The experiment codes and the amount of chemicals used in the photopolymerization of DMPCL, PEGMA-950 and TMPTA were demonstrated in Table 2.1. The reaction mixtures were prepared by altering the ratio of DMPCL in the total of DMPCL and PEGMA-950 (mole/mole), referred as the total macromonomers in Table 2.1.

Figure 2.5 : Photopolymerization setup performed in vial for DMPCL, PEGMA-950 and TMPTA.

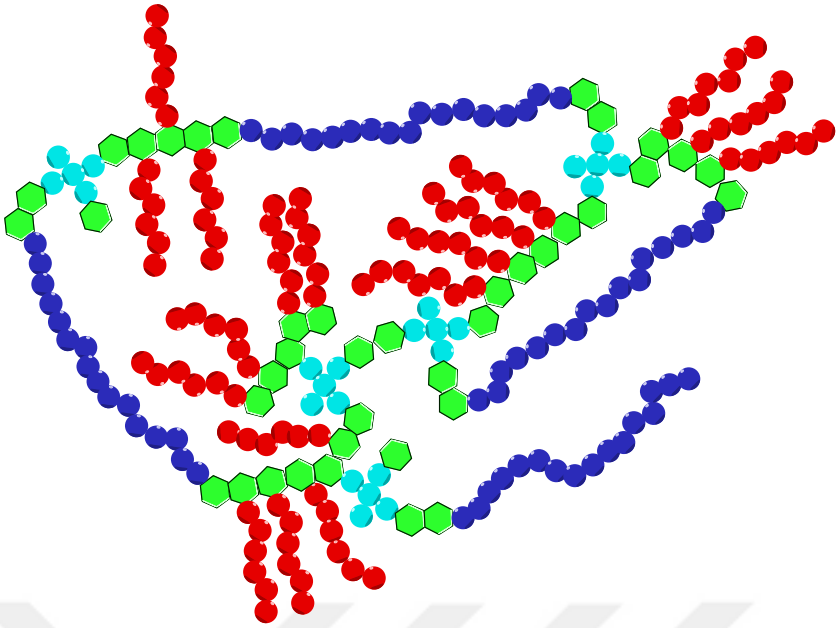

Figure 2.6 : The proposed network structure after the photopolymerization of DMPCL, PEGMA-950 and TMPTA via Irgacure-819.

Concurrently, the ratio of TMPTA in the summation of DMPCL, PEGMA-950 was kept constant as 10.5 % (weight/weigth). The amount of Irgacure-819 was calculated as the 3 % (weight/weight) of the summation of DMPCL, PEGMA-950 and TMPTA, referred as total momonomers.

Table 2.1 : The amount of chemicals and sample codes of the photopolymerized DMPCL, PEGMA-950 and TMPTA as Irgacure-819 was the photoinitiator and $CHCl_3$ was the solvent. Total macromonomer referred to the total amount of DMPCL and PEGMA-950; total monomer was the total of DMPCL, PEGMA-950 and TMPTA.

Experiment Code	DMPCL / (Total macromonomer) (mole/mole)	PEGMA-950 / (Total macromonomer) (mole/mole)	DMPCL (mmole) x 10^{-2}	TMPTA / (Total macromonomer) (w./w.)	Irgacure-819 / Total monomer (w./w.)
S-PCLPEG-1.00	1	0	2.27	0.105	0.03
S-PCLPEG-0.75	0.75	0.25	2.27	0.105	0.03
S-PCLPEG-0.50	0.5	0.5	2.27	0.105	0.03
S-PCLPEG-0.25	0.25	0.75	2.27	0.105	0.03
S-PCLPEG-0.00	0	1	0	0.105	0.03
V-PCLPEG-1.00	1	0	2.27	0.105	0.03
V-PCLPEG-0.75	0.75	0.25	2.27	0.105	0.03
V-PCLPEG-0.50	0.5	0.5	2.27	0.105	0.03
V-PCLPEG-0.25	0.25	0.75	2.27	0.105	0.03
V-PCLPEG-0.00	0	1	0	0.105	0.03

$CHCl_3$ which was utilized as the solvent was added to to the reaction mixtures, as the (solvent volume)/(total monomers) was kept constant at 1.5 (μL/mg). The experiment codes were given according to the rule:

The first initial was the medium where the photopolymerization was conducted. For example, in S-PCLPEG-1.00, S referred to "solvent casting" and in V-PCLPEG-1.00, V refferred to "glass vial". The expression PCLPEG denoted the photopolymerizations were performed by altering the ratios of DMPCL and PEGMA-950. The latter expression in numbers indicated the ration of DMPCL in total DMPCL and PEGMA-950 (Table 2.1).

2.2.6.3 Photopolymerizations initiated by the PCL based macrophotoinitiator

Enzymatic synthesis of PCL based macrophotoinitiator

Irgacure 2959 was dissolved in CL at room temperature and the mixture was treated with freshly activated 4°A molecular sieves for two days. This procedure was repeated for three times, in order to remove water from the reaction media. Novozyme-435 (200 mg) was dried at 50°C for 3 days in a vacuum oven; the glass reactor was treated with flame under vacuum and closed with rubber septum. Monomer and initiator mixture were added with syringe to the reactor and the reaction proceeded for 8 hours at 80°C. CL/initiator ratio (mole/mole) was 10 and the total mixture was 4.5 g. The reaction was stopped by adding chloroform and enzyme was filtered. Excess chloroform was evaporated from the mixture and the polymer was precipitated via ice-cold methanol for 4 times.

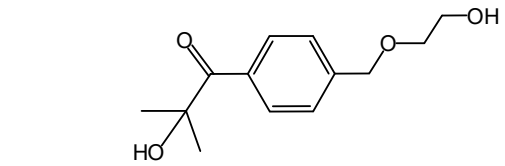

Irgacure-2959

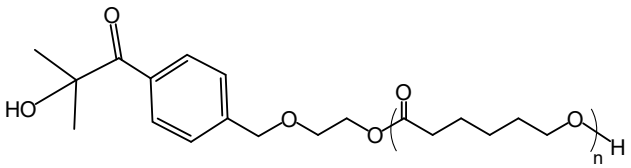

Irgacure-2959 end-functionalized Polycaprolactone (PCL)

Figure 2.7 : Chemical structures of the photoinitiator Irgacure-2959 and Irgacure-2959 end-functionalized PCL macrophotoinitiator.

The resulting polymer was washed with methanol, filtered and dried under vacuum at 30°C for 4 days. The reaction mechanism for general enzymatic ring opening polymerization of ε-caprolactone was demonstrated in Figure 1.26. The structure of Irgacure-2959 and Irgacure-2959 end-capped PCL macrophotoinitiator was shown in Figure 2.7.

Light Emitting Diode (LED) lamps with 360-400 nm wavelength emission were used. 15° of optical lenses were used for focusing. The advantage of the LED lamps is substantial decrease in heating of the reaction medium, prevention of the solvent evaporation, consequent loss of solvent from the reaction medium. The experimental setup for the photopolymerization reactions when BuA, BzA, TFEA and THFA were the acrylate monomers was demonstrated in Figure 2.8. The experimental setup for the photopolymerization reactions when PEGMEA-480 and HEA were the acrylate monomers were shown in Figure 2.5.

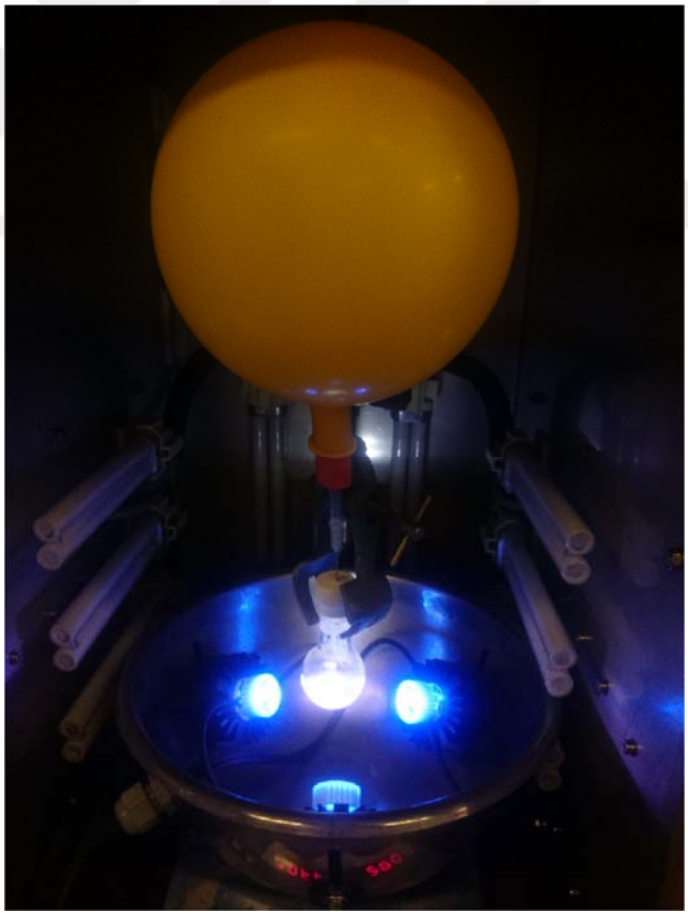

Figure 2.8 : The photopolymerization setup of the reactions made with BuA, BzA, TFEA and THFA.

PCL based macrophotoinitiator, monomer, magnetic stirring bar and 0.4 mL of dimethylacetamide (DMA) were put into a 10 mL snap-capped glass vial. The vial was purged with Ar gas. The mixture was kept at 35°C for 2-3 min and subsequently in ultrasonic bath again for 2-3 min to ensure good solubility of the compounds in the solvent. Then UV polymerization was started; the reaction time was kept as 20 minutes for each monomer. The amount of the macrophotoinitiator was 40 mg, the ratio of acrylate/macromonomer (mole/mole) was kept constant at 200, the reaction time was 20 min, and the solvent amount was 0.4 mL in all photopolymerization experiments.

The resulting polymers were dissolved in chloroform in the case when BuA, BzA, THFA and TFEA were used as monomers and precipitated in ice cold diethyl ether for two times. However, since there was gel formation observed when HEA and PEGMEA were used as monomers, it was not possible to dissolve the polymer networks in chloroform, dichloromethane, dimethylacetamide, dimethylsulfoxide, toluene and tetrahydrofurane. Hence, the gels were rinsed with chloroform and ice cold methanol for several times to remove the residual macrophotoinitiator and the monomers trapped inside. Precipitated polymers and rinsed gels were dried under vacuum oven at 40°C for 2 days.

2.2.6.4 Synthesis of PCL-based terpolymer with of poly(ethylene glycol) methyl ether acrylate-480 and sulfobetaine methacrylate

Synthesis of brominated PCL

The poly(ε-caprolactone) was synthesized via enzymatic ring-opening polymerization at 80°C for 6 hours. The polymerization yield calculated from dry polymer was 23 %. The bromination of the PCL was proceeded similar to a previously reported recipe (Çanak et al, 2012) as follows:

2.5 g PCL was first dissolved in 12.5 mL of dry toluene. Then, 0.100 mL triethylamine was added under the protection of Ar atmosphere and the mixture was cooled in an ice bath at 0°C for 10 min. Under stirring, a solution of 2-bromoisobutyryl bromide (0.315 g in 0.55 mL toluene was added dropwise to the reaction mixture for 30 min. The mixture was kept in an ice–ethanol bath for 30 min, and then stirred at room temperature for 48 h.

The product solution was filtered to remove insoluble salt, concentrated by a rotary evaporator and precipitated into a large excess of cold methanol. The product was

purifed by two rounds of re-precipitation from dichloromethane –methanol, and dried in a vacuum oven overnight at room temperature. Afterwards, the polymer was extracted with 0.1 M $NaHCO_3$ aqueous solution for three times to remove the salt formed during bromination. The final collected organic phase was treated with $Mg(SO_4)$ to remove residual water inside the polymer. Finally the brominated polymer was dried in vacuum oven overnight at 40°C. The synthesis reactions of eROP of CL and the bromination of the enzymatically synthesized PCL were demonstrated in Figure 2.9.

Synthesis of AB type block copolymers of PEGMEA-480 and CL

The brominated PCL was further used as atom-transfer-radical-polymerization (ATRP) macroinitiator to allow PEGMEA-480 polymerization. Toluene was used as the solvent. To conduct the ATRP polymerizations, the solid chemicals (HOOC-PCL-Br, bipyridyl and CuCl) were kept in the main reactor which was a 25 mL round bottom flask. The main reactor and the liquid portion (PEGMEA-480 macromonomer was dissolved in toluene) were deoxygenised with N_2 for 20 minutes. Subsequently, the liquid portion was transferred to the reactor by strictly avoiding any air leakage to the reactor and the liquid portion. The feed molar ratio of the PEGMEA-480 macromonomers to the PCL based macroinitiator was 40. CuCl and bipyridyl ratios to the Br end-groups of the PCL based macroinitiator were kept as 1 and 2 respectively. There were two reaction performed, one for 18 hours and one for 48 hours, both of

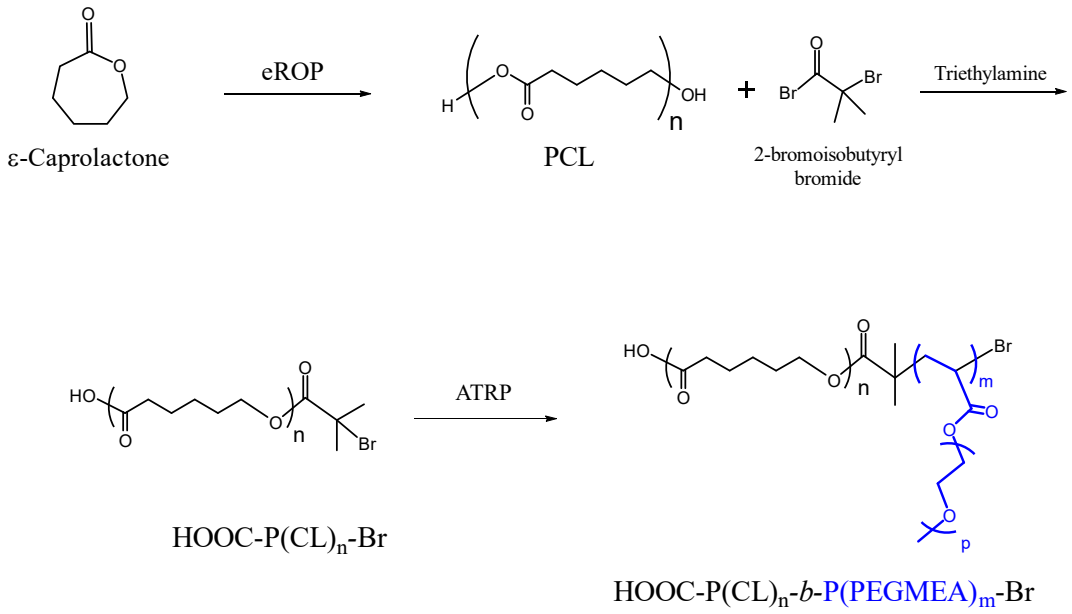

Figure 2.9 : Synthesis reactions of eROP of CL, bromination of the PCL and the ATRP of PEGMEA-480 macromonomer by using PCL based ATRP macroinitiator.

which were at 80°C. The excess toluene was removed via rotary evaporator and the polymer was precipitated in ice-cold hexane for three times and the copper was removed from the polymer by passing the polymer solution through alumina. The solvent (dichloromethane and ethanol mixture) from the polymer solution was further removed via rotary evaporator and polymer was dried afterwards at 40°C for 48 hours. The synthesis reaction was shown in Figure 2.9.

Synthesis of ABC type block copolymers of SBMA, PEGMEA-480 and CL

The AB type copolymer P(CL)$_n$-*b*-P(PEGMEA)$_m$ was further used as atom-transfer-radical-polymerization (ATRP) macroinitiator to allow zwitterionic SBMA polymerization. Ethanol/water mixture (60/40 (v./v.)) was used as the solvent. To

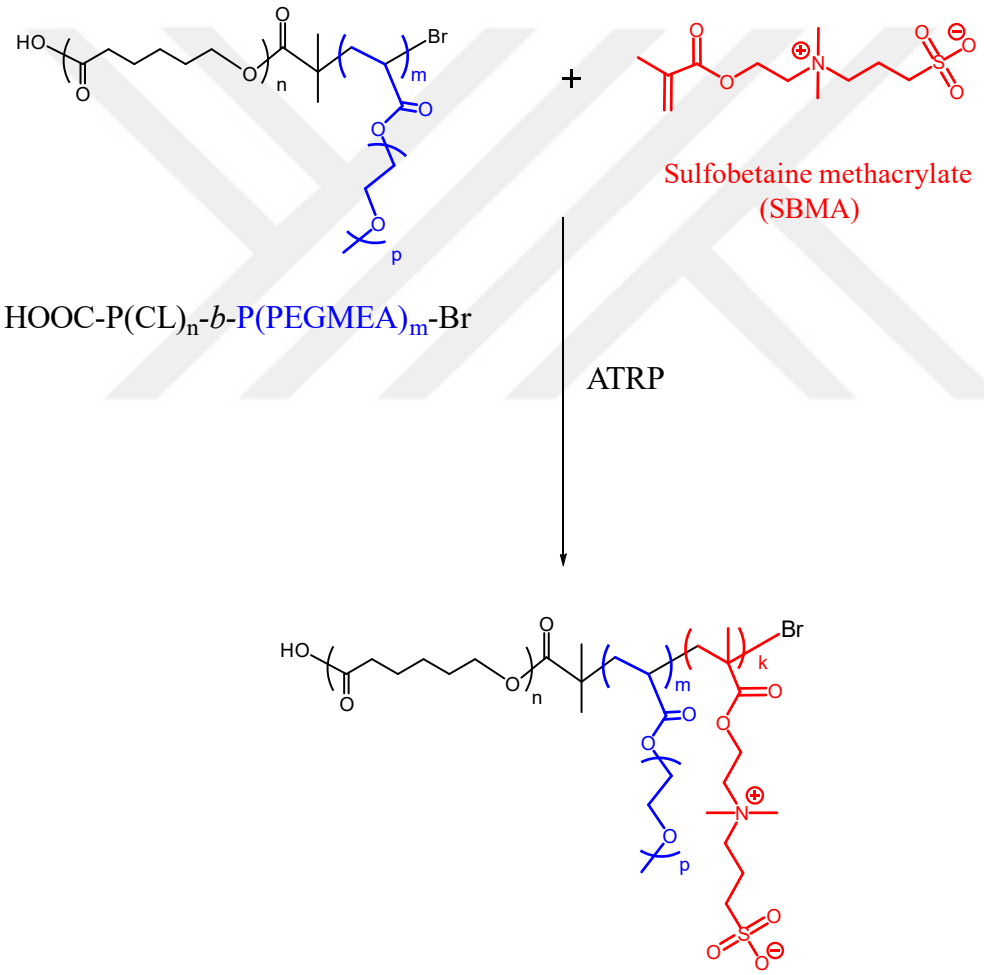

Figure 2.10 : ATRP reaction of SBMA monomer using AB type macroinitiator HOOC-P(CL)$_n$-*b*-P(PEGMEA)$_m$-Br.

conduct the ATRP polymerizations, the solid parts (Bipyridyl and CuCl) were kept in the main reactor which was a 10 mL round bottom flask. The main reactor and the

liquid portion (SBMA monomer and AB macroinitiator were dissolved in ethanol/water mixture) were deoxygenised with N_2 for 20 minutes. Subsequently, the liquid portion was transferred to the reactor by strictly avoiding any air leakage to the reactor and the liquid portion. The feed molar ratio of the SBMA monomer to the AB type macroinitiator was 100. CuCl and bipyridyl ratios to the Br end-groups of the AB type macroinitiator were kept 1 and 2 respectively. The reaction was performed for 24 hours at 80°C. The residual SBMA monomer was removed from the reaction mixture via dialysis for 2 days by changing the dialysis water 6 times per day and the copper was removed from the polymer by passing the polymer solution through alumina. The solvent (chloroform, methanol and ethanol mixture) from the polymer solution was further removed via rotary evaporator and polymer was dried afterwards at 40°C for 48 hours. In Figure 2.10, the reaction scheme of ABC type block copolymer can be found.

3. RESULTS AND DISCUSSION

3.1 HEMA Initiated PCL via eROP

The characteristic peaks of the structures illustrated in Figure 1.22 and 3.1 were as follows: for HEMA end-groups, **h** (4H, m, CH_2=C(CH_3)C(O)O***C*H₂*C*H₂***OCH₂-) δ = 4.31–4.38 ppm; for methacrylate end-groups, **m** (2H, t, -CH_2***C*H₂***OC(O)C(CH_3)=CH_2) δ = 4.12–4.17 ppm; for CL repeating units along the chains, **c** (2H, t, -CH_2***C*H₂***OCO-) δ=4.01–4.12 ppm; for EG inside the chains, **e** (4H, s, -CH_2C(O)O***C*H₂*C*H₂***OC(O)CH_2-) δ=4.27–4.30 ppm; **v** (2H, m, HO***C*H₂***CH_2OC(O)CH_2-) δ= 3.81–3.86 ppm; for hydroxyl groups adjacent to aliphatic methylenes of CL unit, **w** (2H, t, -CH_2***C*H₂***OH) δ = 3.62–3.70 ppm; for double-bond hydrogens of HEMA end-functionalities; $\mathbf{x_1}$ and $\mathbf{y_1}$ (1H each, s, ***C*H₂***=C(CH_3)C(O)OCH_2CH_2O-) δ = 6.12–6.15 ppm and δ = 5.58–5.63 ppm, respectively; for vinylic H atoms of methacrylate end-groups, $\mathbf{x_2}$ and $\mathbf{y_2}$ (1H each, s, ***C*H₂***=C(CH_3)C(O)OCH_2CH_2-) δ = 6.08–6.11 ppm and δ = 5.53–5.57 ppm, respectively (Kaya and Guvenilir, 2015).

The quantitative evaluation of the end-groups of macromonomers was performed using the peak areas achieved via ^{1}H NMR measurements. HEMA, methacrylate, total methacrylate, hydroxyl end-groups, and ethylene glycol (EG) inside the chains were calculated as it was demonstrated in Equation 3.1-3.4. In calculations, the peak areas acquired with vinylic protons of HEMA and methacrylate groups ($\mathbf{x_1}$ and $\mathbf{x_2}$ or $\mathbf{y_1}$ and $\mathbf{y_2}$) had almost the same results with those demonstrated as **h** and **m** (Kaya and Guvenilir, 2015).

$$HEMA\ end\text{-}groups = \frac{(h/4)}{((h/4)+(m/2)+(v/2)+(w/2))} \tag{3.1}$$

$$Methacrylate\ end\text{-}groups = \frac{(m/2)}{((h/4)+(m/2)+(v/2)+(w/2))} \tag{3.2}$$

$$Total\ methacrylate\ end\text{-}groups = \frac{(h/4) + (m/2)}{((h/4)+(m/2)+(v/2)+(w/2))} \quad (3.3)$$

$$Hydroxyl\ end\text{-}groups = \frac{(v/2) + (w/2)}{((h/4)+(m/2)+(v/2)+(w/2))} \quad (3.4)$$

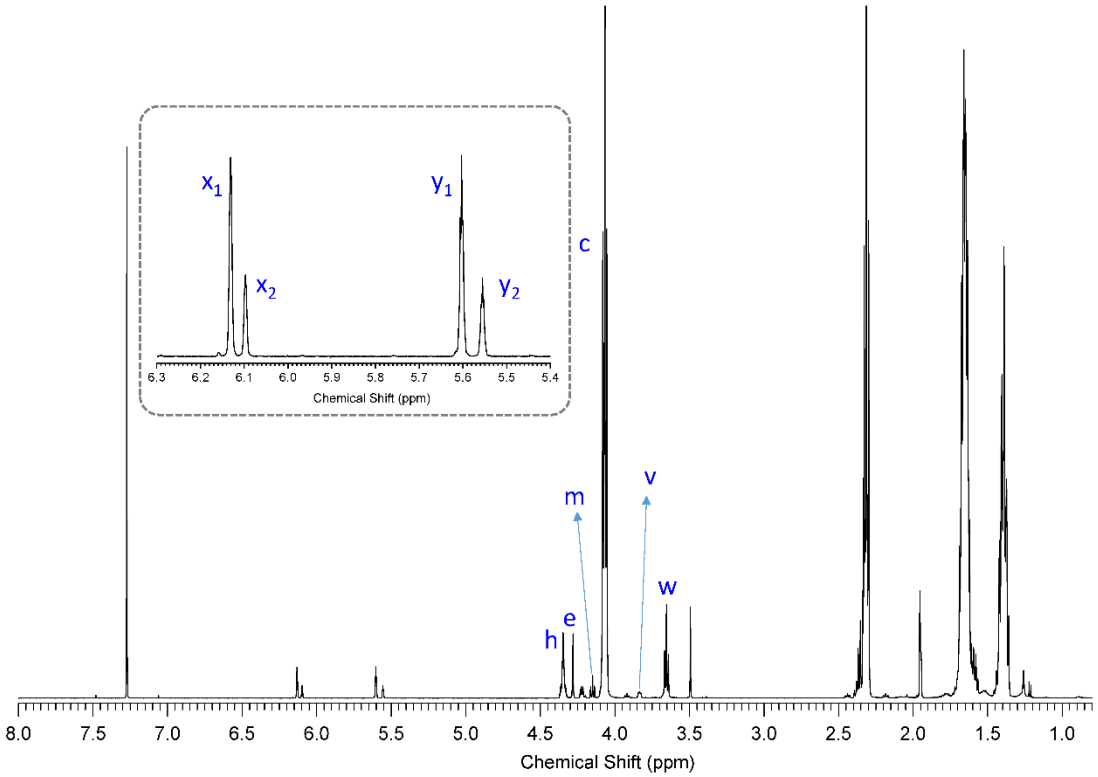

Figure 3.1 : ^{1}H NMR demonstration of the dried macromonomer synthesized at 70°C, 4 h, 100mg N435, 0.2 HEMA/CL (mmole/mmole), and 45mmole CL.

3.1.1 The effect of reaction time

Macromonomers synthesized at 70°C, with 100 mg N435 and 9 mmole/45 mmole HEMA/CL ratio were obtained at 4 different reaction times (2h, 3h, 5h, and 6h). 2h reaction had the lowest number average molecular weight ($\overline{M_n}$) (2116 g/mole) and 6 h reaction had the highest $\overline{M_n}$ (3049 g/mole). Polydispersity index (PDI) ($\overline{M_w}/\overline{M_n}$) raised from 1.13 to 1.21 through the reaction proceeded from 2h to 6h (Figure 2.2). The polymerization yields for the reactions were 6.6%, 9.4%, 17.7%, and 21.5% for 2h, 3h, 5h, and 6h, respectively (Kaya and Guvenilir, 2015).

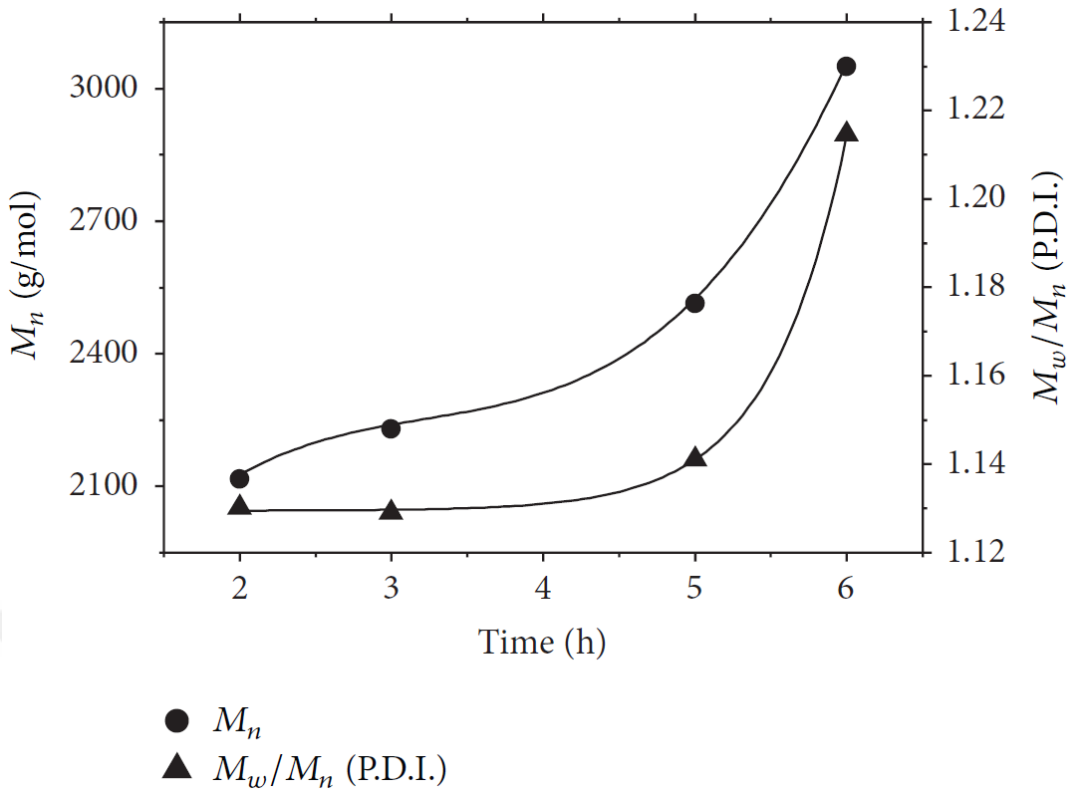

Figure 3.2 : The effect of reaction time on $\overline{M_n}$ and PDI at 2h, 3h, 5h and 6h (Kaya and Guvenilir, 2015).

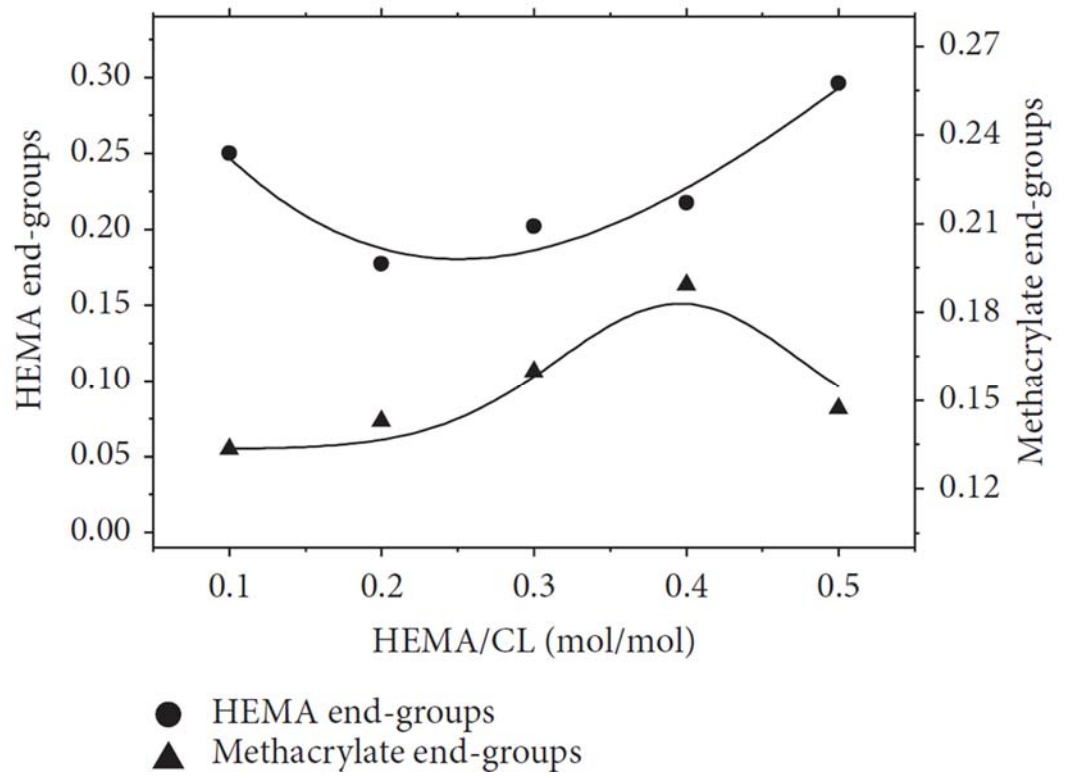

Figure 3.3 : The effect of reaction time on HEMA and methacrylate end-groups formation at 2h, 3h, 5h and 6h (Kaya and Guvenilir, 2015).

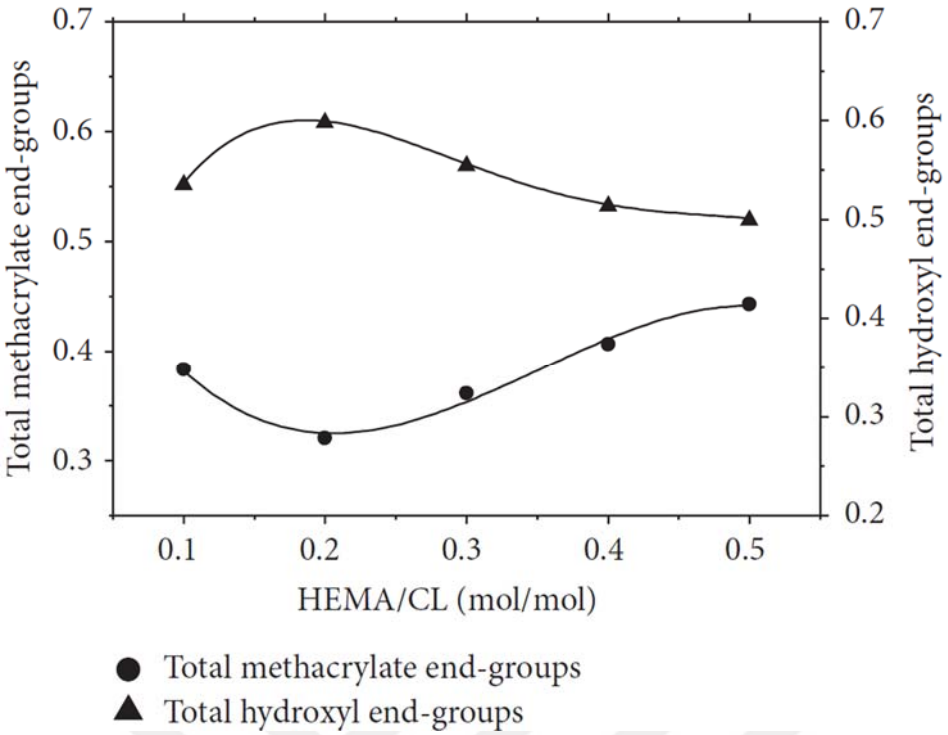

Figure 3.4 : The effect of reaction time on total methacrylate and hydroxyl end-group formation at 2h, 3h, 5h and 6h (Kaya and Guvenilir, 2015).

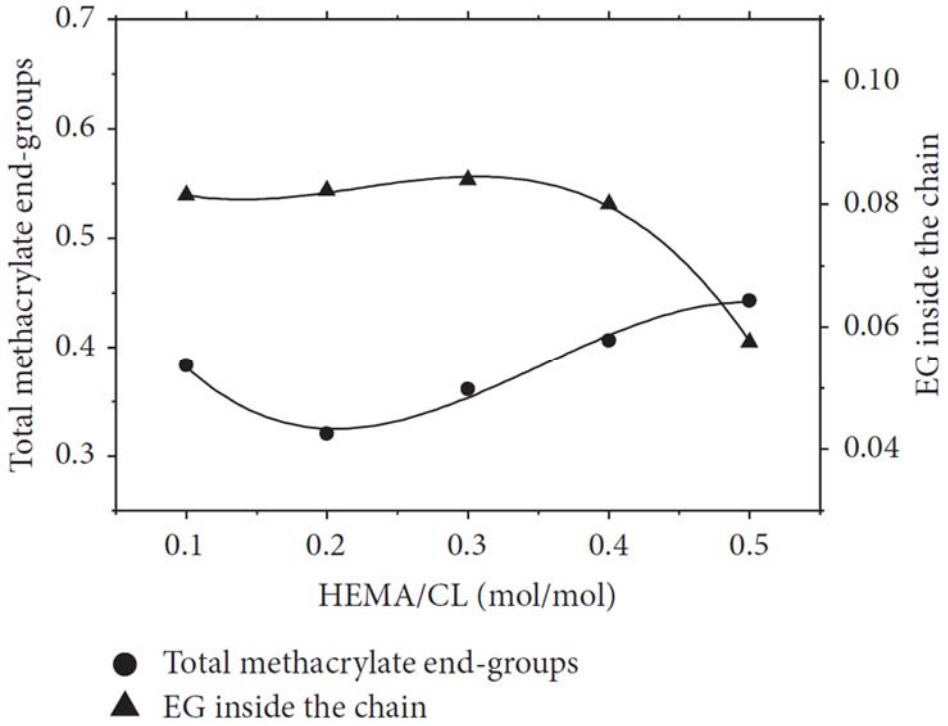

Figure 3.5 : The effect of reaction time on total methacrylate and EG inside the chains formation at 2h, 3h, 5h and 6h (Kaya and Guvenilir, 2015).

It can be seen (Figure 3.3) that, even at 2h, the macromonomers which comprised HEMA (0.235) end-groups together with remarkable amount of methacrylate end-groups (0.124) revealed the first side reaction (methacrylate transfer) had been

progressing in the early parts of polymerization. At 3h, there were a maximum point of HEMA end-groups (0.289) and a minimum point of the methacrylate endgroups (0.113). Afterwards, the HEMA end-groups decreased and methacrylate transfer began increasing as the reaction proceeded. Besides, the total methacrylate end-groups showed a resembling trend with the HEMA end-groups (Figure 3.4 and 3.5). The hydroxyl end-groups demonstrated a minimum point between 3h and 5h and subsequently increased. EG inside the chains mounted for longer reaction times indicates that the secondary side reaction became more obvious (Figure 3.5). Approximately in the first 3h of the reaction the HEMA addition seemed to be rising faster than methacrylate transfer. On the other hand, after 3h, the methacrylate transfer (the first side reaction) became more dominant than HEMA initiation of the enzyme-monomer complex (EM). Concurrently, the total methacrylate end-groups, which is the sum of HEMA and methacrylate (product of the first side reaction) end-groups, and hydroxyl end-groups had coherent trends as the endgroups might either be a methacrylate type (**h** and **m**) or a hydroxyl type (**v**, **w**). The diminish in total methacrylates might be caused by concurrent deceleration of HEMA initiation and higher rate of reactions which ended with hydroxyl end-groups than methacrylate end-groups during acyl transfer to methacrylate (first side reaction) (Kaya and Guvenilir, 2015).

3.1.2 The effect of HEMA/CL ratio

The effect of HEMA/CL (mole/mole) ratio was investigated at two different temperatures (60°C and 70°C) and two different enzyme amounts (100mg and 200mg). In this section, only the effect of HEMA/CL (mole/mole) ratio (at two different enzyme amounts (100mg and 200mg)) was investigated. In Figure 3.6, it could be seen that the HEMA/CL ratio was altered between 0.1 and 0.5 (mmole/mmole) at 70°C, 6 hours of reaction, and 9/45 (mmole/mmole) of HEMA/CL. $\overline{M_n}$ and polydispersity had a declining trend as the initiator amount increased in the medium which increased the chain number, converging the chain sizes. The polydispersity between 0.1 and 0.5 HEMA/CL ratios had values between 1.23 and 1.08. The polydispersity at 0.5 HEMA/CL ratio had a remarkable value as 1.08 which might be comparable with that of a controlled radical polymerization product. This behavior was again attributed to the difficulty in purifying the polymer and loss of low molecular weight oligomers. On the other hand, the polymerization yield of the 0.1, 0.2, 0.3, 0.4, and 0.5 HEMA/CL

was 27.6%, 21.5%, 15.0%, 13.8%, and 11.2%, respectively. The dry polymer weight was descending as the HEMA/CL was increasing. This trend might be due to higher number of polymer chains in higher initiator/monomer ratios, since chains having lowest molecular weight (e.g., dimers, trimers) might be lost during polymer purification (Kaya and Guvenilir, 2015).

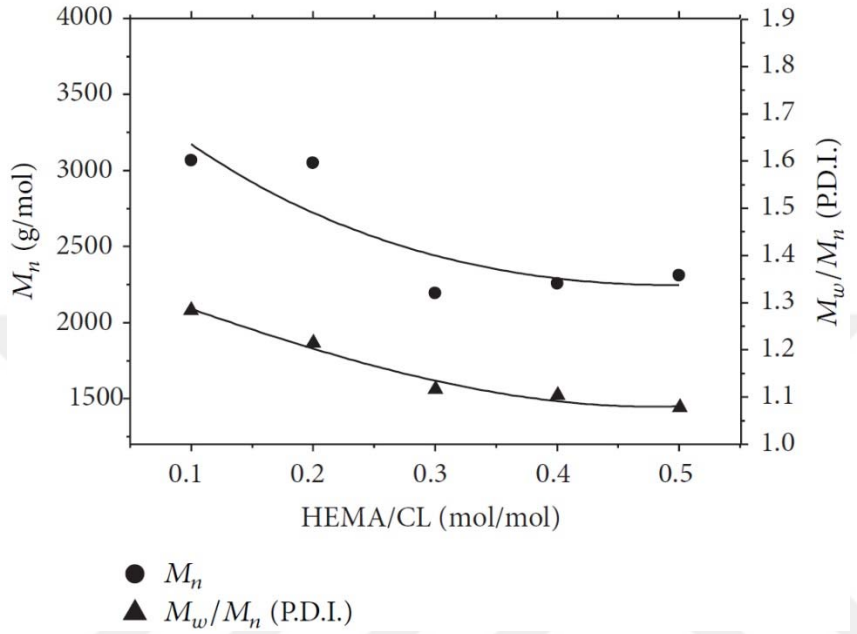

Figure 3.6 : The effect of HEMA/CL (mole/mole) ratio on $\overline{M_n}$ and PDI at 70°C, 6h and with 100mg N435 (Kaya and Guvenilir, 2015).

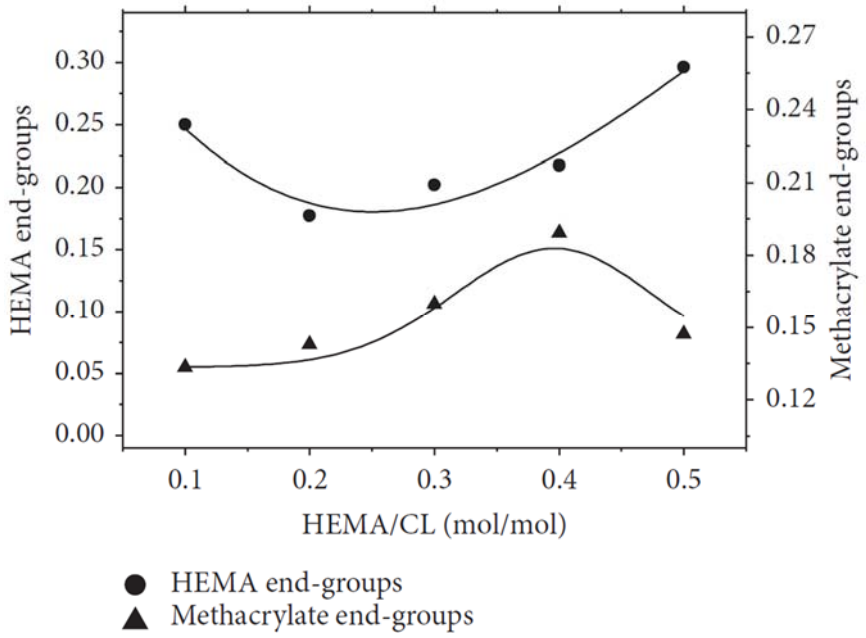

Figure 3.7 : The effect of HEMA/CL (mole/mole) ratio on HEMA and methacrylate end-groups at 70°C, 6h and with 100mg N435 (Kaya and Guvenilir, 2015).

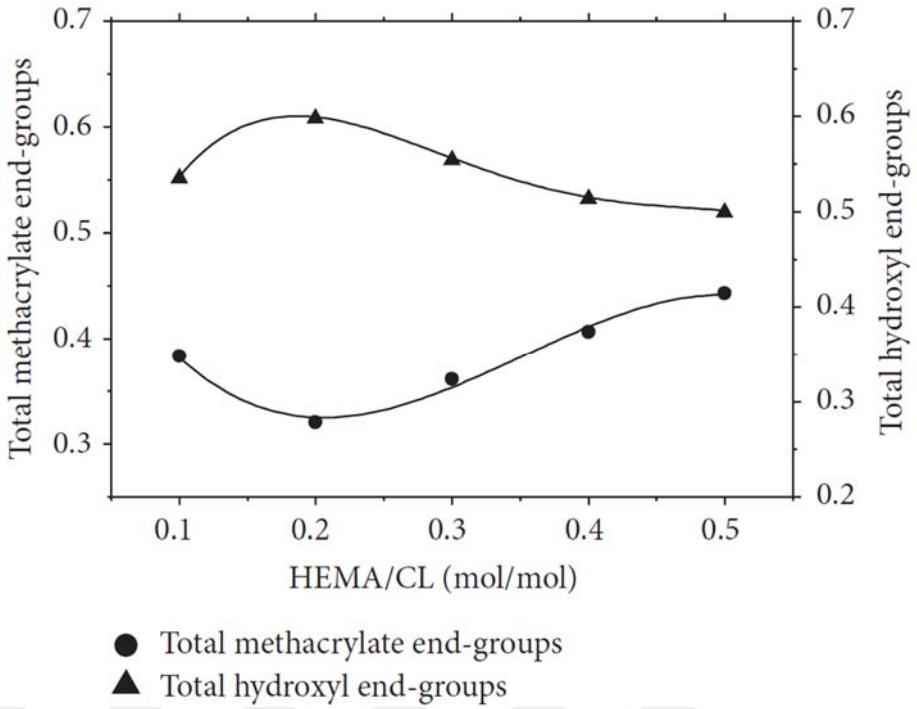

Figure 3.8 : The effect of HEMA/CL (mole/mole) ratio on total methacrylate and total hydroxyl end-groups at 70°C, 6h and with 100mg N435 (Kaya and Guvenilir, 2015).

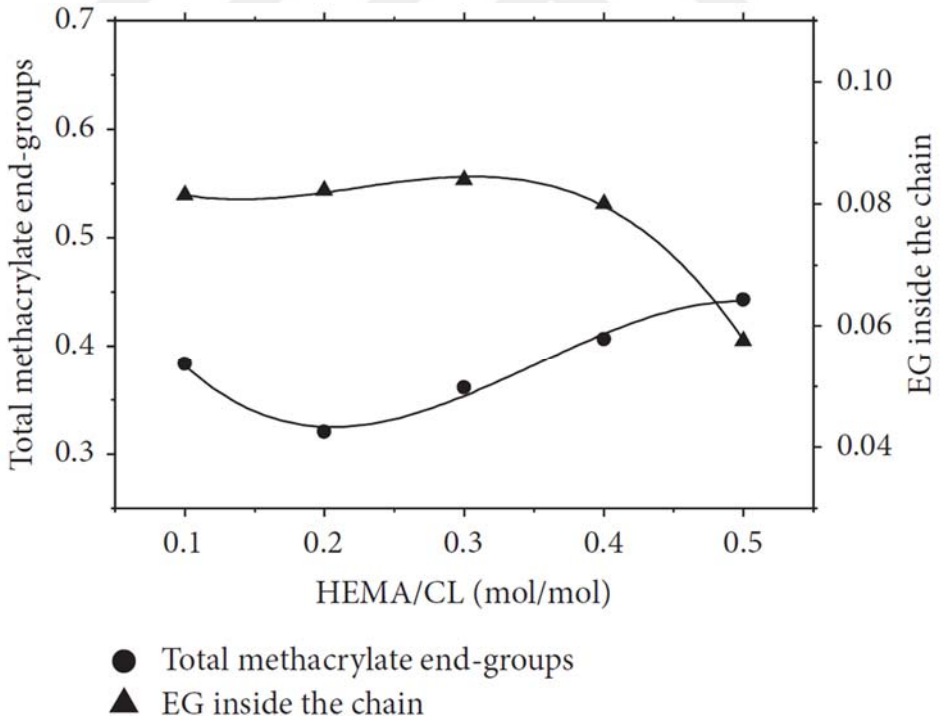

Figure 3.9 : The effect of HEMA/CL (mole/mole) ratio on total methacrylate end-groups and EG inside the chains formation at 70°C, 6h and with 100mg N435 (Kaya and Guvenilir, 2015).

For the reactions conducted at 70°C and with 100mg N435, the HEMA addition performed a parabolic-like curve having closed values of 0.250 at 0.5 HEMA/CL and

0.296 at 0.1 HEMA/CL. The minimum value for HEMA addition seemed to be between 0.2 and 0.3 HEMA/CL ratio. The methacrylate end-groups had a maximum at 0.4 HEMA/CL ratio. The gap between the HEMA and methacrylate endgroups had the highest value at 0.5 and lowest values at 0.4 HEMA/CL ratio (Figure 3.7). Consistently, the hydroxyl end-groups had a curve resembling the x-axis symmetry of the trend of total methacrylate end-groups. The total methacrylate end-groups had a similar trend with the HEMA end-groups representing a minimum at 0.2 HEMA/CL ratio (Figure 3.8). The EG inside the chains had no significant difference within 0.1 and 0.4, although there was a steep decrease at 0.5 HEMA/CL ratios. This might be the result of the influence of polyester transfer which became lesser as well as the methacrylate transfer and the enzyme continued to participate in the addition of HEMA onto the PCL chains and propagation (Figure 3.9). The side reactions could be observed not only at the propagating polymer chains but also at the monomers.The side products might also be 1,2-ethanediol methacrylate and EG (Kaya and Guvenilir; Takwa et al, 2008a). Thus, at the excess amount of the ester comprising initiator, it was a possibility of the enzyme to prefer attacking the methacrylate monomer rather than the edge of the propagating chains. Consequently, it is encouraging to study at low HEMA/CL ratios or at excess HEMA amounts (Kaya and Guvenilir, 2015).

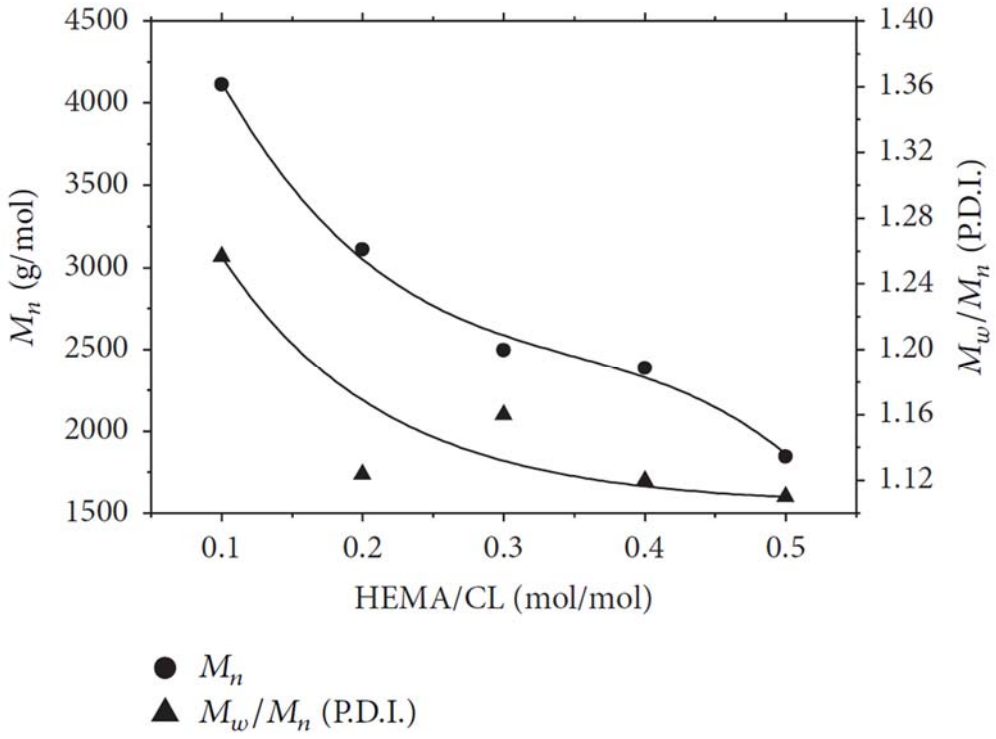

Figure 3.10 : The effect of HEMA/CL (mole/mole) ratio on $\overline{M_n}$ and PDI at 70°C, 6h and with 200mg N435 (Kaya and Guvenilir, 2015).

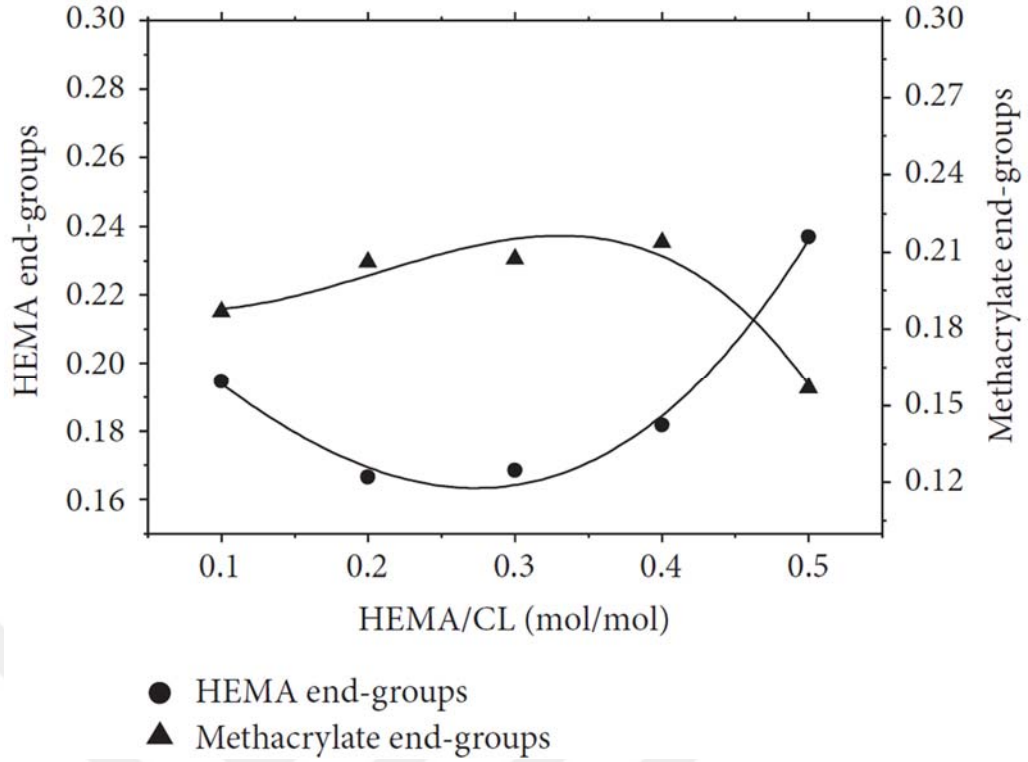

Figure 3.11 : The effect of HEMA/CL (mole/mole) ratio on HEMA and methacrylate end-groups at 70°C, 6h and with 200mg N435 (Kaya and Guvenilir, 2015).

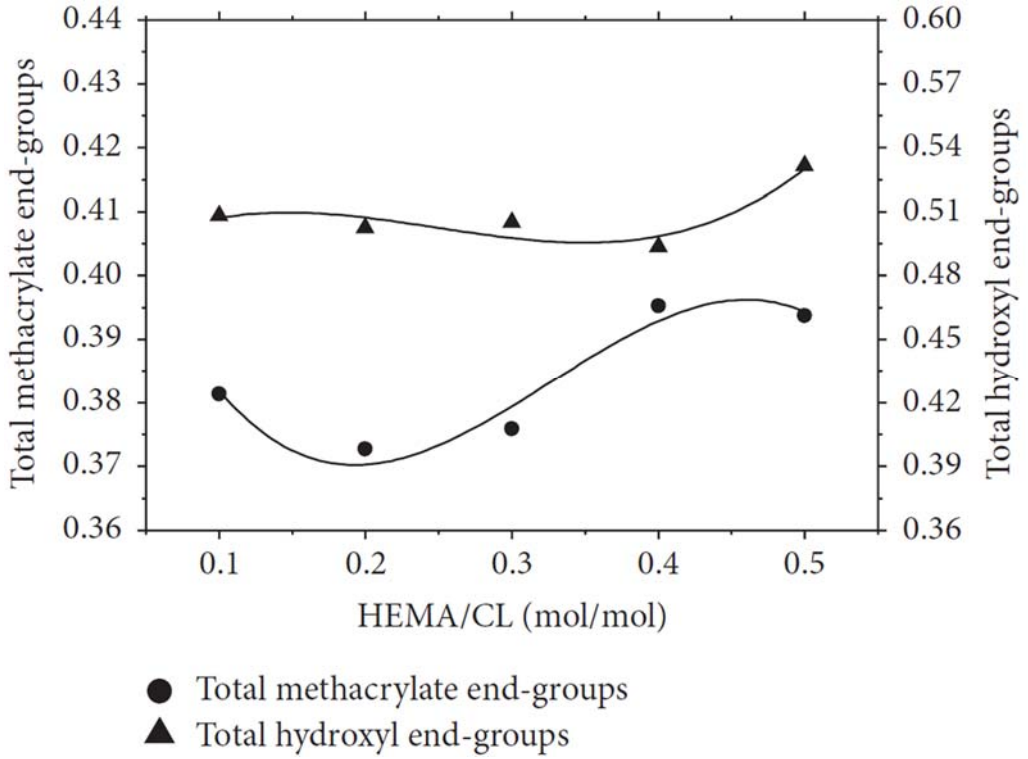

Figure 3.12 : The effect of HEMA/CL (mole/mole) ratio on total methacrylate and total hydroxyl end-groups at 70°C, 6h and with 200mg N435 (Kaya and Guvenilir, 2015).

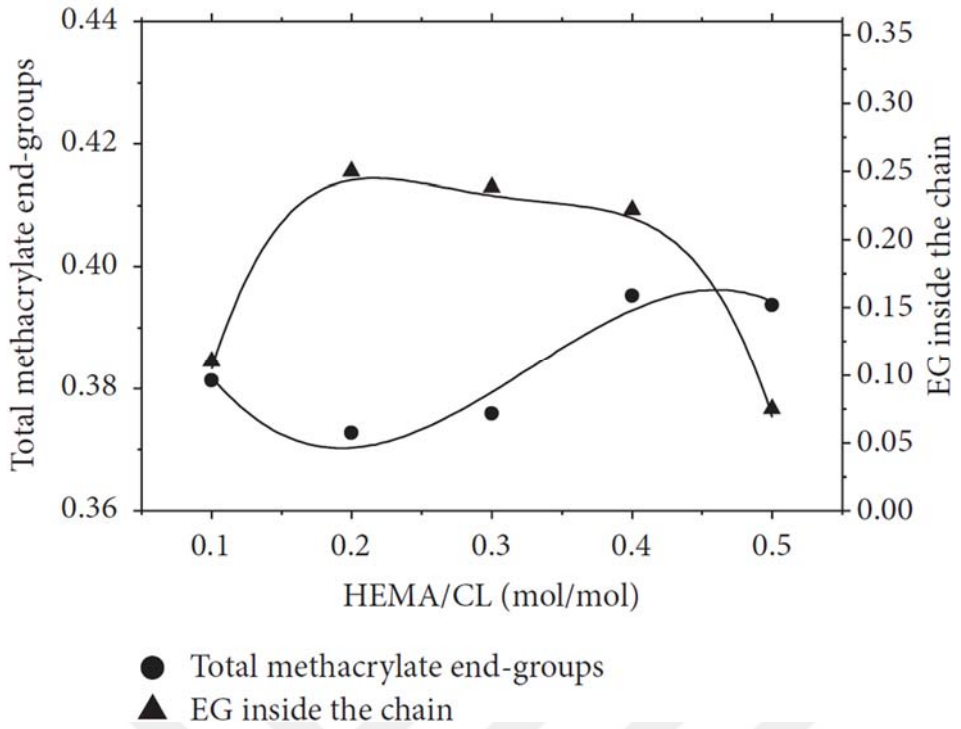

Figure 3.13 : The effect of HEMA/CL (mole/mole) ratio on total methacrylate end-groups and EG inside the chains formation at 70°C, 6h and with 100mg N435 (Kaya and Guvenilir, 2015).

As the N435 amount was increased to 200mg from 100mg, the other reaction parameters were kept the same (70°C, 6 hours, and 9/45 (mmole/mmole) of HEMA/CL). In Figure 3.10, it was shown that $\overline{M_n}$ and PDI were decreasing as the initiator/monomer ratio was increasing, similar to that of the 100mg reaction. Additionally, the $\overline{M_n}$ value was higher for the 200 mg reaction, essentially the result of the increase of propagation ability at higher enzyme amount. The PDI was 1.10 for 0.2 HEMA/CL ratio. Dry polymer weight of the polymers was 33.6%, 31.9%, 28.1%, 19.7%, and 15.3% for 0.1, 0.2, 0.3, 0.4, and 0.5 of HEMA/CL, respectively. The same trend of the polymerization yield is similar to that of the reactions conducted with 100mg enzyme. Nevertheless, enzyme amount had the effect of increasing the polymerization yield (Kaya and Guvenilir, 2015).

The HEMA addition was also a parabolic-like curve having closed values of 0.237 at 0.5 HEMA/CL and 0.195 at 0.1 HEMA/CL. The minimum value for HEMA addition was 0.167 at 0.2 initiator/monomer. Likewise, the methacrylate end-groups demonstrated a peak behavior between 0.2 and 0.4 initiator/lactone ratio resembling a similar trend with the inverse of the HEMA addition as the first side reaction (the methacrylate transfer) was the consequence of cleavage of the ester bond on HEMA

end-group, transferring as the methacrylate end-group (Figure 3.11). The total methacrylate end-group had no remarkable change, having the highest value of 0.373 and minimum value of 0.395 at 0.2 and 0.4 HEMA/CL ratios, respectively (Figure 3.12 and 3.13). On the other hand, the total hydroxy end-groups had almost a constant trend along with the altered HEMA/CL ratio (Figure 2.12). In spite of the fact that there was an insignificant change in total methacrylate end-groups, the EG inside the chains had a major amount of variations as the highest value is 0.249 (0.2 HEMA/CL) and the lowest value was 0.075 (0.5 HEMA/CL). It is worth to mention that this value was 0.110 at 0.1 initiator/lactone ratio which was relatively close to the lowest value (Figure 3.13). Obviously, at 0.1 and 0.5 initiator/lactone ratios, both of the side reactions seemed to be less dominant than the other values (Kaya and Guvenilir, 2015).

3.1.3 The synergetic effect of temperature and initiator/lactone ratio

In Figure 3.14-3.17, the comparison of the influence of two different temperatures (at 60°C and 70°C), while the HEMA/CL (mole/mole) ratio changed was demonstrated.

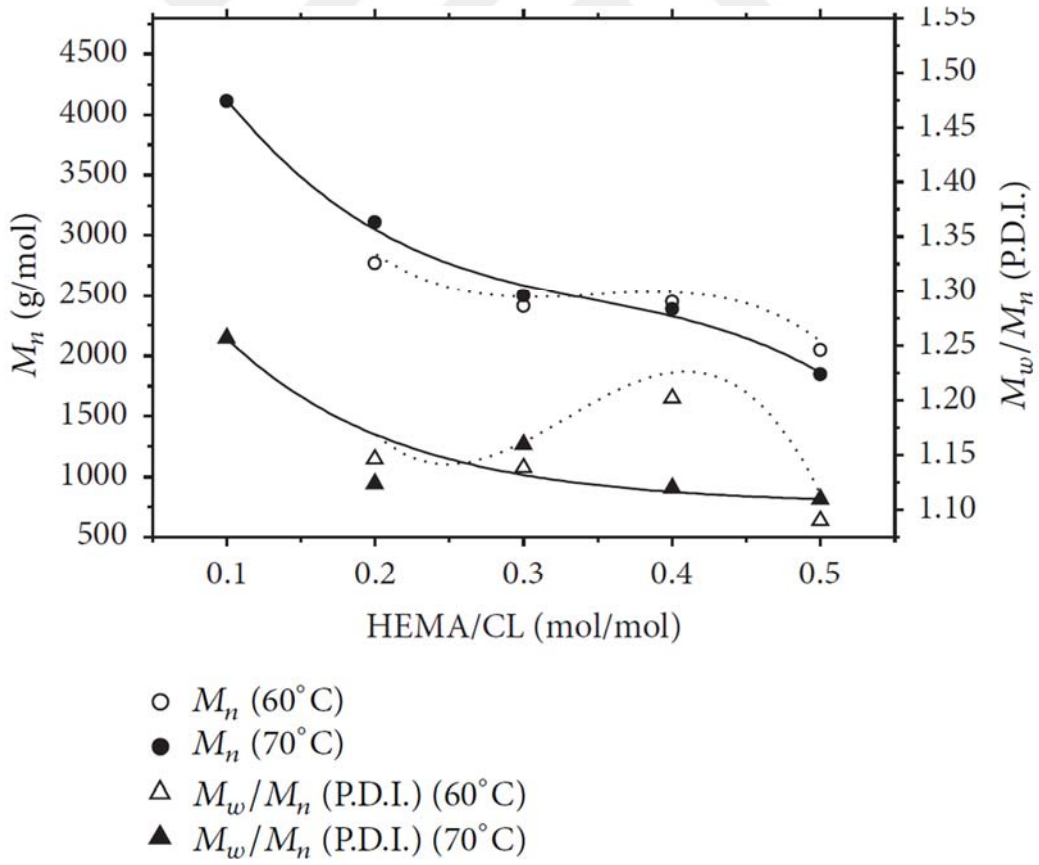

Figure 3.14 : The effect of HEMA/CL (mole/mole), at 60°C and 70°C, on $\overline{M_n}$ and PDI (Constant paratmeters were 6 hours, and 200mg/45mmole N435/CL) (Kaya and Guvenilir, 2015).

The constant reaction parameters were the reaction time and the enzyme amount/lactone ratio at 6 hours and 200mg/45mmole N435/CL respectively. The enzyme amount was kept high in order to investigate the effect of parameters more obviously. The $\overline{M_n}$ values were close together at all values of HEMA/CL ratio that resemble the PDI except for the maximum point at 0.4 HEMA/CL ratio for both temperatures. Polymerization yields were calculated as 24.7%, 21.9%, 14.6%, and 11.5 for 0.5, 0.4, 0.3, and 0.2 HEMA/CL ratios at the 60°C reactions. The polymerization yield had a diminishing trend inversely to the initiator/lactone ratio which is in parallel with the 70°C reactions (Kaya and Guvenilir, 2015).

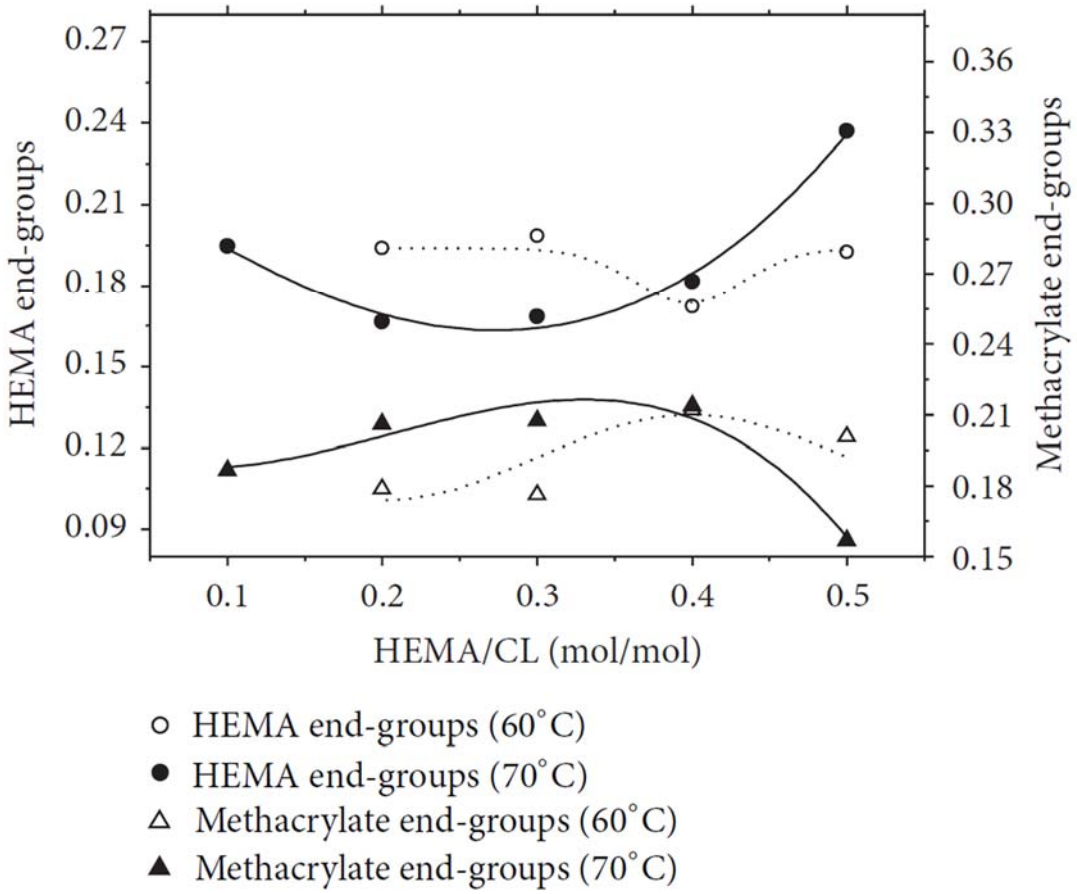

Figure 3.15 : The effect of HEMA/CL (mole/mole), at 60°C and 70°C, on HEMA and methacrylate end-groups (Constant paratmeters were 6 hours, and 200mg/45mmole N435/CL) (Kaya and Guvenilir, 2015).

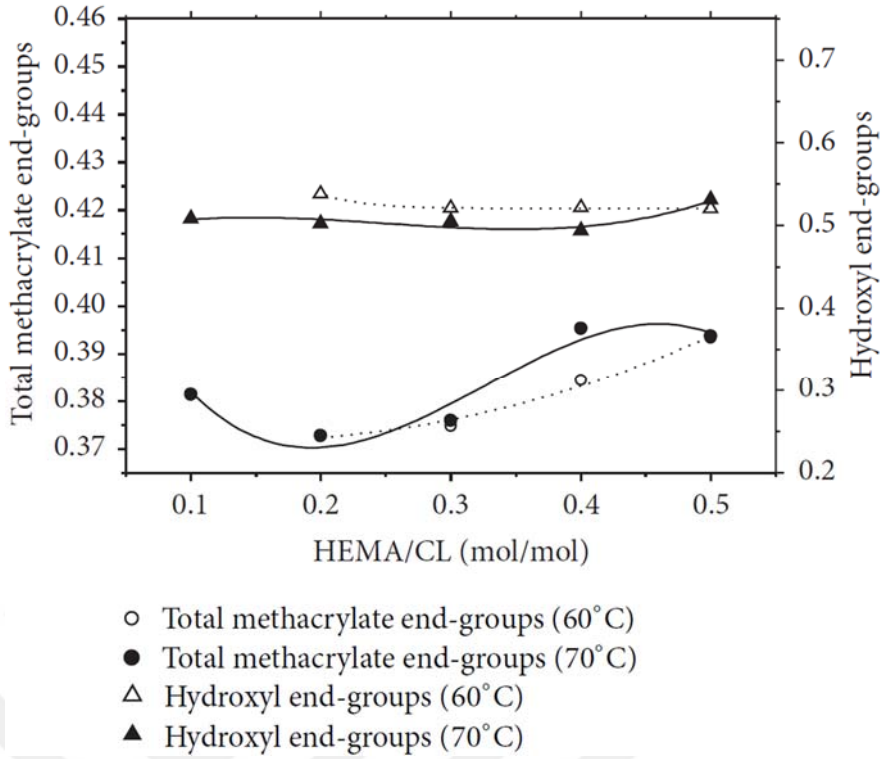

Figure 3.16 : The effect of HEMA/CL (mole/mole), at 60°C and 70°C, on total methacrylate and hydroxyl end-groups (Constant paratmeters were 6 hours, and 200mg/45mmole N435/CL) (Kaya and Guvenilir, 2015).

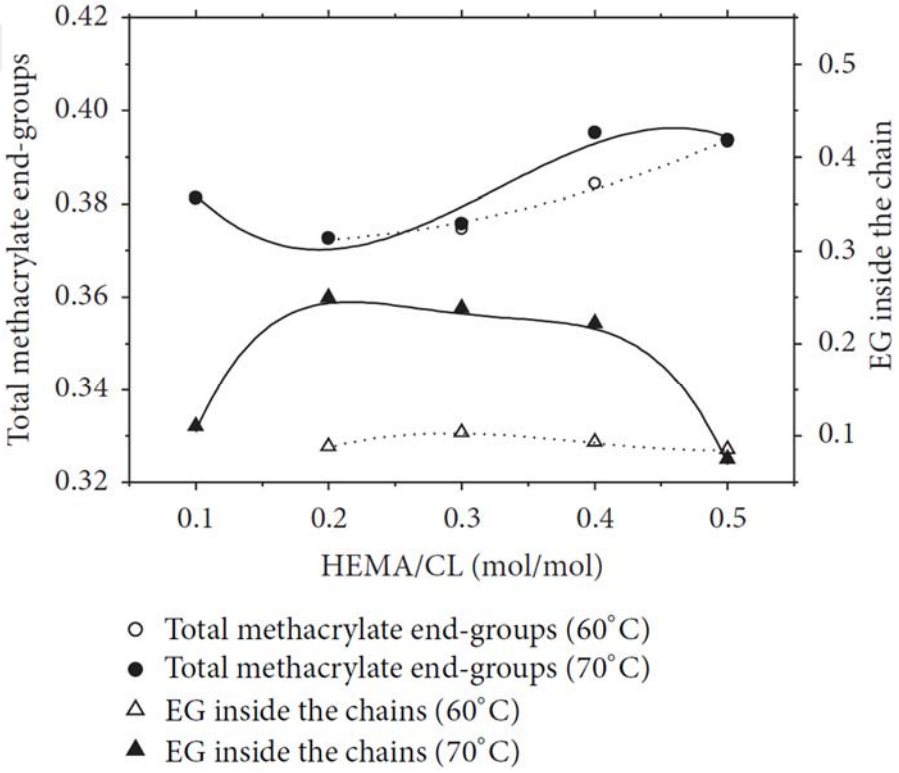

Figure 3.17 : The effect of HEMA/CL (mole/mole), at 60°C and 70°C, on total methacrylate end-groups and EG inside the chains (Constant paratmeters were 6 hours, and 200mg/45mmole N435/CL) (Kaya and Guvenilir, 2015).

For HEMA and methacrylate end-groups, the minimum point of HEMA addition and the maximum point of methacrylate end-groups were at 0.4 HEMA/CL ratio for the reactions at 60°C. It was noted that this convergence seemed to be apparent in between 0.2 and 0.4 (probably close to 0.3) for the reactions at 70°C. Additionally, the gap between the highest and lowest values for HEMA and methacrylate end-groups were higher at 70°C reactions (Figure 3.15). The hydroxyl end-group formation proceeded almost constantly and at close values with the changing HEMA/CL functionality for 60°C and 70°C reactions (Figure 3.16). The total methacrylate end-groups also had a similar ascending trend with small differences except for the 0.4 HEMA/CL ratio, in which the 70°C reaction gave a slightly higher amount. On the other hand, while the EG inside the chains had a high variation at 70°C, there was a relatively lower difference of this value at 60°C as the initiator/lactone increased (Figure 3.17). Hence, it might be favorable to perform the reactions at lower temperatures.

All of the indications revealed that N435 had high activity enough to catalyze EM formation, initiation, and propagation, cleaving the ester bond of the hydroxyl bearing acrylate initiator at the same time. Therefore, it might to be preferable to study at lower reaction temperatures to reduce the side reactions inside the sufficient activity range of N435 or other lipase types. In the first two hours of reaction, approximately the same amount of HEMA was successfully introduced into macromonomers with the sixth hour of reaction; HEMA addition only increased until the third hour and tended to diminish in the following hours. Total methacrylate end-groups had also increased up to three hours, following a decrease along with reaction time. EG inside the chains, which is the indicator of polyester transfer, increased with time. Thus, as the reaction progressed, the first side reaction (methacrylate transfer) increased, the total methacrylate end-groups did not change remarkably or diminished, and the second side reaction (polyester transfer) increased. It is obvious to finalize the eROP at low reaction times and conversions in order to obtain lower side reactions and comparable HEMA addition. Furthermore, the lower enzyme amount might be preferable in order to realise higher HEMA addition, lower methacrylate transfer, comparable total methacrylate end-groups, and minimum EG inside the chains. HEMA/CL ratio can also be chosen minimum as both of the side reactions seemed to be lower at both temperatures and enzyme amounts, still conserving the total methacrylate amount sufficient. In addition to these, higher molecular weight and polymerization yield of

macromonomers can be obtained at lower initiator/lactone ratios. There might be further investigation of the effects of lower conversions, temperatures, and HEMA/CL ratios and less active lipases on the addition of HEMA onto the edge of PCL macromonomers with minimized side reactions.

3.2 Photopolymerization of poly(Ethylene glycol) methyl ether methacrylate with α,ω-methacrylated PCL

Since, the methacrylation reactions occured in a resembling way to that of the HEMA initiated PCL synthesis via eROP, the ^{1}H NMR assignments were conducted likewise. Therefore, the characteristic peaks of the structures were briefly referred in Figure 3.18. There were 4 different end-groups occured. These 4 different end-groups might have existed in different combinations in PCL chains. The assignments were: **a_1** and **b_1** (1H each, s, *C**H**₂*=C(CH₃)(C=O)OCH₂CH₂O-) δ=6.12–6.15 ppm and δ=5.58–5.63 ppm, respectively; **a_2** and **b_2** (1H each, s, *C**H**₂*=C(CH₃)(C=O)OCH₂CH₂CH₂CH₂CH₂-) δ=6.08–6.11 ppm and δ=5.53–5.57 ppm, respectively; **c** (4H, m, CH₂=C(CH₃)C(O)O*C**H**₂C**H**₂*OCH₂-) δ=4.31–4.38 ppm; **f** (4H, s, -CH₂(C=O)O *C**H**₂C**H**₂*O(C=O)CH₂-) δ=4.27–4.30 ppm; **d** (2H, t, -CH₂*C**H**₂*O(C=O)C(CH₃)=CH₂) δ=4.12–4.17 ppm; **5** (2H, t, -O(C=O)CH₂CH₂CH₂CH₂*C**H**₂*-O(C=O)-) δ=4.01–4.12 ppm; **g** (2H, m, HO*C**H**₂*CH₂O(C=O)CH₂-) δ=3.81–3.86 ppm; **h** (2H, t, -CH₂CH₂CH₂CH₂*C**H**₂*OH) δ=3.62–3.70 ppm; **1** (2H, t, -O(C=O)*C**H**₂*CH₂CH₂CH₂CH₂-O(C=O)-) δ= 2.26–2.40 ppm; **e** (3H, s, -CH₂=C(*C**H**₃*)(C=O)O-) δ=1.93–1.96 ppm; **2, 4** (4H, m, -O(C=O)CH₂*C**H**₂*CH₂*C**H**₂*CH₂-O(C=O)-) δ=1.56–1.74 ppm; **3** (2H, m, -O(C=O)CH₂CH₂*C**H**₂*CH₂CH₂-O(C=O)-) δ =1.35–1.47 ppm.

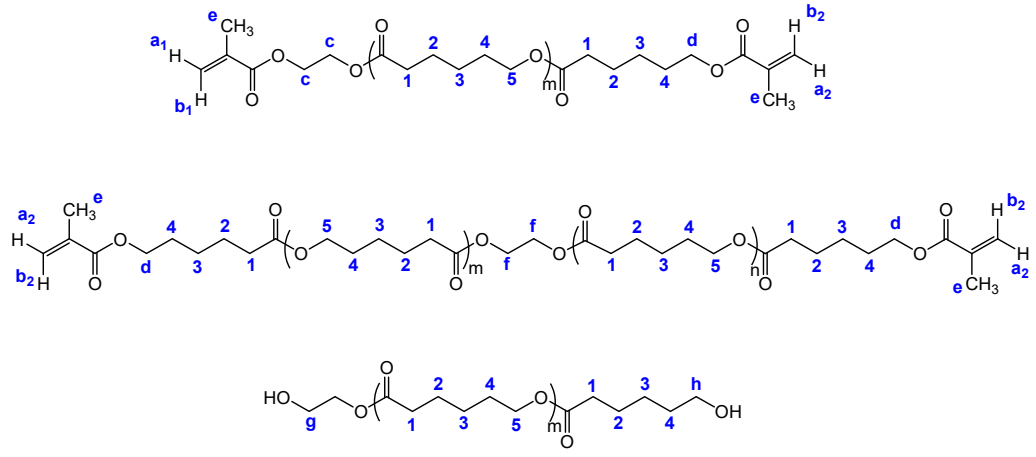

Figure 3.18 : Representation of the end-groups occuring during the eROP synthesis of DMPCL (Takwa et al, 2008b; Xiao et al, 2009).

The ^{1}H NMR spectrums of DMPCL were depicted in Figure 3.19-3.20.

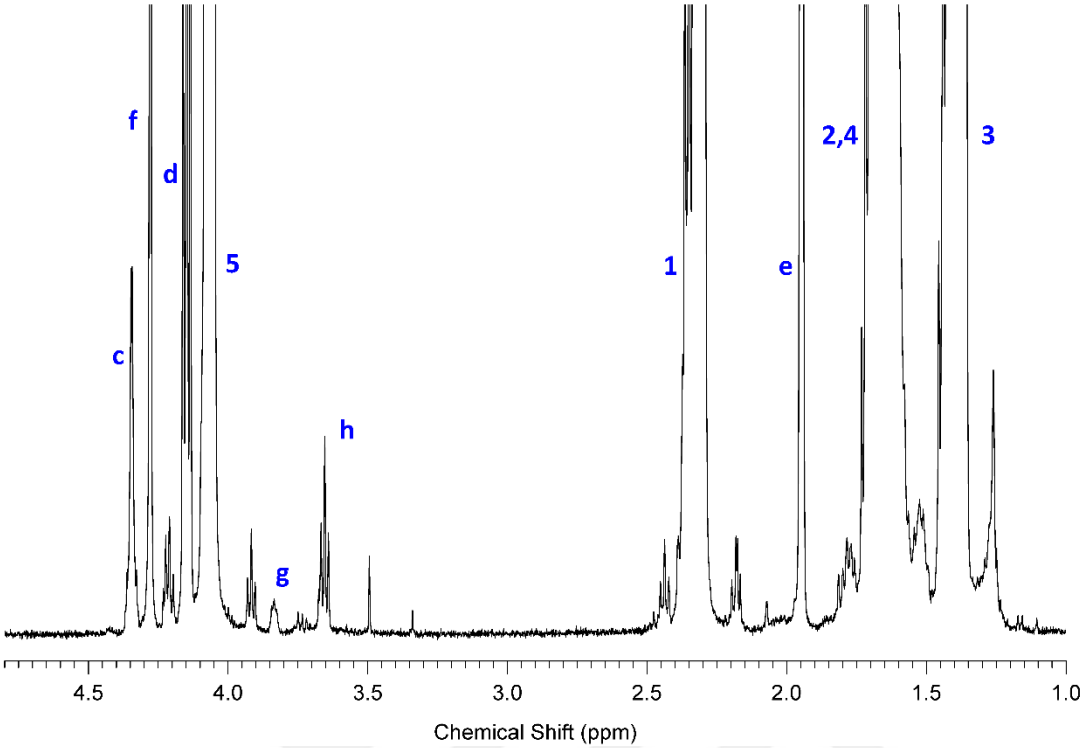

Figure 3.19 : ^{1}H NMR spectrum of the DMPCL synthesized via eROP (1.00-4.80 ppm).

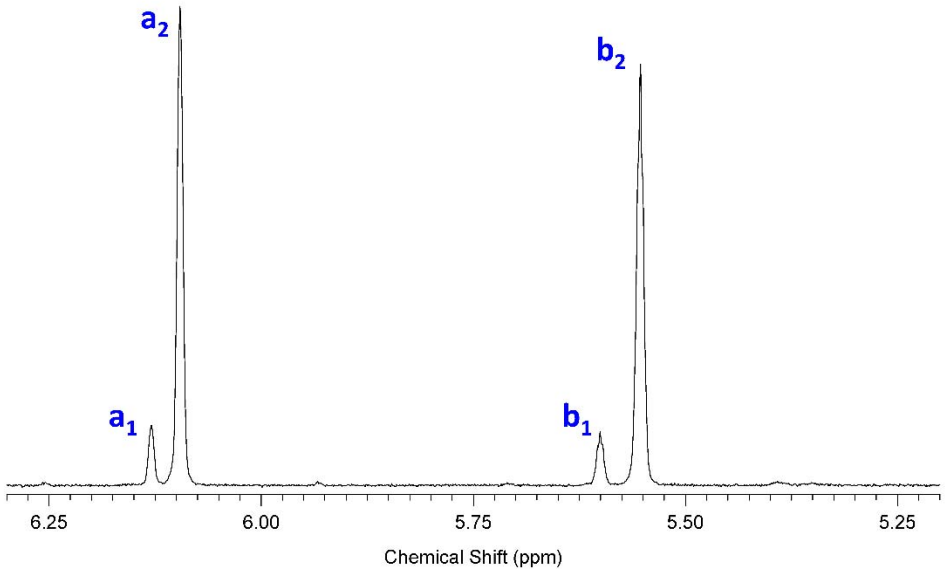

Figure 3.20 : ^{1}H NMR spectrum of the DMPCL synthesized via eROP (5.20-6.30 ppm).

The quantitative evaluation of the end-groups of macromonomers was performed using the peak areas achieved via ^{1}H NMR measurements. Since it was shown that there were two types of methacrylate end-groups and two types of hydroxyl end-groups together with ethylene glycol moieties inside the chains, the enzymatically

synthesized polymer was the mixture of PCL chains with numerous end-group combinations. Hence, it was better to define the polymer mixture with the total methacrylate end-groups. HEMA, methacrylate, total methacrylate and hydroxyl end-group ratios were calculated as it was demonstrated in Equations 3.5-3.8. Total methacrylate end-groups were the summation of HEMA end-groups (referred by peak **c**) and the methacrylate end-groups (referred by peak **d**). In calculations, the peak areas belonging to the vinylic protons of HEMA and methacrylate groups (**a_1** and **a_2** or **b_1** and **b_2**) had almost the same results with those demonstrated as **c** and **d** (Kaya and Guvenilir, 2015). Therefore, the total methacrylate end-groups of the enzymatically synthesized DMPCL was calculated as 0.84 and total hydroxyl end-groups were 0.16. I_c, I_d, I_g and I_h were the peak integrals belonging to the peaks **c**, **d**, **g** and **h** respectively. The $\overline{M_n}$ and PDI values were measured as 4400 g/mole and 1.35 respectively according to SEC measurements.

$$HEMA\ end\text{-}groups = \frac{(I_c/4)}{((I_c/4)+(I_d/2)+(I_g/4)+(I_h/2))} \tag{3.5}$$

$$Methacrylate\ end\text{-}groups = \frac{(I_d/4)}{((I_c/4)+(I_d/2)+(I_g/4)+(I_h/2))} \tag{3.6}$$

$$Total\ methacrylate\ end\text{-}groups = \frac{(I_c/4)+(I_d/2)}{((I_c/4)+(I_d/2)+(I_g/4)+(I_h/2))} \tag{3.7}$$

$$Total\ hydroxyl\ end\text{-}groups = \frac{(I_g/4)+(I_h/2)}{((I_c/4)+(I_d/2)+(I_g/4)+(I_h/2))} \tag{3.8}$$

The DSC measurements were evaluated calculating the melting point (T_m), the glass transition temperature (T_g), the enthalpy of fusion per gram of polymer (ΔH_f) and the specific heat change per gram of polymer (ΔC_p). All of the values were shown in Table 3.1.

Table 3.1 : Calculated T_m, T_g, ΔH_f and ΔC_p, values of DMPCL, PEGMA-950 and the photopolymerized networks.

Experiment Code	ΔH_f *(J/g)*		ΔC_p *(J/g.K)*	T_g *(°C)*	T_m *(°C)*	
	$\Delta H_{f,1}$ *(J/g)*	$\Delta H_{f,2}$ *(J/g)*			$T_{m,1}$ *(°C)*	$T_{m,2}$ *(°C)*
DMPCL	111.95		0.0466	-65.3	55.0	
PEGMA-950	152.08		0.0125	-62.5	35.5	
S-PCLPEG-1.00	13.21		0.1055	-57.5	42.8	
S-PCLPEG-0.75	10.13		0.1040	-57.4	44.3	
S-PCLPEG-0.50	8.93		0.1141	-58.3	44.7	
S-PCLPEG-0.25	5.95	4.02	0.1666	-61.3	16.9	42.1
S-PCLPEG-0.00	68.25		0.0472	-55.3	28.8	
V-PCLPEG-1.00	6.93		0.1219	-56.6	29.7	
V-PCLPEG-0.75	1.82		0.1507	-57.3	29.3	
V-PCLPEG-0.50	12.77		0.1306	-60.0	26.5	
V-PCLPEG-0.25	11.00		0.1745	-60.4	21.9	
V-PCLPEG-0.00	76.74		0.0632	-45.7	33.0	

For DMPCL, an endothermic peak for melting was observed at 55°C respectively indicating the crystalline domains presented in non-reacted DMPCL. Also a small endothermic peak presented at 42.8°C which might point out the reacting DMPCL molecules in small portion. Enthalpy of fusion (ΔH_f) was calculated by integrating the melting curve, as 111.95 J/g (Figure 3.21). The degree of crystallinity, χ_c, was calculated as 82.9 % according to the Equation 3.9, in which ΔH_f^c was the enthalpy of fusion for 100 % crystalline PCL. ΔH_f^c was taken as 139.5 J/g (Gupta et al, 2012). A wide exothermic peak might be observed starting from around 85-90°C to around 140°C (Figure 3.21).

$$\textit{The degree of crystallinity, \%, } \chi_c = \frac{\Delta H_f}{\Delta H_f^c} \text{ x } 100 \qquad (3.9)$$

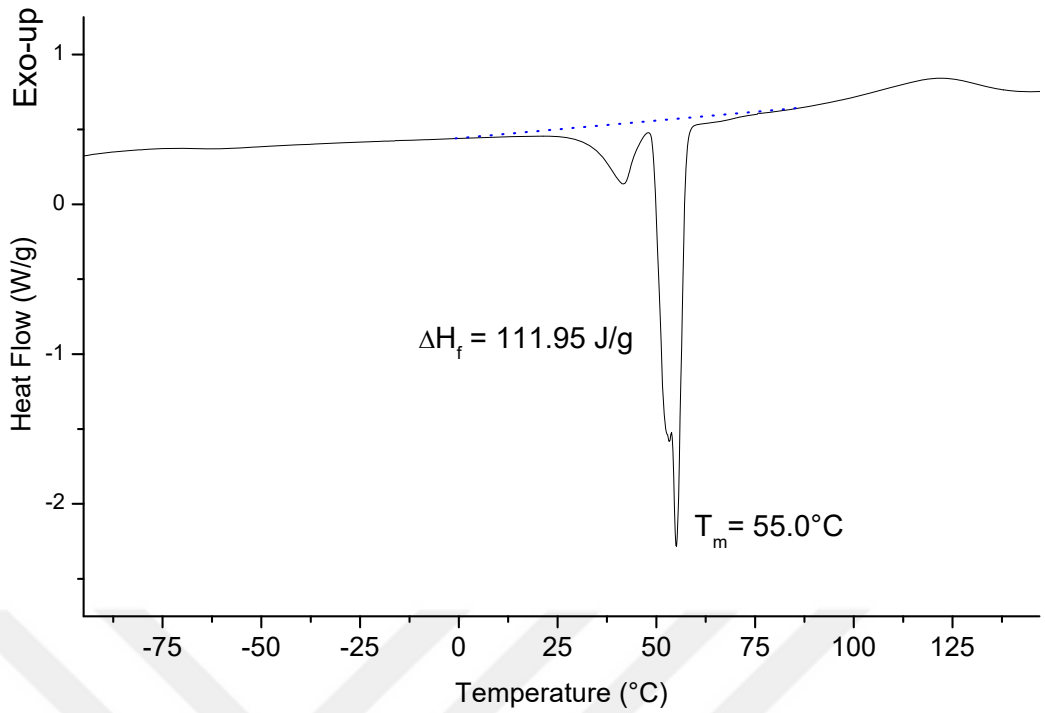

Figure 3.21 : Melting of DMPCL (2nd heating).

The endothermic glass transition occurred at -65.3°C, and specific heat change per gram of polymer (ΔC_p) was calculated as 0.0466 J/g.K for crude DMPCL (Figure 3.22). The T_g and T_m of PCL are generally around -60°C and 60°C respectively, which were comparable with the values in this study (Sarasam and Madihally, 2005).

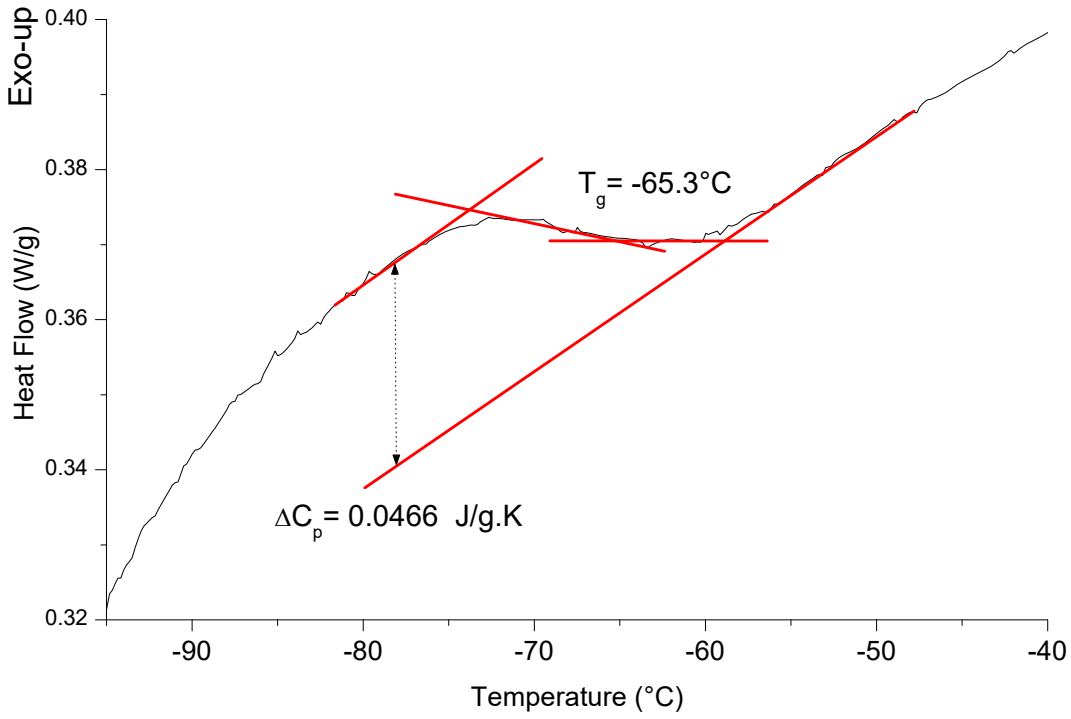

Figure 3.22 : Glass transition and ΔC_p of crude DMPCL.

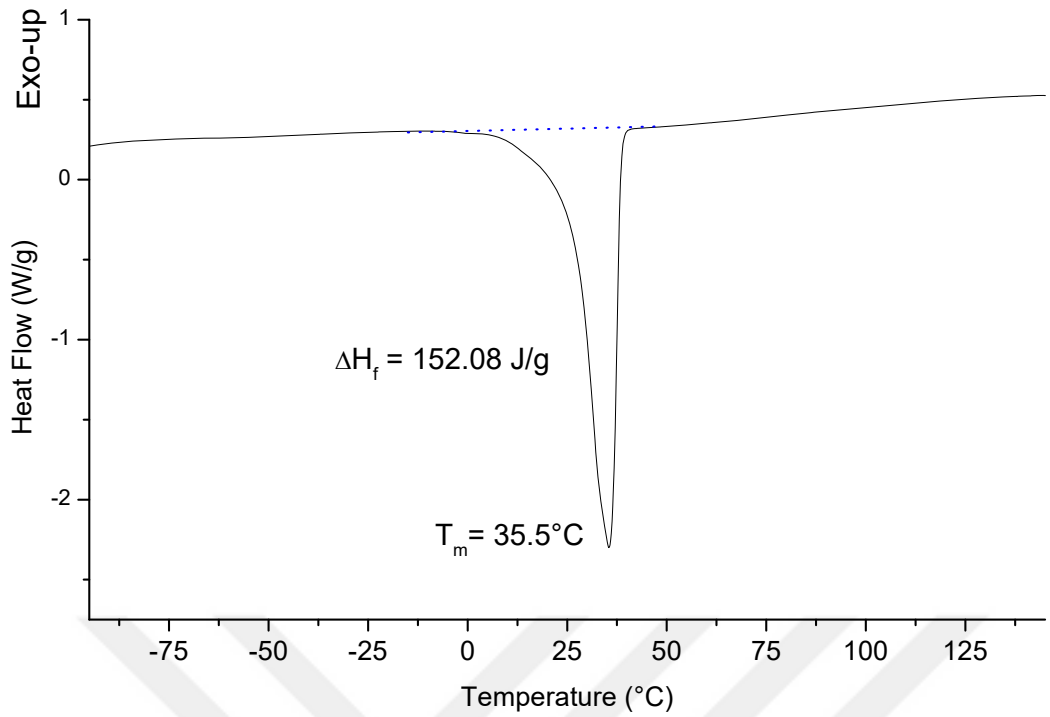

Figure 3.23 : Melting of PEGMA-950 (2nd heating).

For PEGMA, a single endothermic peak was observed, T_m at 35.5°C indicating the crystalline domain presented in non-reacted PEGMA-950. Enthalpy of fusion (ΔH_f) was calculated by integrating the melting curve, as 152.08 J/g (Figure 3.23). The degree of crystallinity, χ_c, was calculated as 77.3 % according to the Equation 3.9, in which ΔH_f^c was the enthalpy of fusion for 100 % crystalline PEG. ΔH_f^c was taken as 196.8 J/g (Wei, 2014).

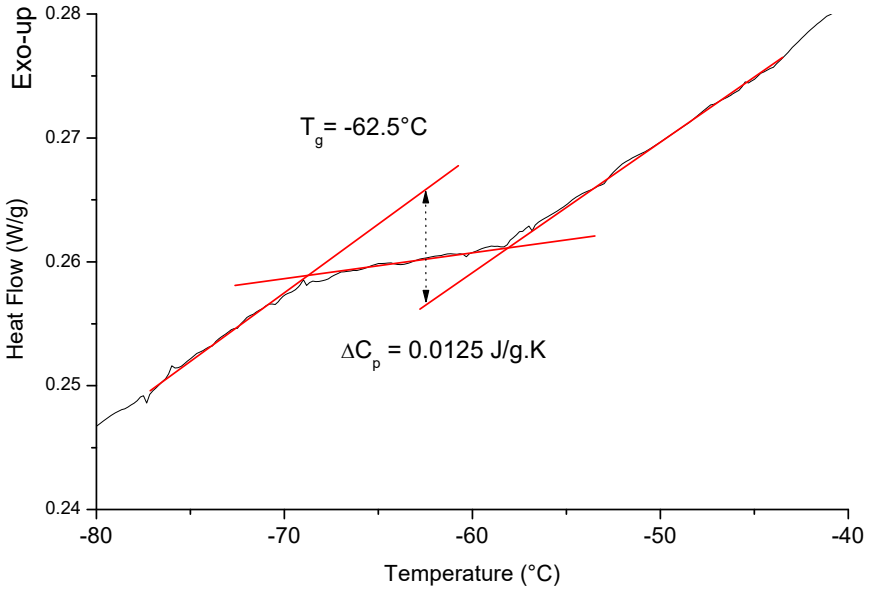

Figure 3.24 : Glass transition and ΔC_p of crude PEGMA-950.

The glass transition occurred at -62.5°C, and specific heat change per gram of polymer (ΔC_p) was calculated as 0.0125 J/g.K for crude PEGMA-950 (Figure 3.24).

For S-PCLPEG-1.00, a single endothermic peak was observed, T_m at 42.8°C revealing the crystalline region which remained after photocrosslinking as the non-reacted DMPCL macromonomers. This diminish in T_m might be attributed to the increase in the amorphous region and the decrease in the crystalline region, thus the suppression of the crystalline domains by the crosslinks. This behavior was also reported in the crosslinking of high molecular weight (7k and 10k) PCL based triacrylates (Wang, 2011). Enthalpy of fusion (ΔH_f) was calculated by integrating the melting curve, as 13.21 J/g (Figure 3.25). This value was very low compared to the nonreacted DMPCL implying the progressive diminish of the crystalline domains after photopolymerization. The T_g was calculated as -57.5°C which was a 7.8°C of rise compared to the crude DMPCL. ΔC_p was calculated as 0.1055 J/g.K. The high C_p change was also in agreement with photocrosslinking.

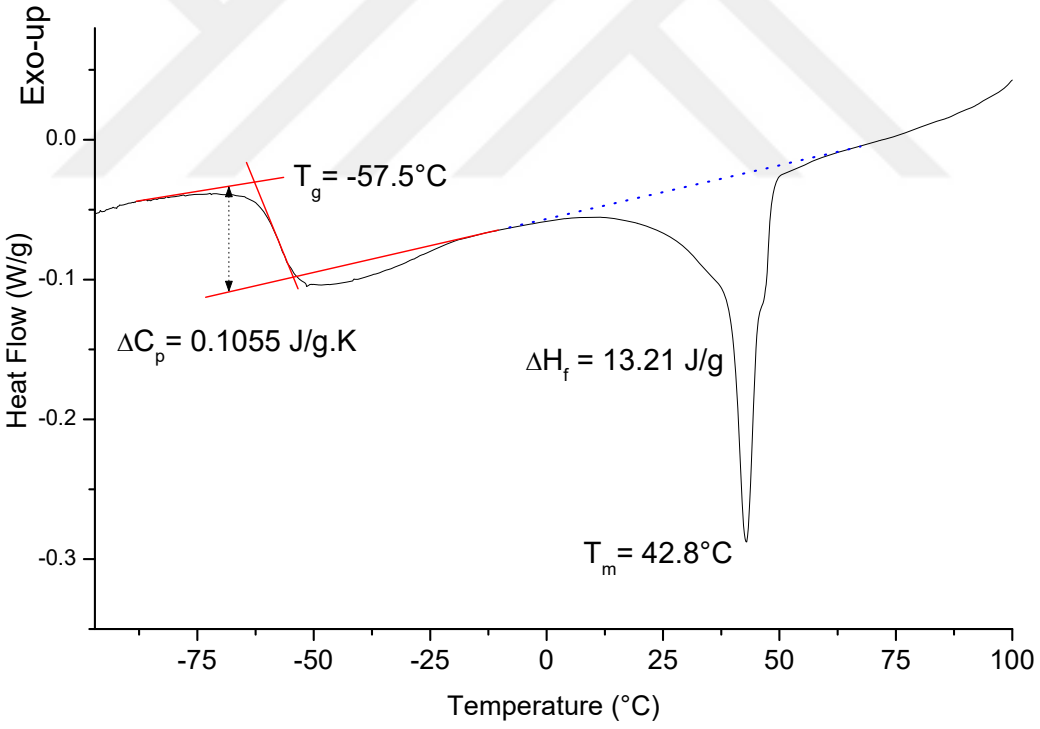

Figure 3.25 : 2nd heating curve of S-PCLPEG-1.00 (The photocrosslinked network performed via solvent casting including 1.00 ratio of DMPCL (mole/mole) in feed).

For S-PCLPEG-0.75, a single sharp endothermic peak at 44.3°C with a small shoulder around 30°C was observed. The lower and single T_m value revealed the crystalline regions which remained after photocrosslinking as non-reacted DMPCL and PEGMA-950 macromonomers. This diminish in T_m might be attributed to the increase in the

amorphous region and the decrease in the crystalline region, thus the suppression of the crystalline domains by the crosslinks. Enthalpy of fusion (ΔH_f) was calculated by integrating the melting curve, as 10.13 J/g (Figure 3.26), which was very low compared to the nonreacted DMPCL and PEGMA-950 implying the progressive diminish of the crystalline domains after photopolymerization. The T_g was calculated as -57.4°C, which was more than both of crude DMPCL and PEGMA-950, however very close to that of S-PCLPEG-1.00. ΔC_p was calculated as 0.1040 J/g.K. The high C_p change was also in agreement with photocrosslinking.

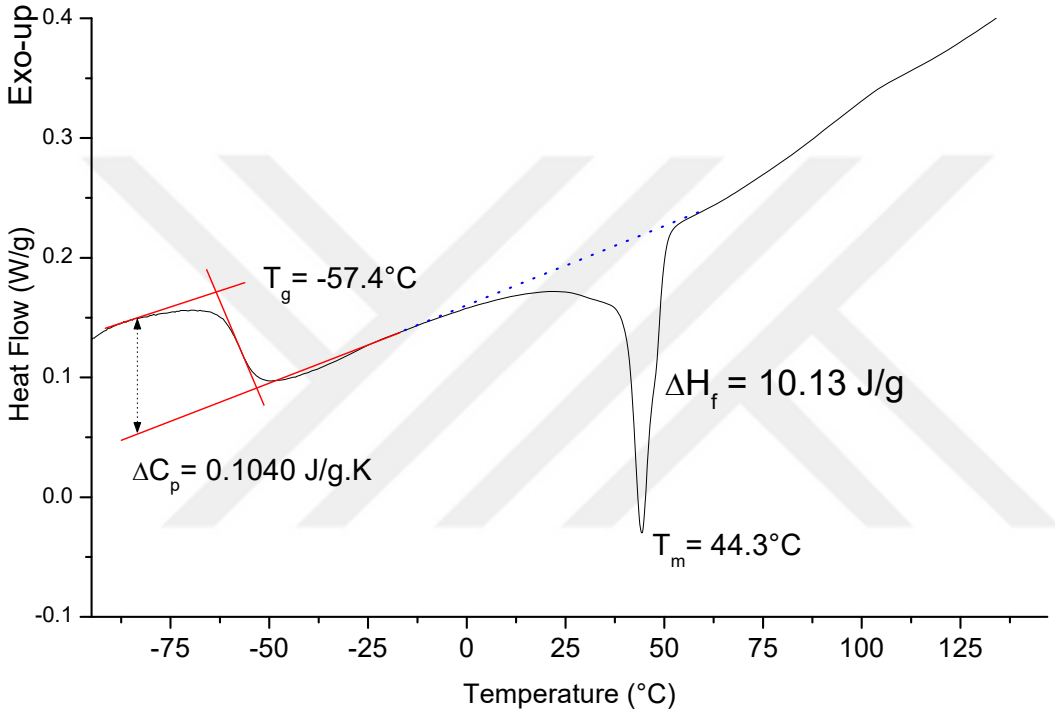

Figure 3.26 : 2nd heating curve of S-PCLPEG-0.75 (The photocrosslinked network performed via solvent casting including 0.75 portion of DMPCL and 0.25 portion of PEGMA (mole/mole) in feed).

For S-PCLPEG-0.50, a single sharp endothermic peak at 44.7°C with a bigger shoulder, as compared to S-PCLPEG-0.75, around 25°C was observed. The lower and single T_m value revealed the crystalline regions which remained after photocrosslinking as non-reacted DMPCL and PEGMA-950 macromonomers. The increased melting shoulder around 25°C might be attributed to the greater number of remaining unreacted PEGMA-950. This diminish in T_m might be attributed to the increase in the amorphous region and the decrease in the crystalline region, thus the suppression of the crystalline domains by the crosslinks. Enthalpy of fusion (ΔH_f) was calculated by integrating the melting curve, as 8.93 J/g (Figure 3.27), which was very low compared to the nonreacted DMPCL and PEGMA-950 expressing the substantial

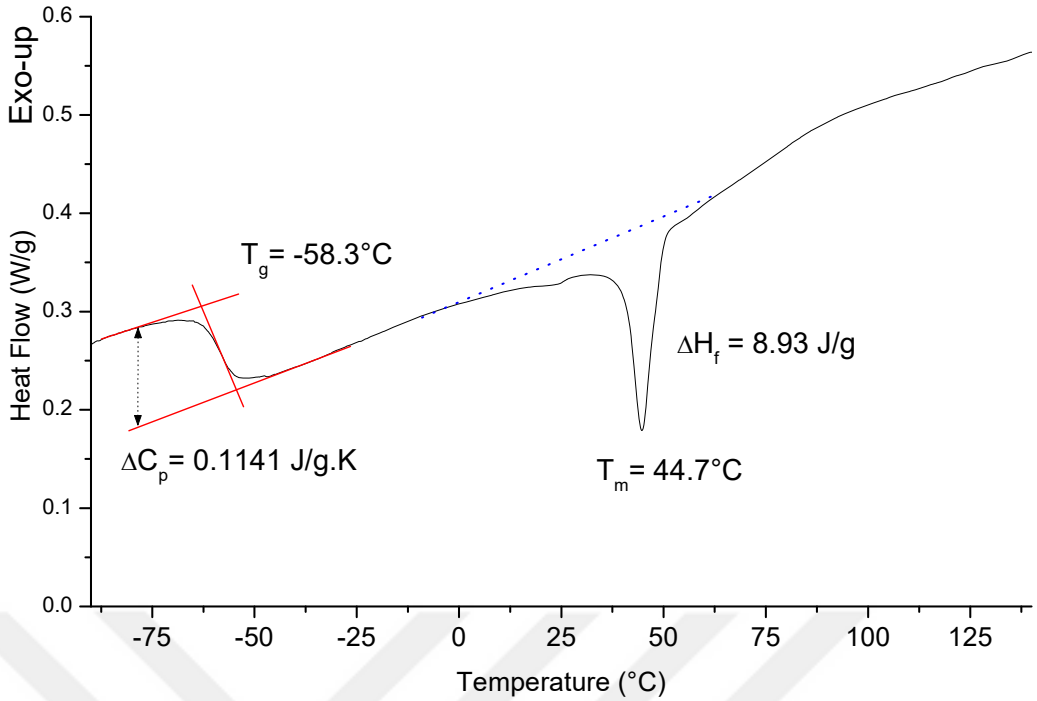

Figure 3.27 : 2nd heating curve of S-PCLPEG-0.50 (The photocrosslinked network performed via solvent casting including 0.50 portion of DMPCL and 0.50 portion of PEGMA (mole/mole) in feed).

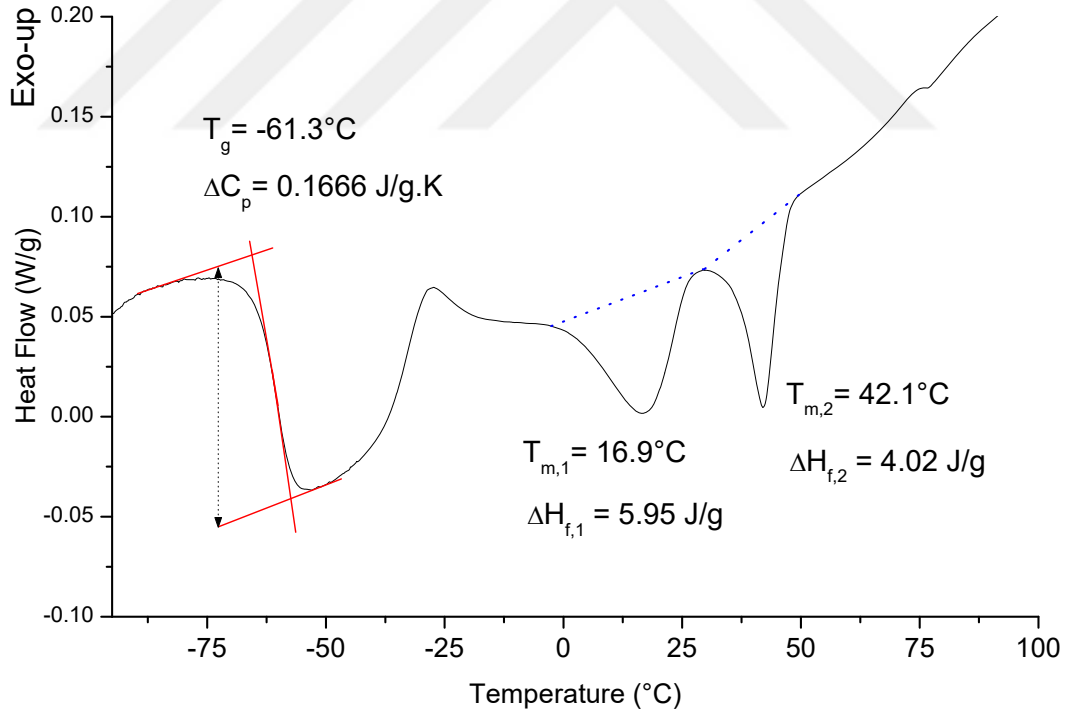

Figure 3.28 : 2nd heating curve of S-PCLPEG-0.25 (The photocrosslinked network performed via solvent casting including 0.25 portion of DMPCL and 0.75 portion of PEGMA (mole/mole) in feed).

depletion of the crystalline domains after photopolymerization. The Tg was calculated as -58.3°C, which was more than both of crude DMPCL and PEGMA-950, however very close to that of S-PCLPEG-1.00 and S-PCLPEG-0.75. ΔCp was calculated as

0.1141 J/g.K. The high Cp change and the augmentation in Tg were in agreement with photocrosslinking.For S-PCLPEG-0.25, a double endothermic peak was observed at 16.9°C and 42.1°C. The lower T_m value at 42.1°C revealed the crystalline regions which remained after photocrosslinking as non-reacted DMPCL macromonomers. On the other hand, the melting at 16.9°C was associated with the new crystalline domains after the photopolymerization. This diminish in T_m values might be attributed to the increase in the amorphous region and the decrease in the crystalline region, thus the suppression of the crystalline domains by the crosslinks. Enthalpy of fusion (ΔH_f) was calculated separately for both of the peaks by integrating the melting curves, as 5.95 and 4.02 J/g respectively and 9.97 in total (Figure 3.28), which was again very low compared to the nonreacted DMPCL and PEGMA-950 expressing the substantial depletion of the crystalline domains after photopolymerization. The T_g was calculated as -61.3°C, which was slightly more than both of crude DMPCL and PEGMA-950. However ΔC_p was calculated as 0.1666 J/g.K.

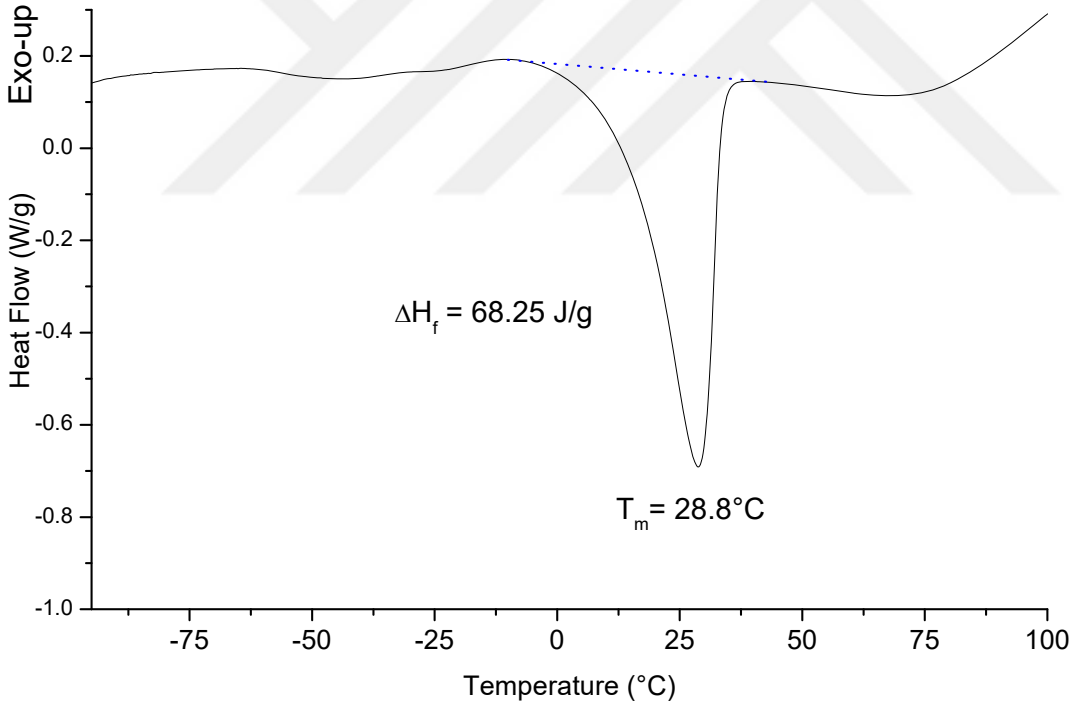

Figure 3.29 : 2nd heating curve of S-PCLPEG-0.00 showing the melting region (The photocrosslinked network performed via solvent casting not including DMPCL and 1.00 portion of PEGMA (mole/mole) in feed).

The drammatically high C_p change, the progressive diminish in enthalpy of fusion and melting points showed effective photocrosslinking, on the other hand the slight increase in T_g might be the consequence of the plasticizing effect of remaining unreacted TMPTA, DMPCL and PEGMA-950. The exothermic peak appeared around

-25°C was related with cold-crystallization of the remaining unreacted macromonomers.

For S-PCLPEG-0.00, a single endothermic peak was observed, T_m at 28.8°C revealing the crystalline region which remained after photocrosslinking as the non-reacted PEGMA-950 macromonomers. This diminish in T_m might be attributed to the increase in the amorphous region and the decrease in the crystalline region, thus the suppression of the crystalline domains by the crosslinks. Enthalpy of fusion (ΔH_f) was calculated by integrating the melting curve, as 68.25 J/g (Figure 3.29). This value was lower compared to the nonreacted PEGMA-950 implying the inefficient decrease of the crystalline domains after photopolymerization. Since, the diminish in ΔH_f was reported notably higher in DMPCL including photocuring experiments, DMPCL can be evaluated as an efficient crosslinking agent for the photopolymerization of PEGMA-950, even though DMPCL had a high molecular weight.

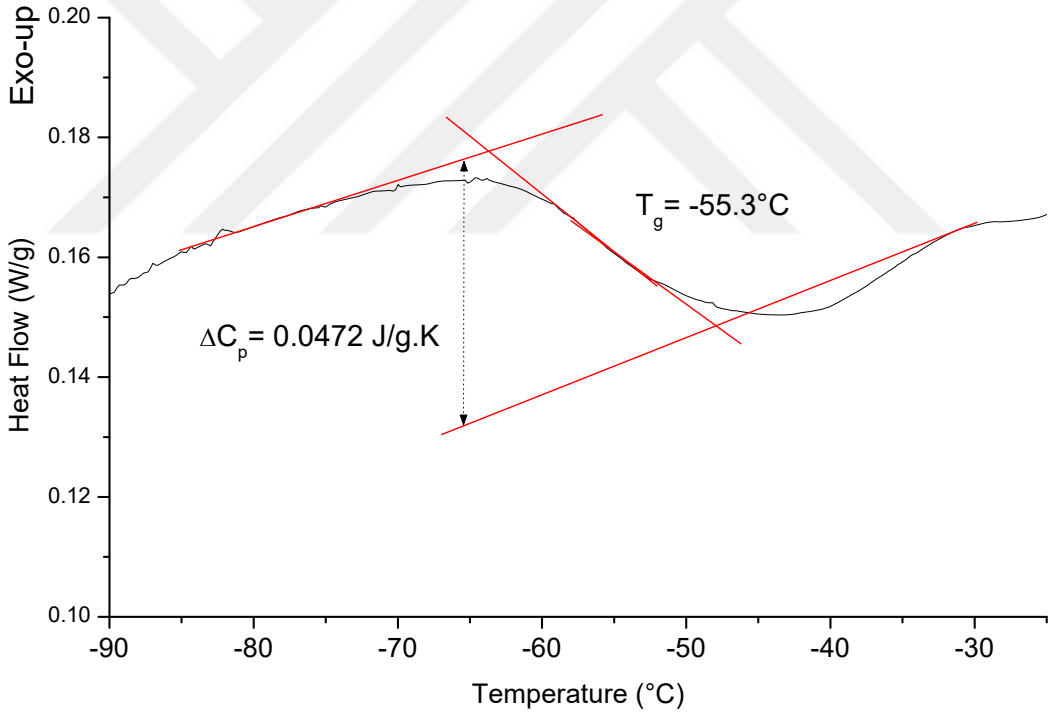

Figure 3.30 : 2nd heating curve of S-PCLPEG-0.00 showing the glass transition region (The photocrosslinked network performed via solvent casting not including DMPCL and 1.00 portion of PEGMA (mole/mole) in feed).

The T_g was calculated as -55.3°C which was a 7.2°C of rise compared to the crude PEGMA-950. ΔC_p was calculated as 0.0472 J/g.K (Figure 3.30). The comparably lower C_p rise was also in agreement with inefficient photocrosslinking and the relatively better effectiveness of DMPCL.

For V-PCLPEG-1.00, a single endothermic peak was observed, T_m at 29.7°C revealing the crystalline region which remained after photocrosslinking as the non-reacted DMPCL macromonomers. This diminish in T_m might be attributed to the increase in the amorphous region and the decrease in the crystalline region, thus the suppression of the crystalline domains by the crosslinks. This behavior was also reported in the crosslinking of high molecular weight (7k and 10k) PCL based triacrylates (Wang, 2011). On the other hand, this melting point value was notably lower than that of crude DMPCL and S-PCLPEG-1.00 (the same reaction perfomed via solvent casting). Enthalpy of fusion (ΔH_f) was calculated by integrating the melting curve, as 6.93 J/g (Figure 3.31), which was again substantially lower than the values observed in crude DMPCL and the S-PCLPEG-1.00. The T_g was calculated as -56.6°C which was a 8.7°C of rise compared to the crude DMPCL. ΔC_p was calculated as 0.1219 J/g.K.

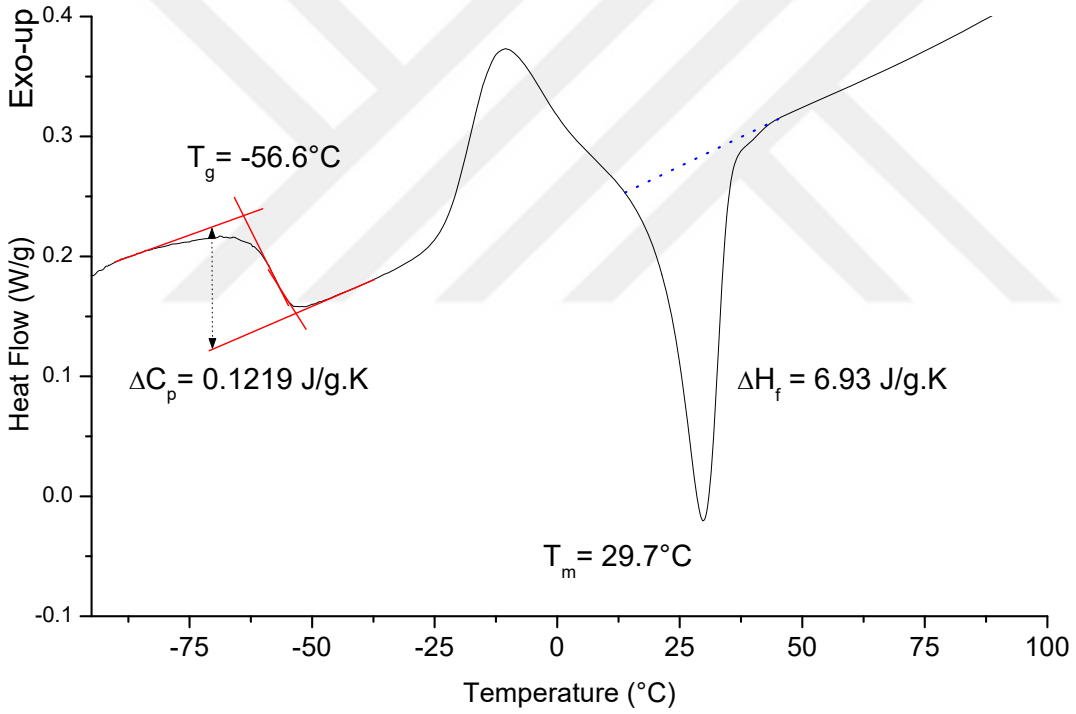

Figure 3.31 : 2nd heating curve of V-PCLPEG-1.00 (The photocrosslinked network performed in glass vial including 1.00 ratio of DMPCL (mole/mole) in feed).

The higher changes in T_m, ΔH_f, T_g and C_p elucidated more efficient photocrosslinking of DMPCL in continuously stirred and Ar purged reaction media. The exothermic peak rose around -10°C was related with the cold-crystallization of the remaining unreacted DMPCL macromonomers.

For V-PCLPEG-0.75, a single sharp endothermic peak at 29.3°C with a small shoulder around 43°C was observed. It should be noted that the T_m of S-PCLPEG-0.75 (the

same reaction performed in glass vial) was reported as 44.3 with a slight shoulder aroun 30°C. The substantially lower T_m value revealed the decrease of the crystalline regions which remained after photocrosslinking as non-reacted DMPCL and PEGMA-950 macromonomers. Enthalpy of fusion (ΔH_f) was calculated by integrating the melting curve, as 1.87 J/g (Figure 3.32), which was very low compared to the nonreacted DMPCL and PEGMA-950 implying the progressive diminish of the crystalline domains after photopolymerization. This value was also lower than that of the S-PCLPEG-0.75 which was reported as 10.13 J/g. The T_g was calculated as -57.3°C, which was more than both of crude DMPCL and PEGMA-950, however very close to that of V-PCLPEG-1.00. ΔC_p was calculated as 0.1507 J/g.K.

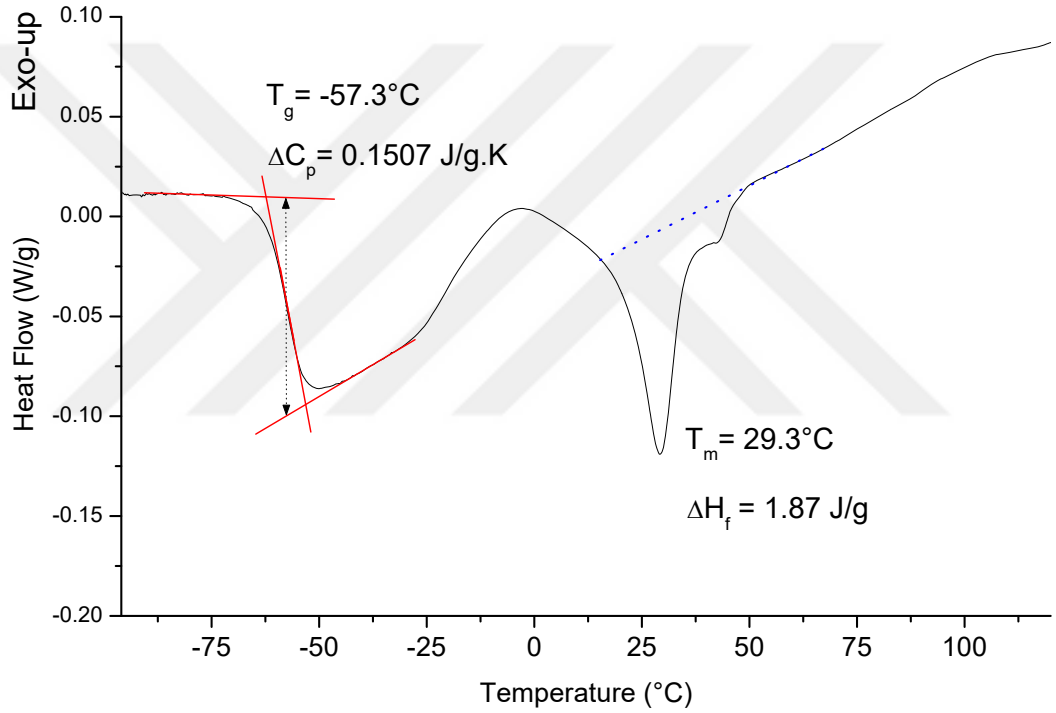

Figure 3.32 : 2nd heating curve of V-PCLPEG-0.75 (The photocrosslinked network performed in the glass vial including 0.75 portion of DMPCL and 0.25 portion of PEGMA (mole/mole) in feed).

The higher changes in T_m, ΔH_f, T_g and C_p elucidated more efficient photocrosslinking of DMPCL, PEGMA-950 and TMPTA in continuously stirred and Ar purged reaction media. The exothermic peak rose around 0°C was related with the cold-crystallization of the remaining unreacted DMPCL and PEGMA-950 macromonomers.

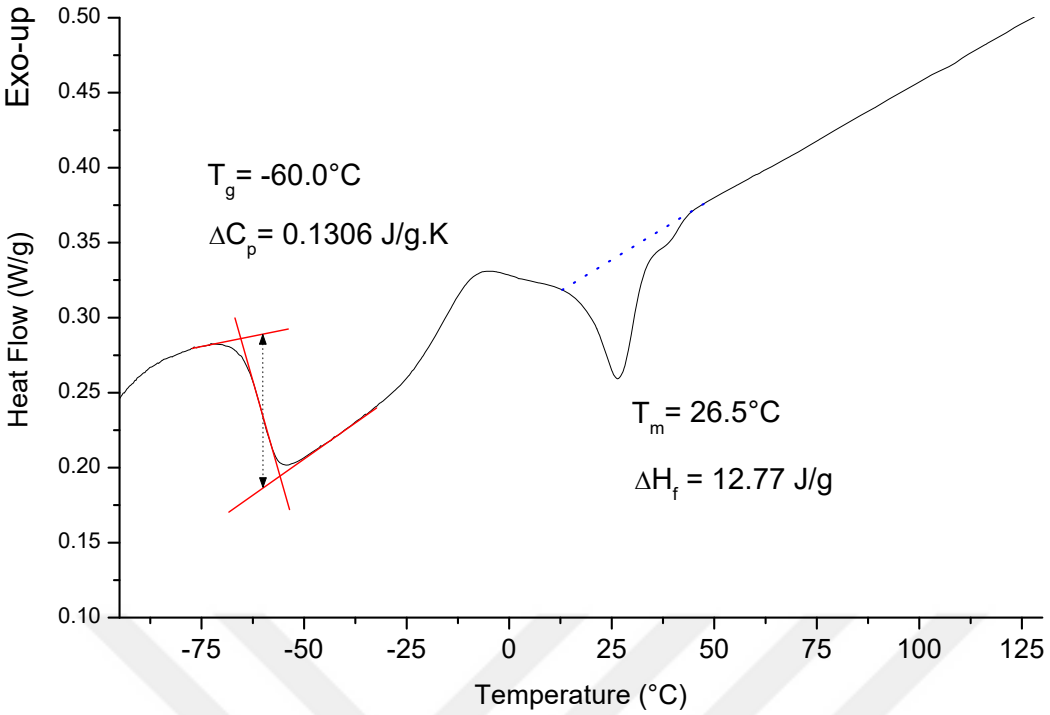

Figure 3.33 : 2nd heating curve of V-PCLPEG-0.50 (The photocrosslinked network performed in glass vial including 0.50 portion of DMPCL and 0.50 portion of PEGMA (mole/mole) in feed).

For V-PCLPEG-0.50, a single sharp endothermic peak at 26.5°C with a small shoulder around 40°C was observed. It should be noted that the T_m of S-PCLPEG-0.50 (the same reaction performed in glass vial) was reported as 44.7 with a slight shoulder aroun 25°C. The substantially lower T_m value revealed the decrease of the crystalline regions which remained after photocrosslinking as non-reacted DMPCL and PEGMA-950 macromonomers. Enthalpy of fusion (ΔH_f) was calculated by integrating the melting curve, as 12.77 J/g (Figure 3.33), which was lower compared to the nonreacted DMPCL and PEGMA-950 implying the progressive diminish of the crystalline domains after photopolymerization.

Figure 3.34 : UV-cured V-PCLPEG-0.50.

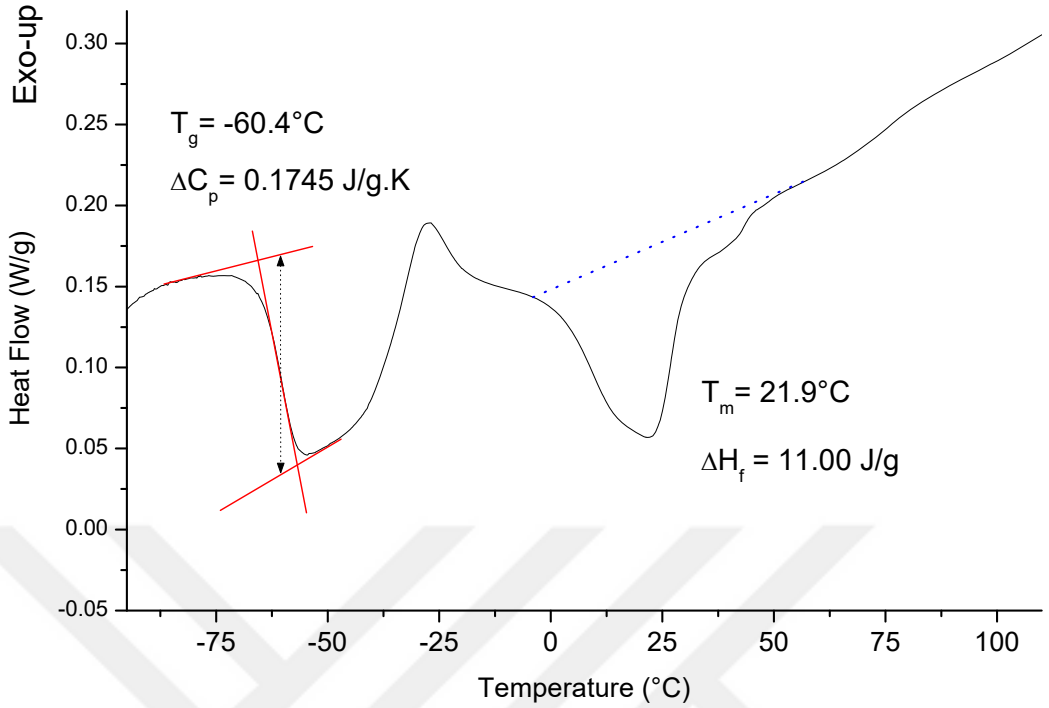

Figure 3.35 : 2nd heating curve of V-PCLPEG-0.25 (The photocrosslinked network performed in glass vial including 0.25 portion of DMPCL and 0.75 portion of PEGMA (mole/mole) in feed).

However, this value was also higher than that of the S-PCLPEG-0.50 which was reported as 8.93 J/g. The T_g was calculated as -60.0°C, which was more than both of crude DMPCL and PEGMA-950. ΔC_p was calculated as 0.1306 J/g.K which was higher than the value observed for S-PCLPEG-0.50.

The higher changes in T_m and C_p elucidated more efficient photocrosslinking of DMPCL, PEGMA-950 and TMPTA in continuously stirred and Ar purged reaction media. On the other hand, the remaining monomers decreased the T_g and ΔH_f as compared with the same reaction conducted in glass vial. The exothermic peak rose around 0°C was related with the cold-crystallization of the remaining unreacted DMPCL and PEGMA-950 macromonomers. The UV-cured V-PCLPEG-0.50 sample 1 day after photopolymerizaiton might be seen in Figure 3.35.

For V-PCLPEG-0.25, a single endothermic peak at 21.9°C with a small shoulder around 40°C was observed. It should be noted that S-PCLPEG-0.25 (the same reaction performed in glass vial) had a distinct double endothermic peak occured at 16.9°C and 42.1°C. The convergence of those two distinct melting peaks to each other, the proximity of the peak at 21.9°C to 35.5°C (T_m of the crude PEGMA-950) and the

substantial damping of the peak at 42.1°C ($T_{m,2}$ in S-PCLPEG-0.25) points out much better consumption of DMPCL in glass vial than on glass slide substrate. However, there still remained unreacted DMPCL and PEGMA-950 macromonomers. Enthalpy of fusion (ΔH_f) was calculated by integrating the melting curve, as 11.00 J/g (Figure 3.34), which was lower compared to the nonreacted DMPCL and PEGMA-950 showing the considerable depletion of the crystalline domains after photopolymerization. Although, this value was still slightly lower and close to the sum of ΔH_f belonging to the two endothermic melting peaks of S-PCLPEG-0.25 which was reported as 9.97 J/g. The T_g was calculated as -60.4°C, which was more than both of crude DMPCL and PEGMA-950. ΔC_p was calculated as 0.1745 J/g.K which was higher than the value observed for S-PCLPEG-0.50.

Despite the proximate ΔH_f and T_g values of the reactions performed in the glass vial and on the glass slide substrate, the noteworthy changes in T_m and C_p prove better photocrosslinking efficiency of DMPCL, PEGMA-950 and TMPTA in continuously stirred and Ar purged reaction media. On the other hand, the remaining monomers decreased the T_g and ΔH_f as compared with the same reaction conducted in glass vial. The exothermic peak rose around -25°C was related with the cold-crystallization of the remaining unreacted DMPCL and PEGMA-950 macromonomers.

The demonstration of the sample V-PCLPEG-0.25 inside the reaction vial in the normal and the inverted stands were shown in Figure 3.36.

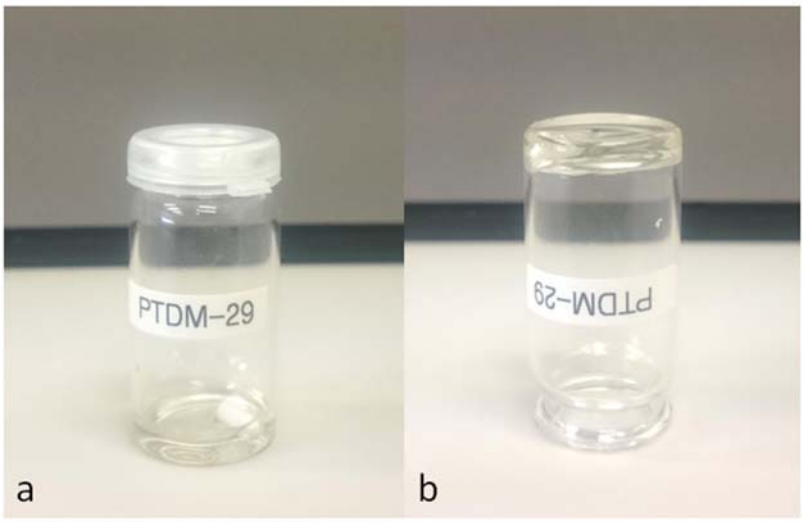

Figure 3.36 : Demonstration of V-PCLPEG-0.25 after photopolymerization (a) Normal stand of the vial, (b) The inverted vial.

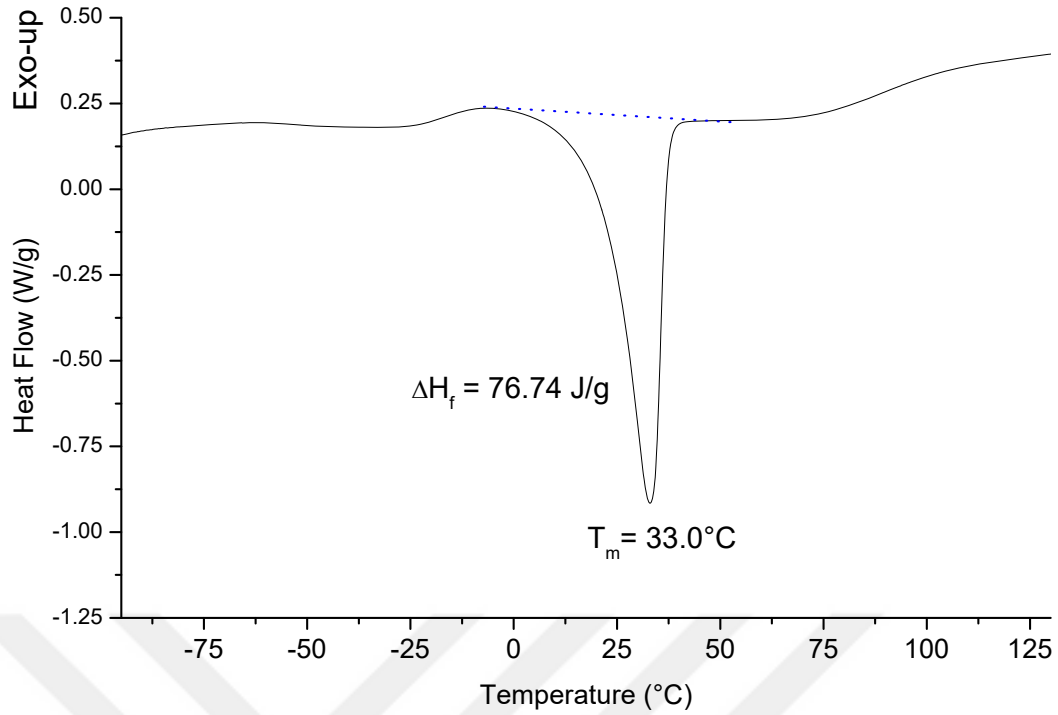

Figure 3.37 : 2nd heating curve of V-PCLPEG-0.00 showing the melting region (The photocrosslinked network performed in glass vial not including DMPCL and 1.00 portion of PEGMA (mole/mole) in feed).

For V-PCLPEG-0.00, a single endothermic peak was observed, T_m at 33.0°C revealing the crystalline region which remained after photocrosslinking as the non-reacted PEGMA-950 macromonomers. This diminish in T_m might be attributed to the increase in the amorphous region and the decrease in the crystalline region, thus the suppression of the crystalline domains by the crosslinks. Enthalpy of fusion (ΔH_f) was calculated by integrating the melting curve, as 76.74 J/g (Figure 3.37). This value was lower compared to the nonreacted PEGMA-950 implying the inefficient decrease of the crystalline domains after photopolymerization, which was in parallel with the experiment performed on glass slide substrate with the same reaction conditions.

The T_g was calculated as -45.7°C which was a 17.0°C of rise compared to the crude PEGMA-950. ΔC_p was calculated as 0.0632 J/g.K (Figure 3.38). The comparably lower C_p rise was also in agreement with inefficient photocrosslinking and the relatively better effectiveness of DMPCL utilization.

The FTIR-ATR assignments of the macromonomers were briefly demonstrated in Table 3.2. DMPCL had absorbance values followingly: end-group O-H stretching at 3442 cm^{-1}; asymmetric CH_2 stretching at 2945 cm^{-1}; symmetric CH_2 stretching at 2864 cm^{-1}; C=O carbonyl stretching of ester groups at 1720 cm^{-1} (belonging to the ester

groups along the backbone and the methacrylate end-groups); C=C double bonds stretching at 1637 cm^{-1} (belonging to the methacrylate end-groups); C-O and C-C stretching in

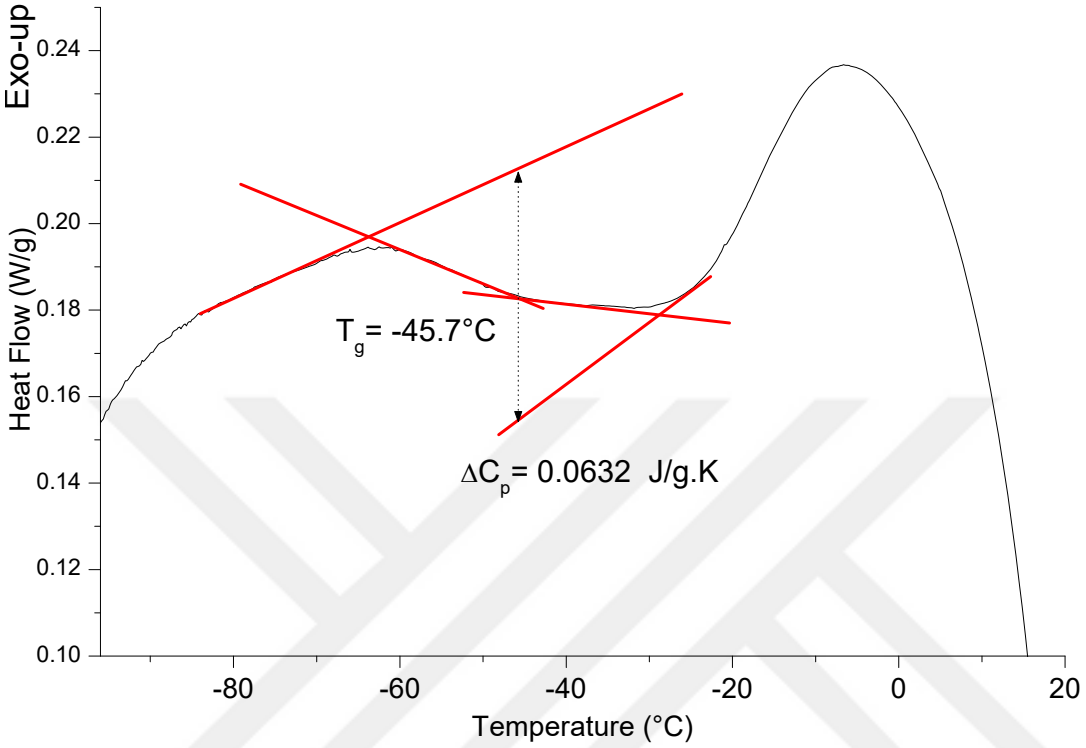

Figure 3.38 : 2nd heating curve of V-PCLPEG-0.00 showing the glass transition region (The photocrosslinked network performed in glass vial not including DMPCL and 1.00 portion of PEGMA (mole/mole) in feed).

the crystalline phase at 1293 cm^{-1}; asymmetric C-O-C stretching at 1237 cm^{-1}; symmetric C-O-C stretching at 1160 cm^{-1}. PEGMA-950 had absorbance values as: a broad peak comprising both symmetric and asymmetric CH_2 stretchings at 2880 cm^{-1}; C=O carbonyl stretching of ester groups at 1720 cm^{-1} (belonging to the methacrylate end-groups); C=C double bonds stretching at 1637 cm^{-1} (belonging to the methacrylate end-groups); C-O-C stretching at 1237 cm^{-1}; C-H scissoring at 1467 cm^{-1}; C-O, C-C stretching and C-H rocking (trans) at 1103 cm^{-1}; C-C stretching and C-H rocking (gauche) at 947 cm^{-1} (Dubois et al, 1991; Elzein et al, 2004; Matsuura and Miyazawa, 1969; Stansbury and Dickens, 2001; Zhou et al, 2003).

In Figure 3.39, full FTIR-ATR spectrums of DMPCL and PEGMA-950 were demonstrated. As it can be seen, a very slight peak was observed at 3442 cm^{-1} revealing only a slight portion of hydroxyl end-groups remained during the synthesis of DMPCL via eROP with transesterification side reactions.

Table 3.2 : FTIR-ATR assignments of the macromonomers utilized in photopolymerization (Dubois et al, 1991; Elzein et al, 2004; Matsuura and Miyazawa, 1969; Stansbury and Dickens, 2001; Zhou et al, 2003).

Chemical type	Wavenumber (cm^{-1})	Vibrational band assignment
DMPCL	3442	O-H stretching
DMPCL	2945	Asymmetric CH_2 stretching
DMPCL	2864	Symmetric CH_2 stretching
DMPCL, PEGMA-950	1720	C=O Carbonyl stretching of ester groups
DMPCL, PEGMA-950	1637	C=C bonds stretching
DMPCL	1293	C-O and C-C stretching in the crystalline phase
DMPCL, PEGMA-950	1237	Asymmetric C-O-C stretching
DMPCL	1160	Symmetric C-O-C stretching
PEGMA-950	2880	C-H stretching (symmetric and asymmetric)
PEGMA-950	1467	C-H scissoring
PEGMA-950	1103	C-O, C-C stretching, C-H rocking (trans)
PEGMA-950	947	C-C stretching, C-H rocking (gauche)

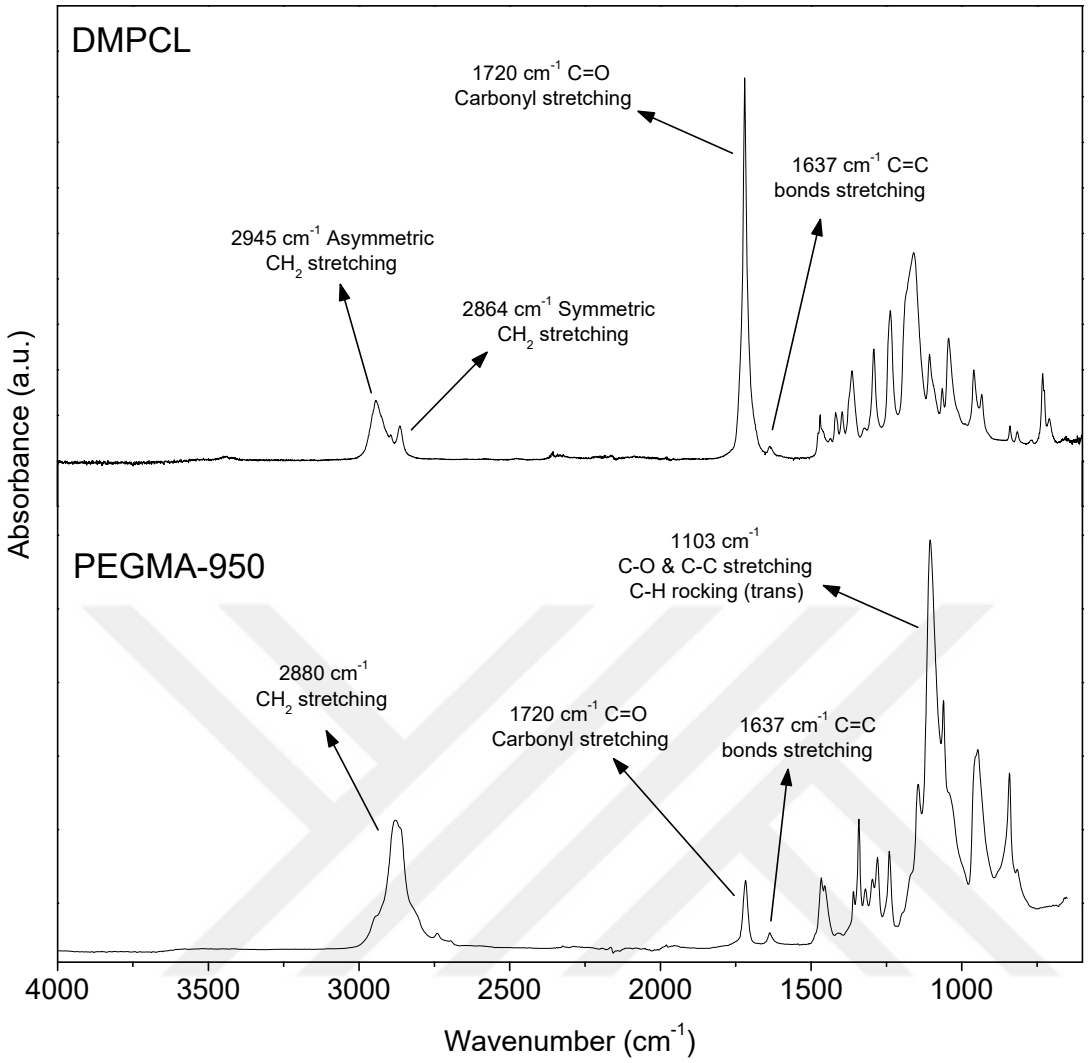

Figure 3.39 : FTIR-ATR spectrums of DMPCL and PEGMA-950.

The FTIR-ATR spectrums of the reactions conducted in glass vials and by solvent casting method, in the range between 1575-1800 cm^{-1}, for each DMPCL feed ratio were demonstrated in Figure 3.40-3.44. It can obviously be realized that the peak intensity of the C=C double bonds at 1637 cm^{-1} dimished after UV exposure. Furthermore, the absorbance at 1637 cm^{-1} decreased even more for the photopolymerizations performed in glass vials except for the reaction made on glass slide substrate. In Figure 3.44, a peak appeared at 1610 cm^{-1} was assigned to the residual unreacted TMPTA crosslinking agent.

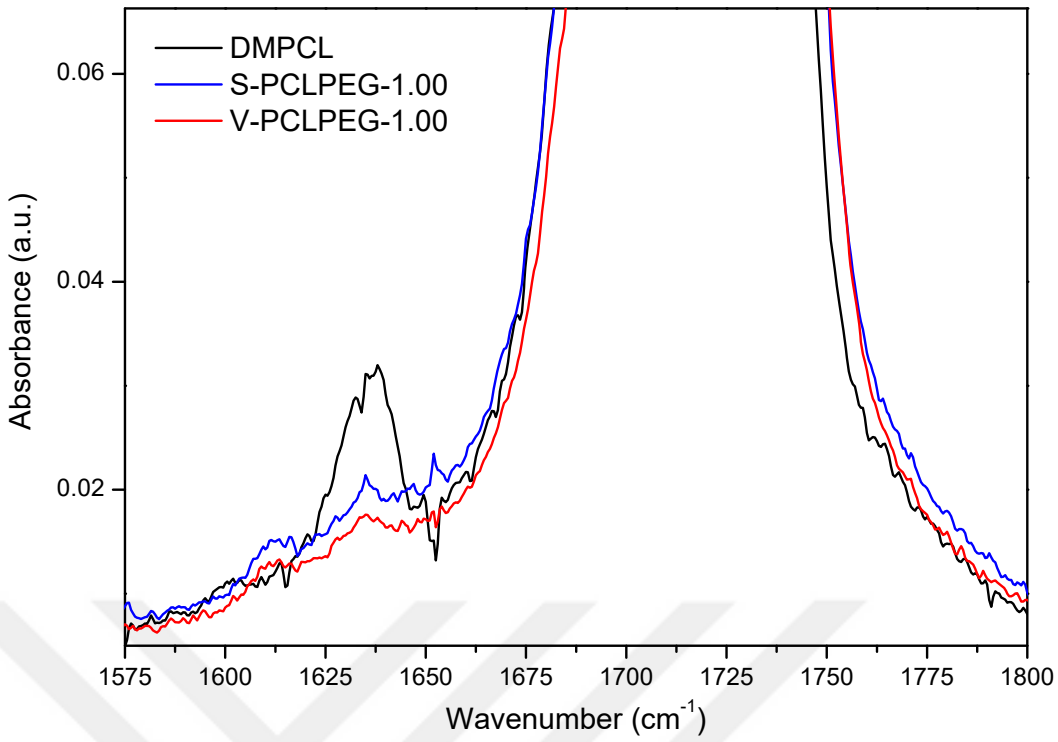

Figure 3.40 : FTIR-ATR spectrums of DMPCL, S-PCLPEG-1.00 and V-PCLPEG-1.00 between 1575-1800 cm^{-1}.

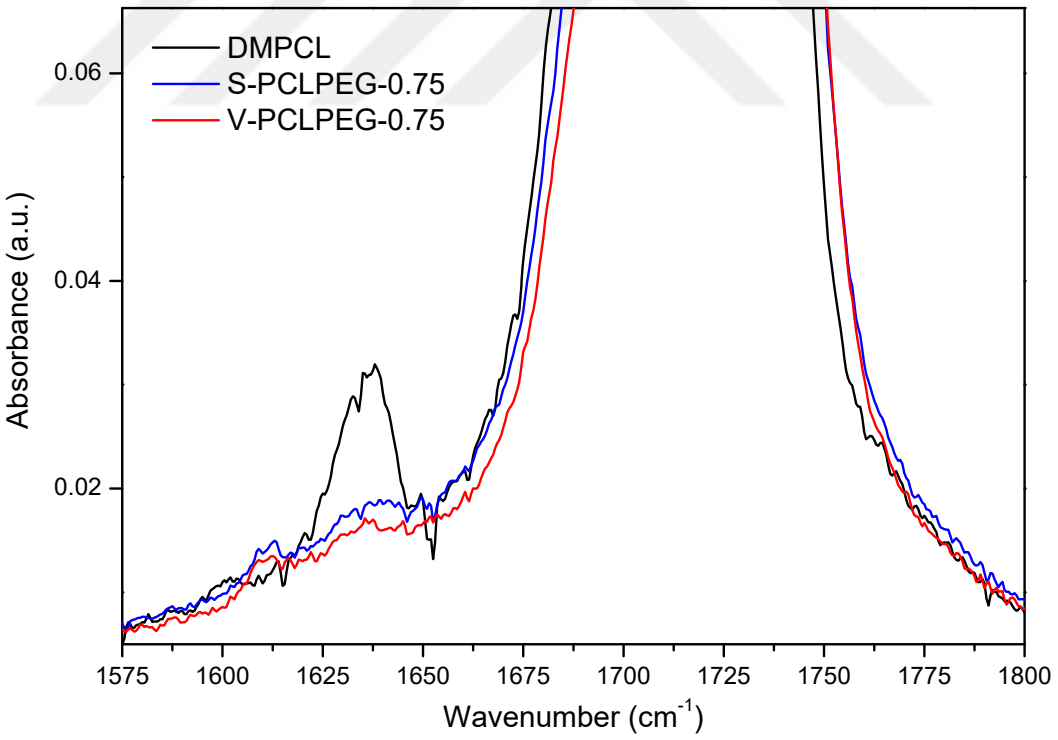

Figure 3.41 : FTIR-ATR spectrums of DMPCL, S-PCLPEG-0.75 and V-PCLPEG-0.75 between 1575-1800 cm^{-1}.

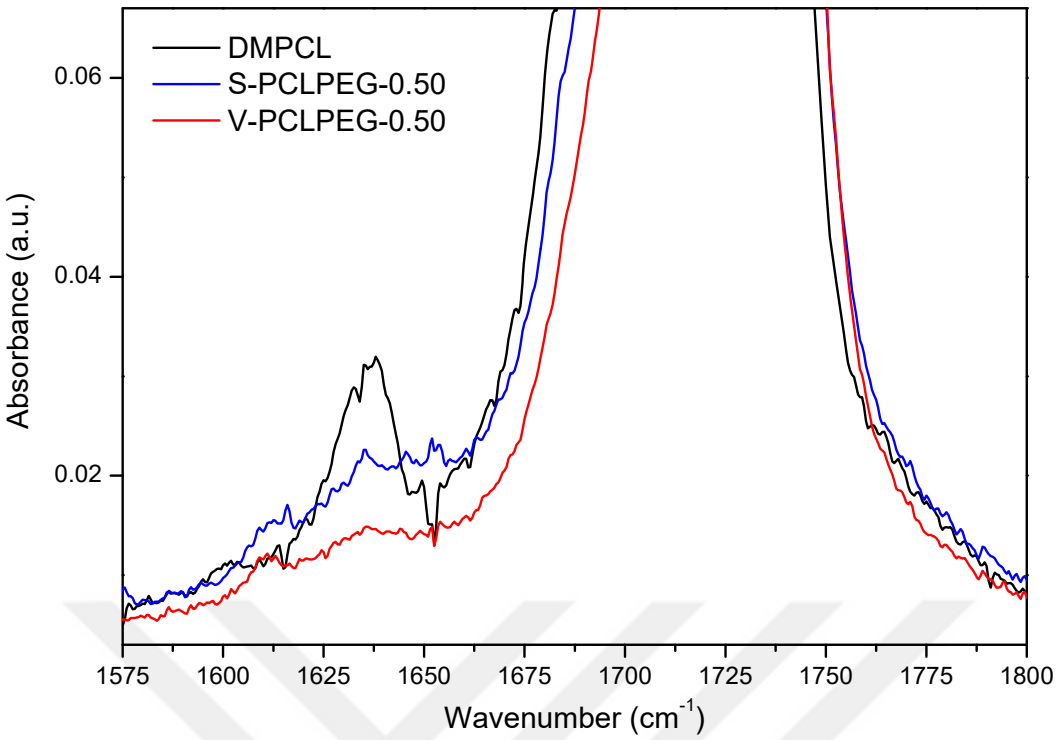

Figure 3.42 : FTIR-ATR spectrums of DMPCL, S-PCLPEG-0.50 and V-PCLPEG-0.50 between 1575-1800 cm^{-1}.

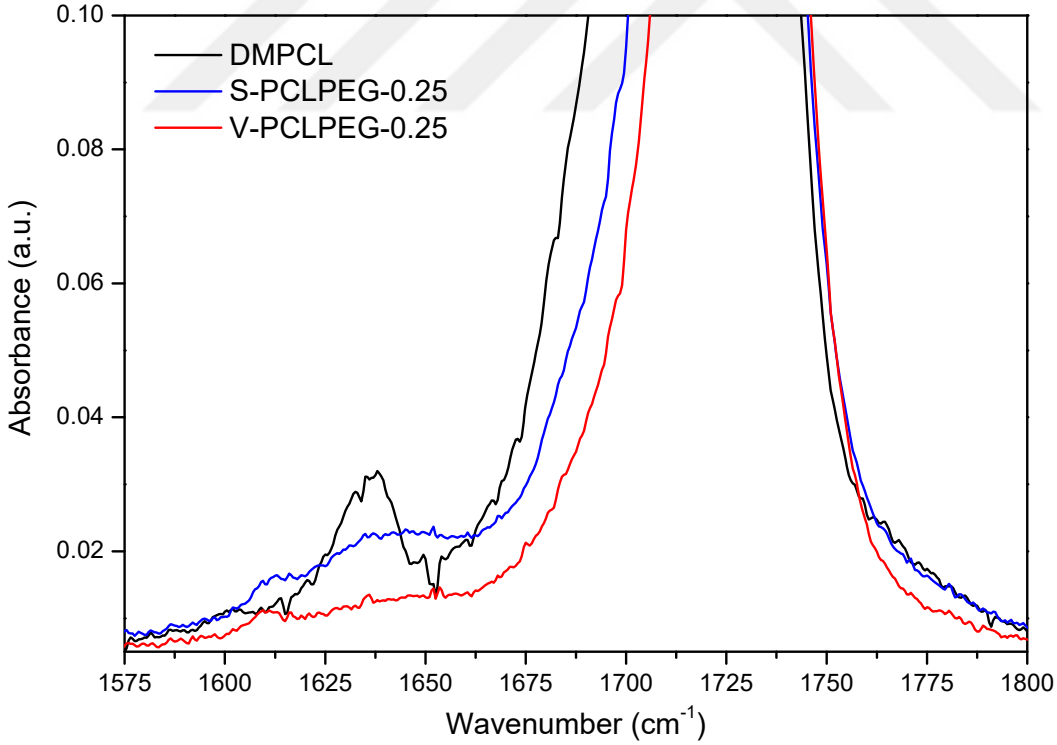

Figure 3.43 : FTIR-ATR spectrums of DMPCL, S-PCLPEG-0.25 and V-PCLPEG-0.25 between 1575-1800 cm^{-1}.

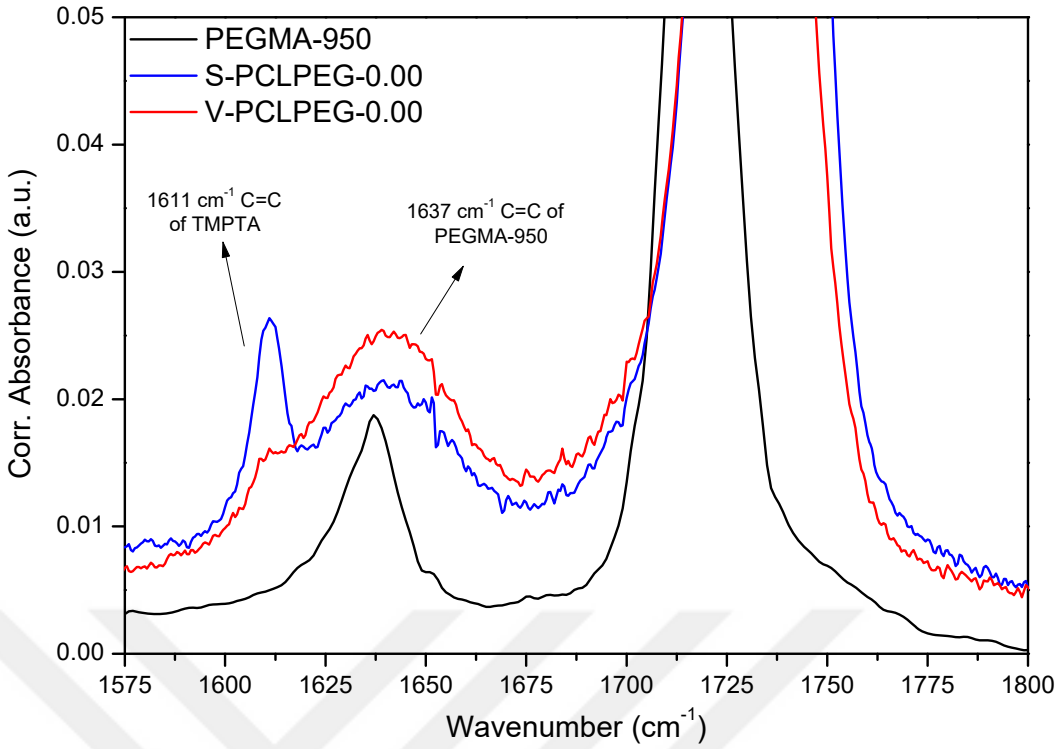

Figure 3.44 : FTIR-ATR spectrums of PEGMA-950, S-PCLPEG-0.00 and V-PCLPEG-0.00 between 1575-1800 cm^{-1}.

The converison (%) of PEGMA-950 and DMPVL macromonomers in the photopolymerization experiments were calculated according to the equations 3.10-3.14. PR^0_{DMPCL} and $PR^0_{PEGMA-950}$ were the peak height ratios of the peaks at 1637 cm^{-1} and 1720 cm^{-1} belonging to the crude DMPCL and PEGMA-950 respectively. $PR^p_{Exp.}$ was referred to the peak height ratio of the aforementioned peaks in the regarding experiment after photopolymerization. EPR^0_{Exp} was the estimated total peak height ratios of the aforementioned peaks in the regarding experiment before photopolymerization. χ_{DMPCL} and $\chi_{PEGMA-950}$ were the feed molar fractions of DMPCL and PEGMA-950 in the experiment respectively. The peak height (absorbance) values were employed in the calculations of the peak ratios and the peak height values were calculated by subtracting the values on the baseline of each spectrum from the values in the actual spectrum.

$$PR^0_{DMPCL} = \frac{[1637\ cm^{-1}]^0_{DMPCL}}{[1637\ cm^{-1}]^0_{DMPCL} + [1720\ cm^{-1}]^0_{DMPCL}} \quad (3.10)$$

$$PR^{0}_{PEGMA-950} = \frac{[1637\ cm^{-1}]^{0}_{PEGMA-950}}{[1637\ cm^{-1}]^{0}_{PEGMA-950} + [1720\ cm^{-1}]^{0}_{PEGMA-950}} \quad (3.11)$$

$$PR^{p}_{Exp} = \frac{[1637\ cm^{-1}]^{p}_{Exp.}}{[1637\ cm^{-1}]^{p}_{Exp.} + [1720\ cm^{-1}]^{p}_{Exp.}} \quad (3.12)$$

$$EPR^{0}_{Exp} = PR^{0}_{DMPCL} \cdot (\chi_{DMPCL}) + PR^{0}_{PEGMA-950} \cdot (\chi_{PEGMA-950}) \quad (3.13)$$

$$Conversion, \% = \frac{EPR^{0} - PR^{p}_{Exp.}}{EPR^{0}} \times 100 \quad (3.14)$$

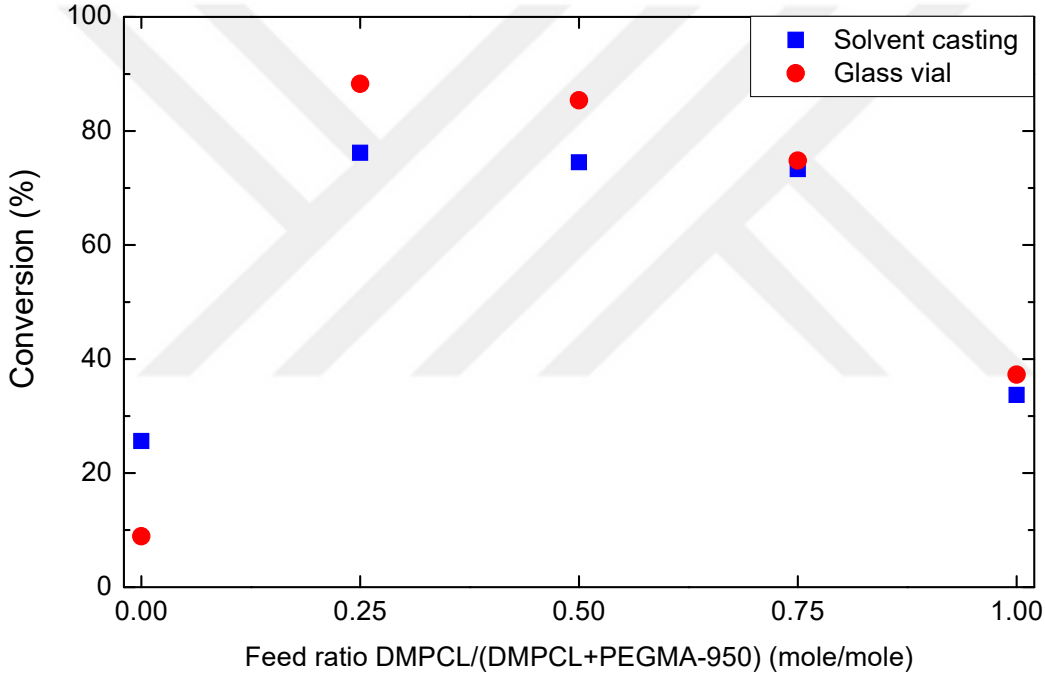

Figure 3.45 : Comparison of the conversions of the reactions processed in glass vials or via solvent casting method according to the feed ratio change of DMPCL in the total amount of DMPCL and PEGMA-950.

As it was demonstrated in Figure 3.45 and Table 3.3, the conversion values of the experiments processed in glass vials or by solvent casting method were compared. In both methods, the conversion values of the experiments involving solely DMPCL or PEGMA-950 had substantially lower values as compared with the experiments including both of the macromonomers. This result reveals the synergetic advantegous of the usage of both macromonomers which might be attributed to the crosslinking effect of the α,ω-methacrylated PCL macromonomers on the PEGMA-950 macromonomers. Since, DMPCL had a high molecular weight for a crosslinking agent,

it was relatively hard to react via photopolymerization even TMPTA was used as a trifunctional crosslinking agent.

Table 3.3 : The conversion (%) values of the experiments with respect to the feed mole ratios of DMPCL and PEGMA-950 macromonomers according to FTIR-ATR measurements

Experiment Code	DMPCL/ (Total macromon.) (mole/mole)	PEGMA-950/ (Total macromon.) (mole/mole)	Conversion (%)
S-PCLPEG-1.00	1	0	34
S-PCLPEG-0.75	0.75	0.25	73
S-PCLPEG-0.50	0.5	0.5	75
S-PCLPEG-0.25	0.25	0.75	76
S-PCLPEG-0.00	0	1	26
V-PCLPEG-1.00	1	0	37
V-PCLPEG-0.75	0.75	0.25	75
V-PCLPEG-0.50	0.5	0.5	85
V-PCLPEG-0.25	0.25	0.75	88
V-PCLPEG-0.00	0	1	9

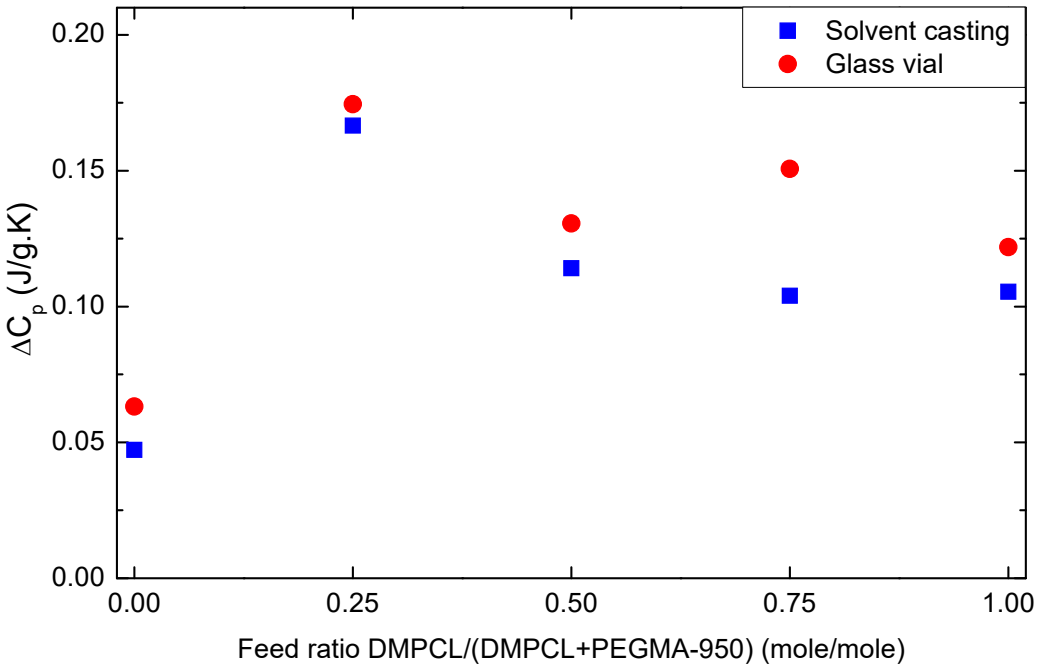

Figure 3.46 : Comparison of the ΔC_p values of the reactions processed in glass vial or via solvent casting method according to the feed ratio change of DMPCL in the total amount of DMPCL and PEGMA-950.

In Figure 3.46, the same synergetic effect with the conversion of double bonds was observed for ΔCp which was an indicator of reaction efficiency. The higher ΔC_p values revealed better conversion. It was worth to mention that in the experiment coded as S-PCLPEG-0.25 and V-PCLPEG-0.25 (with 0.25 and 0.75 feed mole ratios of DMPCL and PEGMA-950 together with TMPTA which was 10.5% of the total macromonomers by weight and Irgacure-819 which 3% of the total monomers) had the highest photopolymerization efficiency regarding the conversion calculated peak height ratios via FTIR-ATR and ΔC_p values via DSC measurements. The soxhlet extraction of the sample V-PCLPEG-0.75 was also performed. The conversion value of this sample was calculated as 75% (Table 3.3) according to FTIR-ATR measurements. After soxhlet extraction, the gel content was found to be 68 % which was consistent with the result acquired with FTIR-ATR measurements.

Considering the synthesis of double methacrylated PCL macromonomers, eROP was evaluated as an efficient method. For the synthesis of amphiphilic networks, photopolymerization with LED lamps was found to be sufficient observing the substantial decrease in the ΔH_f and increase in ΔC_p values confirmed the efficient conversions, calculated from FTIR-ATR results, of photocuring in the experiments having DMPCL feed mole ratios of 0.25, 0.50 and 0.75 revealing the synergetic effect of the utilization of α,ω-methacrylated PCL macromonomers on the PEGMA-950 macromonomer.

3.3 Photopolymerization Of Acrylates Via Enzymatically Synthesized PCL Based Macrophotoinitiator

^{1}H NMR spectrum of the Irgacure-2959 end-functionalized PCL based macrophotoinitiator was demonstrated in Figure 3.47. The characteristic peaks of the structure were as follows: **a** (2H, m, HO-C-$(CH_3)_2$-C(O)-C-***(CH)***$_2$-$(CH)_2$-C-O-) δ= 7.90–7.95 ppm; **b** (2H, m, HO-C-$(CH_3)_2$-C(O)-C $(CH)_2$-***(CH)***$_2$-C-O-) δ = 6.93–6.98 ppm; **c** (2H, t, -C(O)-C-$(CH)_2$-$(CH)_2$-C-O-***CH$_2$***-CH_2-) δ = 4.23–4.27 ppm; **d** (2H, t, -C(O)-C-$(CH)_2$-$(CH)_2$-C-O-CH_2-***CH$_2$***-) δ=4.43–4.47 ppm; **e** (6H, s, HO-C-***(CH$_3$)***$_2$-C(O)-C-$(CH)_2$-$(CH)_2$-C-O-) δ=1.22–4.27 ppm; **1** (2H, t, -O-$(CH_2)_2$-O-C(O)-***CH$_2$***-CH_2-CH_2-CH_2-CH_2-) δ=2.23–2.38 ppm; **2, 4** (4H, m, -O-$(CH_2)_2$-O-C(O)-CH_2-***CH$_2$***-CH_2-***CH$_2$***-CH_2-) δ=1.50–1.75 ppm; **3** (2H, t, -O-$(CH_2)_2$-O-C(O)-CH_2-*C*H_2-***CH$_2$***-*C*H_2-CH_2-) δ= 1.30–1.45 ppm; **5** (2H, t, -O-$(CH_2)_2$-O-C(O)-CH_2-*C*H_2-CH_2-*C*H_2-***CH$_2$***-) δ=

4.00–4.15 ppm; **5'** (2H, t, -O-$(CH_2)_2$-O-C(O)-CH_2-CH_2-CH_2-CH_2-CH_2-OH) δ= 3.61–3.67 ppm. Therefore, the end-group fidelity of the macrophotoinitiator was found according to the equation 3.15, where I_a and $I_{5'}$ were the peak inteagrals of the peaks **a** and **5'** respectively. Since, the peak **5'** presented in every polymer chain and the peak **a** only presented in the successfully Irgacure-2959 initiated PCL chains, the end-group fidelity (the molar ratio of Irgacure-2959 end-functionalized PCL chain to the total PCL chains in the dry polymer mixture) was calculated as the direct ratios of the peak areas of the two peaks.

$$End\text{-}group\ fidelity = \frac{I_a}{I_{5'}} \tag{3.15}$$

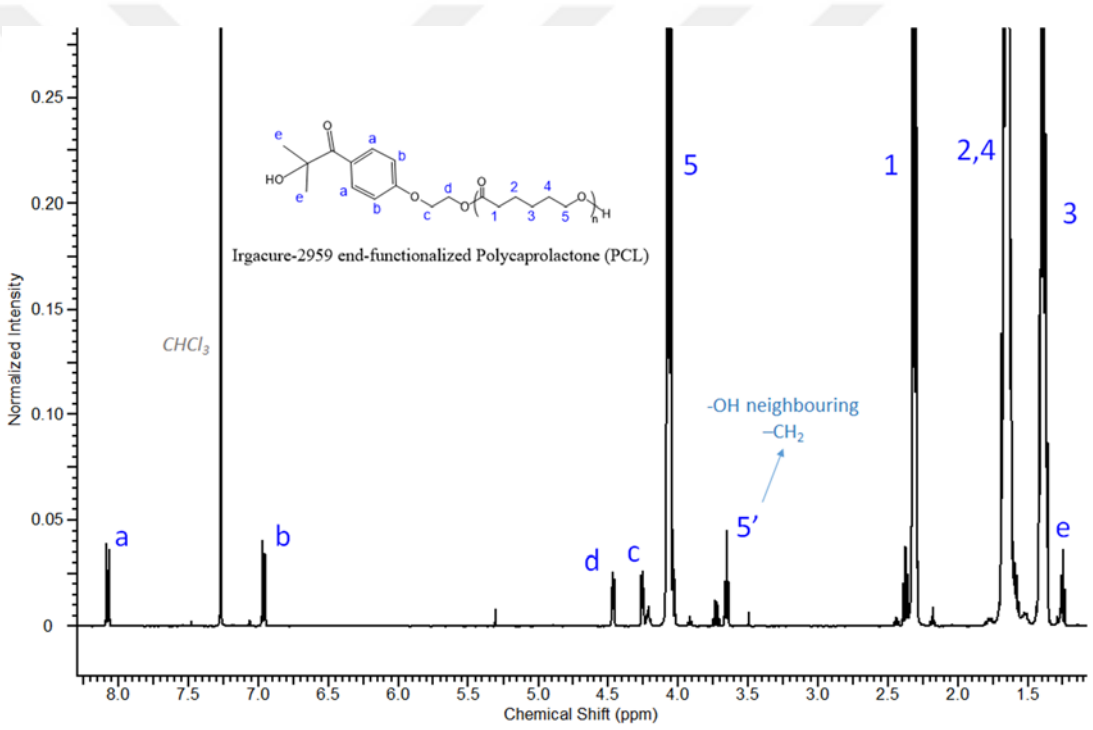

Figure 3.47 : ^{1}H NMR spectrum of the PCL based Irgacure-2959 end-functionalized macrophotoinitiator.

According to DSC measurement of the macrophotoinitiator, T_m was measured as 52.3°C (Figure 3.48) and T_g was measured as -53.3°C (Figure 3.49).

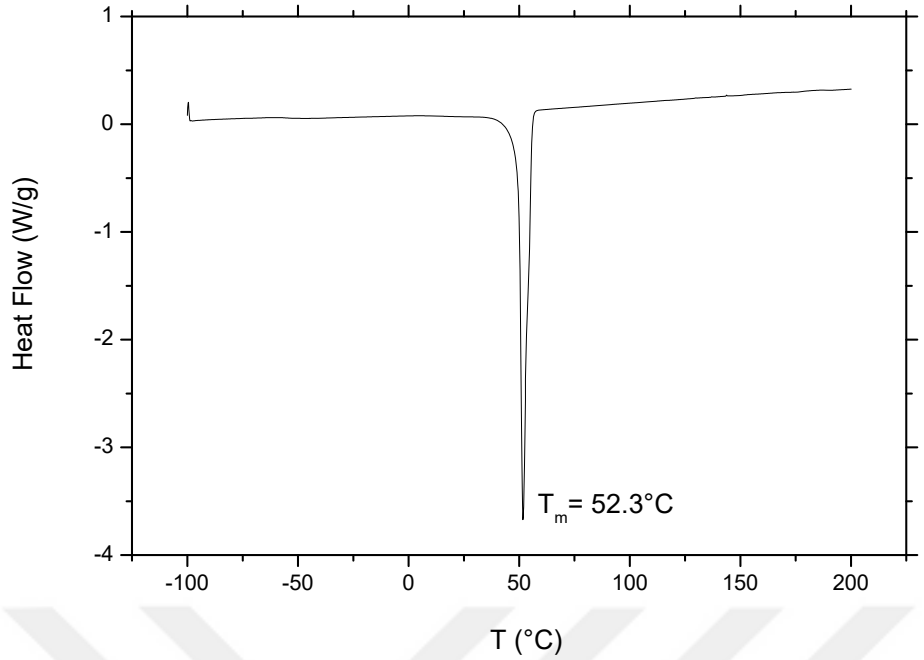

Figure 3.48 : T_m peak of the macrophotoinitiator.

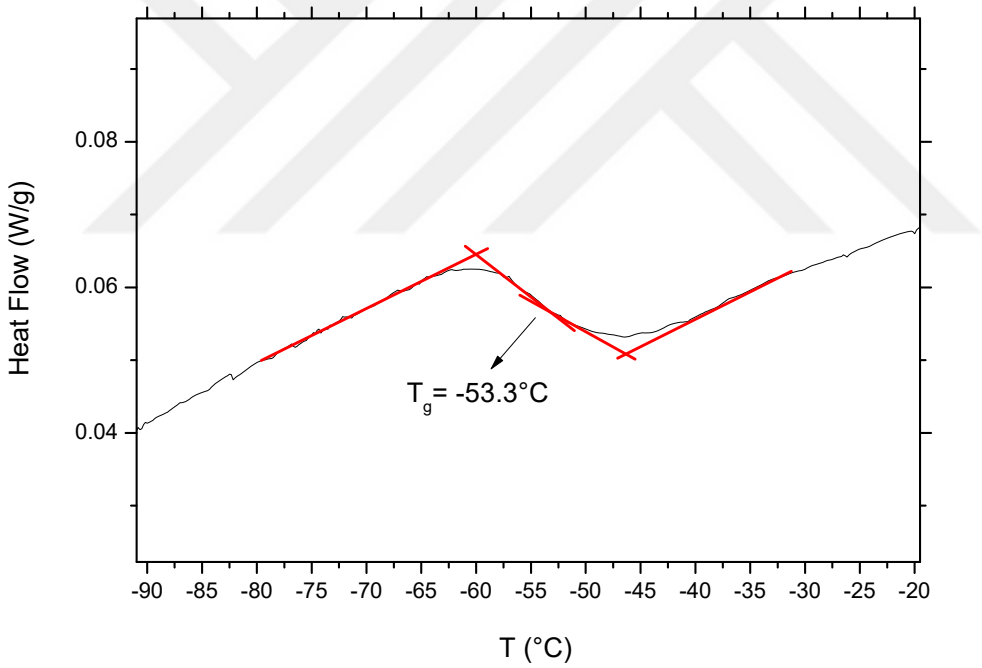

Figure 3.49 : T_g of the macrophotoinitiator.

3.3.1 Photopolymerization of butyl acrylate

The conversion of BuA was calculated from the reaction mixture. The ^{1}H NMR of the reaction mixture was demonstrated in Figure 3.51. The conversion of BuA monomer was calculated as 54 % according to the equation 3.16. The integration of one of the unreacted H atoms belonging to the vinyl bonds and H atoms belonging to –CH_3 of both reacted and unreacted butyl acrylate units were used in the equation, as $I_{G'}$, $I_{C'}$

and I_C were the peak integrals of the peaks **G'**, **C'** and **C** belonging to the H atoms of the vinylic double bonds in the uncreacted BuA monomers, methyl groups in the unreacted and reacted BuA monomers respectively. The chemical structures of the target block copolymer $P(CL)_n$-*b*-$P(BuA)_m$ and BuA monomer were demonstrated in Figure 3.50.

$$Conversion\ of\ Butyl\ Acrylate\ (\%) = (1 - \frac{I_{G'} \times 3}{I_{C'} + I_C}) \times 100 \qquad (3.16)$$

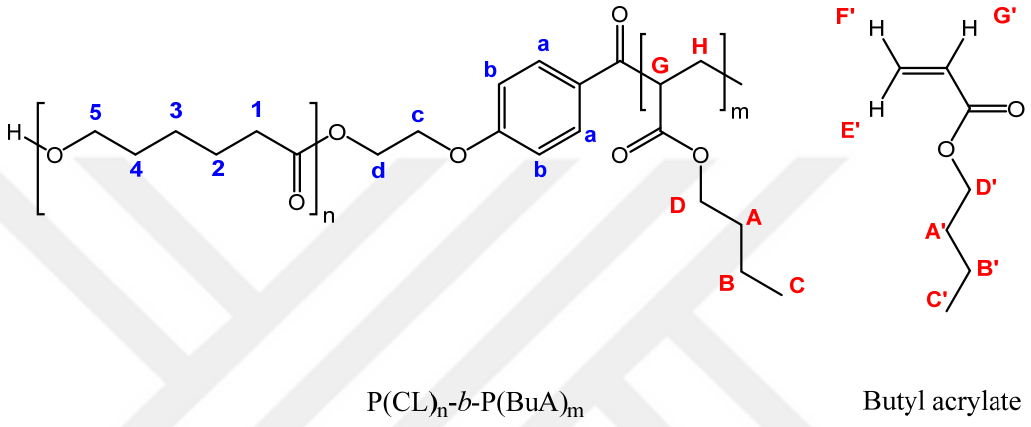

$P(CL)_n$-*b*-$P(BuA)_m$ Butyl acrylate

Figure 3.50 : Chemical structures of the target block copolymer of $P(CL)_n$-*b*-$P(BuA)_m$ and BuA monomer.

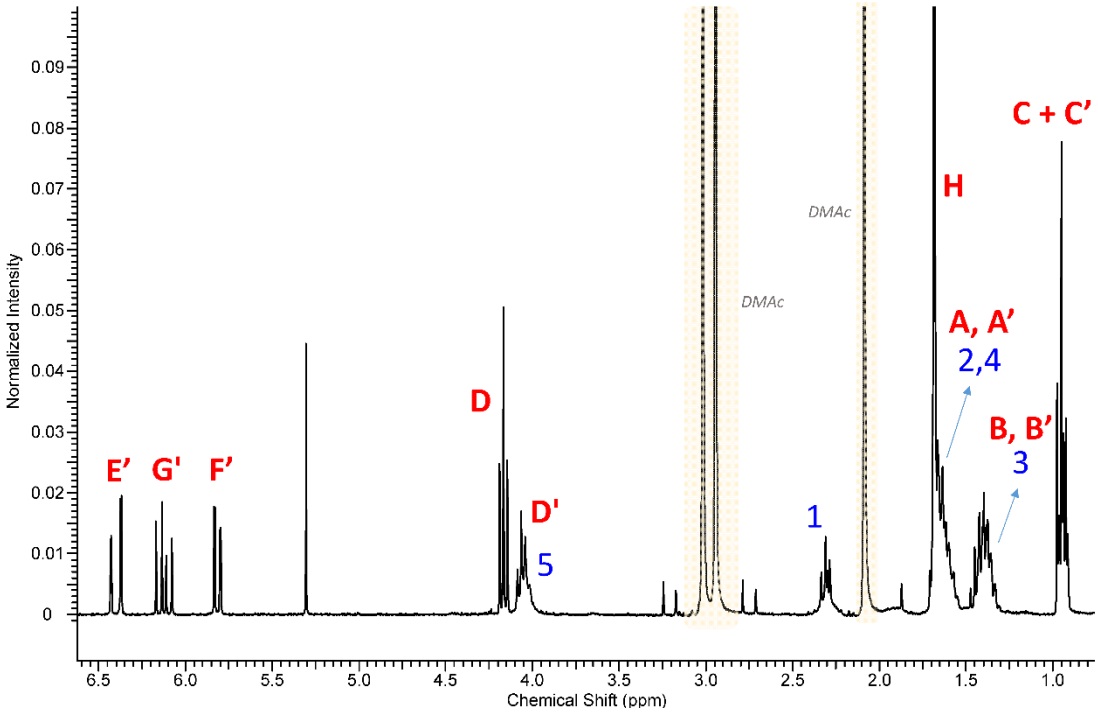

Figure 3.51 : ^{1}H NMR spectrum of the reaction mixture after photopolymerization of BuA via PCL based Irgacure-2959 end-functionalized macrophotoinitiator.

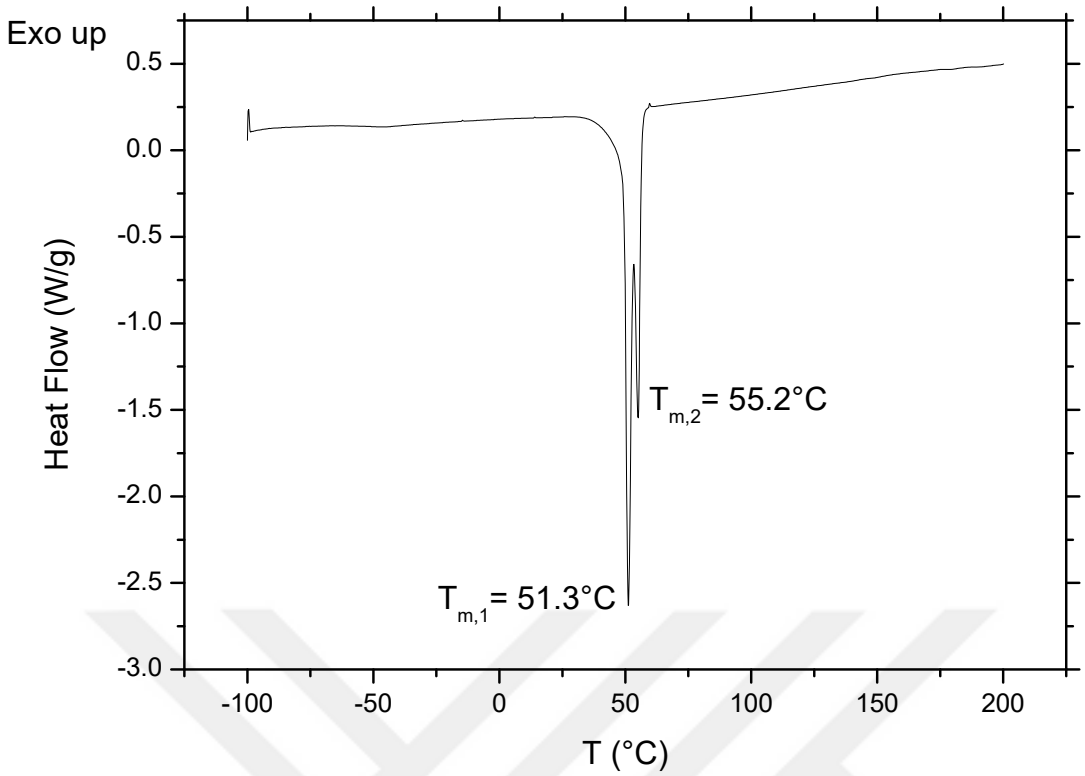

Figure 3.52 : The T_m peaks of the photopolymerization product of BuA.

The DSC results of the photopolymerization product of BuA revealed that there were two T_m peaks (at 51.3°C and 55.2°C) one of which might be belonging to unreacted PCL based macrophotoinitiator or the homopolymer of BuA which was formed as a side reaction. This might be caused due to the formation of two free-radicals under UV exposure of the macrophotoinitiator, one of which was not including PCL chain and the other comprised the PCL chain. The other T_m peak might be belonging to the target block copolymer (Figure 3.53). The T_g of the polymer was calculated as -53.1°C which was very close to that of the macrophotoinitiator (Figure 3.49).

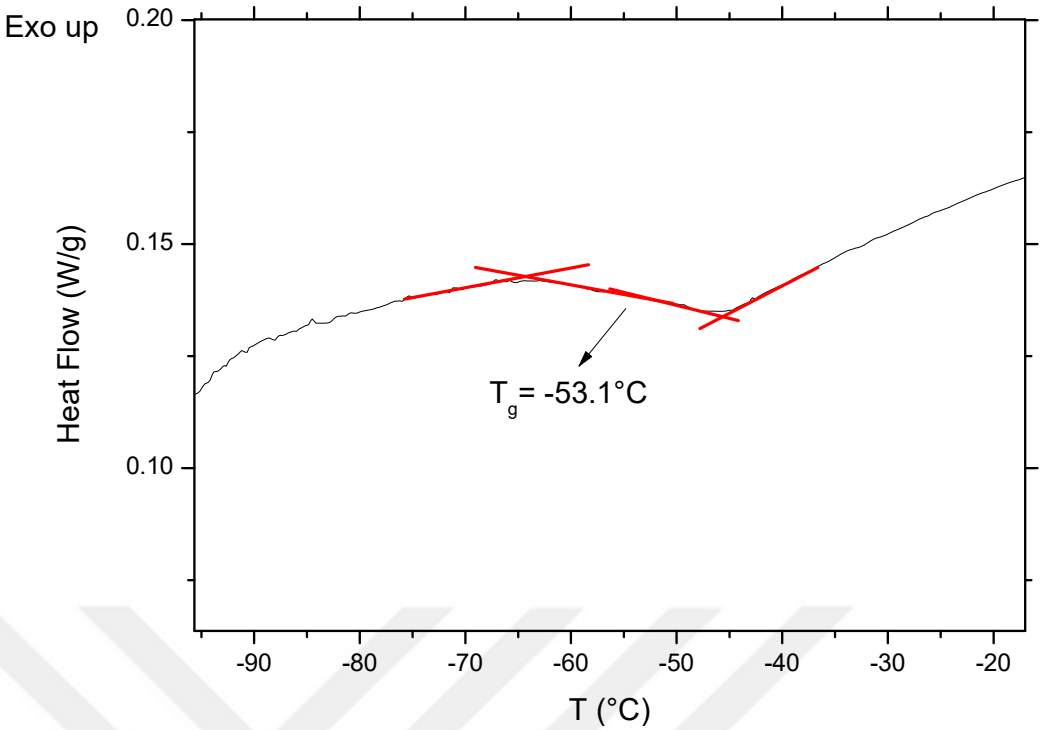

Figure 3.53 : The T_g of the photopolymerization product of BuA.

3.3.2 Photopolymerization of benzyl acrylate

The conversion of BzA was calculated from the reaction mixture. The ^{1}H NMR of the reaction mixture was demonstrated in Figure 3.55. The conversion of BuA monomer was calculated as 54 % according to the equation 3.17. The integration of the unreacted and reacted H atoms belonging to the ester neighbouring -CH_2- groups of the benzyl acrylate units were used in the equation, as I_D, and $I_{D'}$ were the peak integrals of the peaks D and D' belonging to the H atoms of the ester neighbouring -CH_2- groups in the reacted and unreacted BzA monomers, respectively. The chemical structures of the target block copolymer P$(CL)_n$-*b*-P$(BzA)_m$ and BzA monomer were demonstrated in Figure 3.54. The conversion of BzA monomer was calculated as 90 % according to the equation below:

$$\textit{Conversion Benzyl Acrylate (\%)} = \frac{I_D}{I_D + I_{D'}} \times 100 \qquad (3.17)$$

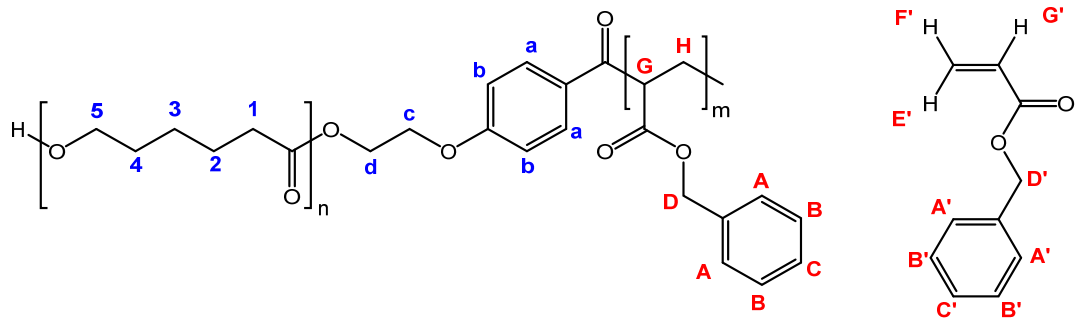

$P(CL)_n$-*b*-$P(BzA)_m$ Benzyl acrylate

Figure 3.54 : Chemical structures of the target block copolymer of $P(CL)_n$-*b*-$P(BzA)_m$ and BzA monomer.

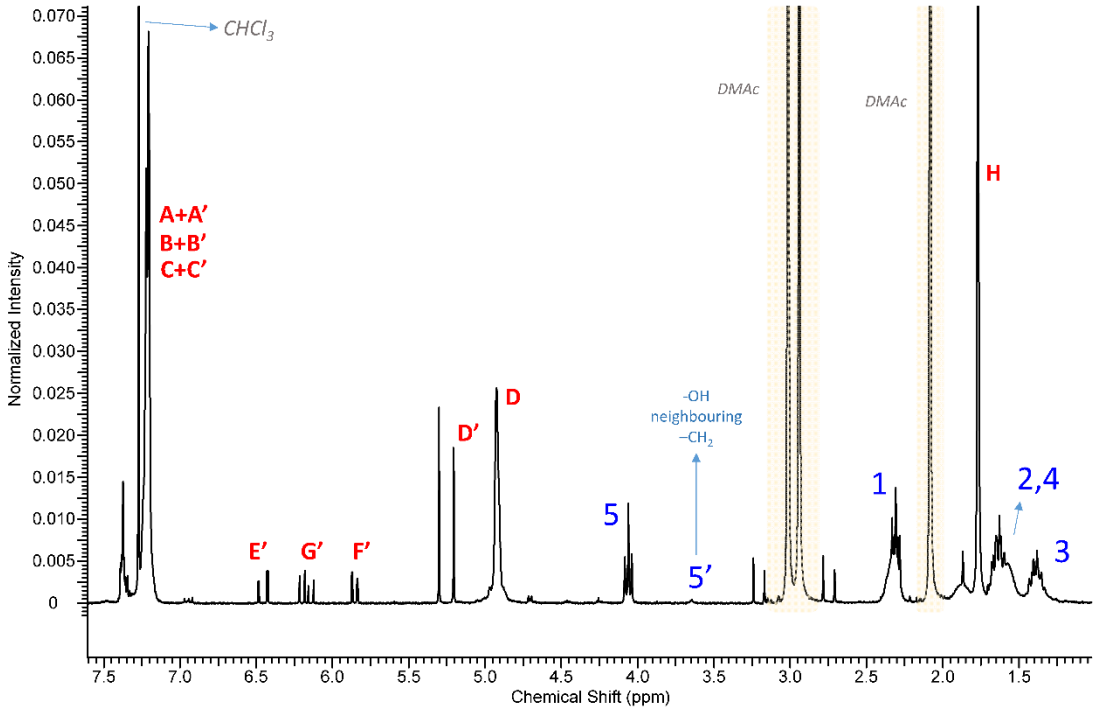

Figure 3.55 : ^{1}H NMR spectrum of the reaction mixture after photopolymerization of BzA via PCL based Irgacure-2959 end-functionalized macrophotoinitiator.

According to the ^{1}H NMR of purified dry polymer of this reaction (Figure 3.56) the conversion was calculated as 93 % confirming the conversion calculation from the crude reaction mixture, where $[I]_D^d$ and $[I]_5^d$ were the peak integrals of the peaks ***D*** and ***5*** of the dry polymer and $[I]_D^f$, and $[I]_5^f$ were the peak integrals of the peaks ***D'*** and ***5*** of the feed before photopolymerization (Equation 3.18).

$$Dry\ Polymer\ Conversion\ Benzyl\ Acrylate\ (\%) = \frac{[I]_D^d / [I]_5^d}{[I]_{D'}^f / [I]_5^f} \times 100 \qquad (3.18)$$

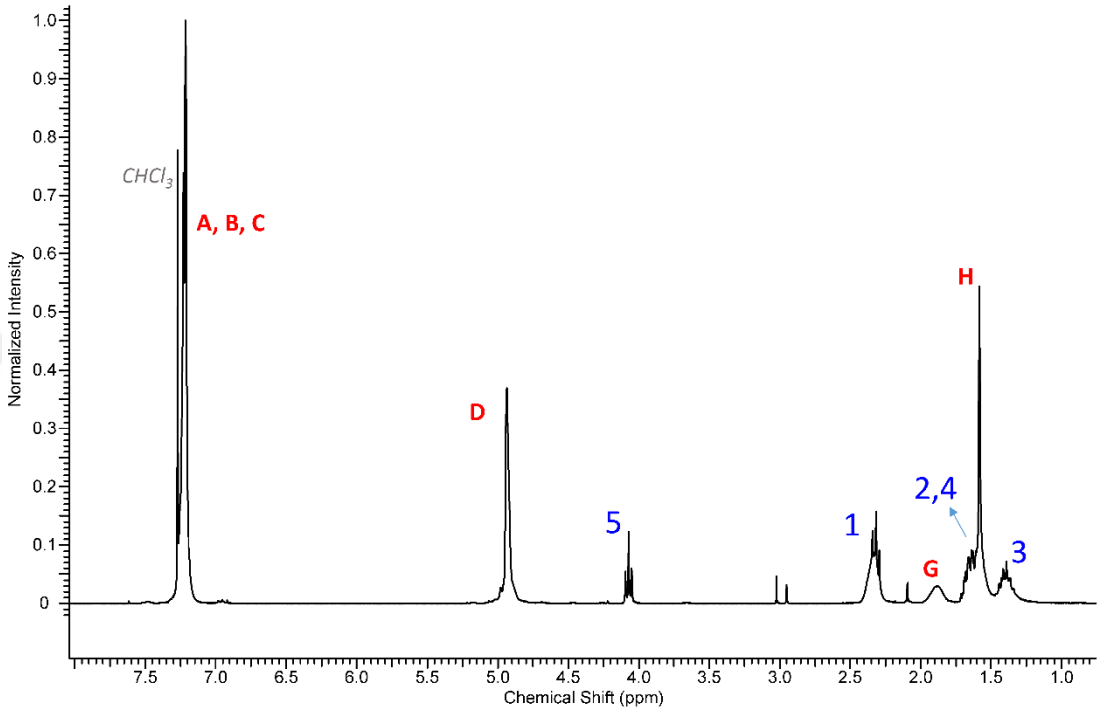

Figure 3.56 : ^{1}H NMR spectrum of the dry polymer after photopolymerization of BzA via PCL based Irgacure-2959 end-functionalized macrophotoinitiator.

In Figure 3.57, the DSC of the photopolymerization product of BzA was demonstrated. The only endothermic transition was the broad glass transition of the block copolymer. The T_g of the block copolymer was evaluated as -6.5°C proving there was no unreacted macrophotoinitiator or homo PBzA present in polymer. Thus, the resulting polymer had a completely amorphous structure.

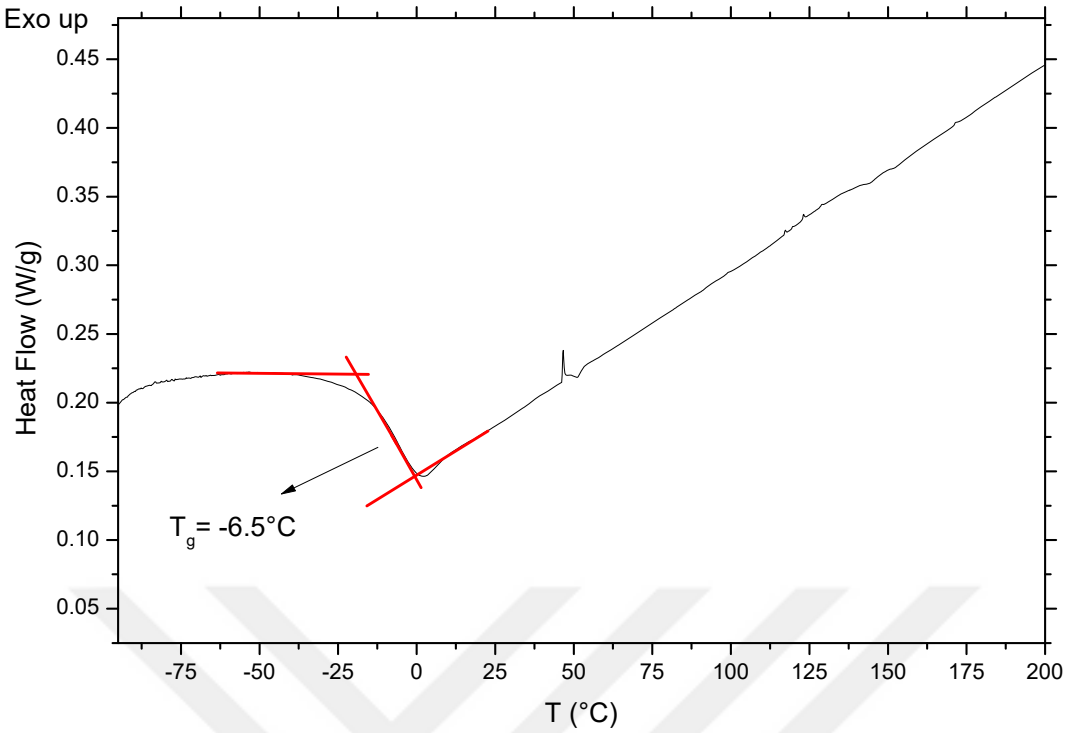

Figure 3.57 : The DSC 2nd heating curve of the photopolymerization product of BzA.

3.3.3 Photopolymerization of tetrahydrofurfuryl acrylate

The conversion of THFA was calculated from the reaction mixture. The ^{1}H NMR of the reaction mixture was demonstrated in Figure 3.59. The conversion of THFA monomer was calculated as 94 % according to the Equation 3.19. The integration of H atoms of the unreacted double bonds and the reacted and unreacted H atoms on the monomer ring were used in the equation, as $I_{F'}$, and I_H were the peak integrals of the peaks **F'** and **H** belonging to the H atoms of the double bonds of the unreacted THFA monomer and indicating the H atoms of $–CH_2-$ along the PTHFA bacbone respectively. The chemical structures of the target block copolymer $P(CL)_n$-*b*-$P(THFA)_m$ and THFA monomer were demonstrated in Figure 3.58.

$$\textit{Conversion of THFA (\%)} = \left(1 - \frac{(I_{F'} \times 2)}{(I_{F'} \times 2) + I_H}\right) \times 100 \qquad (3.19)$$

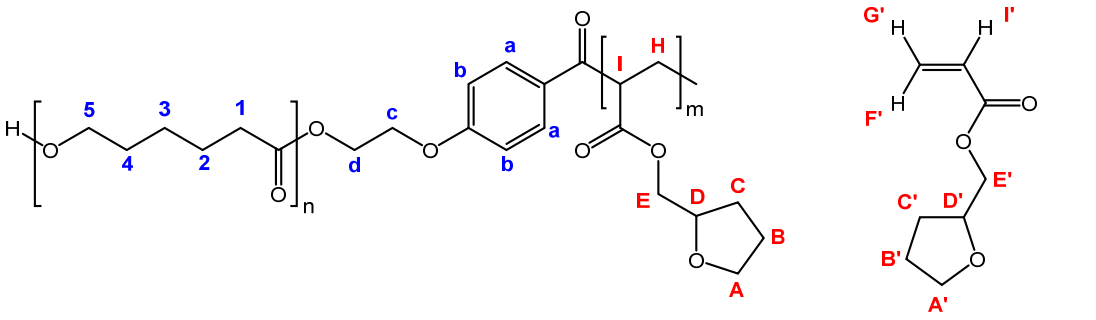

$P(CL)_n$-*b*-$P(THFA)_m$ Tetrahydrofurfuryl acrylate

Figure 3.58 : Chemical structures of the target block copolymer of $P(CL)_n$-*b*-$P(THFA)_m$ and THFA monomer.

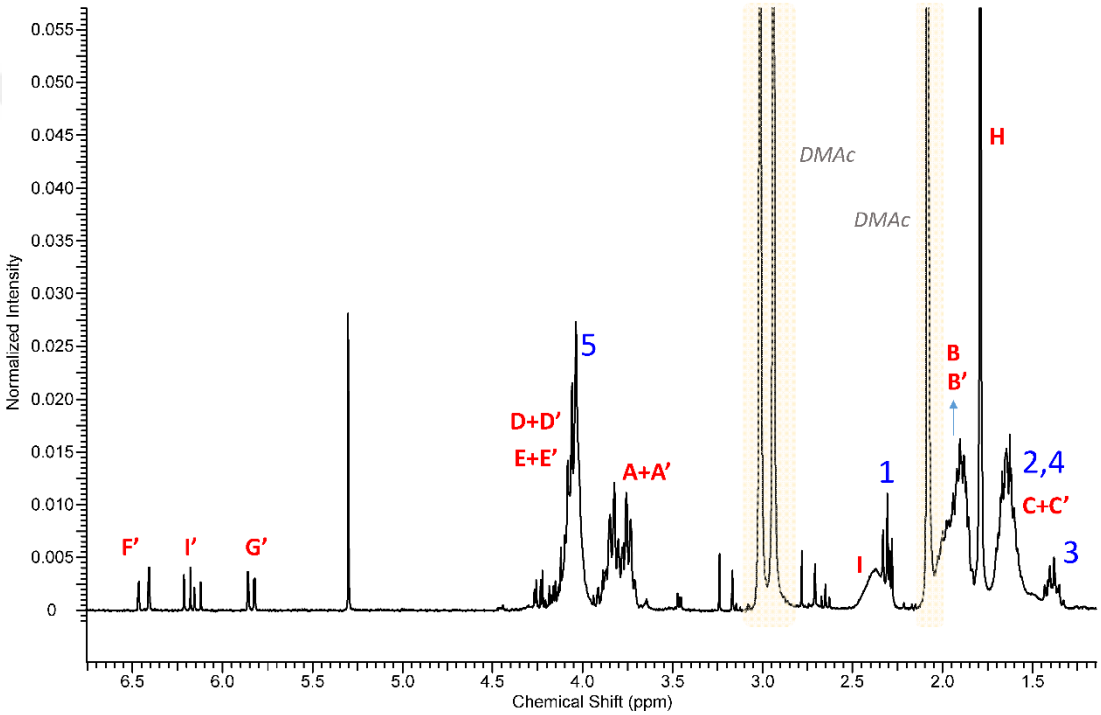

Figure 3.59 : ^{1}H NMR spectrum of the reaction mixture after photopolymerization of BzA via PCL based Irgacure-2959 end-functionalized macrophotoinitiator.

In Figure 3.60, the ^{1}H NMR of the dry polymer was demonstrated. The dry polymer conversion was calculated following Equations 3.20-3.22. *m/n* referred to the ratio of the number of the repeating units of THFA to the repeating units of CL on the macrophotoinitiator backbone which was calculated according to Equations 2.21-2.22. I_A, I_D, I_E and I_5 and were the integral values of the peaks **A**, **D**, **E** and **5** respectively. $(m_{feed})/(n_{feed})$ was the feed ratio of the THFA monomer to the CL repeating units in the feed before the light induced polymerization, which was the same as BuA, BzA, TFEA, HEA and PEGMEA-480 photopolymerization, 200/31 (mole/mole). However,

due to the loss of some of the chains during the purification procedure, the dry polymer conversion was calculated as 73%.

$$Dry\ Polymer\ Conversion\ of\ THFA\ \ (\%) = \frac{m/n}{(m_{feed})/(n_{feed})} \times 100 \tag{3.20}$$

$$I_D + I_E + I_5 = 3m + 2n \tag{3.21}$$

$$I_A = 2n \tag{3.22}$$

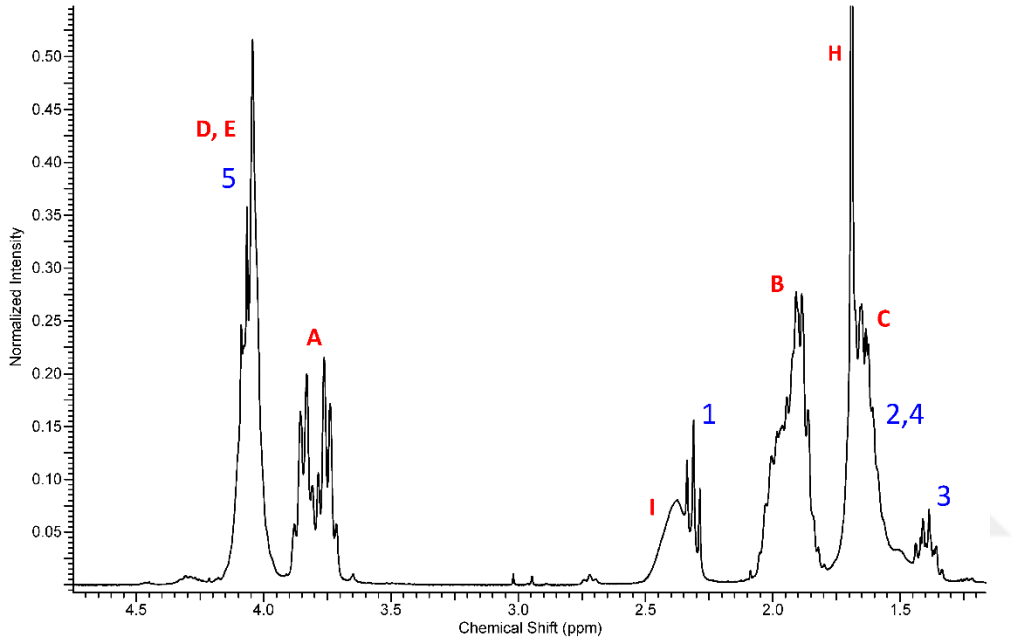

Figure 3.60 : ^{1}H NMR spectrum of the dry polymer after photopolymerization of THFA via PCL based Irgacure-2959 end-functionalized macrophotoinitiator.

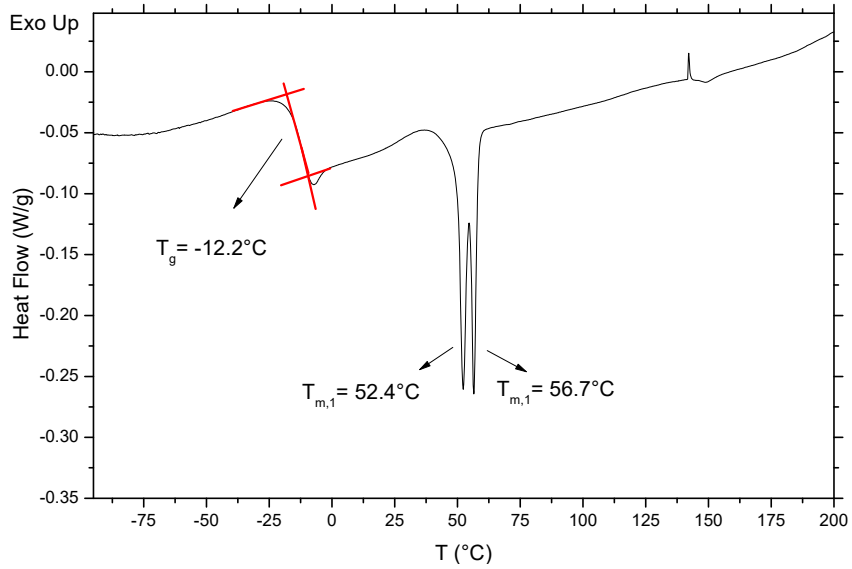

Figure 3.61 : The DSC 2nd heating curve of the photopolymerization product of THFA showing a single T_g and a double T_m peak.

The DSC thermogram of the photopolymerization product of THFA was depicted in Figure 3.61. The broad and high step change in the glass transition of the polymer reveal a highly amorphous structure as compared with the homopolymer of Irgacure-2959 end-functionalized PCL macrophotoinitiator. However, the two melting point at very closed values (at 52.4°C and 56.7°C) might be an indication of either two different crystalline domains, an uncreacted PCL macrophotoinitiator or homopolymer of THFA.

3.3.4 Photopolymerization of 2,2,2-Trifluoroethyl acrylate

The conversion of TFEA was calculated from the reaction mixture. The ^{1}H NMR of the reaction mixture was demonstrated in Figure 3.63. The integration of H atoms of the unreacted double bonds and the reacted and unreacted H atoms on the -CH_2- group neighbouring the ester and CF_3 functionality were used in the equation, as $I_{B'}$, I_A and $I_{A'}$ were the peak integrals of the peaks **B'**, **A** and **A'**. The chemical structures of the target block copolymer P(CL)$_n$-*b*-P(TFEA)$_m$ and TFEA monomer were demonstrated in Figure 3.62. The conversion of TFEA monomer was calculated as 93 % according to the equation 3.23.

$$Conversion\ of\ TFEA\ (\%) = \left(1 - \frac{I_{B'} \times 2}{I_A + I_{A'}}\right) \times 100 \qquad (3.23)$$

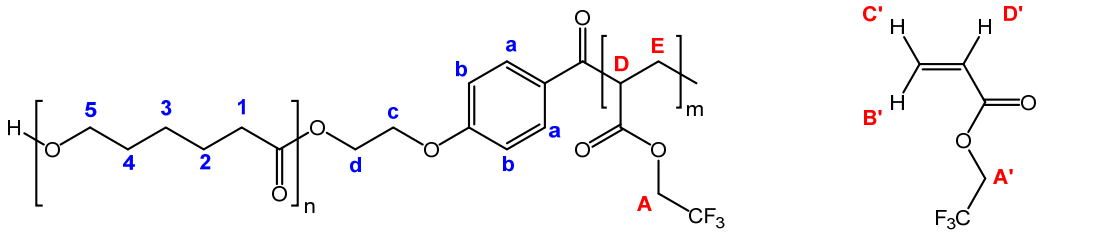

P(CL)$_n$-*b*-P(TFEA)$_m$ *2,2,2-Trifluoroethyl acrylate*

Figure 3.62 : Chemical structures of the target block copolymer of P(CL)$_n$-*b*-P(TFEA)$_m$ and TFEA monomer.

$$Dry\ Polymer\ Conversion\ TFEA\ (\%) = \frac{[I]_A^d \Big/ [I]_5^d}{[I]_{A'}^f \Big/ [I]_5^f} \times 100 \qquad (3.24)$$

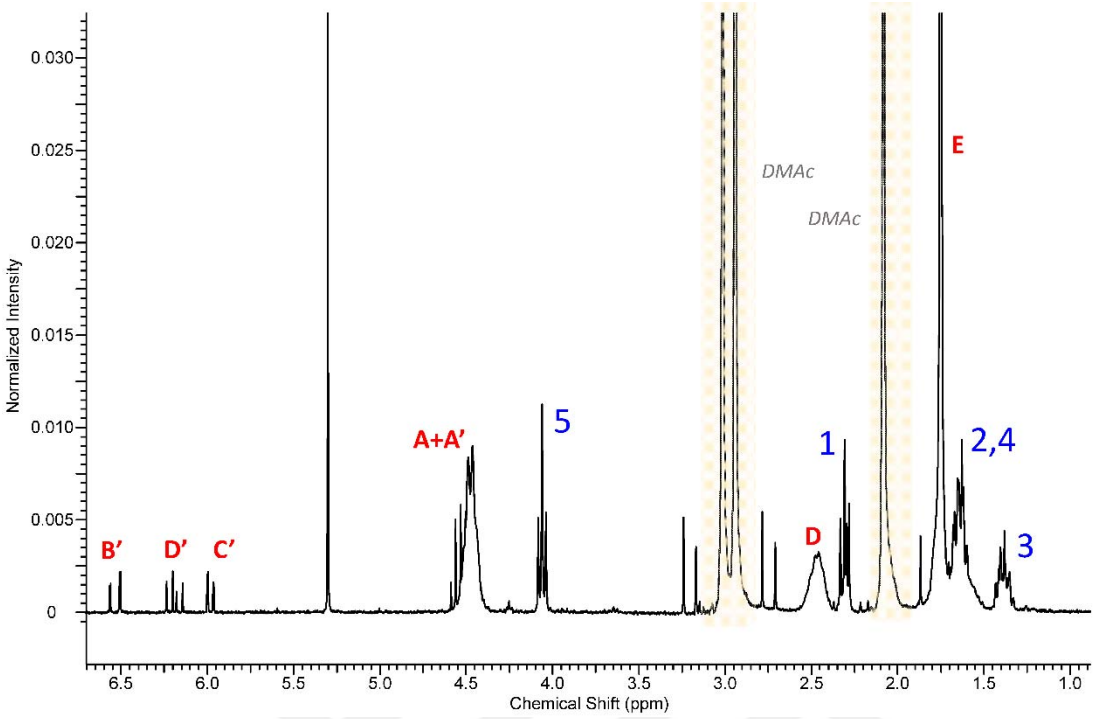

Figure 3.63 : ^{1}H NMR spectrum of the reaction mixture after photopolymerization of TFEA via PCL based Irgacure-2959 end-functionalized macrophotoinitiator.

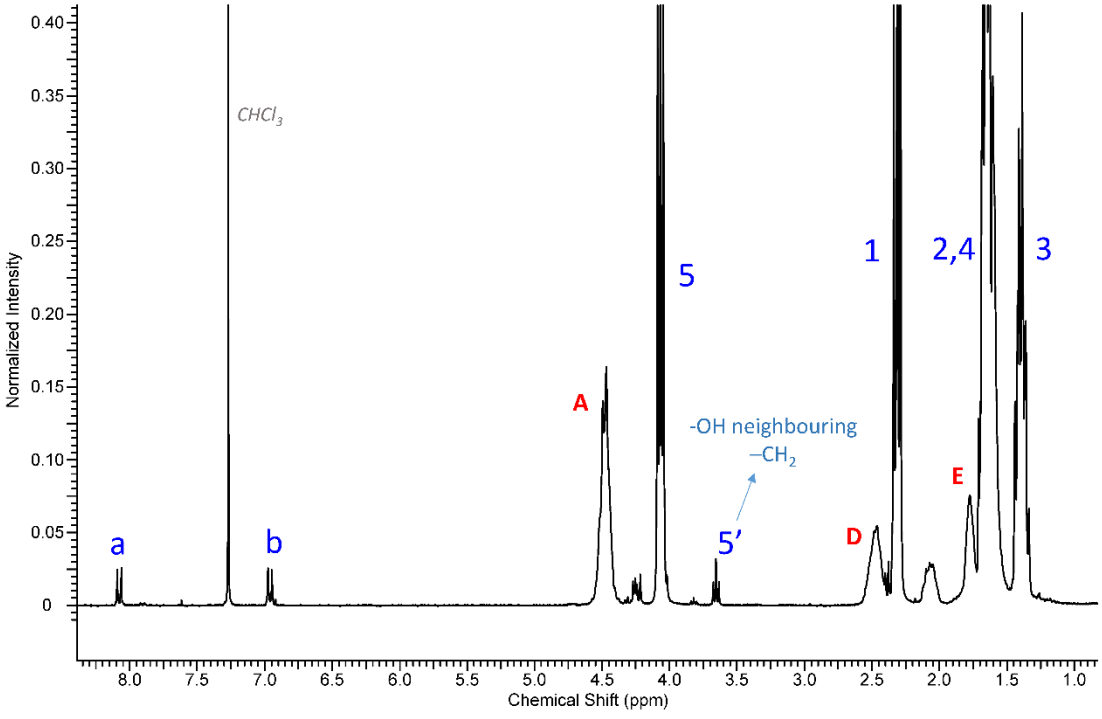

Figure 3.64 : ^{1}H NMR spectrum of the dry polymer after photopolymerization of TFEA via PCL based Irgacure-2959 end-functionalized macrophotoinitiator.

On the other hand, when the conversion of TFEA was calculated from ^{1}H NMR of the dry polymer, the conversion value was calculated as %13 (Figure 3.64 and Equation

3.24), which revealed that roughly 24 tetrahydrofurfuryl acrylate units were installed on PCL based macrophotoinitiator, resulting in block copolymer. The substantial decrease in the conversion might be caused from the purification procedure of the polymer. Oligomers of TFEA might be dissolved in diethyl ether and removed from the copolymer. This polymerization might be repeated. In equation 2.24, $[I]_A^d$ and $[I]_5^d$ were the peak integrals of the peaks ***A*** and ***5*** of the dry polymer and $[I]_A^f$, and $[I]_5^f$ were the peak integrals of the peaks ***A'*** and ***5*** of the feed before photopolymerization.

The DSC results of the photopolymerization product of TFEA revealed that there were 2 T_m peaks (at 51.3°C and 55.2°C) one of which might be belonging to unreacted PCL based macrophotoinitiator (Figure 3.65). The other T_m peak might be belonging to the block copolymer or another block copolymer crystalline domain.

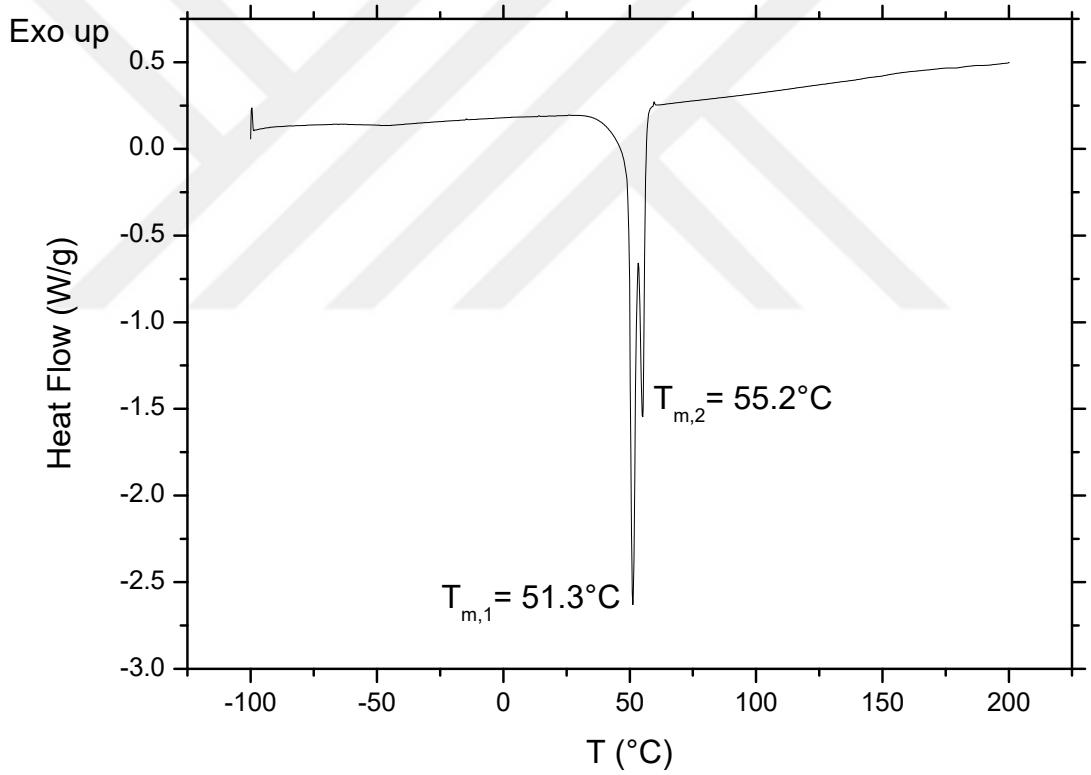

Figure 3.65 : The T_m peaks of the photopolymerization product of TFEA.

In Figure 3.66 the T_g of the polymer was evaluated as -0.3°C which was substantially higher than that of the macrophotoinitiator, which might be an indication of the amorphous region belonging to the homoblock copolymer as there was only one endothermic glass transition. Because, the glass transition related to the macrophotoinitiator was not observed in the heating curve.

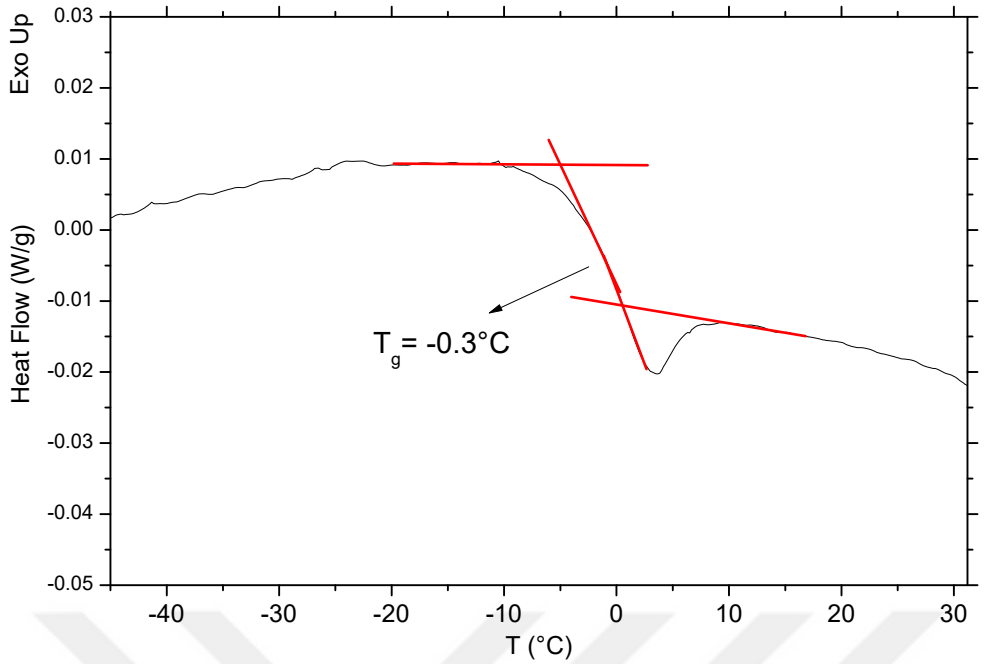

Figure 3.66 : The T_g of the photopolymerization product of TFEA.

3.3.5 Photopolymerization of 2-hydroxyethyl acrylate

The ^{1}H NMR of the photopolymerization product of HEA couldn't be measured because of the the insolubility of the resulting polymer in neither of the solvents such as $CHCl_3$, dichloromethane (CH_2Cl_2), dimethylformamide $HCON(CH_3)_2$, dimethylsulfoxide ($(CH_3)_2SO$), N,N-dimethylacetamide ($CH_3CON(CH_3)_2$), toluene ($C_6H_5CH_3$), hexane ($CH_3(CH_2)_4CH_3$), acetonitrile (CH_3CN) and water. Therefore only DSC and FTIR-ATR measurements of the resulting gel was formed. The chemical structures of the target block copolymer, $P(CL)_n$-*b*-$P(HEA)_m$ and HEA were shown in Figure 3.67.

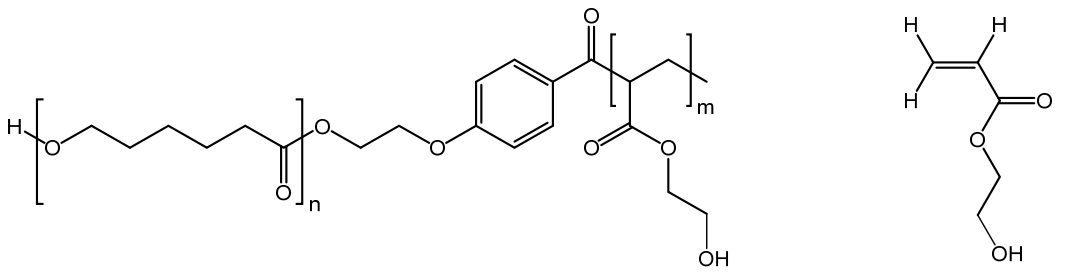

$P(CL)_n$-*b*-$P(HEA)_m$ *2-Hydroxyethyl acrylate*

Figure 3.67 : Chemical structures of the target $P(CL)_n$-*b*-$P(HEA)_m$ and HEA monomer.

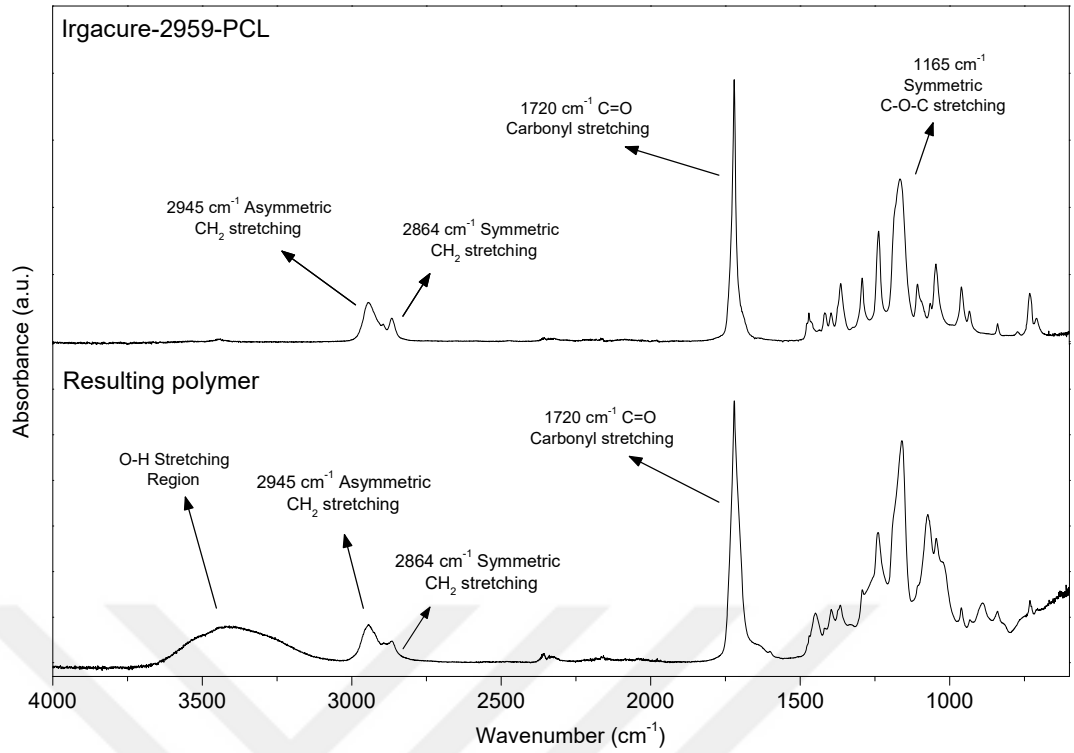

Figure 3.68 : FTIR-ATR spectrum of the Irgacure-2959 end-functionalized PCL macrophotoinitiator and the gel obtained after the photopolymerization of HEA.

The FTIR-ATR spectrum of the Irgacure-2959 end-functionalized PCL macrophotoinitiator and the gel obtained after the photopolymerization of HEA were demonstrated in Figure 3.68. It can be seen that after the photopolymerization of HEA, the resulting polymer had a wide O-H stretching region between 3000-3700 cm^{-1}, which was attributed the hydroxyl group after the installation of the HEA monomers. All of the other peaks relating to PCL structure were kept such as asymmetric stretching at 2945 cm^{-1}, symmetric stretching at 2864 cm^{-1}, carbonyl stretching at 1720 cm^{-1} and C-O-C stretching at 1165 cm^{-1}. On the other hand, FTIR-ATR technique is not sufficient enough to reveal whether the resulting polymer was a mixture of polymers or a block copolymer. Therefore, DSC measurement was performed.

For the photopolymerization of HEA, since there were two distinct glass transitions (at -55.3°C and 16.5°C) and two melting peaks (at 55.9°C and a broad peak around 160°C) were observed, the resulting polymer might be evaluated as the mixture of the unreacted PCL, homopolymer of HEA and the block copolymer $P(CL)_n$-*b*-$P(HEA)_m$. The T_g value at -55.3°C and Tm value at 55.9°C were the characteristic peaks of the PCL based macrophotoinitiator. On the other hand, the broad and highly inclined T_g value at 16.5°C was ascribed to the block copolymer and/or the homopolymer of HEA. Therefore, the photopolymerization product was in the rubbery state and had an elastic

behavior (Figure 3.69). The broad endothermic transition around 160°C was due to the high melting point of HEA including polymer chains equipped with dense hydrogen bonds due to the hydroxyl functionality of HEA repeating units, which was also confirmed by FTIR-ATR measurements.

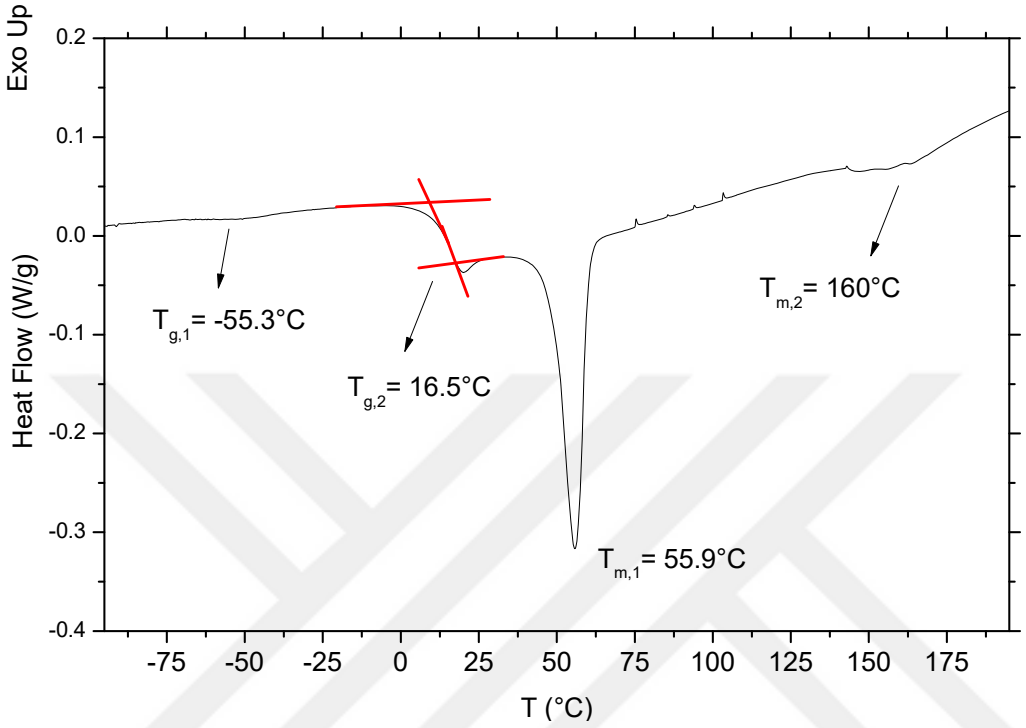

Figure 3.69 : The DSC 2nd heating curve of the photopolymerization product of HEA via PCL based macrophotoinitiator.

3.3.6 Photopolymerization of poly (ethylene glycol) methyl ether acrylate-480

The ^{1}H NMR of the photopolymerization product of PEGMEA-480 macromonomer couldn't be measured because of the the insolubility of the resulting polymer in neither of the solvents such as $CHCl_3$, dichloromethane (CH_2Cl_2), dimethylformamide $HCON(CH_3)_2$, dimethylsulfoxide ($(CH_3)_2SO$), N,N-dimethylacetamide ($CH_3CON(CH_3)_2$), toluene ($C_6H_5CH_3$), hexane ($CH_3(CH_2)_4CH_3$), acetonitrile (CH_3CN) and water. Therefore only DSC and FTIR-ATR measurements of the resulting gel was formed. The chemical structures of the target block copolymer, $(CL)_n$-*b*-$P(PEGMEA)_m$ and PEGMEA-480 macromonomer were shown in Figure3.70.

The FTIR-ATR spectrum of the Irgacure-2959 end-functionalized PCL macrophotoinitiator and the gel obtained after the photopolymerization of PEGMEA-480 were demonstrated in Figure 3.71. It can be seen that after the photopolymerization of

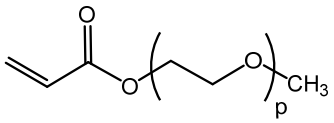

Poly (ethylene glycol) methyl ether acrylate

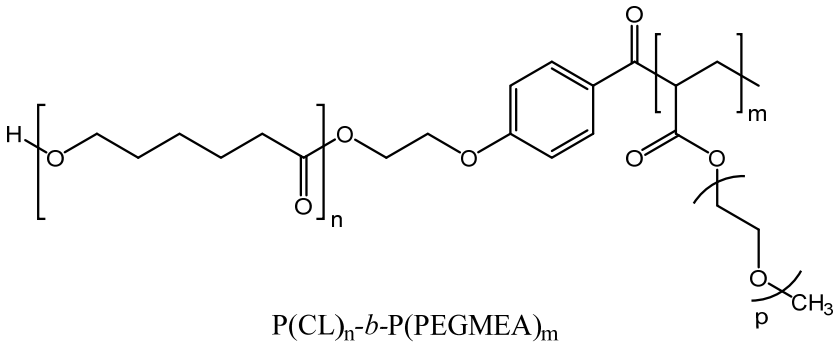

$P(CL)_n$-*b*-$P(PEGMEA)_m$

Figure 3.70 : Chemical structures of the target $P(CL)_n$-*b*-$P(PEGMEA)_m$ and PEGMEA-480 macromonomer.

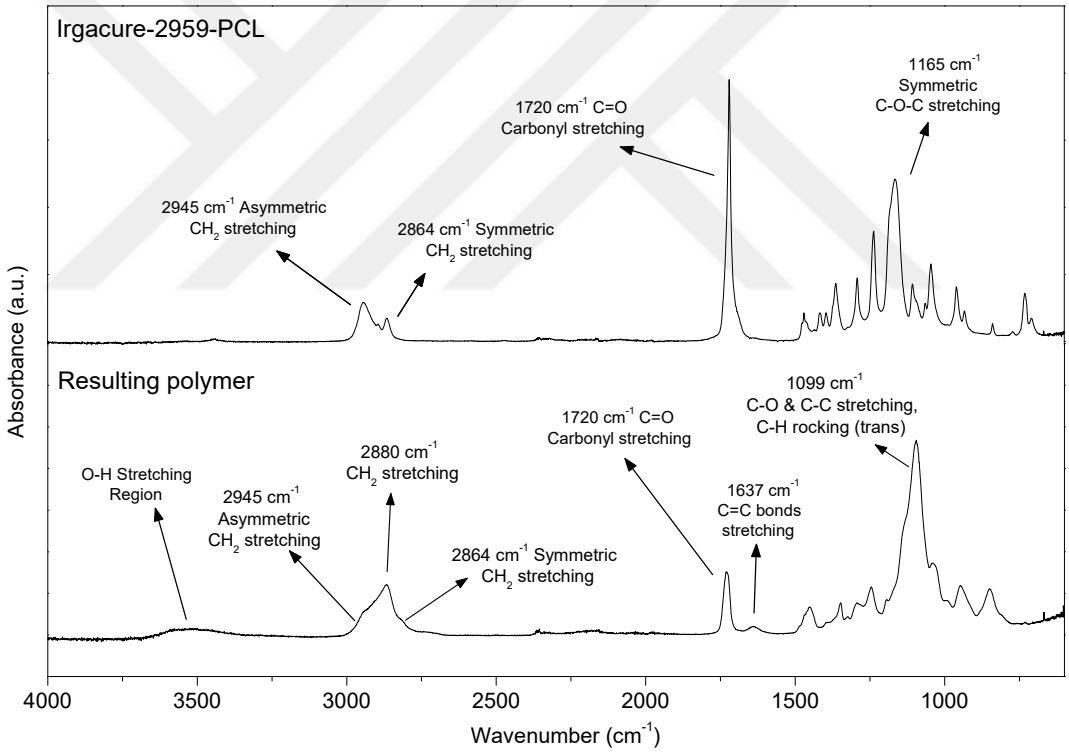

Figure 3.71 : FTIR-ATR spectrum of the Irgacure-2959 end-functionalized PCL macrophotoinitiator and the gel obtained after the photopolymerization of PEGMEA-480.

PEGMEA-480, the resulting polymer had a slight wide O-H stretching region between 3000-3700 cm^{-1}, which was attributed the moisture uptake of the PEGMEA segments in the final polymer. All of the other peaks relating to PCL structure were kept such as asymmetric stretching at 2945 cm^{-1}, symmetric stretching at 2864 cm^{-1}, carbonyl stretching at 1720 cm^{-1} and C-O-C stretching at 1165 cm^{-1}. Additionally, the peak with

small aborbance at 1637 cm^{-1} was associated with the double bonds of the unreacted PEGMEA-480 macromonomer residue trapped inside the gel, even though the resulting gel was rinsed with dichloromethane for numerously. The peak with highest absorbance value at 1099 cm^{-1}, which was the result of C-O, C-C stretching together with C-H rocking (trans) vibrations, implied the PEGMEA-480 segments in the resulting polymer.

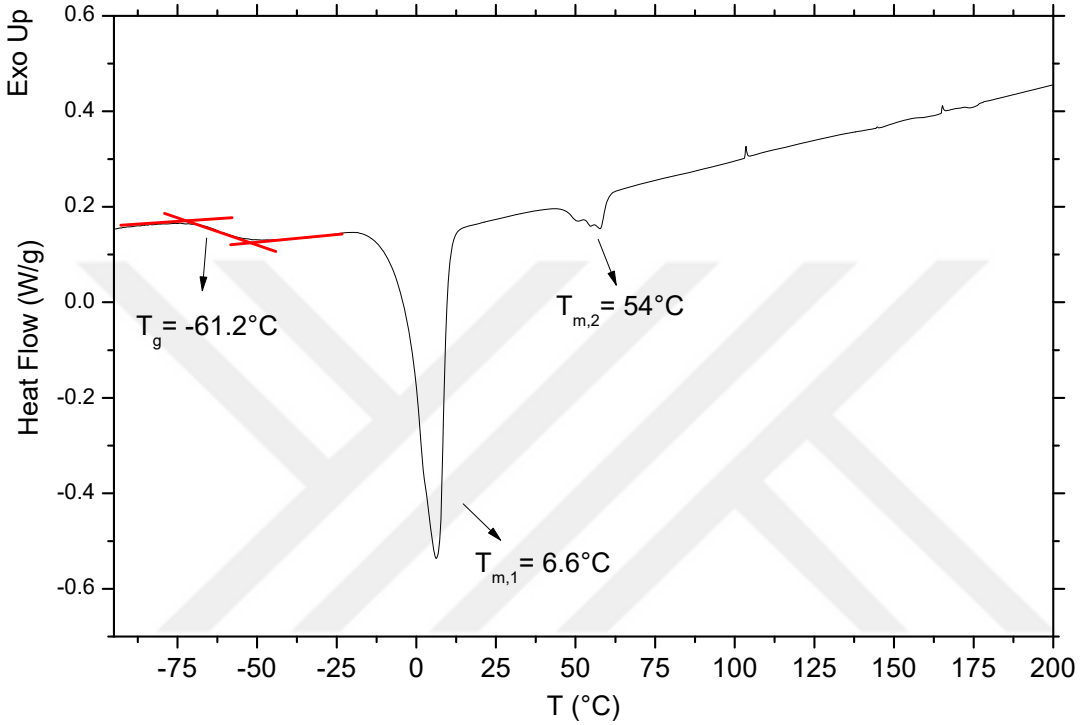

Figure 3.72 : The DSC 2nd heating curve of the photopolymerization product of PEGMEA-480 via PCL based macrophotoinitiator.

For the photopolymerization reaction of PEGMEA-480, the only one glass transition (at -61.2°C) temperature was attributed to either the homo-brush polymer of PEGMEA-480 macromonomer, or the block copolymer $P(CL)_n$-*b*-$P(PEGMEA)_m$. Additionally, there were two melting transitions (a peak at 6.6°C and a small peak with multiple shoulders around 54°C) were observed. The T_m at 54°C was considered as the residual unreacted PCL chains, and the T_m at 6.6°C as the melting of the block copolymer. The low T_g and T_m values signified the rubbery and elastic state of the resulting polymer similar to the photopolymerization products conducted with the other monomers (Figure 3.72).

SEC results of the photopolymerization reactions performed by using BuA, BzA, THFA and PCL-based macrophotoinitiator were demonstrated in Figure 3.73 The PCL-based macrophotoinitiator had a PDI value of 1.46 and $\overline{M_n}$ of 5150 g/moles

calculated from SEC measurement. The SEC curve of the dry polymer including BuA segments had two distinct peaks revealing the majority of the unreacted PCL-based macrophotoinitiator residue inside the resulting polymer mixture. In the polymerization made with THFA, there is a wide peak comprising three shoulders all of which shifted to higher molecular weight values as compared with the macrophotoinitiator. The peak with highest response had the highest molecular weight and the lowest response had the lowest molecular weight. The SEC curve of the product of the experiment conducted with BzA, had the smoothest curve among the other photopolymerization experiments.

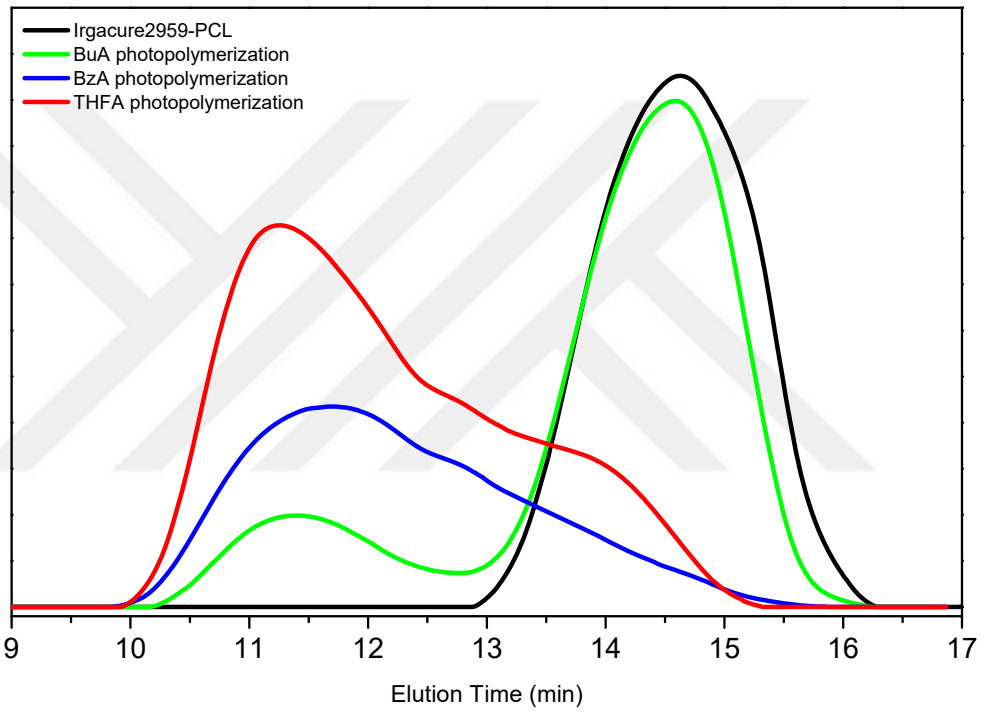

Figure 3.73 : SEC results of the photopolymerization reactions performed by using BuA, BzA, THFA and PCL-based macrophotoinitiator.

However, it can also be seen that there was a slight shoulder and the curve had a tendency to the higher molecular weight values. The average molecular weight of the photopolymerization products of the monomers BuA, BzA and THFA were calculated as 36,000 g/mole, 113,000 g/mole and 108,000 g/mole. It should be noted that the PDI values of the photopolymerization products had values more than 2.5.

The results of the enzymatic macrophotoinitiator synthesis and the photopolymerizations conducted with it might be found in Table 3.4. The enzymatic synthesis of PCL-based macrophotoinitiator was performed successfully. The macrophotoinitiator successfully photopolymerized the acrylate monomers: butyl

acrylate, benzyl acrylate, tetrahydrofurfuryl acrylate, 2,2,2-trifluoroethyl acrylate, 2-hydroxyethyl acrylate and poly (ethylene glycol) methyl ether acrylate ~ 480g/mole). Benzyl acrylate and tetrahydrofurfuryl acrylate had the highest conversion values according to ^{1}H NMR spectrum values of the reaction mixture after photopolymerization. However, the conversion value of benzyl acrylate according to the dry polymer ^{1}H NMR spectrum could be calculated. Despite the SEC curve of the photopolymerizatin performed with benzyl acrylate monomer demonstrated a broad peak with a slight shoulder, the block copolymer structure of poly(CL-*b*-BzA) and high conversion was confirmed with a single and broad T_g value with a high step decrease of the specific heat capacity.

Table 3.4 : The $\overline{M_n}$, *PDI*, *monomer conversion*, *dry polymer conversion*, T_g and T_m values of the macrophotoinitiator and the polymers obtained via photopolymerization of BuA, BzA, THFA, TFEA, HEA and PEGMEA-480. [a] Monomer conversion was calculated from the ^{1}H NMR of the reaction mixture after photopolymerization. [b] Dry polymer conversion was calculated via ^{1}H NMR. [c] Calculated from the dry polymer weight.

Experiment Code	$\overline{M}_n^{SEC}$ *(g/mole)*	*PDI*	*Monomer Conv. (%)* [a]	*Dry Polymer Conv.(%)* [b]	T_g *(°C)*		T_m *(°C)*	
					$T_{g,1}$ *(°C)*	$T_{g,2}$ *(°C)*	$T_{m,1}$ *(°C)*	$T_{m,2}$ *(°C)*
Macrophotoinitiator	5150	1.46	-	52[c]	-53.3	-	52.3	
BuA Photop.	36,000	-	54	16	-53.1	-	51.3	55.2
BzA Photop.	113,000	-	90	93	-6.5	-	-	-
THFA Photop.	108,000	-	94	73	-12.2	-	52.4	56.7
TFEA Photop.	-	-	93	13	0.3	-	51.3	55.2
HEA Photop.	-	-	-	65[c]	-55.3	16.5	55.9	160
PEGMEA-480 Photop.	-	-	-	48[c]	-61.2	-	6.6	54

3.4 PCL-based terpolymer with of poly(ethylene glycol) methyl ether acrylate and sulfobetaine methacrylate

^{1}H NMR spectrum of the PCL synthesized via enzymatic ring-opening polymerization was demonstrated in Figure 3.74. The molecular weight of the PCL was calculated according to the equation 3.25 as 7300 g/mole (roughly 64 repeating units of CL), where I_5 and $I_{5'}$ were the peak integrals associated with the peaks **5** and **5**'.

$$Molecular\ weight\ according\ to\ ^1H\ NMR\ = \frac{I_5}{I_{5'}} \tag{3.25}$$

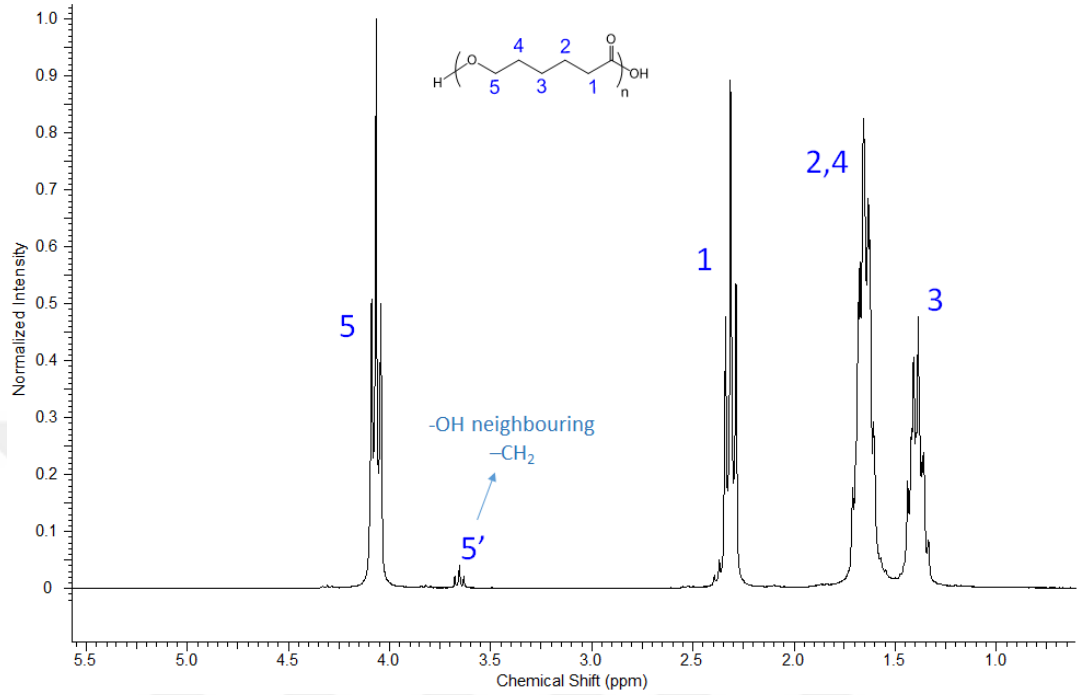

Figure 3.74 : ^{1}H NMR spectrum of the PCL synthesized via enzymatic ring-opening polymerization.

^{1}H NMR spectrum of the brominated PCL that was previously synthesized via enzymatic ring-opening polymerization was demonstrated in Figure 3.75. The bromination efficiency was calculated according to the equation 3.26 as 96 %, where I_7 and $I_{5'}$ were the peak integrals associated with the peaks **7** (methyl groups on the 2-bromoisobutyryl bromide end-groups) and **5'** (H atoms of -CH_2- neighbouring the hydroxyl end-groups) which remained from the unreacted hydroxyl end-groups of the enzymatically synthesized PCL.

$$Bromination\ efficiency\ PCL\ (\%)\ = \frac{I_7/_6}{(I_7/_6)+(I_{5'}/_2)} \tag{3.26}$$

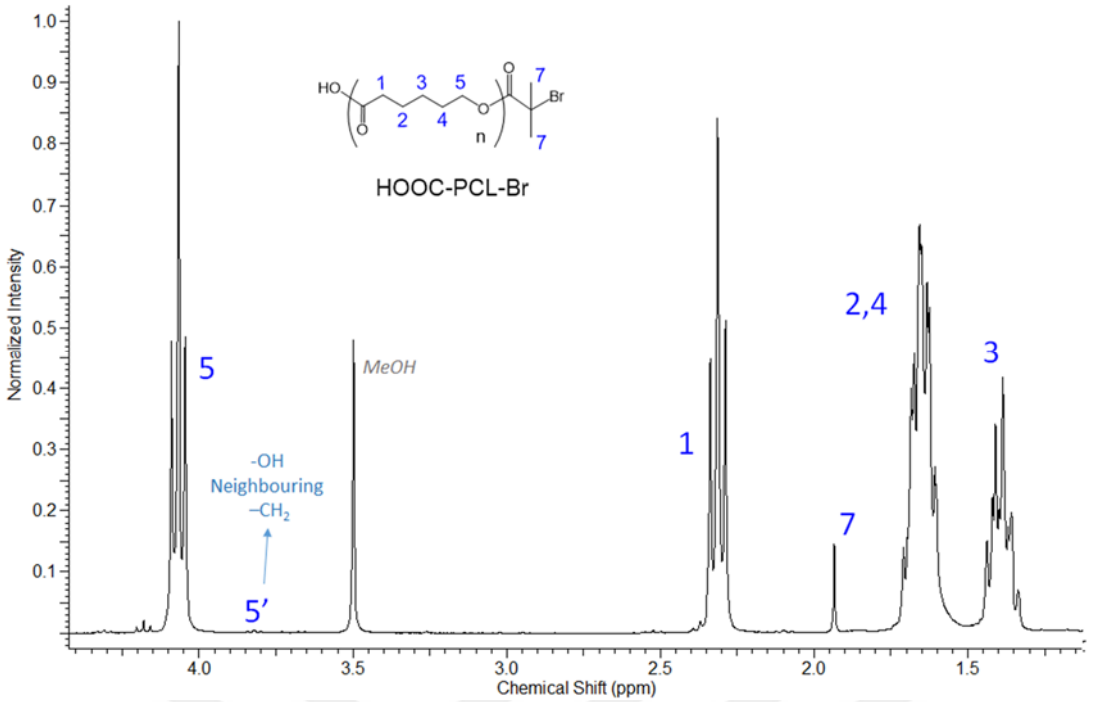

Figure 3.75 : ^{1}H NMR spectrum of the brominated PCL.

The monomer conversion of the ATRP polymerization of PEGMEA-480 macromonomer was calculated from the ^{1}H NMR spectrum (Figure 3.76) of the reaction mixture of ATRP. The conversion of the reaction performed for 48h was calculated as 65% from the equation 3.27, where $I_{A'}$, I_F and $I_{F'}$ were corresponding to the peaks **A'**, **F** and **F'**. Since 40 moles of PEGMEA-480 macromonomers per HOOC-PCL-Br was fed to the reaction, the resulting AB type copolymer included approximately 26 units of PEGMEA-480 macromonomer. On the other hand, the conversion of the reaction performed for 18 hours was calculated as only 32%, in other words 13 macromonomer units installation. The dry polymer yield was calculated as 59% according to dry polymer weight.

$$\textit{Monomer conversion of PEGME-480 (\%)} = 100 \times \frac{(I_{A'})\times 3}{I_F + I_{F'}} \qquad (3.27)$$

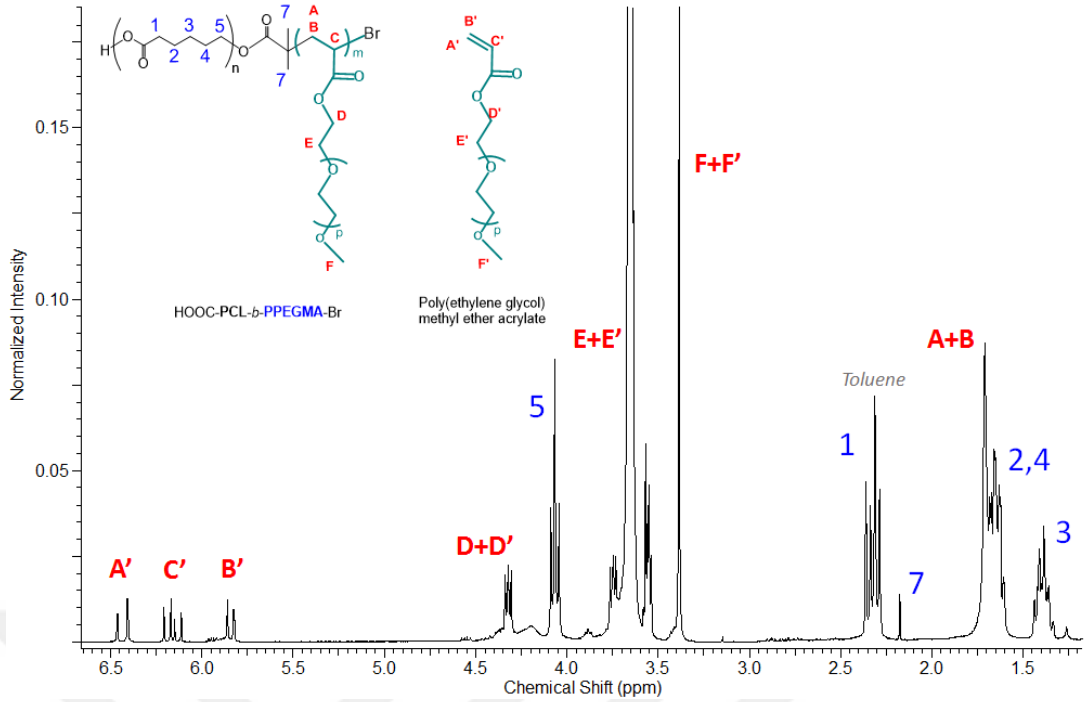

Figure 3.76 : ^{1}H NMR spectrum of the reaction mixture of the ATRP synthesis of AB type P(CL)$_n$-*b*-P(PEGMEA)$_m$ block copolymer.

The resulting polymer after the ATRP polymerization of SBMA monomer was insoluble in solvents such as $CHCl_3$, dichloromethane (CH_2Cl_2), dimethylformamide $HCON(CH_3)_2$, dimethylsulfoxide ($(CH_3)_2SO$), N,N-dimethylacetamide ($CH_3CON(CH_3)_2$), toluene ($C_6H_5CH_3$), hexane ($CH_3(CH_2)_4CH_3$), acetonitrile (CH_3CN) and water at room temperature. Therefore the ^{1}H NMR measurement of the purified and dried polymer was performed in D_2O at 80°C. However, the conversion calculation of the SBMA monomer from ^{1}H NMR couldn't be performed due to the incoherence of the peak integrals. But, still the peak assignments proved the triblockcopolymer structure (Figure 3.77 and 3.78). The dry polymer yield was calculated as 43% according to dry polymer weight.

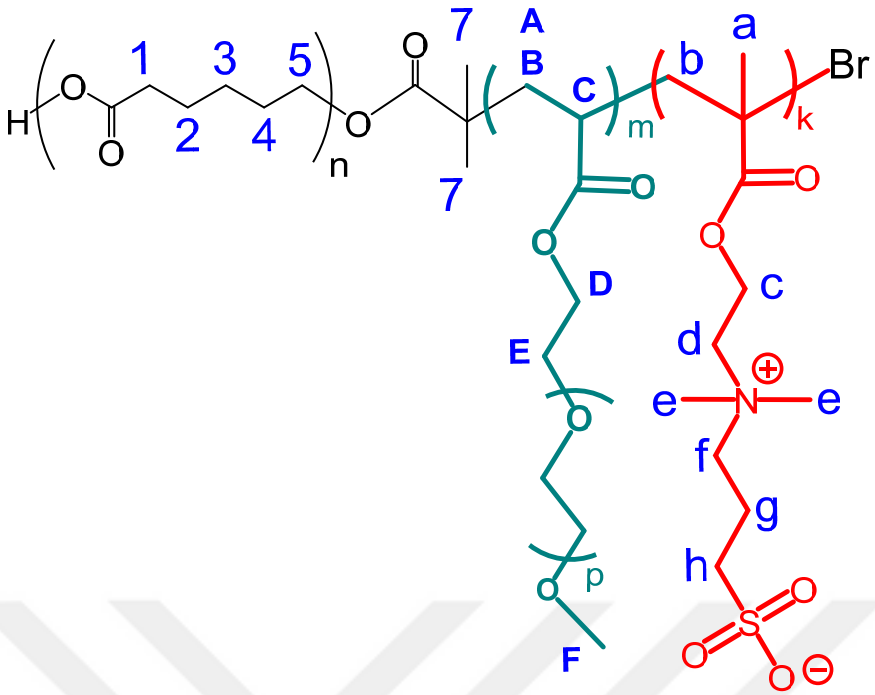

HOOC-**P(CL)$_n$**-*b*-**P(PEGMA)$_m$**-*b*-**P(SMBA)$_k$**-Br

Figure 3.77 : The chemical structure of the ABC type triblock HOOC-P(CL)$_n$-*b*-P(PEGMA)$_m$-*b*-P(SMBA)$_k$ copolymer.

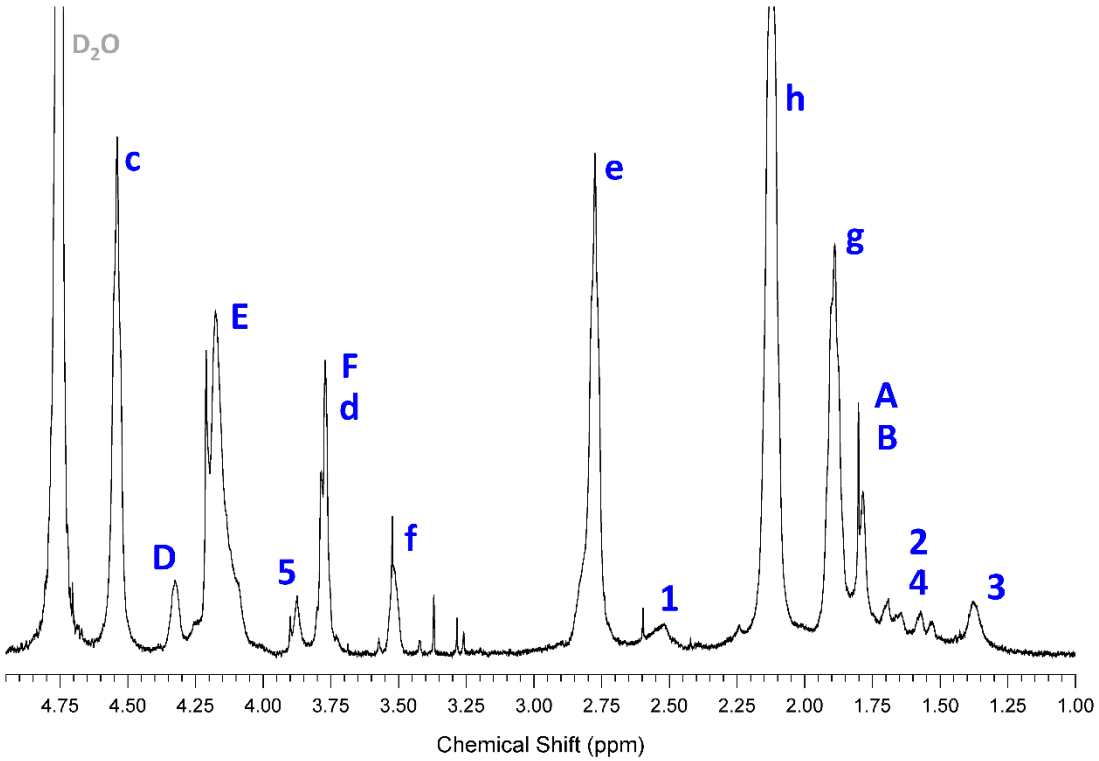

Figure 3.78 : ^{1}H NMR spectrum of the dry polymer obtained via ATRP synthesis of ABC type P(CL)$_n$-*b*-P(PEGMEA)$_m$-*b*-P(SMBA)$_k$ triblock copolymer.

The chemoenzymatic route was utilized in order to synthesize AB type amphiphilic diblock copolymer, P(CL)$_n$-*b*-P(PEGMA)$_m$ and an amphiphilic ABC type triblock copolymer comprising zwitterionic monomer units P(CL)$_n$-*b*-P(PEGMEA)$_m$-*b*-P(SMBA)$_k$. It should be noted that the third polymer segment was installed by the synthesis of a methacrylate via ATRP onto an polyacrylate based diblock macroinitiator. Furthermore, the low solubility of the diblock copolymer in the reaction solvent ethanol/water mixture was also one of the challenging points of the third monomer addition. Another barrier for both PEGMEA-480 and SBMA ATRP polymerizations might be the steric hinderence of PEGMEA-480 brush segments together with the possible entaglements of the PEG chains. However, PEGMEA-480 conversion was calculated as 65% and SBMA was proven to be polymerized with diblock ATRP macroinitiator.

3.5 Antibacterial Tests Results

Mueller-Hinton agar was used for the growth medium of the microorganisms. Petri dishes were used for the assay. Microbial cultures were homogeneously spread onto the selected agar petri dish, and the sample (in either powder, granule or flake forms) was placed into the middle of the petri dish. After an incubation period of 24 hours, the samples were observerd in order to reveal whether there was a non-microbial zone surrounding the sample. In case a zone was observed, the sample was assessed to hold antimicrobial property.

The zone inhibition assay was performed in order to investigate the antibacterial and antifungal properties of the samples (1) PCL synthesized via enzymatic ring opening polymerization, (2) diblock copolymer P(CL)$_n$-*b*-P(PEGMA)$_m$ synthesized via ATRP method with PCL based macroinitiator, (3) triblock copolymer P(CL)$_n$-*b*-P(PEGMEA)$_m$-*b*-P(SMBA)$_k$ via ATRP method synthesized with diblock copolymer P(CL)$_n$-*b*-P(PEGMA)$_m$ based macroinitiator, (4) photopolymerization products of BuA, BzA, THFA, TFEA, HEA and PEGMEA-480 synthesized via photopolymerization with enzymatically synthesized PCL based macrophotoinitiaor (5) photopolymerization products of DMPCL, PEGMA-950 and TMPTA. *Staphylococcus aureus* as the gram positive, *Escherichia coli* as the gram negative bacteria and *Aspergillus niger* as the fungus were the microorganisms tested for the

antibacterial evaluation of the abovementioned samples. The test results were illustrated in Table 3.5.

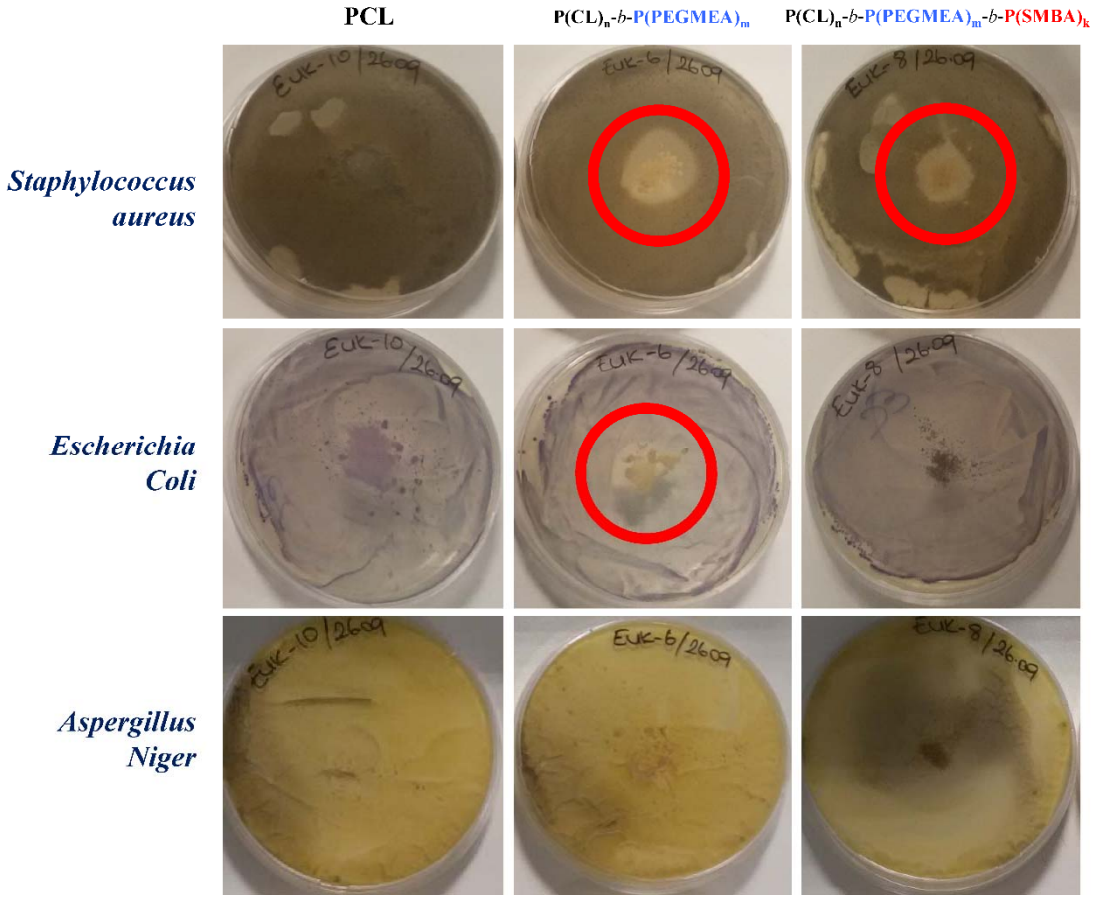

Figure 3.79 : Antibacterial and antifungal feature evaluation of enzymatically synthesized PCL, AB type diblock copolymer P(CL)$_n$-*b*-P(PEGMEA)$_m$ and ABC type triblock copolymer P(CL)$_n$-*b*-P(PEGMEA)$_m$-*b*-P(SMBA)$_k$ via zone inhibition test.

The antibacterial and the antifungal properties of the samples (1) PCL synthesized via enzymatic ring opening polymerization, (2) diblock copolymer PCL-*b*-PPEGMEA synthesized via ATRP method with PCL based macroinitiator, (3) triblock copolymer P(CL)$_n$-*b*-P(PEGMEA)$_m$-*b*-P(SMBA)$_k$ via ATRP method synthesized with diblock copolymer P(CL)$_n$-*b*-P(PEGMA)$_m$ based macroinitiator were shown in Figure 3.79. The unmodified PCL couldn' t perform antibacterial and antifungal characteristics against etiher of the microorganisms. On the other hand the P(CL)$_n$-*b*-P(PEGMA)$_m$ diblock copolymer had antibacterial activity against both of the *Staphylococcus aureus* and *Escherichia coli*, whereas the triblock copolymer P(CL)$_n$-*b*-P(PEGMEA)$_m$-*b*-P(SMBA)$_k$ could only have antibacterial feature against *Staphylococcus aureus*. But neither of the materials could perform antifungal activity.

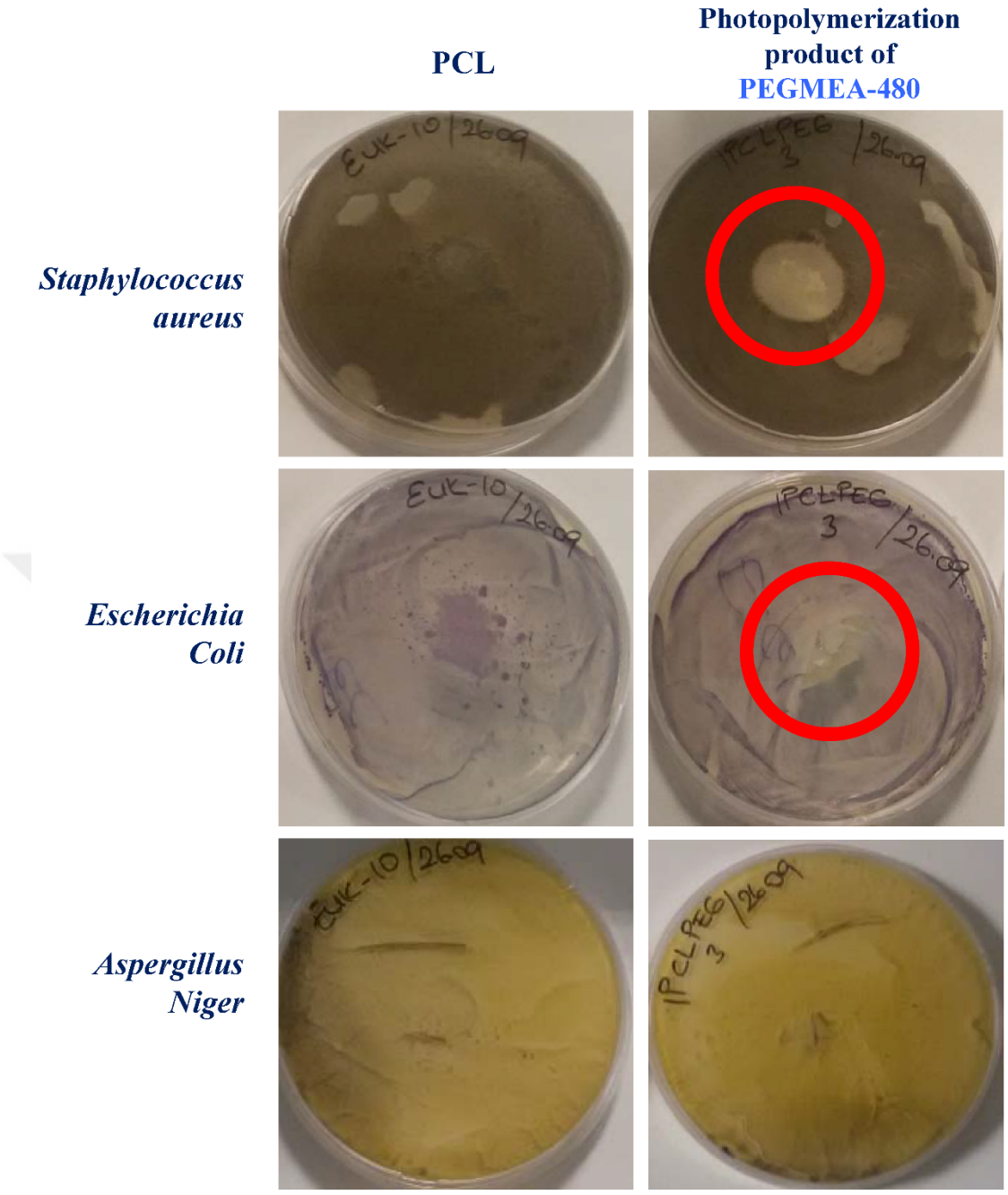

Figure 3.80 : Antibacterial and antifungal feature evaluation with zone inhibition test of the enzymatically synthesized PCL and the block copolymer PCL-b-PPEGMEA synthesized via photopolymerization using Irgacure-2959 end-functionalized PCL based macrophotoinitiator.

The antibacterial and the antifungal properties of the samples PCL synthesized via enzymatic ring opening polymerization and the photopolymerization product of PEGMEA-480 by the PCL based macrophotoinitiaor were depicted in Figure 3.80. The photopolymerization product of of PEGMEA-480 had antibacterial activity against *Staphylococcus aureus* and *Escherichia coli*, but no antifungal activity against *Aspergillus niger*. However, the photopolymerization products of BuA, BzA, THFA,

TFEA and HEA couldn't exhibit any antibacterial and antifungal activity. The antibacterial feature of the PEGMEA-480 moacromonomer insertion to the PCL chains was ascribed to the dense sequencing of the PEG macromonomers, hence providing a brush-like structure with high hydrophilic nature causing a hydration layer which hinders the intermolecular interaction between the surface and the protein of the bacteria. HEA utilized photopolymerization product showed that the amount of inserted HEA repeating units was not sufficient enough to provide antibacterial and antifungal activity.

The photopolymerized PEGMA-950 macromonomers crosslinked with DMPCL and TMPTA also couldn't provide antibacterial and antifungal characteristics even though the conversion values were higher than that of the photopolymerization product of PEGMEA-480 synthesized by PCL based macrophotoinitiator. This case was attributed to the denser macromonomer repeating units of PEGMEA-480 as compared to PEGMA-950, providing a better hydration layer.

It can be seen that the photopolymerization product of PEGMEA-480 via PCL based macrophotoinitiator had similar antibacterial characteristics with the diblock copolymer $P(CL)_n$-*b*-$P(PEGMEA)_m$ synthesized via ATRP. Both of the polymers were comprised of PCL with similar molecular weight values (7300 g/mole for PCL ATRP initiator and 5150 g/mole for Irgacure-2959 end-functionalized macrophotoinitiator and the same molecular weight of PEGMEA as 480 g/mole.

In Table 3.5, the zone inhibition test results of all of the samples were illustrated. None of the the polymeric structures, except the ones including PEGMEA-480 obtained via macrophotoinitiator method and ATRP method, could exhibit antibacterial feature against *S. aureus* and *E. coli*. This output was attributed to the densely tailoring of the PEGMEA-480 macromonomers, consequently supplying a sufficient hydration layer to inhibit the approaching of the bacteria.

Table 3.5 : Zone inhibition test results of crude PCL; the polymers obtained with the photocuring of DMPCL with PEGMA-950; photopolymerization of BuA, BzA, THFA, TFEA, HEA and PEGMEA-480 by the enzymatically synthesized PCL based macrophotoinitiator; diblock and triblock copolymers obtained via the combination of enzymatic and ATRP methods.

	Staphylococcus aureus	*Escherichia coli*	*Aspergillus niger*
PCL	x	x	x
V-PCLPEG-1.00	x	x	x
V-PCLPEG-0.75	x	x	x
V-PCLPEG-0.50	x	x	x
V-PCLPEG-0.25	x	x	x
V-PCLPEG-0.00	x	x	x
Ir2959-PCL	x	x	x
BuA Photopolymerization product	x	x	x
BzA Photopolymerization product	x	x	x
THFA Photopolymerization product	x	x	x
TFEA Photopolymerization product	x	x	x
HEA Photopolymerization product	x	x	x
PEGMEA-480 Photopolymerization product	✓	✓	x
$P(CL)_n$-*b*-$P(PEGMEA)_m$	✓	✓	x
$P(CL)_n$-*b*-$P(PEGMEA)_m$-*b*-$P(SMBA)_k$	✓	x	x

4. CONCLUSION AND RECOMMENDATIONS

It was revealed that N435 has high activity enough to catalyze enzyme-monomer complex formation, initiation, and propagation, cleaving the ester bond of the hydroxyl bearing acrylate initiator at the same time. Therefore, it might to be preferable to study at lower reaction temperatures to reduce the side reactions inside the sufficient activity range of N435 or other lipase types. In the first two hours of reaction, approximately the same amount of HEMA was successfully introduced into macromonomers with the sixth hour of reaction; HEMA addition only increased until the third hour and tended to diminish in the following hours. Total methacrylate end-groups had also increased up to three hours, following a decrease along with reaction time. EG inside the chains, which is the indicator of polyester transfer, increased with time. Thus, as the reaction progressed, the first side reaction (methacrylate transfer) increased, the total methacrylate end-groups did not change remarkably or diminished, and the second side reaction (polyester transfer) increased. It is obvious to finalize the eROP at low reaction times and conversions in order to obtain lower side reactions and comparable HEMA addition. Furthermore, the lower enzyme amount might be preferable in order to realise higher HEMA addition, lower methacrylate transfer, comparable total methacrylate end-groups, and minimum EG inside the chains. HEMA/CL ratio can also be chosen minimum as both of the side reactions seemed to be lower at both temperatures and enzyme amounts, still conserving the total methacrylate amount sufficient. In addition to these, higher molecular weight and polymerization yield of macromonomers can be obtained at lower initiator/lactone ratios. There might be further investigation of the effects of lower conversions, temperatures, and HEMA/CL ratios and less active lipases on the addition of HEMA onto the edge of PCL macromonomers with minimized side reactions. However the numerous side-reactions during the enzymatic ring-opening polymerizaiton in the presence of an ester containing initiator seemed to be inevitable. Hence, in order to synthesize better defined PCL macromonomers via eROP holding a reactive functionality only in the α position initiators holding hydroxyl groups but not ester

groups (i.e., allyl, epoxides, dienes, triazolinediones, thiolactones, amines) against which lipases do not possess any activity.

Another alternative was to benefit from the activity of N-435 against the ester groups of the initiators in a sense to synthesize a α,ω-methacrylated macromonomer for the application as a crosslinking agent. The double methacrylation of the PCL chains was evaluated to be a successful route, since the one-pot synthesis comprised of the primary synthesis of PCL enzymatically, and subsequent tailoring of the methacrylate groups onto the chains provided that all the water molecules were removed from the reaction mixture with high vacuum for high a conversion time. It should be noted that there were still unreacted hydroxyl end-groups left belonging to the mixture of PCL macromonomer types. The utilization of this highly methacrylated PCL macromonomers as a crosslinking agent in the photopolymerizaiton of PEGMA-950 (α-methacrylated PEG monomer with average molecular weight of 950 g/mole) was performed successfully with high conversions which were confirmed with FTIR-ATR and DSC Furthermore, the conversion values without the usage of either PEGMA-950 or DMPCL didn't give high conversion values of DMPCL and PEGMA-950. Therefore, the concurrent usage of DMPCL and PEGMA-950 in photopolymerization provided a synergetic influence for the conversion of both macromonomers with the help of TMPTA. The feed mole ratios 0.25, 0.50 and 0.75 for DMPCL (DMPCL/Total macromonomers) inside the photopolymerization mixture all gave high polymerization yields. Consequently, enzymatically polymerized dimethacrylated PCL macromonomer with average molecular weight of 4400 g/mole was found to be an efficient crosslinking agent in photopolymerization and obtaining amphiphilic networks. It was noteworthy that the low T_g and T_m values of the amphiphilic networks revealed the rubbery and elastic behaviour of the materials, hence enabling their usage in biomedical applications since they do not comprise any toxic chemicals.

The macrophotoinitiator approach was employed to achieve amphiphilic copolymers. Correspondingly, the enzymatic synthesis of PCL based macrophotoinitiator was performed successfully as photocleavable Irgacure-2959 was exerted as the nucleophilic initiator. The macrophotoinitiator successfully photopolymerized the acrylate monomers: butyl acrylate, benzyl acrylate, tetrahydrofurfuryl acrylate, 2,2,2-trifluoroethyl acrylate, 2-hydroxyethyl acrylate and poly (ethylene glycol) methyl ether acrylate ~ 480 g/mole). Benzyl acrylate and tetrahydrofurfuryl acrylate had the

highest conversion values according to the ^{1}H NMR spectrum values of the reaction mixture after photopolymerization. Despite the fact that, there was only one glass transition value of the photopolymerization product of BzA, the SEC result revealed there are two other molecular weight distributions which might point the unreacted PCL chains and homopolymer of BzA. Resembling SEC curve was observed for THFA as well with more visible shoulders. The dry polymer conversions for gel formation by using HEA and PEGMEA-480 monomers in photopolymerization also proved the efficient amphiphilic polymer synthesis via PCL based macrophotoinitiator. The low T_g value, thus the rubbery state, of the amphiphilic gels also made it possible for their usage in biomedical applications together with the biocompatible nature of the employed macromonomers.

A chemoenzymatic approach was also utilized in order to synthesize amphiphilic polymers with a different strategy than the combination of photopolymerization and eROP. The amphiphilic AB type diblock copolymer, P(CL)$_n$-*b*-P(PEGMEA)$_m$ and an amphiphilic ABC type triblock copolymer comprising zwitterionic monomer units P(CL)$_n$-*b*-P(PEGMEA)$_m$-*b*-P(SMBA)$_k$ were obtained via the combination of eROP and ATRP. Even though the conversion of PEGMEA-480 to reach the diblock copolymer was acceptible, the conversion of SBMA in the synthesis of the triblock copolymer couldn not be evaluated quantitatively. Therefore, the triblock copolymer structure could only be proven qualitatively by ^{1}H NMR. The challenging characterization of the triblock copolymer was caused by the insolubility of the product in many soluvents. It should be noted that the third polymer segment was installed by the synthesis of a methacrylate via ATRP onto an polyacrylate based diblock macroinitiator. Furthermore, the low solubility of the diblock copolymer in the reaction solvent ethanol/water mixture was also one of the challenging points of the third monomer addition. Another barrier for both PEGMEA-480 and SBMA ATRP polymerizations might be the steric hinderence of PEGMEA-480 brush segments together with the possible entaglements of the PEG chains. However, PEGMEA-480 conversion was calculated as 65% and SBMA was proven to be polymerized with diblock ATRP macroinitiator. However, the troublesome purification procedure of the synthesized diblock and triblock copolymers due to the obligation of residual Cu elements for biomedical applications made this approach rather complicated. As an alternative, metal free click reactions such organic photoredox catalyst

(phenylphenothiazine) based ATRP, reversible addition-fragmentation chain-transfer polymerization (RAFT) and nitroxide mediated polymerization (NMP) (Delplace and Nicolas, 2015; Fairbanks et al, 2015; Trat et al, 2014) might be employed to synthesize biocompatible amphiphilic PCL based polymers.

Amphiphilic diblock copolymers comprised of PCL and PEG synthesized via photopolymerization and ATRP approaches both had antibacterial activity against *S. aureus* (Gram positive) and *E. coli* (Gram negative). The triblock copolymer, based on PCL, PEG and PSMBA was only antibacterial against *S. aureus*. On the other hand, none of the the polymeric structures, except the ones including PEGMEA-480 obtained via macrophotoinitiator method and ATRP method, could exhibit antibacterial feature against *S. aureus* and *E. coli*. This output was attributed to the densely tailoring of the PEGMEA-480 macromonomers, consequently supplying a sufficient hydration layer to inhibit the approaching of the bacteria. It's note to mention neither of the polymers provided antifungal activity against *A. niger*. Another analysis methods might also be performed for the synthesized polymers such as protein adsoption, since composing antifouling surfaces is one of the candidate routes to obtain antibacterial activity due to their capability of inhibition of the protein based molecules which are employed by microorganisms to simplify their settlemt on surfaces. Consequently, enzymatic ring-opening polymerization in combination with photopolymerization or ATRP was found to be an approach to achieve amphiphilic polymers performing antibacterial properties which might find applications in biomedical and marine uses.

REFERENCES

Al-Azemi, T. F., Bisht, K.S. (2002). One-step synthesis of polycarbonates bearing pendant carboxyl groups by lipase-catalyzed ring-opening polymerization. *Journal of Polymer Science Part A: Polymer Chemistry, 40*, 1267–1274. doi:10.1002/pola.10212

Albertsson, A.-C., Srivastava, R.K. (2008). Recent developments in enzyme-catalyzed ring-opening polymerization. *Advanced Drug Delivery Reviews, 60*, 1077–1093. doi:10.1016/j.addr.2008.02.007

Álvarez-Chávez, C. R., Edwards, S., Moure-Eraso, R., Geiser, K. (2012). Sustainability of bio-based plastics: general comparative analysis and recommendations for improvement. *Journal of Cleaner Production, 23*, 47-56.

Aran, B., Sankır, M., Vargün, E., Sankır, N. D., Usanmaz, A. (2010). Tailoring the swelling and glass-transition temperature of acrylonitrile/hydroxyethyl acrylate copolymers. *Journal of Applied Polymer Science, 116*, 628–635. doi:10.1002/app.30854

Arciola, C. R., Campoccia, D., Speziale, P., Montanaro, L., Costerton, J.W. (2012). Biofilm formation in Staphylococcus implant infections. A review of molecular mechanisms and implications for biofilm-resistant materials. *Biomaterials, 33*, 5967-5982. doi:10.1016/j.biomaterials.2012.05.031

Armentano, I., Arciola, C.R., Fortunati, E., Ferrari, D., Mattioli, S., Amoroso, C.F., Rizzo, J., Kenny, J.M., Imbriani, M., Visai, L. (2014). The interaction of bacteria with engineered nanostructured polymeric materials: A review. *Scientific World Journal, 2014*. doi:10.1155/2014/410423

Balke, K., Kadow, M., Mallin, H., Saß, S., Bornscheuer, U.T. (2012). Discovery, application and protein engineering of Baeyer–Villiger monooxygenases for organic synthesis. *Organic & Biomolecular Chemistry, 10*, 6249–6265. doi:10.1039/c2ob25704a

Banerjee, I., Pangule, R.C., Kane, R.S. (2011). Antifouling coatings: Recent developments in the design of surfaces that prevent fouling by proteins, bacteria, and marine organisms. *Advanced Materials, 23*, 690–718. doi:10.1002/adma.201001215

Basso, A., Froment, L., Hesseler, M., Serban, S. (2013). New highly robust divinyl benzene/acrylate polymer forimmobilization of lipase CALB. *European Journal of Lipid Science and Technology, 115*, 468–472. doi:10.1002/ejlt.201200419

Behlau, I., Mukherjee, K., Todani, A., Tisdale, A.S., Cade, F., Wang, L., Leonard, E.M., Zakka, F.R., Gilmore, M.S., Jakobiec, F.A., Dohlman, C.H., Klibanov, A.M. (2011). Biocompatibility and biofilm inhibition of

N,N-hexyl,methyl-polyethylenimine bonded to Boston Keratoprosthesis materials. *Biomaterials, 32*, 8783–8796. doi:10.1016/j.biomaterials.2011.08.010

Bisht, K. S., Svirkin, Y.Y., Henderson, L.A., Gross, R.A., Kaplan, D.L., Swift, G. (1997). Lipase-catalyzed ring-opening polymerization of trimethylene carbonate. *Macromolecules, 30*, 7735-7742. doi:10.1021/ma9708858

Brady, L., Brzozowski, A.M., Derewenda, Z.S,, Dodson, E., Dodson, G., Tolley, S., Turkenburg, J.P., Christiansen, L., Huge-Jensen, B., Norskov, L., Thim, L., Menge, U. (1990). A serine protease triad forms the catalytic centre of a triacylglycerol lipase. *Nature, 343*, 767-770.

Brandenburg, L. O., Merres, J., Albrecht, L.J., Varoga, D., Pufe, T. (2012). Antimicrobial peptides: Multifunctional drugs for different applications. *Polymers, 4*, 539-560. doi:10.3390/polym4010539

Brzozowski, A. M., Derewenda, U., Derewenda, Z.S., Dodson, G.G., Lawson, D.M., Turkenburg, J.P., Bjorkling F., Huge-Jensen, B., Patkar, S.A., Thim, L. (1991). A model for interfacial activation in lipases from the structure of a fungal lipase-inhibitor complex. *Nature, 351*, 491 ± 494.

Campoccia, D., Montanaro, L., Arciola, C.R. (2013). A review of the biomaterials technologies for infection-resistant surfaces. *Biomaterials, 34*, 8533-8554. doi:10.1016/j.biomaterials.2013.07.089

Camps, M., Briand, J.F., Guentas-Dombrowsky, L., Culioli, G., Bazire, A., Blache, Y. (2011). Antifouling activity of commercial biocides vs. natural and natural derived products assessed by marine bacteria adhesion bioassay. *Marine Pollution Bulletin, 62*, 1032-1040. doi:10.1016/j.marpolbul.2011.02.031

Carlsson, N., Gustafsson, H., Thörn, C., Olsson, L., Holmberg, K., Åkerman, B. (2014). Enzymes immobilized in mesoporous silica: A physical–chemical perspective. *Advances in Colloid and Interface Science, 205*, 339–360.

Carteau, D., Vallée-Réhel, K., Linossier, I., Quiniou, F., Davy, R., Compère, C., Delbury, M., Faÿ, F. (2014). Development of environmentally friendly antifouling paints usingbiodegradable polymer and lower toxic substances. *Progress in Organic Coatings, 77*, 485-493. doi:10.1016/j.porgcoat.2013.11.012

Casas-Godoy, L., Duquesne, S., Bordes, F., Sandoval, G., Marty, A. (2012). Lipases: An Overview. In G. Sandoval (Ed.), *Lipases and Phospholipases: Methods and Protocols*.

Chahinian, H., Nini, L., Boitard, E., Dubès, J.P., Comeau, L.C., Sarda, L. (2002). Distinction between esterases and lipases: a kinetic study with vinyl esters and TAG. *Lipids, 37*, 653-662.

Chatti, S., Behnken, G., Langanke, D., Kricheldorf, H.R. (2006). Biodegradable polyesters based on cis-1,4-butenediol. *Macromolecular Chemistry and Physics, 207*, 1474–1484. doi:10.1002/macp.200600105

Chen, H., Zhao, C., Zhang, M., Chen, Q., Ma, J., Zheng, J. (2016). Molecular understanding and structural-based design of polyacrylamides and

polyacrylates as antifouling materials. *Langmuir, 32*, 3315−3330. doi:10.1021/acs.langmuir.6b00386

Chen, S., Hu, T., Tian, Y., Chen, L., Pojman, J. A. (2007). Facile synthesis of poly(hydroxyethyl acrylate) by frontal free-radical polymerization. . *Journal of Polymer Science Part A: Polymer Chemistry, 45*, 873–881. doi:10.1002/pola.21865

Chirife, J., Herszage, L., Joseph, A., Bozzini, J.P., Leardini, N., Kohn, E.S. (1983). In vitro antibacterial activity of concentrated polyethylene glycol 400 solutions. *Antimicrobial Agents and Chemotherapy, 24*, 409–412.

Cornell, R. J., Donaruma, L.G. (1965). 2-Methacryloxytroponones. Intermediates for synthesis of biologically active polymers. *Journal of Medicinal Chemistry, 8*, 388–390. doi:10.1021/jm00327a025

Costa, L., Brissos, V., Lemos, F., Ribeiro, F.R., Cabral, J. M. S. (2009). Enhancing the thermal stability of lipases through mutagenesis and immobilization on zeolites. *Bioprocess and Biosystems Engineering, 32*, 53–61.

Coulembier, O., Josse, T., Guillerm, B., Gerbaux, P., Dubois, P. (2012). An imidazole-based organocatalyst designed for bulk polymerization of lactide isomers: inspiration from Nature. *Chemical Communications, 48*, 11695–11697.

Çanak, T. Ç., Kızılcan, N., Serhatlı, İ. E. (2012). Synthesis of cyclohexanone formaldehyde resin-methylmethacrylate block-graft copolymers via ATRP. *Journal of Applied Polymer Science, 123*, 2628–2635. doi:10.1002/app.34547

Dai, S., Xue, L., Li, Z. (2011). Enzymatic ring-opening polymerization of trimethylene carbonate with macrodiol: Synthesis of block poly(ester-co-carbonate) for biomaterial preparation. *ACS Catalysis, 1*, 1421–1429. doi:10.1021/cs200407n

Dann, A. B., Hontela, A. (2011). Triclosan: environmental exposure, toxicity and mechanisms of action. *Journal of Applied Toxicology, 31*, 285-311. doi:10.1002/jat.1660

de Regil, R., Sandoval, G. (2013). Biocatalysis for biobased chemicals. *Biomolecules, 3*, 812-847. doi:10.3390/biom3040812

Degirmenci, M., Hizal, G., Yagci, Y. (2002). Synthesis and characterization of macrophotoinitiators of poly(ε-caprolactone) and their use in block copolymerization. *Macromolecules, 35*, 8265-8270. doi:10.1021/ma020668t

Degirmenci, M., Urun, T., Durgun, M., Barim, E. (2015). Synthesis of mid-chain functional macrophotoinitiators of poly(D,L-lactide) homopolymer and tetrablock poly(D,L-lactide)-poly(ε-caprolactone) copolymer by ring-opening polymerization. *Designed Monomers & Polymers, 18*, 669–677. doi:10.1080/15685551.2015.1070499

Delplace, V., Nicolas, J. (2015). Degradable vinyl polymers for biomedical applications. *Nature Chemistry, 7*, 771–784. doi:10.1038/nchem.2343

Divakar, S. (2004). Porcine pancreas lipase catalyzed ring-opening oolymerization of ϵ-Caprolactone. *Journal of Macromolecular Science, Part A, 41*, 537-546. doi:10.1081/MA-120030923

Dobretsov, S., Dahms, H.U., Qian, P.Y. (2006). Inhibition of biofouling by marine microorganisms and their metabolites. *Biofouling, 22*, 43-54. doi:10.1080/08927010500504784

Donoghue, N. A., Norris, D.B., Trudgill, P.W. (1976). The purification and properties of cyclohexanone oxygenase from Nocardia globerula CL1 and Acinetobacter NCIB 9871. *European Journal of Biochemistry, 63*, 175-192. doi:10.1111/j.1432-1033.1976.tb10220.x

Dubois, P., Jerome, R., Teyssie, P. (1991). Macromolecular engineering of polylactones and polylactides. 3. Synthesis, characterization, and applications of poly(iε-caprolactone) macromonomers. *Macromolecules, 24*, 977-981. doi:10.1021/ma00005a002

Dunne, W. M. (2002). Bacterial adhesion: Seen any good biofilms lately? *Clinical Microbiology Reviews, 15*, 155-166. doi:10.1128/CMR.15.2.155–166.2002

Düşkünkorur, H. Ö., Pollet, E., Phalip, V., Güvenilir, Y., Avérous, L. (2014). Lipase catalyzed synthesis of polycaprolactone and clay-based nanohybrids. *Polymer, 55*, 1648–1655. doi:10.1016/j.polymer.2014.02.016

Elzein, T., Nasser-Eddine, M., Delaite, C, Bistac, S., Dumas, P. (2004). FTIR study of polycaprolactone chain organization at interfaces. *Journal of Colloid and Interface Science, 273*, 381–387. doi:10.1016/j.jcis.2004.02.001

Endres, H.-J., Siebert-Raths, A. (2011). *Engineering Biopolymers: Markets, Manufacturing, Properties and Applications* Carl Hanser Verlag.

Faÿ, F., Linossier, I., Langlois, V., Renard, E., Vallée-Réhel, K. (2006). Degradation and controlled release behavior of ε-Caprolactone copolymers in biodegradable antifouling coatings. *Biomacromolecules, 7*, 851-857. doi:10.1021/bm0509669

Faÿ, F., Renard, E., Langlois, V., Linossier, I., Vallée-Réhel, K. (2007). Development of poly(ε-caprolactone-co-L-lactide) and poly(ε-caprolactone-co-δ-valerolactone) as new degradable binder used for antifouling paint. *European Polymer Journal, 43*, 4800–4813. doi:10.1016/j.eurpolymj.2007.07.045

Fairbanks, B. D., Gunatillake, P.A., Meagher, L. (2015). Biomedical applications of polymers derived by reversible addition - fragmentation chain-transfer (RAFT). *Advanced Drug Delivery Reviews, 91*, 141–152. doi:10.1016/j.addr.2015.05.016

Faucher, S. (2013). United States of America Patent No. US 8507571 B2. U. S. P. a. T. Office.

Fisher, J. P., Dean, D., Engel, P. S., Mikos, A. G. (2001). Photoinitiated polymerization of biomaterials. *Annual Review of Materials Research, 31*, 171-181. doi:10.1146/annurev.matsci.31.1.171

Fojan, P., Jonson, P.H., Petersen, M.T.N., Petersen, S.B. (2000). What distinguishes an esterase from a lipase: a novel structural approach. *Biochimie, 82*, 1033–1041.

Foster, T. J., Höök, M. (1998). Surface protein adhesins of Staphylococcus aureus. *Trends in Microbiology, 6*, 484-488. doi:10.1016/S0966-842X(98)01400-0

Fusetani, N. (2011). Antifouling marine natural products. *Natural Product Reports, 28*, 400-410. doi:10.1039/C0NP00034E

Gabriel, G. J., Som, A., Madkour, A.E., Eren, T., Tew, G.N. (2007). Infectious disease: Connecting innate immunity to biocidal polymers. *Materials Science and Engineering, 57*, 28–64. doi:10.1016/j.mser.2007.03.002

Garrett, T. R., Bhakoo, M., Zhang, Z. (2008). Bacterial adhesion and biofilms on surfaces. *Progress in Natural Science, 18*, 1049–1056. doi:10.1016/j.pnsc.2008.04.001

Gijsen, H. J. M., Qiao, L., Fitz W., Wong, C.-H. (1996). Recent advances in the chemoenzymatic synthesis of carbohydrates and carbohydrate mimetics. *Chemical Reviews, 96*, 443–474.

González, J. E., Keshevan, N.D. (2006). Messing with bacterial quorum sensing. *Microbiology and Molecular Bİology Reviews, 70*, 859–875. doi:10.1128/MMBR.00002-06

Gross, R. A., Ganesh, M., Lu, W. (2010). Enzyme-catalysis breathes new life into polyester condensation polymerizations. *Trends in Biotechnology, 28*, 435–443. doi:10.1016/j.tibtech.2010.05.004

Guo, L., Zhang, Z., Zhu, Y., Li, J., Xie, Z. (2008). Synthesis of polysiloxane–polyester copolymer by lipase-catalyzed polycondensation. *Journal of Applied Polymer Science, 108*, 1901–1907. doi:10.1002/app.27807

Gupta, B. G., Ray, A.R. (2012). Preparation of poly(ε-caprolactone)/poly(ε-caprolactone-co-lactide) (PCL/PLCL) blend filament by melt spinning. *Journal of Applied Polymer Science, 123*, 1944–1950. doi:10.1002/app.34728

Hasan, J., Crawford, R.J., Ivanova, E.P. (2013). Antibacterial surfaces: the quest for a new generation of biomaterials. *Trends in Biotechnology, 31*, 295–304. doi:10.1016/j.tibtech.2013.01.017

He, F., Zhuo, R.X., Liu, L.J., Jin, D.B., Feng, J., Wang, X.L. (2001). Immobilized lipase on porous silica beads: preparation and application for enzymatic ringopening polymerization of cyclic phosphate. *Reactive & Functional Polymers, 47*, 153–158. doi:10.1016/S1381-5148(01)00027-X

Henderson, L. A., Svirkin, Y.Y., Gross, R.A. (1996). Enzyme-catalyzed polymerizations of ε-Caprolactone: Effects of initiator on product structure, propagation kinetics, and mechanism. *Macromolecules, 29*, 7759–7766. doi:10.1021/ma960821h

Hong, S. Y., Young, J.Y. (2013). Activity enhancement of candida antarctica lipase B by flexibility modulation in helix region surrounding the active site. *Applied Biochemistry and Biotechnology, 170*, 925–933.

Hu, F. X., Neoh, K.G., Cen, L., Kang, E.T. (2005). Antibacterial and antifungal efficacy of surface functionalized polymeric beads in repeated applications. *Biotechnology and Bioengineering, 89*, 474-484. doi:10.1002/bit.20384

Hui, F., Debiemme-Chouvy, C. (2013). Antimicrobial N-Halamine polymers and coatings: A review of their synthesis, characterization, and applications. *Biomacromolecules, 14*, 585–601. doi:10.1021/bm301980q

Hunsen, M., Azim, A., Mang, H., Wallner, S.R., Ronkvist, A., Xie, W., Gross, R.A. (2007). A cutinase with polyester synthesis activity. *Macromolecules, 40*, 148–150. doi:10.1021/ma062095g

I.K. Varma, A.-C. A., R. Rajkhowaa, R.K. Srivastava. (2005). Enzyme catalyzed synthesis of polyesters. *Progress in Polymer Science, 30*, 949–981.

Ikada, Y., Tsuji, H. (2000). Biodegradable polyesters for medical and ecological applications. *Macromolar Rapid Communications, 21*, 117–132. doi:10.1002/(SICI)1521-3927(20000201)21:3<117::AID-MARC117>3.0.CO;2-X

Ishimaru, N., Tsukegi, T., Wakisaka, M., Shirai, Y., Nishida, H. (2012). Effects of poly(L-lactic acid) hydrolysis on attachment of barnacle cypris larvae. *Polymer Degradation and Stability, 97*, 2170-2176. doi:10.1016/j.polymdegradstab.2012.08.012

Jaeger, K. E. D., B.W.; Reetz, M.T. (1999). Molecular biology, three-dimensional structures, and biotechnological applications of lipases. *Annual Review of Microbiology, 53*, 315–351. doi:10.1146/annurev.micro.53.1.315

Jérôme, C., Lecomte, P. (2008). Recent advances in the synthesis of aliphatic polyesters by ring-opening polymerization. *Advanced Drug Delivery Reviews, 60*, 1056–1076. doi:http://dx.doi.org/10.1016/j.addr.2008.02.008

Jiang, H., Wang, X.B., Li, C.Y., Li, J.S., Xu, F.J., Mao, C., Yang, W.T., Shen, J. (2011). Improvement of hemocompatibility of polycaprolactone film surfaces with zwitterionic polymer brushes. *Langmuir, 27*, 11575-11581. doi:10.1021/la202101q

Jiang, Y., Loos, K. (2016). Enzymatic synthesis of biobased polyesters and polyamides. *Polymers, 8*. doi:10.3390/polym8070243

Jiang, Z. (2008). Lipase-catalyzed synthesis of aliphatic polyesters via copolymerization of lactone, dialkyl diester, and diol. *Biomacromolecules, 9*, 3246–3251. doi:10.1021/bm800814m

Juda, L. (2010). The European Union and the Marine Strategy Framework Directive: Continuing the development of European ocean use management. *Ocean Development & International Law, 41*, 34–54. doi:10.1080/00908320903285463

Jun, F., Renxi, Z., Feng, H.E. (2003). Enzymatic ring-opening copolymerization of trimethylene carbonate and ethylene ethyl phosphate. *Science in China Series B-Chemistry, 46*, 160-167. doi:10.1360/03yb9023

Kato, M., Toshima, K. Matsumura, S. (2009). Direct enzymatic synthesis of a polyester with free pendant mercapto groups. *Biomacromolecules, 10*, 366–373. doi:10.1021/bm801132d

Kato, M., Toshima, K., Matsumura, S. (2007). Enzymatic synthesis of polythioester by the ring-opening polymerization of cyclic thioester. *Biomacromolecules, 8*, 3590–3359. doi:10.1021/bm700623s

Kaya, N. U., Guvenilir, Y.A. (2015). End-group evaluation of HEMA initiated poly(ε-caprolactone) macromonomers via enzymatic ring-opening polymerization. *International Journal of Polymer Science, 2015*. doi:10.1155/2015/458756

Kenawy, E. R., Salem, I.A., Abo-Elghit, E.M., Al-Owais, A.A. (2014). New trends in antimicrobial polymers: A state-of-the-art review. *International Journal of Chemical and Applied Biological Sciences, 1*, 95-105. doi:10.4103/2348-0734.146922

Kenawy, E. R., Worley, S.D., Broughton, R. (2007). The chemistry and applications of antimicrobial polymers: A state-of-the-art review. *Biomacromolecules, 8*, 1359–1384. doi:10.1021/bm061150q

Knani, D., Gutman, A.L., Kohn, D. (1993). Enzyme-catalyzed synthesis of linear polyesters. *Journal of Polymer Science Part A: Polymer Chemistry, 31*, 1221-1232.

Kobayashi, S. (2009). Recent developments in lipase-catalyzed synthesis of polyesters. *Macromolecular Rapid Communications, 30*, 237-266. doi:10.1002/marc.200800690

Kobayashi, S. (2011). *Enzymatic Polymerization*: John Wiley & Sons, Inc.

Kobayashi, S. (2015). Enzymatic ring-opening polymerization and polycondensation for the green synthesis of polyesters. *Polymers for Advanced Technologies, 26*, 677–686. doi:10.1002/pat.3564

Kobayashi, S., Kashiwa, K., Kawasaki, T., Shoda, S. (1991). Novel method for polysaccharide synthesis using an enzyme: the first in vitro synthesis of cellulose via a nonbiosynthetic path utilizing cellulase as catalyst. *Journal of American Chemical Society, 113*, 3079–3084.

Kobayashi, S., Uyama, H., Ohmae, M. (2001b). Enzymatic polymerization for precision polymer synthesis. Bull Chem Soc Jpn 74:613–635. *Bulletin of the Chemical Society of Japan, 74*, 613-635. doi:10.1246/bcsj.74.613

Krasowska, A., Sigler, K. (2014). How microorganisms use hydrophobicity and what does this mean for human needs? *Frontiers in Cellular and Infection Microbiology, 4*. doi:10.3389/fcimb.2014.00112

Kricheldorf, H. R. (2009). Syntheses of biodegradable and biocompatible polymers by means of bismuth catalysts. *Chemical Reviews, 109*, 5579–5594. doi:10.1021/cr900029e

Krishnan, S. (2013). Marine bioadhesion on polymer surfaces and strategies for its prevention. In H. Zeng (Ed.), *Polymer Adhesion, Friction, and Lubrication*. U.S.A.: Wiley.

Kumar, R., Tyagi, R., Parmar, V.S., Samuelson, L.A., Kumar, J., Watterson, A.C. (2004). Biocatalytic "green" synthesis of PEG-based aromatic polyesters: optimization of the substrate and reaction conditions. *Green Chemistry, 6*, 516-520. doi:10.1039/B407700H

Labet, M., Thielemans, W. (2009). Synthesis of polycaprolactone: A review. *Chemical Society Reviews, 38*, 3484–3504. doi:10.1039/b820162p

Ladd, J., Zhang, Z., Chen, S., Hower, J.C., Jiang, S. (2008). Zwitterionic polymers exhibiting high resistance to nonspecific protein adsorption from human serum and plasma. *Biomacromolecules, 9*, 1357-1361. doi:10.1021/bm701301s

Langlois, V., Vallee-Rehel, K., Peron, J.J., le Borgne, A., Walls, M., Guerin, P. (2002). Synthesis and hydrolytic degradation of graft copolymers containing poly(lactic acid) side chains: In vitro release studies of bioactive molecules. *Polymer Degradation and Stability, 76*, 411–417. doi:10.1016/S0141-3910(02)00042-3

Li, C., Tan, T., Zhang, H., Feng, W. (2010). Analysis of the conformational stability and activity of candida antarctica lipase B in organic solvents. *The Journal of Biological Chemistry, 285*, 28434–28441.

Li, P., Poon, Y.F., Li, W., Zhu, H.Y., Yeap, S.H., Cao, Y., Qi, X., Zhou, C., Lamrani, M., Beuerman, R.W., Kang, E.T., Mu, Y., Li, C.M., Chang, M.W., Leong, S.S., Chan-Park, M.B. (2011). A polycationic antimicrobial and biocompatible hydrogel with microbe membrane suctioning ability. *Nature Materials, 10*, 149–156. doi:10.1038/nmat2915

Li, Q., Li, G., Yu, S., Feng, L.Y. (2011). Ring-opening polymerization ofε-caprolactone catalyzed by a novel thermophilic lipase from Fervidobacterium nodosum. *Process Biochemistry, 46*, 253-257. doi:10.1016/j.procbio.2010.08.019

Li, Q., Wang, Z., Zhang, S., Zheng, W., Zhao, Q., Zhang, J., Wang, L., Wang, S., Kong, D. (2013). Functionalization of the surface of electrospun poly(epsilon-caprolactone) mats using zwitterionic poly(carboxybetaine methacrylate) and cell-specific peptide for endothelial progenitor cells capture. *Materials Science and Engineering: C, 33*, 1646–1653. doi:10.1016/j.msec.2012.12.074

Liljeblad, A., Kallio, P., Vainio, M., Niemi, J., Kanerva, L.T. (2010). Formation and hydrolysis of amide bonds by lipase A from Candida antarctica; exceptional features. *Organic & Biomolecular Chemistry, 8*, 886-895. doi:10.1039/b920939p

Liu, Q., Singh, A., Liu, L. (2013). Amino acid-based zwitterionic poly(serine methacrylate) as an antifouling material. *Biomacromolecules, 14*, 226–231. doi:10.1021/bm301646y

Lowe, S., O'Brien-Simpson, N.M., Connal, L.A. (2015). Antibiofouling polymer interfaces: poly(ethylene glycol) and other promising candidates. *Polymer Chemistry, 6*, 198–212. doi:10.1039/c4py01356e

M. Takwa, Y. X., N. Simpson, E. Malmström, K. Hult, C.E. Koning, A. Heise, M. Martinelle. (2008). Lipase catalyzed HEMA initiated Ring-Opening Polymerization: In Situ Formation of Mixed Polyester Methacrylates by Transesterification. *Biomacromolecules, 9*, 704-710.

Ma, J., Li, Q., Song, B., Liu, D., Zheng, B., Zhang, Z., Feng, Y. (2009). Ring-opening polymerization of ε-caprolactone catalyzed by a novel thermophilic esterase from the archaeon Archaeoglobus fulgidus. *Journal of Molecular Catalysis B: Enzymatic, 56*, 151-157. doi:10.1016/j.molcatb.2008.03.012

MacDonald, R. T., Pulapura, S.K., Svirkin, Y.Y., Gross, R.A. (1995). Enzyme-catalyzed ε-Caprolactone ring-opening polymerization. *Macromolecules, 28*, 73-78. doi:10.1021/ma00105a008

Mahapatro, A., Kumar, A., Kalra, B., Gross, R.A. (2004). Solvent-free adipic acid/1,8-octanediol condensation polymerizations catalyzed by Candida antartica lipase B. *Macromolecules, 37*, 35-40. doi:10.1021/ma025796w

Målberg, S., Finne-Wistrand, A., Albertsson, A-.C. (2010). The environmental influence in enzymatic polymerization of aliphatic polyesters in bulk and aqueous mini-emulsion. *Polymer, 51*, 5318-5322. doi:10.1016/j.polymer.2010.09.016

Martinelle, M., Holmquist, M., Hult, K. (1995). On the interfacial activation of candida antarctica lipase A and B as compared with Humicola lanuginosa lipase. *Biochimica et Biophysica Acta (BBA) - Lipids and Lipid Metabolism, 1258*, 272-276. doi:10.1016/0005-2760(95)00131-U

Matsumura, S., Tsukada, K. Toshima, K. (1999). Novel lipase-catalyzed ring-opening copolymerization of lactide and trimethylene carbonate forming poly(ester carbonate)s. *International Journal of Biological Macromolecules, 2*, 161–167. doi:10.1016/S0141-8130(99)00030-6

Matsuura, H., Miyazawa, T. (1969). Vibrational analysis of molten poly(ethylene glycol) *Journal of Polymer Science Part B: Polymer Physics, 7*, 1735–1744. doi:10.1002/pol.1969.160071009

Mochizuki, A., Hatakeyama, T., Tomono, Y., Tanaka, M. (2009). Water structure and blood compatibility of poly(tetrahydrofurfuryl acrylate). *Journal of Biomaterials Science, 20*, 591-603. doi:10.1163/156856209x426411

Montanaro, L., Campoccia, D., Arciola, C.R. (2007). Advancements in molecular epidemiology of implant infections and future perspectives. *Biomaterials, 28*, 5155–5168. doi:10.1016/j.biomaterials.2007.08.003

Mülhaupt, R. (2013). Green Polymer Chemistry and Bio-based Plastics: Dreams and Reality. *Macromolecular Chemistry and Physics, 214*, 159−174.

Niaounakis, M. (2013). *Biopolymers Reuse, Recycling, and Disposal: A volume in Plastics Design Library* (1 ed.). U.S.A.: Elsevier Inc.

Niaounakis, M. (2015). Biopolymers: Processing and Products (pp. 1-2).

Oberti, T. G., Schiavoni, M. M., Cortizo, M. S. (2008). Structure and properties of poly(benzyl acrylate) synthesized under microwave energy. *Radiation Physics and Chemistry, 77*, 597-604. doi:10.1016/j.radphyschem.2007.09.015

Odent, J., Raquez, J.M., Duquesne, E., Dubois, P. (2012). Random aliphatic copolyesters as new biodegradable impact modifiers for polylactide materials. *European Polymer Journal, 48*, 331-340. doi:10.1016/j.eurpolymj.2011.11.002

Olsson, A., Lindström, M., Iversen, T. (2007). Lipase-catalyzed synthesis of an epoxy-functionalized polyester from the suberin monomer cis-9,10-epoxy-18-hydroxyoctadecanoic acid. *Biomacromolecules, 8*, 757-760. doi:10.1021/bm060965w

Öztürk-Düşkünkorur, H., Pollet, E., Deberie, P., Phalip, V., Güvenilir, Y., Avérous, L. (2014). Lipase catalyzed synthesis of biopolyester and related clay-based nanohybrids. *Polymer, 55*, 1648-1655.

Palza, H. (2015). Antimicrobial polymers with metal nanoparticles *International Journal of Molecular Sciences, 16*, 2099-2116. doi:10.3390/ijms16012099

Poojari, Y., Clarson, S.J. (2013). Thermal stability of candida antarctica lipase B immobilized on macroporous acrylic resin particles in organic media. *Biocatalysis and Agricultural Biotechnology, 2*, 7-11.

Poulhès, F., Mouysset, D., Gil, G., Bertrand, M.P., Gastaldi, S. (2012). CAL-B catalyzed synthesis of chiral polyamides. *Tetrahedron: Asymmetry, 23*, 867–875. doi:10.1016/j.tetasy.2012.05.021

Pugh, C., Liu, T., Yan, J., Kobayashi, S. (2015). *Enzymatic polymerizations*.

Puskas, J. E., Sen, M.Y., Seo, K.S. (2009). Green polymer chemistry using nature's catalysts: enzymes. *Journal of Polymer Science Part A: Polymer Chemistry, 47*, 2959–2976.

Radheshkumar, C. M. H. (2006). Antimicrobial polymers from polypropylene/silver composites—Ag+ release measured by anode stripping voltammetry. *Reactive and Functional Polymers, 66*, 780-788. doi:10.1016/j.reactfunctpolym.2005.11.005

Renner, L. D., Weibel, D.B. (2011). Physicochemical regulation of biofilm formation. *MRS Bulletin, 36*, 347–355. doi:10.1557/mrs.2011.65

Sadu, R. B., Chen, D.H., Kucknoor, A.S., Guo, Z., Gomes, A.J. (2014). Silver-doped TiO_2/polyurethane nanocomposites for antibacterial textile coating. *BioNanoScience, 4*, 136-148. doi:10.1007/s12668-014-0125-x

Salmon, S., Hudson, S.M. (1997). Crystal morphology, biosynthesis, and physical assembly of cellulose, chitin and chitosan. *Journal of Macromolecular Science, Part C, 37*, 199-276.

Santhosh, S. M., Natarajan, K. (2015). Antibiofilm activity of epoxy/Ag-TiO_2 polymer nanocomposite coatings against Staphylococcus Aureus and Escherichia Coli. *Coatings, 5*, 95-114. doi:10.3390/coatings5020095

Santos, M. R. E., Fonseca, A.C., Mendonça, P.V., Branco, R., Serra, A.C., Morais, P.V., Coelho, J.F.J. (2016). Recent developments in antimicrobial polymers: A review. *Materials, 9*, 599. doi:doi:10.3390/ma9070599

Sarasam, A., Madihally, S.V. (2005). Characterization of chitosan–polycaprolactone blends for tissue engineering applications. *Biomaterials, 26*, 5500–5508. doi:10.1016/j.biomaterials.2005.01.071

Scardino, A. J., de Nys, R. (2011). Mini review: Biomimetic models and bioinspired surfaces for fouling control. *Biofouling, 27*, 73–86. doi:10.1080/08927014.2010.536837

Schmid, R. D., Verger, R. (1998). Lipases: interfacial enzymes with attractive applications. *Angewandte Chemie International Edition, 37*, 1609-1633.

Schmidt, S., Scherkus, C., Muschiol, J., Menyes, U., Winkler, T., Hummel, W., Gröger, H., Liese, A., Herz, H.-G., Bornscheuer, U.T. (2015). An enzyme cascade synthesis of ε-caprolactone and its oligomers. *Angewandte International Edition Communications, 54*, 2784 –2787. doi:10.1002/anie.201410633

Schwab, L. W., Kroon, R., Schouten, A.J., Loos, K. (2008). Enzyme-catalyzed ring-opening polymerization of unsubstituted β-lactam. *Macromolar Rapid Communications, 29*, 794–797. doi:10.1002/marc.200800117

Sellenet, P. H., Allison, B., Applegate, B.M., Youngblood, J.P. (2007). Synergistic activity of hydrophilic modification in antibiotic polymers. *Biomacromolecules, 8*, 19-23. doi:10.1021/bm0605513

Shah, S. A. S., Nag, M., Kalagara, T., Singh, S., Manorama, S.V. (2008). Silver on PEG-PU-TiO_2 polymer nanocomposite films: An excellent system for antibacterial applications. *Chemistry of Materials, 20*, 2455–2460. doi:10.1021/cm7033867

Shoda, S., Uyama, H., Kadokawa, J., Kimura, S., Kobayashi, S. (2016). Enzymes as green catalysts for precision macromolecular synthesis. *Chemical Reviews, 116*, 2307–2413. doi:10.1021/acs.chemrev.5b00472

Siedenbiedel, F., Tiller, J.C. (2012). Antimicrobial polymers in solution and on surfaces: Overview and functional principles. *Polymers, 4*, 46-71. doi:10.3390/polym4010046

Sivalingam, G., Madras, G. (2004). Modeling of lipase catalyzed ring-opening polymerization of ε-caprolactone. *Biomacromolecules, 5*, 603–609. doi:10.1021/bm0344405

Skjøt, M., De Maria, L., Chatterjee, R., Svendsen, A., Patkar, S.A., Østergaard, P.R., Brask, J. (2009). Understanding the plasticity of the alpha/beta hydrolase fold: lid swapping on the candida antarctica lipase B results in chimeras with interesting biocatalytic properties. *ChemBioChem, 10*, 520-527. doi:10.1002/cbic.200800668

Stansbury, J. W., Dickens, S.H. (2001). Determination of double bond conversion in dental resins by near infrared spectroscopy. *Dental Materials, 17*, 71-79. doi:10.1016/S0109-5641(00)00062-2

Stauch, B., Fisher, S.J., Cianci, M. (2015). Open and closed states of Candida antarctica lipase B: protonation and the mechanism of interfacial activation. *Journal of Lipid Research, 56*, 2348-2358.

Stavila, E., Loos, K. (2015). Synthesis of polyamides and their copolymers via enzymatic polymerization. *Journal of Renewable Materials, 3*, 268-280. doi:10.7569/JRM.2015.634102

Stepankova, V., Bidmanova, S., Koudelakova, T., Prokop, Z., Chaloupkova, R., Damborsky, J. (2013). Strategies for stabilization of enzymes in organic solvents. *ACS Catalysis, 3*, 2823–2836. doi:10.1021/cs400684x

Taden, A., Antonietti, M., Landfester, K. (2003). Enzymatic Polymerization towards Biodegradable Polyester Nanoparticles. *Macromolecular Rapid Communications, 24*, 512–516. doi:10.1002/marc.200390079

Takwa, M., Hult, K., Martinelle, M. (2008b). Single-step, solvent-free enzymatic route to α,ω-functionalized polypentadecalactone macromonomers. *Macromolecules, 41*, 5230-5236. doi:10.1021/ma800074a

Takwa, M., Xiao, Y., Simpson, N., Malmström, E., Hult, K., Koning, C.E., Heise, A., Martinelle, M. (2008a). Lipase catalyzed HEMA initiated ring-

opening polymerization: In situ formation of mixed polyester methacrylates by transesterification. *Biomacromolecules, 9*, 704-710. doi:10.1021/bm7010449

Tanaka, M., Sato, K., Kitakami, E., Kobayashi, S., Hoshiba, T., Fukushima, K. (2015). Design of biocompatible and biodegradable polymers based on intermediate water concept. *Polymer Journal, 47*, 114-121. doi:10.1038/pj.2014.129

Tang, S.-J., Shaw, J.-F., Sun, K.-H., Sun, G.-H., Chang, T.-Y., Lin, C.-K., Lo, Y.-C., Lee, G.-C. (2001). Recombinant expression and characterization of the Candida rugosa lip4 lipase in Pichia pastoris: Comparison of glycosylation, activity, and stability. *Archives of Biochemistry and Biophysics, 387*, 93-98.

Timofeeva, L., Kleshcheva, N. (2011). Antimicrobial polymers: Mechanism of action, factors of activity, and applications. *Applied Microbiology and Biotechnology, 89*, 475–492. doi:10.1007/s00253-010-2920-9

Treat, N. J., Sprafke, H., Kramer, J.W., Clark, P.G., Barton, B.E., de Alaniz, J.R., Fors, B.P., Hawker, C.J. (2014). Metal-Free Atom Transfer Radical Polymerization. *Journal of American Chemical Society, 136*, 16096–16101. doi:10.1021/ja510389m

Trodler, P., Pleiss, J. (2008). Modeling structure and flexibility of candida antarctica lipase B in organic solvents. *BMC Structural Biology, 2008*, 9.

Tufvesson, P., Törnvall, U., Carvalho, J., Karlsson, A.J., Hatti-Kaul, R. (2011). Towards a cost-effective immobilized lipase for the synthesis of specialty chemicals. *Journal of Molecular Catalysis B: Enzymatic, 68*, 200–205. doi:10.1016/j.molcatb.2010.11.004

Ulber, R., Dieter, S., Hirth, T. (2011). Renewable Raw Materials: New Feedstocks for the Chemical Industry (pp. 238). Federal Republic of Germany: Wiley-VCH.

Uppenberg, J., Hansen, M.T., Patkar, S., Jones, T.A. (1994). The sequence, crystal structure determination and refinement of two crystal forms of lipase B from Candida antarctica. *Structure, 2*, 293-308.

Url-1 <*http://www.rcsb.org/pdb/home/home.do***>**, date retrieved 24.12.2016.

Uyama, H., Kobayashi, S. (2002). Enzyme-catalyzed polymerization to functional polymers. *Journal of Molecular Catalysis B: Enzymatic, 19-20*, 117–127. doi:10.1016/S1381-1177(02)00158-3

Uyama, H., Namekawa, S., Kobayashi, S. (1997). Mechanistic studies on the lipase-catalyzed ring-opening polymerization of lactones. *Polymer Journal, 29*, 299-301. doi:10.1295/polymj.29.299

Uyama, H., Takeya, K., Hoshi, N. Kobayashi, S. (1995). Lipase-catalyzed ring-opening polymerization of 12-dodecanolide. *Macromolecules, 28*, 7046-7050. doi:10.1021/ma00125a002

Uyuma, H., Kobayashi, S. (1993). Enzymatic ring-opening polymerization of lactones catalyzed by lipase. *Chemistry Letters, 35*, 1149-1150. doi:10.1246/cl.1993.1149

Vakhlu, J., Kour, A. (2006). Yeast lipases: enzyme purifi cation, biochemical properties and gene cloning. *Electronic Journal of Biotechnology, 9*, 69–85.

van Loosdrecht, M. C., Lyklema, J., Norde, W., Schraa, G., Zehnder, A.J. (1987). The role of bacterial cell wall hydrophobicity in adhesion. *Applied and Environmental Microbiology, 53*, 1893–1897.

Varma, I. K., Albertsson, A.-C., Rajkhowaa, R., Srivastava, R.K. (2005). Enzyme catalyzed synthesis of polyesters. *Progress in Polymer Science, 30*, 949–981. doi:10.1016/j.progpolymsci.2005.06.010

Veld, M. A. J., Palmans, A.R.A. (2010). Hydrolases part I: Enzyme mechanism, selectivity and control in the synthesis of well-defined polymers. *Advances in Polymer Science, 237*, 55–78.

Verger, R. (1997). 'Interfacial activation' of lipases: facts and artifacts. *Trends in Biotechnology, 15*, 32-38.

Vert, M., Li, S.M., Spenlehauer, G., Guerin, P. (1992). Bioresorbability and biocompatibility of aliphatic polyesters. *Journal of Materials Science: Materials in Medicine, 3*, 432-446. doi:10.1007/BF00701240

Wang, G. (2014). Human antimicrobial peptides and proteins. *Pharmaceuticals, 7*, 545-594. doi:10.3390/ph7050545

Wang, H.-F., Su, W., Zhang, C., Luo, X., Feng, J. (2010). Biocatalytic fabrication of fast-degradable, water-soluble polycarbonate functionalized with tertiary amine groups in backbone. *Biomacromolecules, 11*, 2550–2557. doi:10.1021/bm1001476

Wang, K. (2011). *Roles of polymer crosslinking density and crystallinity in regulating surface characteristics and pre-osteoblastic MC3T3 cell behavior.* (Doctoral Dissertation), University of Tennessee. Retrieved from http://trace.tennessee.edu/utk_graddiss/1138

Wang, Y., Shen, J., Yuan, J. (2016). Design of hemocompatible and antifouling PET sheets with synergistic zwitterionic surfaces. *Journal of Colloid and Interface Science, 480*, 205–217. doi:10.1016/j.jcis.2016.07.022

Warwel, S., Demes, C., Steinke, G. (2001). Polyesters by lipase-catalyzed polycondensation of unsaturated and epoxidized long-chain α,ω-dicarboxylic acid methyl esters with diols. *Journal of Polymer Science Part A: Polymer Chemistry, 39*, 1601–1609. doi:10.1002/pola.1137

Wei, T., Zheng, B., Yi, H., Gao, Y., Guo, W. (2014). Thermal Analysis and Non-Isothermal Kinetics of poly(ethylene glycol) with different molecular weight. *Polymer Engineering and Science, 54*, 2872–2876. doi:10.1002/pen.23846

Wen, J., Zhuo, R.-X. (1998). Enzyme-catalyzed ring-opening polymerization of ethylene isopropyl phosphate. *Macromolar Rapid Communications, 19*, 641-642. doi:10.1002/(SICI)1521-3927(19981201)19:12<641::AID-MARC641>3.0.CO;2-I

West, S. L., Salvage, J.P., Lobb, E.J., Armes, S.P., Billingham, N.C., Lewis, A.L., Hanlon, G.W., Lloyd, A.W. (2004). The biocompatibility of crosslinkable copolymer coatings containing sulfobetaines and phosphobetaines. *Biomaterials, 25*, 1195–1204. doi:10.1016/j.biomaterials.2003.08.010

Whitehead, N. A., Barnard, A.M., Slater, H., Simpson, N.J., Salmond, G.P. (2001). Quorum-sensing in Gram-negative bacteria. *FEMS Microbiology Reviews, 25*, 365-404. doi:10.1111/j.1574-6976.2001.tb00583.x

Winkler, F. K., D'Arcy, A., Hunziker, W. (1990). Structure of human pancreatic lipase. *Nature, 343*, 771-774.

Wo, Y., Brisbois, E.J., Bartlett, R.H., Meyerhoff, M.E. (2016). Recent advances in thromboresistant and antimicrobial polymers for biomedical applications: just say yes to nitric oxide (NO). *Biomaterials Science, 4*, 1161-1183. doi:10.1039/c6bm00271d

Woodruff, M. A., Hutmacher, D.W. (2010). The return of a forgotten polymer—Polycaprolactone in the 21st century. *Progress in Polymer Science, 35*, 1217–1256. doi:10.1016/j.progpolymsci.2010.04.002

Xiao, Y., Takwa, M., Hult, K., Koning, C.E., Heise, A., Martinelle, M. (2009). Systematic comparison of HEA and HEMA as initiators in enzymatic ring-opening polymerizations. *Macromolecular Bioscience, 13*, 713-720. doi:10.1002/mabi.200800290

Xing, Z., Chae, W.P., Baek, J.Y., Kang, I.K. (2010). In vitro assessment of antibacterial activity and cytocompatibility of silver-containing PHBV nanofibrous ccaffolds for tissue engineering. *Biomacromolecules, 11*, 1248-1253. doi:10.1021/bm1000372

Xue, Y., Xiao, H., Zhang, Y. (2015). Antimicrobial polymeric materials with quaternary ammonium and phosphonium salts. *International Journal of Molecular Sciences, 16*, 3626-3255. doi:10.3390/ijms16023626

Y. Xiao, M. T., K. Hult, C.E. Koning, A. Heise, M. Martinelle. (2009). Systematic comparison of HEA and HEMA as initiators in enzymatic ring-opening polymerizations. *Macromolecular Bioscience, 13*, 713-720.

Y. Yang, Y. Y., Y. Zhuang, C. Liu, W. Shi, Q. Li. (2011). Lipase/esterase-catalyzed ring-opening polymerization: A green polyester synthesis technique. *Process Biochemistry, 46*, 1900–1908.

Yagci, Y., Jockusch, S., Turro, N. J. (2010). Photoinitiated polymerization: Advances, challenges, and opportunities. *Macromolecules, 43*, 6245–6260. doi:10.1021/ma1007545

Yan, G., Zhang, G., Ren, H., Li, Y., Yang, J. (2016). Synthesis and characterization of semiaromatic polyamides with dicyclohexane units. *RSC Advances, 6*, 76490–76497. doi:10.1039/c6ra13021f

Yang, Y., Qi, P., Yang, Z., Huang, N. (2015). Nitric oxide based strategies for applications of biomedical devices. *Biosurface and Biotribology, 1*, 177–201. doi:10.1016/j.bsbt.2015.08.003

Yang, Y., Yu, Y., Zhang, Y., Liu, C., Shi, W., Li, Q. (2011). Lipase/esterase-catalyzed ring-opening polymerization: A green polyester synthesis technique. *Process Biochemistry, 46*, 1900–1908. doi:10.1016/j.procbio.2011.07.016

Zhai, S., Ma, Y., Chen, Y., Li, D., Cao, J., Cai, M., Xie, X., Chen, Y., Luo X. (2014). Synthesis of an amphiphilic block copolymer containing zwitterionic

sulfobetaine as a novel pH sensitive drug carrier. *Polymer Chemistry, 5*, 1285-1297. doi:10.1039/C3PY01325A

Zhang, J., Shi, H., Wu, D., Xing, Z., Zhang, A., Yang, Y., Li, Q. (2014). Recent developments in lipase-catalyzed synthesis of polymeric materials. *Process Biochemistry, 49*, 797–806. doi:10.1016/j.procbio.2014.02.006

Zhang, X., Cai, M., Zhong, Z., Zhuo, R. (2012). A water-soluble polycarbonate with dimethylamino pendant groups prepared by enzyme-catalyzed ring-opening polymerization. *Macromolar Rapid Communications, 33*, 693−697. doi:10.1002/marc.201100765

Zheng, J., Li, L., Chen, S., Jiang, S. (2004). Molecular simulation study of water interactions with oligo (ethylene glycol)-terminated alkanethiol self-assembled monolayers. *Langmuir, 20*, 8931-8938. doi:10.1021/la036345n

Zhou, S., Deng, X., Yang, H. (2003). Biodegradable poly(e-caprolactone)-poly(ethylene glycol) block copolymers: characterization and their use as drug carriers for a controlled delivery system. *Biomaterials, 24*, 3563–3570. doi:10.1016/S0142-9612(03)00207-2

Zisis, T., Freddolino, P.L., Turunen, P., van Teeseling, M.C., Rowan, A.E., Blank, K.G. (2015). Interfacial activation of candida antarctica lipase B: Combined evidence from experiment and simulation. *Biochemistry, 54*, 5969–5979. doi:10.1021/acs.biochem.5b00586

CURRICULUM VITAE

Name Surname : Nazif Uğur Kaya

Place and Date of Birth : Seyhan/Adana/Türkiye, 12.09.1985

E-Mail : naugka12@gmail.com

EDUCATION :

- **B.Sc.** : 2007, Istanbul Technical University, Faculty of Chemical and Metallurgical Engineering, Chemical Engineering Department
- **M.Sc.** : 2010, Istanbul Technical University, Faculty of Graduate School of Science Engineering and Technology, Polymer Science & Technology Department

PROFESSIONAL EXPERIENCE:

- 2012-2013 Technical Specialist in SASA Polyester A.Ş. (Adana/Turkiye).

PUBLICATIONS AND PRESENTATIONS ON THE THESIS:

- **Nazif Ugur Kaya**, Fatoş Yüksel Güvenilir, "End-group evaluation of HEMA initiated Poly(ε-Caprolactone) macromonomers via enzymatic ring-opening polymerization", *International Journal of Polymer Science*, 2015(2015), Article ID 458756.
- **Nazif Ugur Kaya**, Aysen Onen, Yuksel Guvenilir, "Photopolymerization of Acrylates by Enzymatically Synthesized PCL Based Macrophotoinitiator", *Express Polymer Letters* (Accepted).
- **Nazif Ugur Kaya**, Aysen Onen, Yuksel Avcibasi Guvenilir, "Enzymatically Synthesized Polycaprolactone Based Macrophotoinitiator", *Biobased and*

Biodegradable Polymers (BIOPOL 2015), 6-9 October 2015, Donostia-San Sebastián, Spain (Poster).

- **Nazif Ugur Kaya**, Yuksel Avcibasi Guvenilir, "Methacrylate Initiated Poly(ε-Caprolactone) via Enzymatic Ring-Opening Polymerization", *European Polymer Congress 2015 (European Polymer Federation, EPF)*, 21-26 June 2015, Dresden, Germany (Oral Presentation).

OTHER PUBLICATIONS AND PRESENTATIONS

- Ugur Cengiz, Nevin Atalay Gengec, **N. Ugur Kaya**, H. Yildirim Erbil, A. Sezai Sarac, "Mechanical and Thermal Properties of Fluoromethacrylate-Methylmethacrylate Statistical Copolymers Synthesized in Supercritical Carbon Dioxide" *Journal of Fluorine Chemistry*, Vol.132, pp. 348-355, 2011.
- Suat Cetiner, Hale Karakas, Romeo Ciobanu, Marius Olariu, **N. Ugur Kaya**, Cem Unsal, Fatma Kalaoglu, A.Sezai Sarac, "Polymerization of Pyrrole Derivatives on Polyacrylonitrile Matrix, FTIR-ATR and Dielectric Spectroscopic Characterization of Composite Thin Films" *Synthetic Metals*, Vol.160, pp. 1189-1197, 2010.
- **Nazif Ugur Kaya**, Nezha Badi, Filip Du Prez, "Multifunctional Dendrimer Formation Using Thiolactone Chemistry", *Macromolecular Chemistry and Physcis* (Accepted).
- Cristina Resetco, Daniel Frank, **Nazif Uğur Kaya**, Nezha Badi and Filip Du E. Prez Bio-inspired multifunctional polyampholytes prepared in single pot from sustainable thiolactone building blocks" (Submitted).
- Suat Cetiner, Marius Olariu, **N. Ugur Kaya**, Sebastian Aradoaei, "Thermally stimulated discharge currents of poly(Acrylonitrile-co-Acrylic acid)-polypyrrole composites", *Materials and Applications for Sensors and Transducers II, Key Engineering Materials*, Vol.543, pp. 154-158, 2013.
- Cem Unsal, Suat Cetiner, **N. Ugur Kaya**, Fatma Kalaoglu, Hale Karakas, A.Sezai Sarac, "Characterization of Conductive Polyacrylonitrile/Polypyrrole Composite Thin Films", *2nd International Scientific Conference "Textiles of the Future*, 13-15 November 2008, Kortrijk, Belgium.
- Suat Cetiner, Fatma Kalaoglu, Hale Karakas, A.Sezai Sarac, Cem Unsal, **N. Ugur Kaya**, "Conductive Polyacrylonitrile/Polypyrrole Composites", *Uludağ Exporters' Association – R&D Project Market for Textile and Confection*, 19 February 2009, Bursa, Turkey.
- Suat Cetiner, **N. Ugur Kaya**, Cem Unsal, Fatma Kalaoglu, Hale Karakas, A.Sezai Sarac, "Characterization of Conductive Polyacrylonitrile/Poly-N-Methyl Pyrrole Composite Thin Films", *Autex 2009 World Textile Conference*, 26-29 May 2009, İzmir, Turkey.
- **Nazif Ugur Kaya**, Nezha Badi, Filip Du Prez, "Multifunctional PEG-based polymers via thiolactone chemistry", *Belgian Polymer Group (BPG)*, 23-24 May 2016, Hasselt, Belgium.